Fakultät für Physik der Universität Bielefeld

The inhomogeneous Universe:

Its average expansion and cosmic variance

Alexander Wiegand

September 12, 2012

Dissertation an der Fakultät für Physik der Universität Bielefeld

Erstgutachter: Prof. Dr. Dominik J. Schwarz
Zweitgutachter: Prof. Dr. Dietrich Bödeker

To the masters of the Universe

Abstract

Despite its global homogeneity and isotropy, the local matter distribution in the late Universe is manifestly inhomogeneous. Understanding the various effects resulting from these inhomogeneities is one of the most important tasks of modern cosmology. In this thesis, we investigate two aspects of the influence of local structure: firstly, *to what extent do local structures modify the average expansion of spatial regions with a given size*, and secondly, *how strongly does the presence of structure limit the possible accuracy of measurements in our cosmic neighborhood*.

To address these questions we first characterize the properties of the local inhomogeneities; we recall basic measures of fluctuations and go beyond them using the robust morphological tool of the Minkowski functionals. In particular, we apply these measures to the Sloan Digital Sky Survey data release seven. We find that the morphology of the luminous red galaxy data is marginally consistent with the one derived from simulations within the ΛCDM framework. In addition we illustrate, how the Minkowski functionals provide a description of clustering properties, and why this description goes beyond the standard two-point statistics. Minkowski functionals do therefore provide a measure for the amount of non-Gaussianity that we find in the galaxy data.

With this information on the amount of structure in the observed Universe, we choose to model these structures by employing the relativistic Zel'dovich approximation (RZA) to find out, whether they can affect the average evolution. To this end, we use the Buchert scheme of averaging and evaluate the magnitude of the kinematical backreaction term, which is one modification with respect to the equations without structure. The other modification is a change in evolution of the averaged curvature. We find that, within the RZA, kinematical backreaction affects only the evolution on small scales, while curvature may lead to effects on larger scales. More precisely, the contribution of backreaction to the cosmic energy budget, is larger than 1% below 100 Mpc only. We show that our results are consistent with the results obtained by other perturbative methods and also with those of a toy model that tries to capture non-perturbative effects.

The observation of a significant curvature contribution on scales larger than the homogeneity scale finally motivates the investigation of its effects on the accuracy of local measurements. We derive the fluctuations of the cosmological parameters in recent galaxy surveys, and find that domains as big as $540\,h^{-1}$Mpc may still have a curvature contribution to the energy budget of 1%. This may limit our ability to measure the dark energy equation of state. We find that the Hubble rate today can never be directly measured with an accuracy better than 0.5% Finally we show how backreaction and cosmic variance are linked to each other.

The work presented here is based upon the articles:

1. A. Wiegand and D. J. Schwarz
   Inhomogeneity-induced variance of cosmological parameters
   Astronomy & Astrophysics 538, A147 (2012)

2. T. Buchert, C. Nayet and A. Wiegand
   Lagrangian theory of structure formation in relativistic cosmology II: average properties of a generic evolution model
   In preparation

3. A. Wiegand
   Fluctuations of Cosmic Parameters Due to Inhomogeneities
   Acta Physica Polonica B
   Vol. 42, No. 11, November 2011, page 2279

The calculations were performed using Mathematica and Cadabra [127,128].

Contents

1. Introduction

The question of how we may describe the global properties of our locally inhomogeneous Universe within the geometrical framework of General Relativity (GR) is a longstanding and lively discussed problem in cosmology. Since the first simple cosmological models by Einstein [1], the prevailing opinion is, that this can be achieved by assuming that the Universe is homogeneous and isotropic. Then, it is only the homogeneous background energy density that determines the entire global evolution. This evolution is then calculated under the assumption that the Einstein equations of GR give a meaningful result for these large scales as well, as for the local motion of stars and planets. To be able to also describe the inhomogeneous features, the structure ignored in the first step is added in the form of small perturbations to the average density. The resulting theory is then claimed to describe the Universe on large scales where the density perturbations are small enough that this linear treatment holds.

Especially in the last decade, this prescription has been surprisingly successful in providing an effective fitting model to a growing number of cosmological data. In its present form of the concordance Λ cold dark matter (ΛCDM) model, it has been established by observations of the Wilkinson Microwave Anisotropy Probe (WMAP) [2] and the Nobel Price awarded Supernova measurements [3, 4]. Since then, this newly created "standard model of cosmology" has been found to be consistent with all experiments with which it has been tested. These experiments include such complementary probes as gravitational lensing, baryon acoustic oscillations (BAO) distance measurements, the integrated Sachs Wolfe (ISW) effect and more.

Despite (or perhaps just as a consequence of) this remarkable success, the underlying conceptual problems have still not been rigorously solved. At each step of the chain of assumptions above, that leads to the standard model, open questions remain. The assumed homogeneity on large scales is mainly a postulate even if recently there has been experimental progress in testing this assumption [5]. Concerning the isotropy there are hints of dipole features in several observations all pointing into the direction of an "axis of evil" (like e.g. in the CMB [6]). But even for a statistically homogeneous and isotropic Universe the question remains, if the same Einstein equations can be used at the global level for an effective description of the average cosmological fluid, that are used at the local level for the description of motions of stars and planets. In electrodynamics we know, that the macroscopic Maxwell equations pick up effective terms that contain the combined microscopic contributions. So what would be the corresponding prescription in the GR case? This issue is known as the "averaging problem" and has probably most clearly been discussed by George Ellis in [7].

The fact that this problem is very involved results from the tensor structure of GR. To arrive at a theory for the global properties of our Universe that effectively takes into account the local structure, we would have to find something like an average space-time manifold. To this end, we would have to average tensors like the Ricci tensor, that describe the geometry of the space-time. This, however, is not yet possible consistently, even if there are several approaches on the market, for example the bi tensor approach of Zalaletdinov [8, 9], or the Ricci flow approach [10].

So until this question is settled, the use of the standard model implies that we implicitly assume that the average space-time manifold that we will find in the end is the FRW space-time and that the average properties will be given by the single homogeneous and isotropic solution to Einsteins equations. This means, that there is some implicit averaging in this framework, but with the expectation that it will turn out to give the same result as for a completely homogeneous Universe. As there is consensus on the fact that there will be effective terms emerging in a thorough treatment, this expectation is another way of saying that these effective terms are negligible. This belief is at the heart of the current debate on the importance of the backreaction of inhomogeneities on the global evolution: Is the common conviction correct that these corrections are at best a 10^{-5} effect?

The physical motivation for the opinion that the backreaction of inhomogeneities is a 10^{-5} effect comes from results in perturbation theory averaged at the horizon scale. Studies in Newtonian [11, 12, 13] and synchronous gauge [14, 15, 16, 17] consistently come to this conclusion. However, they have to rely on the assumption that the standard framework is correct and structure may be described by small perturbations about the homogeneous background. Yet, the big observational success of this framework then leads to the common conclusion that this proves that the effect is not important.

This however raises the question if this is conclusion is compulsory. If the effective terms merely lead to a change in the background, the perturbations onto this effective background may still describe the structure correctly, but the physical reasons for this particular background would be different. As especially the motivation for the different background components in the standard model is not very convincing at the moment, with a cosmological constant of unmotivated size and a dark matter component of so far unknown nature, there may still be surprises concerning their interpretation.

That such background changing components exist in perturbation theory has been shown by Clarkson [18]. In this particular case they are small, but in a further work [19] he showed that there are many formally diverging integrals in the higher order terms in perturbation theory. With a reasonable cutoff they still would give sizable corrections to the background.

Results of this kind have raised doubts that perturbation theory is still appropriate for a description of the late Universe with high density contrasts. The standard argument is that on larger scales the density fluctuations are still small so perturbation theory would work on those scales. By speaking of the density distribution on large scales, however, the argument implies again the use of implicit averaging. So any effective contribution of

small scale inhomogeneities to the background is lost by definition. This is why as soon as perturbation theory breaks down on small scales, all arguments based on the linearity of large scales become questionable. Under which circumstances this breakdown occurs has nicely been discussed by Räsänen [20].

At latest when this breakdown occurs, it is in addition questionable if the picture of background and perturbations really describes the Universe correctly. Can the large Voids that supposedly are completely empty, be described by small fluctuations from a finite density background? Can an effective description be correct where light that travels in vacuum is now treated as if it travels in a constant density homogeneous Universe? Concerning this latter question Räsänen [21, 22] found that a correct treatment of the background in terms of an explicit averaging is necessary to correctly interpret the observations.

Due to all these issues, the expectation that the results from perturbation theory may not be trustworthy at late times has led to the construction of a number of models that try to avoid perturbation theory. However, they make either ad hoc assumptions about the effective contribution of inhomogeneities [23, 24, 25, 26], or they are only toy models that might oversimplify the problem [27]. Apart from that, there is an interesting proposal by Wiltshire [28, 29], but it is unclear whether its technical issues have all been addressed properly.

In summary one has therefore to conclude that the problem is still open. Even if there is no model that would show a sizable effect without plugging it in by hand from the beginning through the assumptions made, there is also no proof that perturbation theory would give the correct answer.

Independently from the question if the higher order perturbative terms would give a global contribution to the background, the local evolution of the Universe is clearly affected by inhomogeneities. Especially the fluctuations in the cosmic parameters between different locations in the Universe have been shown to be important locally [30, 16, 15, 17]. In the era of precision cosmology, these fluctuations present fundamental limits for the precision with which we can principally know local quantities.

In this work we will contribute to both of these problems. Concerning the question if the averaging renormalizes the background significantly, we explore a new perturbative scheme, introduced in [31]. It has the advantage that it is easily generalizable to higher orders and is therefore expected to help solving the question how trustworthy the perturbative results actually are. As a first step we therefore explore the solutions that this scheme provides at lowest order. We find that it leads to conclusions in agreement with the perturbative studies mentioned above and show under which assumptions it is also formally equivalent to the treatment of Li and Schwarz [15, 16, 17].

The second part treats the question on which scales the local contributions of the inhomogeneities become important. We find that even above the assumed homogeneity scale of 100 Mpc there are sizable contributions to the uncertainties that arise through inhomogeneities. These limit the precision to which we will ultimately know local parameters such as today's Hubble rate.

If the assumed homogeneity is seen in the morphology of the cosmic structures, is finally explored with the help of Minkowski functionals. These provide a robust measure of the nonlinear structure and show significant deviations in the morphology from the homogeneous ΛCDM case. When applied to the cosmic velocity field they would also provide a non-perturbative description of the backreaction term, as it can be expressed in terms of the velocity field Minkowski functionals, see [32].

All in all there are a number of new applications that become possible with the techniques described and explored in this work. In the upcoming golden era of the big structure characterizing surveys, with deep redshift surveys such as GOODS [33], GEMS [34] or COSMOS [35], and even more with the giant surveys like the Baryonic Oscillation Spectroscopic Survey (BOSS) [36], BigBoss [37] and finally Euclid [38] and the square kilometre array (SKA)[1], these techniques will be useful for deriving the real influence of the structure that these surveys will reveal.

The thesis is organized as follows: Sec. 1.1 is used to collect the basic formulas of homogeneous cosmology. Then we will turn to the basics of inhomogeneous cosmology in Chapter 2. Both (perhaps with the exception of Sec. 2.1.2) will not be new to readers working on large scale structure so they may be skipped and only used for reference for the formulas relevant in the later sections. Then in Chapter 3 we present the observations that are used for exploring the inhomogeneous Universe and complement the characterization of structures by our analysis of the Sloan Digital Sky Survey (SDSS) luminous red galaxy (LRG) sample. Chapter 4 addresses the "averaging problem" and presents the results for the backreaction of inhomogeneities in the relativistic Zel'dovich approximation (RZA). Chapter 5 then turns to the influence of inhomogeneities on local observations. While Chapter 2 and Sections 3.1 and 4.1 present the necessary theoretical formalism, the rest of Chapters 3, 4 and 5 mainly contains my own work as published in [39, 40] if not otherwise stated.

1.1. The background evolution of the Universe

Before turning to the description of structures in the Universe in Chapter 2, we will first have a look at the evolution of the overall Universe in this section. As we will ask the question whether the cosmic evolution is modified through the influence of structure, this part is mainly for reference. It allows to compare the results obtained in the context of averaged inhomogeneous cosmologies, to the normally used Friedmann-Robertson-Walker cosmologies.

1.1.1. The Friedmann equations

The Universe is believed to be governed mainly by gravity. This is because of the four known forces it is the only one that acts on cosmologically relevant distance scales, when

[1] http://www.skatelescope.org

we assume that the Universe is electrically neutral. The description of the evolution of our space-time is therefore based on the Einstein equations of general relativity

$$R_{\mu\nu} - \frac{1}{2} R g_{\mu\nu} + \Lambda g_{\mu\nu} = 8\pi G T_{\mu\nu} \,. \tag{1.1}$$

These equations relate the geometry of space-time encoded in the Ricci tensor $R_{\mu\nu}$ and the metric $g_{\mu\nu}$ to the matter content of the Universe encoded in the energy momentum tensor $T_{\mu\nu}$. When we want to apply these equations to the Universe as a whole, we face the problem that they depend on the characteristics at each position x^μ of the manifold that describes our Universe. To derive the overall properties of this space-time manifold we would need to average over the solutions to these equations to get the global behavior. As they consist of 10 independent differential equations of second order for the metric components, obtaining a full inhomogeneous solution is impossible. In addition we would not be able to specify the initial data for the energy momentum tensor in every point in space.

The standard approach to avoid these technical difficulties is now to assume, that the average evolution of the Universe would be given by the solution that is obtained if we use a homogeneous matter source in the equations (1.1). The metric that describes such a space-time with a homogeneous source is the homogeneous and isotropic Robertson Walker (RW) metric

$$\mathrm{d}s^2 = -\mathrm{d}t^2 + a\left(t\right)^2 \left[\frac{\mathrm{d}r^2}{1-kr^2} + r^2\left(\mathrm{d}\theta^2 + \sin\left(\theta\right)^2 \mathrm{d}\phi^2\right)\right] \,. \tag{1.2}$$

This ansatz for the metric drastically reduces the complexity of the equations (1.1). Instead of ten functions of space and time, the metric components now depend only on one function $a\left(t\right)$ and one constant k. $a\left(t\right)$ is the scale factor that describes how the Universe expands and k is the constant spatial curvature. With this ansatz, the Einstein equations (1.1) simplify to

$$H^2 \equiv \left(\frac{\dot{a}}{a}\right)^2 = \frac{8\pi G}{3}\varrho - \frac{k}{a^2} + \frac{\Lambda}{3} \,, \tag{1.3a}$$

$$\frac{\ddot{a}}{a} = -\frac{4\pi G}{3}\left(\varrho + 3p\right) + \frac{\Lambda}{3} \,, \tag{1.3b}$$

$$0 = \dot{\varrho} + 3H\left(\varrho + p\right) \,, \tag{1.3c}$$

which are called the Friedmann equations with the Hubble rate H. After having specified the curvature, the cosmological constant and the homogeneous fluid, they give the overall evolution of the Universe. The specification which type of fluid one uses is done by choosing a relation between its density ϱ and pressure p. In cosmology this relation is always assumed to be of the form $w = p/\varrho$, where w is the equation of state parameter. For most applications it is taken to be a constant, with the two important special cases of $w = 0$ for non-relativistic matter and $w = 1/3$ for highly relativistic matter.

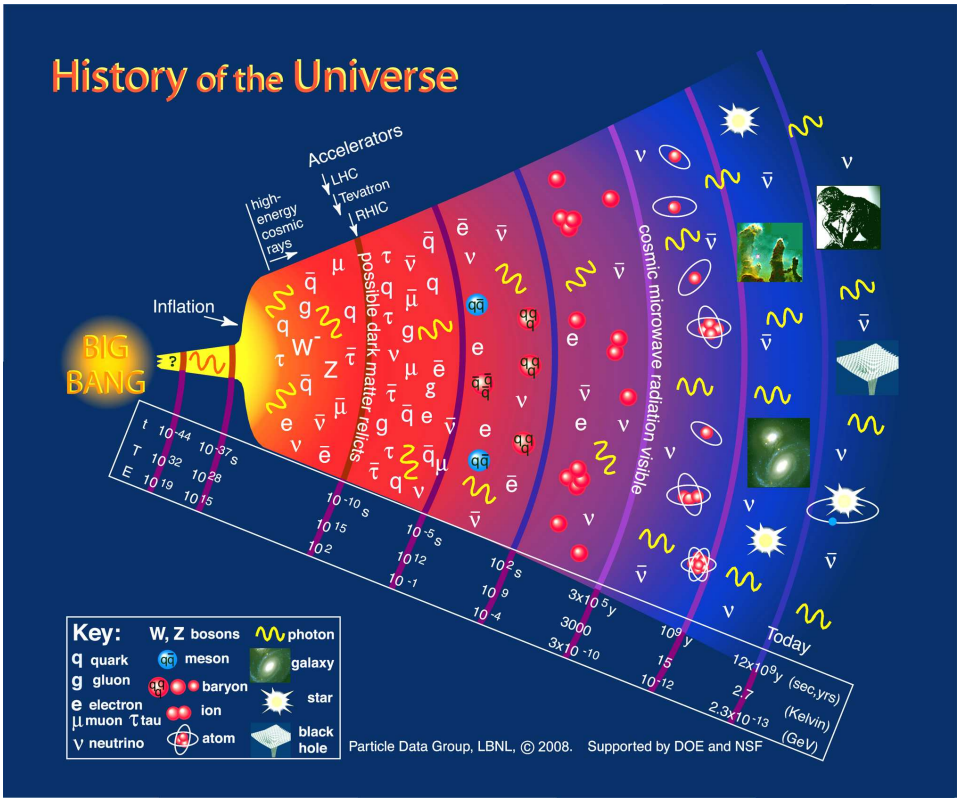

Figure 1.1. Sketch of the evolution history of the Universe. After the initial Big Bang singularity and the era of trans-Planckian physics, cosmological inflation led to a rapid growth of the scale factor. After a short epoch of reheating that created the matter content of the Universe it was mainly radiation dominated and underwent several phase transitions. When the temperature had dropped enough that atoms could form, the Universe became transparent for radiation. From then on, the photons formerly trapped in the hot plasma, streamed freely and gave rise to the radiation that we see today as microwave radiation. Continually expanding, the Universe cooled down to $3K$ today. Credit: Particle Data Group, LBNL 2008.

To characterize the importance of the different energy components one introduces the dimensionless parameters

$$\Omega_i := \frac{8\pi G}{3H^2}\varrho_i \;\; ; \;\; \Omega_k := -\frac{k}{a^2H^2} \;\; ; \;\; \Omega_\Lambda := \frac{\Lambda}{3H^2} \, , \tag{1.4}$$

where i runs over the different fluid components and H is typically evaluated today.

1.1.2. The evolution history

Since the discovery of the expanding Universe, the only solutions of interest to Eq. (1.3a) are those for which the scale factor $a(t)$ is growing with cosmic time. Extrapolating these solutions to early times, one finds that the scale-factor goes to zero at $t = 0$ for most of them, more precisely iff $\varrho + 3p > 0$. There is an interesting solution due to Eddington to Eq. (1.3a) that starts with a finite $a_\mathbf{i}$ and then turns over to the standard expansion, but in general only solutions with an initial singularity are considered. So in the beginning the Universe was arbitrarily smaller and therefore denser and hotter than today. This implies that the baryonic matter component (i.e. protons and electrons), that is non-relativistic today, was in the form of a relativistic plasma in the early Universe. So the Universe has undergone changes in the dominating energy component.

In the Friedmann equation these changes can be seen by looking at the scaling of the different components. The energy conservation equation (1.3c) implies that non-relativistic matter ($w = 0$) scales as $\varrho_m \propto a^{-3}$, whereas relativistic matter ($w = 1/3$) scales as $\varrho_r \propto a^{-4}$. Inserting this into the Friedmann equation (1.3a),

$$H^2 = H_0^2 \left(\Omega_r \left(\frac{a_0}{a}\right)^4 + \Omega_m \left(\frac{a_0}{a}\right)^3 + \Omega_k \left(\frac{a_0}{a}\right)^2 + \Omega_\Lambda \right) \, , \tag{1.5}$$

we see that for small $a(t)$ we find a radiation dominated era, followed by a matter dominated era, followed by a cosmological constant dominated era (as Ω_k seems to be zero). With the measured values (see table 3.1 from [41]) of the Ω-parameters (assuming $\Omega_k = 0$) of

$$\begin{aligned} \Omega_r &= 4.15 \times 10^{-5} h^{-2} \;\; ; \;\; \Omega_m = 0.272 \pm 0.015 \;\; ; \\ \Omega_\Lambda &= 0.725 \pm 0.016 \;\; ; \;\; H_0 = 70.2 \pm 1.4 \; km/s/Mpc \, , \end{aligned} \tag{1.6}$$

we find that matter radiation equality was at $a_{eq}^{-1} \approx 3200$ and that the equality of $\Omega_\Lambda(t)$ and $\Omega_m(t)$ occurs at $a_{\Lambda m}^{-1} \approx 1.39$.

Besides these transitions, in the very early Universe there have been a number of phase transitions in the particle physics sector (see e.g. [42] for a review). The hot and dense initial state allowed the creation of particles that are instable and therefore only appear if they can be constantly reproduced by a thermal bath. Figure 1.1 shows a sketch of the evolution of the Universe including these early stages.

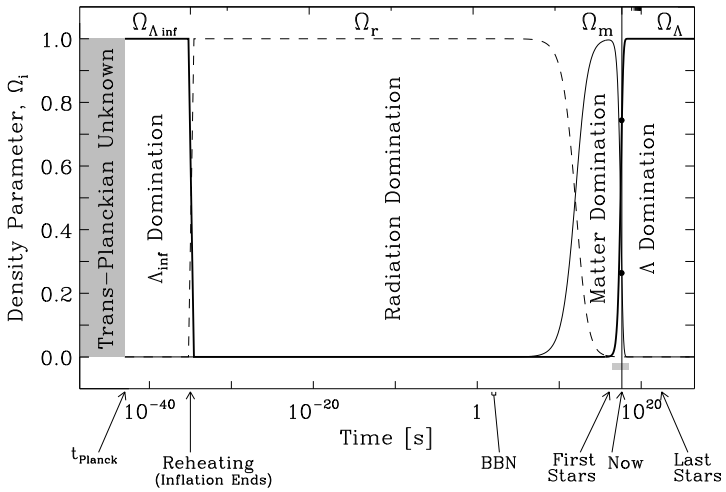

Figure 1.2. Cosmic expansion history. Most of the time the evolution is well described by taking into account the dominant energy contribution. These contributions were the inflaton energy density, the primordial radiation density, the matter density of non-relativistic matter and more recently the energy density of the cosmological constant. The plot also illustrates that we seem to live at a very special instant in time, namely at the transition from the matter dominated phase to the cosmological constant dominated phase. Picture form [43].

Even before this epoch of high energy standard model particle physics, Figure 1.1 shows an era called cosmological inflation. In this era, a yet unknown mechanism is believed to have led to an exponential growth of the scale factor $a(t)$. This period of exponential expansion has been introduced to solve a number of problems of Big Bang cosmology like the horizon problem, the flatness problem or the monopole problem, but provides also an explanation for the origin of structure as we will see in Sec. 2.3.

The complete picture of evolution of the scale-factor $a(t)$ is therefore the following: After an unknown pre-inflationary phase, it grew exponentially during inflation, then as $a \propto t^{1/2}$ during another radiation dominated phase, switching to $a \propto t^{2/3}$ in the matter dominated phase. Finally with the cosmological constant taking over, it seems that we are heading towards another period of exponential growth of $a(t)$. All epochs are shown in Fig. 1.2. We will inspect below, how each of these epochs contributed to the formation of the structures that we see today.

2. The theory of structure formation

Sec. 1.1.2 described the standard picture of the homogeneous evolution of the matter content of the Universe. In this chapter we turn to the more interesting task of characterizing and explaining the formation of structures in the Universe. To this end, Sec. 2.1 and 2.2 collect the basic formalism that is frequently used in this domain. Sec. 2.3 derives with the cold dark matter (CDM) power spectrum the main ingredient for the calculations in the following chapters. Sec. 2.1 is based on the chapters 2 and 3 of [44], whereas sections 2.2 and 2.3 closely follow the presentation in chapters 5 and 6 of [45].

2.1. Methods for characterizing structure

In Sec. 1.1.2 the matter content of the Universe was assumed to be a homogeneous perfect fluid characterized by one number only, its constant energy density ϱ_0. Even if in the real Universe galaxies and stars are rather discrete objects than continuous fluids, at least the expected underlying dark matter background should be well described by a perfect fluid picture. In addition, on the large scales we are mostly considering, also the distribution of galaxies may be treated as a dust fluid with the galaxies as individual fluid particles. We will derive the equations governing the evolution of those fluids in Sec. 2.2. Here, we will introduce the statistical tools used to describe the initial state and to characterize the distribution today.

In this statistical picture, the matter density field of the Universe $\varrho(\mathbf{x})$ is taken to be one realization of a continuous stationary stochastic process (SSP) $\hat{\varrho}(\mathbf{x})$. Its properties are determined by a probability density functional $\mathcal{P}[\varrho(\mathbf{x})]$, which may be seen as the joint probability function of the random variable $\hat{\varrho}(\mathbf{x})$. The condition of stationarity of the process means that it is invariant under translations of the position $\mathbf{x}$, i.e. the statistical properties of $\hat{\varrho}(\mathbf{x})$ are independent of $\mathbf{x}$. The assumption of stationarity is in the cosmological context motivated by the Copernican Principle. There should not be a preferred location in the Universe, so the statistical distribution of its matter content should be translationally invariant.

The properties of the discrete galaxy samples can be modeled by a stochastic point process (SPP). It can be seen as the discretization of the continuous distribution $\varrho(\mathbf{x})$ by partitioning the space into infinitesimal volumes $\mathrm{d}V$. The mass density $\varrho(\mathbf{x}_i)\,\mathrm{d}V = m_i$ can then be modeled by a sum of delta functions

$$\varrho(\mathbf{x}) = \sum_i m_i \delta(\mathbf{x} - \mathbf{x}_i) \ . \tag{2.1}$$

To determine the statistical properties of $\hat{\varrho}(\mathbf{x})$ we need to take ensemble averages $\overline{O}$ (also sometimes written as $\mathbb{E}[O]$ in the following). In the case of the Universe this is unfortunately impossible as we have only one realization of the density field. Therefore we have to assume that the underlying stationary process is ergodic. This means that for a generic observable $O = O(\varrho(\mathbf{x}_1), \varrho(\mathbf{x}_2), \dots)$ the ensemble average $\overline{O}$ may be calculated by a volume average over the whole density field

$$\overline{O} = \lim_{V\to\infty} \frac{1}{V} \int \mathrm{d}^3\mathbf{x}_0 O(\varrho(\mathbf{x}_1 + \mathbf{x}_0), \varrho(\mathbf{x}_2 + \mathbf{x}_0), \dots) \ . \tag{2.2}$$

In real observations we can of course not extend the volume to infinity, so Eq. (2.2) gives only an estimator for the true ensemble average. Therefore we have to ensure that the volume is large enough, if we want to make statements about the underlying stochastic process. Otherwise finite volume effects occur that may lead to misinterpretations of the data, as we will see in Sec. 3.1.

2.1.1. Correlation functions

The most important tool for the description of the statistical properties of the matter distribution of the Universe is the two-point correlation function and its Fourier transform, the power spectrum. The general *complete* ℓ-point correlation function is defined as the ensemble average

$$\overline{\hat{\varrho}(\mathbf{x}_1)\,\hat{\varrho}(\mathbf{x}_2)\dots\hat{\varrho}(\mathbf{x}_\ell)} \ . \tag{2.3}$$

For the stationary case that we are considering, these functions only depend on the relative distances $\mathbf{x}_{ij} = \mathbf{x}_i - \mathbf{x}_j$, but not on the absolute position.

More important than the complete correlation functions above are the reduced or connected correlation functions

$$C_2(\mathbf{x}_{12}) = \overline{(\hat{\varrho}(\mathbf{x}_1) - \varrho_0)(\hat{\varrho}(\mathbf{x}_2) - \varrho_0)} \ , \tag{2.4}$$

$$C_3(\mathbf{x}_{12}, \mathbf{x}_{13}, \mathbf{x}_{23}) = \overline{(\hat{\varrho}(\mathbf{x}_1) - \varrho_0)(\hat{\varrho}(\mathbf{x}_2) - \varrho_0)(\hat{\varrho}(\mathbf{x}_3) - \varrho_0)} \ . \tag{2.5}$$

For a nonzero average density $\overline{\hat{\varrho}(\mathbf{x})} = \varrho_0$ they are mainly used in dimensionless form

$$\tilde{\xi}(\mathbf{x}_{12}) = \frac{C_2(\mathbf{x}_{12})}{\varrho_0^2} = \overline{\hat{\delta}(\mathbf{x}_1)\,\hat{\delta}(\mathbf{x}_2)} \ , \tag{2.6}$$

$$\tilde{\zeta}(\mathbf{x}_{12}, \mathbf{x}_{13}, \mathbf{x}_{23}) = \frac{C_3(\mathbf{x}_{12}, \mathbf{x}_{13}, \mathbf{x}_{23})}{\varrho_0^3} = \overline{\hat{\delta}(\mathbf{x}_1)\,\hat{\delta}(\mathbf{x}_2)\,\hat{\delta}(\mathbf{x}_3)} \ , \tag{2.7}$$

where the dimensionless density contrast $\hat{\delta}(\mathbf{x})$ is defined as $\hat{\delta}(\mathbf{x}_1) = (\hat{\varrho}(\mathbf{x}_1) - \varrho_0)/\varrho_0$.

Cumulants For higher order connected correlation functions the correspondence to the central moments of the distribution is no longer so straightforward as in Eq. (2.4)-(2.5).

We rather have to introduce the joint cumulant generating function for the random variables $X_1, \ldots, X_n$

$$g(t_1, t_2, \ldots, t_n) = \log\left(\mathbb{E}\left[\exp\left(\sum_{j=1}^{n} t_j X_j\right)\right]\right) \ . \tag{2.8}$$

To extract the cumulants from this generating function one has to evaluate their derivatives at $\mathbf{t} = \{t_1, \ldots, t_n\} = \vec{0}$

$$\kappa_n = \partial_{t_1} \ldots \partial_{t_n} g(t_1, t_2, \ldots, t_n)|_{\mathbf{t}=0} \ , \tag{2.9}$$

which leads to the expression[1]

$$\kappa(X_1, \ldots, X_n) = \sum_{\pi}(|\pi| - 1)!(-1)^{|\pi|-1} \prod_{B\in\pi} \mathbb{E}\left[\prod_{i\in B} X_i\right] \tag{2.10}$$

for the joint cumulants in terms of the moments or complete correlation functions. Here, π runs through all partitions of $\{1, \ldots, n\}$, B runs through the list of all blocks of the partition π and $|\pi|$ is the number of parts in the partition. For the first three cumulants we find again the values from above, if we take $X_i = \hat{\varrho}(\mathbf{x}_i)/\varrho_0$

$$\begin{aligned} \kappa(\hat{\varrho}(\mathbf{x}_1)) &= 0!(-1)^0 \mathbb{E}[\hat{\varrho}(\mathbf{x}_1)] = \varrho_0 \ , \\ \kappa(X_1, X_2) &= 1!(-1)^1 \mathbb{E}[X_1]\,\mathbb{E}[X_2] + 0!\,(-1)^0\,\mathbb{E}[X_1 X_2] = \tilde{\xi}(\mathbf{x}_{12}) \ , \\ \kappa(X_1, X_2, X_3) &= \tilde{\zeta}(\mathbf{x}_{12}, \mathbf{x}_{13}, \mathbf{x}_{23}) \ , \end{aligned} \tag{2.11}$$

but for the fourth cumulant we find for example

$$\begin{aligned} \kappa(X_1, X_2, X_3, X_4) &= \overline{\hat{\delta}(\mathbf{x}_1)\,\hat{\delta}(\mathbf{x}_2)\,\hat{\delta}(\mathbf{x}_3)\,\hat{\delta}(\mathbf{x}_4)} - \tilde{\xi}(\mathbf{x}_{12})\,\tilde{\xi}(\mathbf{x}_{34}) \\ &\quad -\tilde{\xi}(\mathbf{x}_{13})\,\tilde{\xi}(\mathbf{x}_{24}) - \tilde{\xi}(\mathbf{x}_{14})\,\tilde{\xi}(\mathbf{x}_{23}) \ . \end{aligned} \tag{2.12}$$

We will need these cumulants, also known as connected correlation functions, in Sec. 3.2.

Power spectrum A description of the clustering properties of over-densities that is complementary to the one by its two-point correlation properties is given by the power spectrum. It may be defined as the Fourier transformation of the two-point correlation function

$$P(\mathbf{k}) = \int d^3 r \tilde{\xi}(\mathbf{r})\, e^{-i\mathbf{k}\cdot\mathbf{r}} \ . \tag{2.13}$$

By this definition it is directly related to the Fourier modes of the over-density field. If $\delta_\varrho(\mathbf{r}) = (\varrho(\mathbf{r}) - \varrho_0)/\varrho_0$, these Fourier modes are

$$\tilde{\delta}_\varrho(\mathbf{k}, V) = \int_V d^3 r \delta_\varrho(\mathbf{r})\, e^{-i\mathbf{k}\cdot\mathbf{r}} \ . \tag{2.14}$$

[1] See Wikipedia https://en.wikipedia.org/wiki/Cumulant in the version of 16.07.2012

The power spectrum (2.13) of the distribution of over-densities $\delta_\varrho(\mathbf{r})$ is then given by the ensemble average

$$P(\mathbf{k}) = \lim_{V\to\infty} \frac{\mathbb{E}\left[\left|\tilde{\delta}_\varrho(\mathbf{k}, V)\right|^2\right]}{V} . \tag{2.15}$$

The power spectrum is useful, because, as we will see in Sec. 2.3, it is this quantity that theories of structure formation in the early Universe naturally work with.

Variance of the density field Another important quantity that is closely related to the power spectrum and the correlation function are the matter fluctuations in a sphere of radius R. They are defined as the variance of the density field by

$$\sigma^2(R) = \frac{\mathbb{E}\left[M(R)^2\right] - \mathbb{E}\left[M(R)\right]^2}{\mathbb{E}\left[M(R)\right]^2} , \tag{2.16}$$

where $M(R)$ is the mass contained in a sphere of radius R and therefore

$$\mathbb{E}\left[M(R)\right] = \int_{\mathcal{B}(R)} d^3r \mathbb{E}\left[\hat{\varrho}(\mathbf{r})\right] = \frac{4\pi}{3}\varrho_0 R^3 \tag{2.17}$$

and

$$\mathbb{E}\left[M(R)^2\right] = \int_{\mathcal{B}(R)} d^3r_1 \int_{\mathcal{B}(R)} d^3r_2 \mathbb{E}\left[\hat{\varrho}(\mathbf{r}_1)\,\hat{\varrho}(\mathbf{r}_2)\right] , \tag{2.18}$$

where $\mathcal{B}(R)$ is the boundary of a ball of radius R. This means that it is related to the correlation function as

$$\sigma^2(R) = \frac{1}{\left(\frac{4\pi}{3}R^3\right)^2} \int_{\mathcal{B}(R)} d^3r_1 \int_{\mathcal{B}(R)} d^3r_2 \tilde{\xi}\left(|\mathbf{r}_1 - \mathbf{r}_2|\right) . \tag{2.19}$$

When passing to Fourier space we can also determine its expression in terms of the power spectrum. The window function of a ball of radius R, also known as the top hat window function,

$$W_{\mathcal{B}(R)}(\mathbf{r}) = \begin{cases} \left(\frac{4\pi}{3}R^3\right)^{-1} & R - |\mathbf{r}| > 0 \\ 0 & \text{else} \end{cases} \tag{2.20}$$

looks in Fourier space like

$$\widetilde{W}_{\mathcal{B}(R)}(\mathbf{k}) = \int d^3r W_{\mathcal{B}(R)}(\mathbf{r})\, e^{-i\mathbf{k}\cdot\mathbf{r}} = \frac{3\left(\sin kR - kR\cos kR\right)}{(kR)^3} \tag{2.21}$$

and with the relation (2.13) this means for σ

$$\sigma^2(R) = \frac{1}{(2\pi)^3} \int d^3k P(\mathbf{k}) \left|\widetilde{W}_{\mathcal{B}(R)}(k)\right|^2 . \tag{2.22}$$

The dependence of σ on the shape of the power spectrum may be found explicitly for the simple class of models that where $P(\mathbf{k})$ simply scales as $P(\mathbf{k}) \propto k^n$. When non-relativistic matter dominates the evolution, the power spectrum of perturbations grows with the scale factor as $\propto a^2$. So for spectra of the form $P(k) = A(a/a_0)^2 k^n$ one finds

$$\sigma^2(R) \propto a^2 R^{-3-n} \tag{2.23}$$

in the range of $-3 < n < 1$. This leads to an interesting effect for the $n = 1$ spectrum for the matter fluctuations on scales of the (particle) horizon. This horizon is in comoving coordinates determined by

$$R_H(t) = \eta(t) = \int \frac{dt}{a(t)} \propto a^{1/2} , \tag{2.24}$$

where the $a^{1/2}$ behavior holds for the matter dominated era. Using this in Eq. (2.23) gives

$$\sigma^2(R_H(t)) \propto a^{2-\frac{3+n}{2}} , \tag{2.25}$$

so in the limit of $n \to 1$, the spectrum becomes scale invariant in the sense that

$$\sigma^2(R = R_H(t)) = \text{const.} \tag{2.26}$$

and therefore the perturbations on the horizon scale are independent of the actual size of that scale.

Gaussian distribution Gaussian matter distributions are important in cosmology, because the initial fluctuations seem to have been Gaussian to a high degree of accuracy. In the discretized picture where we describe the continuous field by its average value in small cells ΔV

$$\varrho(\mathbf{r}_i; \Delta V) = \frac{1}{\Delta V} \int_{\Delta V(\mathbf{r}_i)} \mathrm{d}^3 r \hat{\varrho}(\mathbf{r}) , \tag{2.27}$$

we can think of the field being Gaussian if the probability of a realization $\{\varrho(\mathbf{r}_i; \Delta V)\}$ is given by the joint probability density function

$$p(\{\varrho(\mathbf{r}_i; \Delta V)\}) = B e^{-\frac{1}{2}\sum_{i,j}(\varrho(\mathbf{r}_i;\Delta V)-m_i)A_{ij}(\varrho(\mathbf{r}_j;\Delta V)-m_j)} . \tag{2.28}$$

The values m_i give the average density in the i-th cell and the matrix A is related to the two-point correlation function by $A = C^{-1}$ with C defined as

$$C_{ij} = \varrho_0^2 \tilde{\xi}(\mathbf{r}_i, \mathbf{r}_j) . \tag{2.29}$$

The probability density functional for the continuous case is then obtained by formally sending $\Delta V \to 0$. This gives

$$\mathcal{P}[\varrho(\mathbf{r})] \propto e^{-\frac{1}{2}\int_V \int_V \mathrm{d}^3 r \mathrm{d}^3 r' (\varrho(\mathbf{r})-m(\mathbf{r}))K(\mathbf{r},\mathbf{r}')(\varrho(\mathbf{r}')-m(\mathbf{r}'))} , \tag{2.30}$$

where the correlation kernel is

$$K(\mathbf{r},\mathbf{r}') = \lim_{\Delta V\to 0} \frac{A_{ij}}{\Delta V^2} \ . \tag{2.31}$$

As the stochastic processes we consider are stationary $K(\mathbf{r},\mathbf{r}')$ only depends on the distance between the two points $K(\mathbf{r},\mathbf{r}') = K(\mathbf{r}-\mathbf{r}')$. This correlation kernel is then directly related to the power spectrum of the Gaussian process. With the Fourier transform $\tilde{K}(\mathbf{k}) = FT[K(\mathbf{r})]$, P becomes

$$P(\mathbf{k}) = \frac{1}{\varrho_0^2 \tilde{K}(\mathbf{k})} \ . \tag{2.32}$$

One important property of Gaussian fields is that all the cumulants defined by Eq. (2.10) for $n > 2$ vanish. This leads to Wicks theorem saying that all the central moments of the Gaussian distribution are given by products of the two-point correlation function. This implies that all odd central moments vanish as well. So a Gaussian process is completely characterized by the two-point correlations.

2.1.2. Minkowski functionals

Another tool for the characterization of structure are Minkowski functionals, introduced into cosmology in [46]. They are important quantities of integral geometry and defined as additive translational invariant functionals

$$V_\nu(A) \ \propto \ \int \chi(A\cap E^\nu)\, d\mu(E^\nu) \ , \tag{2.33}$$

$$V_d(A) \ = \ \chi(A) \ , \tag{2.34}$$

where A is a convex body. E^ν is a ν-dimensional hypersurface in a d-dimensional Euclidean space. χ is the Euler characteristic of A, defined as

$$\chi(A) = \begin{cases} 1 & A \text{ convex } A \neq \emptyset \\ 0 & A = \emptyset \ . \end{cases} \tag{2.35}$$

The definition (2.33) is strictly valid for a *single* convex body A only, but may be generalized to *a set* of convex bodies by defining the additivity relation for the Euler characteristic

$$\chi(A\cup B) = \chi(A) + \chi(B) - \chi(A\cap B) \ . \tag{2.36}$$

It can then be shown [47], that the Minkowski functionals form a basis of all possible additive, translation invariant measures in the sense that all these measures may be written as a linear combination of the $d+1$ Minkowski functionals possible in d dimensions.

In the case of three dimensions, the integrals (2.33) have a simple interpretation: V_0 is proportional to the volume V of the convex body, V_1 is proportional to its surface

S, and V_2 is proportional to the integrated mean curvature H. The fourth functional V_3 (Eq. (2.34)) is the Euler characteristic. In three dimensions, when applied to a set of intersecting convex bodies using Eq. (2.36), it gives the sum of isolated components K, plus the sum of cavities C, minus the holes R: $\chi = K + C - R$. This means that for a filled ball $\chi = 1$, for a torus $\chi = 0$ and for a double torus (having the form of the number 8) $\chi = -1$. More explicitly, the relations between the functionals V_ν and their more familiar geometric counterparts are

$$V_0 = V \;\; ; \;\; V_1 = \frac{S}{6} \;\; ; \;\; V_2 = \frac{H}{3\pi} \;\; ; \;\; V_3 = \chi \; . \tag{2.37}$$

Boolean Grain Model To use these Minkowski functionals for the characterization of cosmic structure, one has to specify to which objects we want to apply the above formulae. The data we have is mainly in the form of catalogs of point sources. The integral geometric properties of a set of points, however, are trivial. We have to smooth the points in a way that gives rise to extended bodies that have a well defined volume, surface and curvature.

There are several possibilities to achieve this. One would be to smooth out the point distribution on some given scale, to arrive at a smooth density field. Then, the structures could be identified by connecting all those regions that have an average density higher than a given threshold. Thus, these regions form an excursion set, that has a more interesting morphology than the mere collection of points. This approach has been used for SDSS data in the past in [48].

Here, we want to work with a different scheme, which is called the boolean grain model and has been used for other surveys [49, 50]. To arrive at a set of convex bodies, we decorate every object in a galaxy survey by a sphere of radius R. Then we can calculate the Minkowski functionals of this set of spheres. The results are presented as a function of the radius of the spheres. The Minkowski functionals of the spheres themselves are quite simple. Using (2.37) gives

$$V_0 = \frac{4\pi}{3}R^3 \;\; ; \;\; V_1 = \frac{2}{3}\pi R^2 \;\; ; \;\; V_2 = \frac{4}{3}R \;\; ; \;\; V_3 = 1 \; . \tag{2.38}$$

When combined to a set of balls around the galaxy positions, the R dependence becomes more interesting. In this case one mainly considers the average Minkowski functional densities v_μ. These are the mean values of the functionals per unit volume. It has been shown in [51], that these densities for the boolean grain model may be expressed analytically as

$$\begin{aligned}
v_0 &= 1 - e^{-\varrho_0 \overline{V}_0} \\
v_1 &= \varrho_0 \overline{V}_1 e^{-\varrho_0 \overline{V}_0} \; , \\
v_2 &= \left(\varrho_0 \overline{V}_2 - \frac{3\pi}{8} \varrho_0^2 \overline{V}_1^2 \right) e^{-\varrho_0 \overline{V}_0} \; , \\
v_3 &= \left(\varrho_0 \overline{V}_3 - \frac{9}{2} \varrho_0^2 \overline{V}_1 \overline{V}_2 + \frac{9\pi}{16} \varrho_0^3 \overline{V}_1^3 \right) e^{-\varrho_0 \overline{V}_0} \; ,
\end{aligned} \tag{2.39}$$

where ϱ_0 is the average number density of the galaxy sample, and $\overline{V}_0 - \overline{V}_3$ are the modified Minkowski functionals of the collection of balls given by

$$\overline{V}_\mu = V_\mu(B) + \sum_{n=1}^{\infty} \frac{(-\varrho_0)^n}{(n+1)!} \int_{\mathcal{D}} \mathrm{d}^3x_1 \ldots \mathrm{d}^3x_n \xi_{n+1}(0, \mathbf{x}_1, \ldots \mathbf{x}_n) V_\mu(B \cap B_{\mathbf{x}_1} \cap \cdots \cap B_{\mathbf{x}_n}) \ . \tag{2.40}$$

Here, $\xi_{n+1}(0, \mathbf{x}_1, \ldots \mathbf{x}_n)$ is the connected $n+1$-point correlation function, i.e. the joint cumulants (2.10) of the distribution of galaxies. For a Poisson distribution the non-diagonal part of all connected n-point correlation functions κ_n with $n \geq 2$ vanish. So the $\overline{V}_\mu$'s simply reduce to the standard Minkowski functionals V_μ of a ball (2.38). In this case the Minkowski functional density of the galaxy distribution is therefore known analytically.

The relations (2.39) and (2.40) are very interesting, because they connect the Minkowski functional densities, that may be measured directly from the galaxy surveys, with a series containing all higher order correlation functions. In this way the Minkowski functionals represent a tool for the characterization of structure, that is complementary to the usual methods of measuring only the low order statistics like the correlation function. In Sec. 3.2 we will see what this allows us to learn about the galaxy distribution in the Universe.

2.2. Cosmological perturbation theory

To describe structure in the Universe, the usual approach is to use perturbation theory. It is starting from the assumption described in Sec. 1.1.1, that the average evolution is obtained by using a homogeneous matter source in the Einstein equations (1.1). To add structure to this homogeneous soup, we will assume that the deviations in the energy density may be described by small perturbations of this average. We will see how this produces, even at first order, a set of equations that is much more complicated than the background evolution, described by the Friedmann equations (1.3a)–(1.3c). This section follows closely chapter 5 of [45].

2.2.1. First order perturbations

The split of the metric into a homogeneous background and a position dependent perturbation, may be written in the form

$$g_{\mu\nu} = \bar{g}_{\mu\nu} + h_{\mu\nu} \ , \tag{2.41}$$

where $\bar{g}_{\mu\nu}$ is the background metric and $h_{\mu\nu}$ the small perturbation. In this work, $\bar{g}_{\mu\nu}$ will always be the flat Robertson-Walker metric (1.2), i.e. $\bar{g}_{00} = -1$ and $\bar{g}_{ij} = a^2(t)\,\delta_{ij}$. The space-time perturbation tensor $h_{\mu\nu}$ may be decomposed into a scalar, a vectorial

and a tensorial component. These will be written as[2]

$$h_{00} = -E \;\; ; \;\; h_{i0} = a\left[\partial_i F + G_i\right] \;, \tag{2.42}$$

$$h_{ij} = a^2\left[A\delta_{ij} + \partial_i\partial_j B + 2\partial_{(i}C_{j)} + D_{ij}\right] \;. \tag{2.43}$$

The components of the perturbations are therefore the four scalars functions A, B, E and F, the two divergence free three-vectors C_i and G_i, and the traceless, divergence free spatial tensor D_{ij}.[3]

Analogously, also the energy-momentum tensor on the right hand side of (1.1) is decomposed into the homogeneous background and a perturbation

$$T^{full}_{\mu\nu} = T_{\mu\nu} + \delta T_{\mu\nu} \;. \tag{2.44}$$

The homogeneous part is again the perfect fluid energy momentum tensor

$$T_{\mu\nu} = \bar{p}\bar{g}_{\mu\nu} + \left(\bar{\varrho} + \bar{p}\right)\bar{u}_\mu\bar{u}_\nu \;, \tag{2.45}$$

where $\bar{u}^\mu\bar{u}_\mu = -1$ and $\bar{u}_i = 0$. The perturbations are then

$$\delta T_{00} = -\bar{\varrho}h_{00} + \delta\varrho \;\; ; \;\; \delta T_{i0} = \bar{p}h_{i0} - \left(\bar{\varrho} + \bar{p}\right)\left(\partial_i\delta u + \delta u^V_i\right) \;; \tag{2.46}$$

$$\delta T_{ij} = \bar{p}h_{ij} + a^2\left[\delta_{ij}\delta p + \partial_i\partial_j\pi^S + 2\partial_{(i}\pi^V_{j)} + \pi^T_{ij}\right] \;, \tag{2.47}$$

where these equations may be understood as the defining equations for the quantities $\delta\varrho$, δp, $\delta u_i = \partial_i u + \delta u^V_i$, and the anisotropic stress terms π^S, π^V and π^T that characterize the departure from the perfect fluid form of the energy momentum tensor.

Plugging these formulas into the Einstein equations (1.1) and evaluating them consistently at first order gives a set of nasty looking equations for the perturbations (and the Friedmann equations for the background). As we will not need them in their full generality we will only give them in a particular form, described in the next chapter. The reader who is interested in their full form may find them for example in Weinberg's book on cosmology [45].

2.2.2. Gauges and evolution equations

The equations that result from the perturbative ansatz made in the previous section, will not only contain physical degrees of freedom, but also some that are only related to general coordinate transformations of the unperturbed RW metric. These coordinate transformations may be described by four functions of x^μ and we may, therefore, choose our coordinates in a way that eliminates four components of the perturbations. Fixing the coordinate system in this way is called "choosing a gauge", because the coordinate

[2] The brackets in $\partial_{(i}C_{j)}$ denote symmetrization, i.e. $\partial_{(i}C_{j)} = \frac{1}{2}\left(\partial_i C_j + \partial_j C_i\right)$.
[3] Formally these conditions are $\partial^i C_i = \partial^i G_i = 0$ and $\partial^i D_{ij} = \delta^{ij} D_{ij} = 0$.

transformations may be written in a form that resembles gauge transformations in particle physics. The choice which gauge to use depends on the application. The desired physical quantities may take a simpler form in one gauge than another. The physical content however is the same as long as the perturbations are consistently truncated and there is no residual gauge freedom left. We will discuss two popular choices below.

In addition to using these formal freedom we will also employ two physical restrictions. Firstly, for our purpose it is sufficient to look at the scalar parts of the perturbations (2.42)-(2.43) and (2.46)-(2.47). Secondly, we will only be interested in fluids for which the anisotropic stress π^S vanishes. With these restrictions we may finally write down the sets of equations that determine the evolution of the structure in the Universe in the form of a linear perturbation of the background.

Synchronous gauge In synchronous gauge the coordinate system is chosen such that the scalar sector of the decomposition (2.42)-(2.43) is constrained by $E = 0$ and $F = 0$. This means for the metric that

$$g_{00} = -1 \quad , \quad g_{0i} = 0 \quad , \quad g_{ij} = a^2 \left[(1 + A)\, \delta_{ij} + \partial_i \partial_j B \right] \ . \tag{2.48}$$

So the gauge choice has eliminated the mixed space time components of the metric and the perturbation to the time component. This latter is the reason that the gauge is called synchronous. To simplify the equations we may finally combine the perturbations A and B in the quantity

$$\Psi := \frac{1}{2} \left[3\dot{A} + \nabla^2 \dot{B} \right] = \frac{\partial}{\partial t} \left(\frac{h_{ii}}{2a^2} \right) \ , \tag{2.49}$$

because it will be this combination that will occur in the equations for the fluid perturbations. Note that this potential is not completely gauge fixed by the conditions $E = 0$ and $F = 0$. There is still a gauge transformation left that preserves $E = 0$ and $F = 0$, but changes Ψ. In the late Universe, where we have the independently evolving dark matter component, one may fix this degeneracy by imposing the coordinates to be comoving with the dark matter fluid.

After these preparations the equation derived from (1.1) governing the evolution of the potential Ψ reads

$$\partial_t \left(a^2 \Psi \right) = -4\pi G a^2 \left(\delta\varrho + 3\delta p \right) \ . \tag{2.50}$$

To have a complete system of equations we may either combine other components of the Einstein equations (1.1) or replace them with the conservation equations of the fluid i.e. evaluating the expression $T^{\mu}_{\nu;\mu} = 0$. This leads to

$$\partial_i \left(\delta p + \partial_t \left[(\bar{\varrho} + \bar{p})\, \delta u \right] + 3\frac{\dot{a}}{a} (\bar{\varrho} + \bar{p})\, \delta u \right) = 0 \ , \tag{2.51}$$

$$\delta\dot{\varrho} + 3\frac{\dot{a}}{a} (\delta\varrho + \delta p) + \nabla^2 \left[a^{-2} (\bar{\varrho} + \bar{p})\, \delta u \right] + (\bar{\varrho} + \bar{p})\, \Psi = 0 \ . \tag{2.52}$$

After specification of an equation of state $p(\varrho) = 0$ for the fluid(s) these equations (2.50)-(2.52) form a closed system for the three independent variables $\delta\varrho$, δu and Ψ.

Conformal Newtonian gauge In this gauge we choose the coordinates such that $B = 0$ and $F = 0$ in the decomposition (2.42)-(2.43). This means for the metric if we call $A = -2\Psi$ and $E = 2\Phi$

$$g_{00} = -1 - 2\Phi \quad , \quad g_{0i} = 0 \quad , \quad g_{ij} = a^2\delta_{ij}\left(1 + 2\Psi\right) \ . \tag{2.53}$$

As we have chosen π^S to be zero some of the equations imply that $\Phi = \Psi$. This only remaining potential Ψ is in a certain limit similar to the Newtonian potential of classical gravity, which explains the name of the gauge. The equation for this potential is then

$$\partial_i\left[4\pi G\left(\bar{\varrho} + \bar{p}\right)\delta u + \partial_t\left(a\Psi\right)\right] = 0 \ . \tag{2.54}$$

Adding the energy momentum conservation equations for the perfect fluid to the system of equations, i.e. $T^{\mu}_{\nu;\mu} = 0$, we find

$$\partial_i\left(\delta p + \partial_t\left[\left(\bar{\varrho} + \bar{p}\right)\delta u\right] + 3\frac{\dot{a}}{a}\left(\bar{\varrho} + \bar{p}\right)\delta u + \left(\bar{\varrho} + \bar{p}\right)\Psi\right) \ = \ 0 \ , \tag{2.55}$$

$$\delta\dot{\varrho} + 3\frac{\dot{a}}{a}\left(\delta\varrho + \delta p\right) + \nabla^2\left[a^{-2}\left(\bar{\varrho} + \bar{p}\right)\delta u\right] - 3\left(\bar{\varrho} + \bar{p}\right)\Psi \ = \ 0 \ . \tag{2.56}$$

Assuming an equation of state $p\left(\varrho\right) = 0$, these equations (2.54)-(2.56) again give the evolution for the three independent variables $\delta\varrho$, δu and Ψ, but this time the remaining Einstein equations give an additional time independent constraint

$$a^3\delta\varrho - 3Ha^3\left(\bar{\varrho} + \bar{p}\right)\delta u - \left(\frac{a}{4\pi G}\right)\nabla^2\Psi = 0 \ . \tag{2.57}$$

Gauge invariance and conservation The problem of the gauge dependence can also be evaded by using gauge invariant variables. The concept has been introduced into cosmological perturbation theory by Bardeen [52] and is besides gauge fixing the other way of treating the problem of spurious degrees of freedom.

An important gauge invariant quantity is the curvature perturbation $\mathcal{R}_q$ that can be expressed in terms of synchronous gauge quantities as

$$q^2\mathcal{R}_q = -a^2H\Psi_q + 4\pi Ga^2\delta\varrho_q + q^2H\delta u_q \ , \tag{2.58}$$

where we have introduced the Fourier components of the potential, the over-density field and the velocity field. So the equation holds for all wavenumbers q.

In addition to being gauge invariant, $\mathcal{R}_q$ has the advantage to be conserved outside the Hubble radius i.e. for modes for which $q/a \ll H$. This property will prove useful in Sec. 2.3.1 when we try to make contact to inflationary perturbations.

2.2.3. Statistical nature of the perturbations

The equations for the perturbations of the cosmic fluid derived in the previous section only give us their evolution with cosmic time. To arrive at the full solution we have to specify appropriate initial conditions. This is a problem in cosmology as the initial conditions are not known. But even if they were, for many applications we would not be interested in all positions of over- or under-densities, but rather in the underlying statistical distribution. To learn something about this distribution it is useful to go to Fourier space. As the background with respect to which we defined the perturbations is translationally invariant, we may expand the solutions for the perturbations into plane waves. For two perturbations A and B this leads to

$$\begin{aligned} A(\mathbf{x},t) &= \sum_n \int \mathrm{d}^3 q \alpha_n(\mathbf{q}) A_{nq}(t) e^{i\mathbf{q}\mathbf{x}} , \\ B(\mathbf{x},t) &= \sum_n \int \mathrm{d}^3 q \alpha_n(\mathbf{q}) B_{nq}(t) e^{i\mathbf{q}\mathbf{x}} , \end{aligned} \tag{2.59}$$

where n runs over the number of independent solutions of the perturbative equations presented in Sec. 2.2.2. The fact that these equations, if transformed to Fourier space, only depend on $\mathbf{q}^2$, shows that their solutions are independent of direction. All directional information is therefore encoded in the initial conditions $\alpha_n(\mathbf{q})$. As the equations are linear, the α_n may be chosen to be the same for all perturbations.

Under the assumption that the perturbations are Gaussian, which will prove to be a good approximation for the cosmological context we are considering, all statistical information is contained in bilinear averages of the form

$$\langle A(\mathbf{x},t) B(\mathbf{y},t)\rangle = \sum_{nm} \int \mathrm{d}^3 q \int \mathrm{d}^3 q' A_{nq}(t) B^\star_{mq'}(t) \langle \alpha_n(\mathbf{q}) \alpha^\star_m(\mathbf{q}')\rangle e^{i(\mathbf{q}\mathbf{x}-\mathbf{q}'\mathbf{y})} \tag{2.60}$$

where the average $\langle \dots \rangle$ is an ensemble average over all possible initial conditions. When we assume that the underlying probability distribution of the initial conditions is translationally invariant, $\langle \alpha_n(\mathbf{q}) \alpha^\star_m(\mathbf{q}')\rangle$ may depend on $\mathbf{q}-\mathbf{q}'$ only. If the distribution is also rotationally invariant we have $\langle \alpha_n(\mathbf{q}) \alpha^\star_m(\mathbf{q}')\rangle = M_{nm}(q)\delta^3(\mathbf{q}-\mathbf{q}')$, with a matrix M depending on $|\mathbf{q}|$ only. With the choice of the adapted basis of functions for α_n and A_{nq} we can assure that M is simply δ_{nm}. Then we have

$$\langle \alpha_n(\mathbf{q}) \alpha^\star_m(\mathbf{q}')\rangle = \delta_{nm}\delta^3(\mathbf{q}-\mathbf{q}') , \tag{2.61}$$

which means that in this basis, the different solutions for a particular mode q do not couple. For the ensemble average we then have

$$\langle A(\mathbf{x},t) B(\mathbf{y},t)\rangle = \sum_n \int \mathrm{d}^3 q A_{nq}(t) B^\star_{nq}(t) e^{i\mathbf{q}(\mathbf{x}-\mathbf{y})} . \tag{2.62}$$

The assumption of a rotationally and translationally symmetric probability distribution has simplified the equation considerably.

A particularly important case is when we take $A = B = \delta\varrho$. This results in

$$\langle \delta\varrho\left(\mathbf{x},t\right)\delta\varrho\left(\mathbf{y},t\right)\rangle = \sum_n \int \mathrm{d}^3q \left|\delta\varrho_{nq}\left(t\right)\right|^2 e^{i\mathbf{q}(\mathbf{x}-\mathbf{y})} \ . \tag{2.63}$$

This is the correlation function (2.6) of the over-density field $\delta\varrho$ and related via the Fourier transformation to the power spectrum $\left|\delta\varrho_{nq}\left(t\right)\right|^2$ of the statistical distribution of the field. It is this power spectrum that we will be interested in in the following, because it contains all the information about the density field under the well motivated assumption that it is initially a Gaussian field.

2.3. The origin of today's structure

After the introduction of the basic formalism to describe the evolution of structures in a dynamic space-time background, we will see in this section where these structures come from and how they were influenced by the various epochs of cosmic expansion described in Sec. 1.1.2. The presentation is summarizing the information of interest for us from chapters 10, 6 and 2.4 of [45].

2.3.1. The seeds of cosmic structure

The fundamental reason that we see structures in the Universe around us is nowadays believed to be the quantum fluctuations in the early Universe. The mechanism that links these random fluctuations on microscopic scales to the largest scales in the Universe is inflation, i.e. the exponential growth of the scale factor in an early epoch of the Universe. Although inflation was originally introduced to solve other problems like the horizon or the flatness problem, its most remarkable achievement is, that it predicts the correct form of the perturbation spectrum that we see in the CMB. Because this occurrence is so impressive, we here want to have a closer look on the way that this result emerges.

The most popular models that are used to describe the inflationary phase are models with a scalar field that is slowly rolling down its potential. The Lagrangian of such a field in a general relativistic background, described by the metric $g_{\mu\nu}$, is given by

$$\mathcal{L} = \int d^4x\sqrt{-\det\left(g\right)}\left[-\frac{1}{2}g^{\mu\nu}\frac{\partial\varphi}{\partial x^\mu}\frac{\partial\varphi}{\partial x^\nu} - V\left(\varphi\right)\right] \ . \tag{2.64}$$

This field consists of a homogeneous background and its perturbation

$$\varphi\left(\mathbf{x},t\right) = \bar{\varphi}\left(t\right) + \delta\varphi\left(\mathbf{x},t\right) \ . \tag{2.65}$$

Working in conformal Newtonian gauge the perturbed metric is

$$ds^2 = \left(-1-2\Psi\right)\mathrm{d}t^2 + a^2\left(t\right)\left(1-2\Psi\right)\delta_{ij}\mathrm{d}x^i\mathrm{d}x^j \ . \tag{2.66}$$

Plugging the scalar source and the perturbed metric in the Einstein equations (1.1) first yields the Friedmann equations for the background

$$H^2 = \frac{8\pi G}{3}\left(\frac{1}{2}\dot{\bar{\varphi}}^2 + V\left(\bar{\varphi}\right)\right) \tag{2.67}$$

$$\dot{H} = -4\pi G\dot{\bar{\varphi}}^2 \tag{2.68}$$

and gives the equations for the perturbations

$$\dot{\Psi} + H\Psi = 4\pi G\dot{\bar{\varphi}}\delta\varphi\,, \tag{2.69}$$

$$\delta\ddot{\varphi} + 3H\delta\dot{\varphi} + \frac{\partial^2 V\left(\bar{\varphi}\right)}{\partial\bar{\varphi}^2}\delta\varphi - \left(\frac{\nabla^2}{a^2}\right)\delta\varphi = -2\Psi\frac{\partial V\left(\bar{\varphi}\right)}{\partial\bar{\varphi}} + 4\dot{\Psi}\dot{\bar{\varphi}}\,, \tag{2.70}$$

$$\left(\dot{H} - \frac{\nabla^2}{a^2}\right)\Psi = 4\pi G\left(-\dot{\bar{\varphi}}\delta\dot{\varphi} + \ddot{\bar{\varphi}}\delta\varphi\right)\,. \tag{2.71}$$

Using the definitions (2.59) to pass to momentum space

$$\delta\varphi\left(\mathbf{x},t\right) = \int d^3q\left[\delta\varphi_q\left(t\right)\alpha\left(\mathbf{q}\right)e^{i\mathbf{qx}} + \delta\varphi_q^\star\left(t\right)\alpha^\star\left(\mathbf{q}\right)e^{-i\mathbf{qx}}\right]\,, \tag{2.72}$$

$$\Psi\left(\mathbf{x},t\right) = \int d^3q\left[\Psi_q\left(t\right)\alpha\left(\mathbf{q}\right)e^{i\mathbf{qx}} + \Psi_q^\star\left(t\right)\alpha^\star\left(\mathbf{q}\right)e^{-i\mathbf{qx}}\right]\,, \tag{2.73}$$

we could solve the emerging equations for the time evolution of the perturbations $\delta\varphi_q\left(t\right)$, $\Psi_q\left(t\right)$. However, we are only interested in the quantity

$$\mathcal{R} = -\Psi + H\delta u\,, \tag{2.74}$$

that is constant outside of the Hubble radius for the growing mode. It can be written in terms of the creation and annihilation operators $\alpha\left(\mathbf{q}\right)$ and $\alpha^\star\left(\mathbf{q}\right)$ as

$$\mathcal{R}\left(\mathbf{x},t\right) = \int d^3q\left[\mathcal{R}_q\left(t\right)\alpha\left(\mathbf{q}\right)e^{i\mathbf{qx}} + \mathcal{R}_q^\star\left(t\right)\alpha^\star\left(\mathbf{q}\right)e^{-i\mathbf{qx}}\right]\,, \tag{2.75}$$

where of course

$$\mathcal{R}_q = -\Psi_q - H\frac{\delta\varphi_q}{\dot{\bar{\varphi}}}\,. \tag{2.76}$$

The operators α fulfill the canonical commutation relation $\left[\alpha,\alpha^\dagger\right] = 1$. The vacuum expectation value of $\mathcal{R}_q$, that represents the quantum fluctuations, is then

$$\left\langle 0\right|\mathcal{R}\left(\mathbf{x},t\right)\mathcal{R}\left(\mathbf{y},t\right)\left|0\right\rangle = \int d^3q e^{i\mathbf{q}\left(\mathbf{x}-\mathbf{y}\right)}\left|\mathcal{R}_q\left(t\right)\right|^2\,. \tag{2.77}$$

To characterize the curvature fluctuations $\mathcal{R}$ we therefore need to determine its power spectrum $\left|\mathcal{R}_q\left(t\right)\right|^2$. Using the equations (2.69)-(2.71), introducing the definition (2.74)

and rewriting the equation in terms of conformal time τ, we arrive at an equation for $\mathcal{R}_q(t)$ also known as the Mukhanov-Sasaki equation:

$$\frac{d^2\mathcal{R}_q}{d\tau^2} + \frac{2}{z}\frac{dz}{d\tau}\frac{d\mathcal{R}_q}{d\tau} + q^2\mathcal{R}_q = 0\,. \tag{2.78}$$

where

$$\tau = \int_{t_\star}^{t} \frac{dt'}{a(t')} \;\;;\;\; z = \frac{a\dot{\bar{\varphi}}}{H}\,. \tag{2.79}$$

In the usual slow roll approximation where H is close to constant, the slow roll parameters

$$\epsilon = -\frac{\dot{H}}{H^2} \;\;;\;\; \delta = \frac{\ddot{H}}{2H\dot{H}}\,, \tag{2.80}$$

are small (the background equation $\dot{H} = -4\pi G\dot{\bar{\varphi}}^2$ illustrates why this phase is called slow roll, because it means that the "speed" of the scalar field, $\dot{\bar{\varphi}}$, is small). With the identities

$$\frac{1}{z}\frac{dz}{d\tau} = aH(1+\epsilon+\delta) \;\;;\;\; \frac{d}{d\tau}\left(\frac{1}{aH}\right) = -1+\epsilon \tag{2.81}$$

and assuming that $\dot{\epsilon}$ and $\dot{\delta}$ may be neglected we arrive at the simplified equation

$$\frac{d^2\mathcal{R}_q}{d\tau^2} + \frac{2(1+2\epsilon+\delta)}{\tau}\frac{d\mathcal{R}_q}{d\tau} + q^2\mathcal{R}_q = 0\,, \tag{2.82}$$

which has the two Hankel functions $\tau^\nu H_\nu^{(1)}(-q\tau)$ and $\tau^\nu H_\nu^{(2)}(-q\tau)$ as its solution with $\nu = \frac{3}{2} + 2\epsilon + \delta$. The growing mode is $H_\nu^{(1)}$. As we need $\mathcal{R}$ only in the limit where $q/a \ll H$, i.e. for modes that are much larger than the Hubble radius, we find as asymptotic behavior for the growing mode

$$\mathcal{R}_q^o = i\frac{\sqrt{-\tau}\,\Gamma(\nu)}{2\sqrt{\pi}\,(2\pi)^{3/2}\,z(\tau)} e^{i\pi\nu/2+i\pi/4}\left(\frac{-q\tau}{2}\right)^{-\nu}\,, \tag{2.83}$$

where the o indicates that it is the value of $\mathcal{R}_q$ outside the Hubble radius. This result shows that the power spectrum of the curvature perturbations has the form

$$\mathcal{R}_q^o \propto q^{-3/2-2\epsilon-\delta}\,, \tag{2.84}$$

which, as we will see in Sec. 2.3.3, leads to the nearly scale invariant spectrum seen in the CMB. As $\mathcal{R}_q^o$ is time independent (which may also be shown from the form (2.83) by an explicit calculation), the prefactor in (2.83) can be evaluated at any convenient time. A standard choice is to evaluate it at the time when the mode corresponding to the wavenumber q is leaving the Hubble radius, i.e. when $q/a(t_q) = H(t_q)$ where t_q is the time of crossing of the mode q. This leads to the expression

$$\mathcal{R}_q^o = \mp i\frac{\sqrt{16\pi G}}{8\pi^{3/2}}\frac{H(t_q)}{\sqrt{\epsilon(t_q)}}q^{-3/2}\,, \tag{2.85}$$

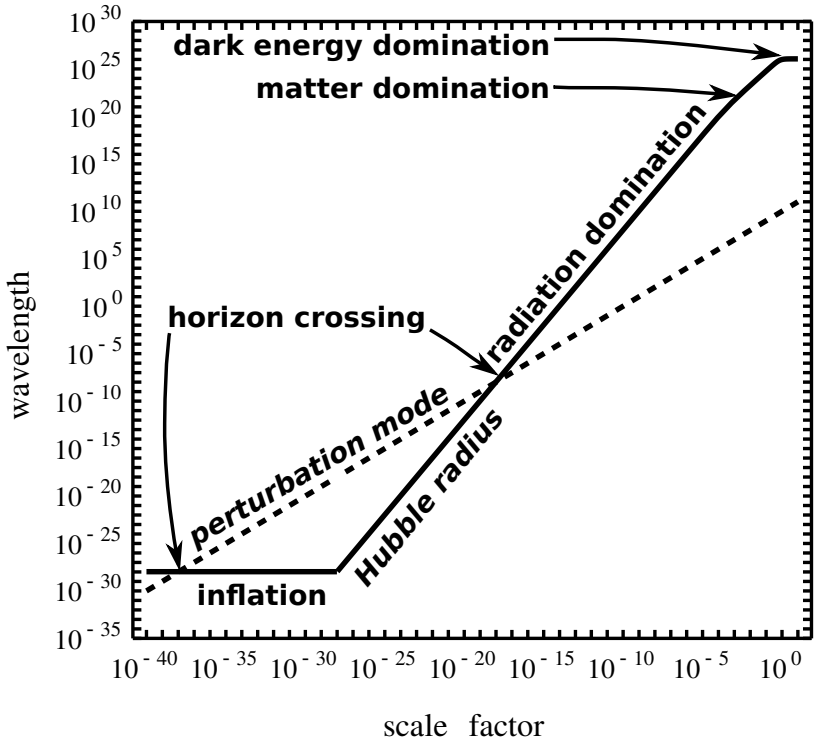

Figure 2.1. Sketch of the evolution of the wavelength of a perturbation as compared to the Hubble radius. As all the length scales, the wavelength grows linearly with the scale-factor $\lambda = a\lambda_0$. The Hubble scale $1/H$ grows differently, depending on the era. It is constant during inflation, grows as a^2 during radiation domination and as $a^{3/2}$ during matter domination. Therefore, a perturbation that is smaller than $1/H$ during inflation may cross this scale, but will eventually reenter the Hubble radius in one of the later eras. Only if the recent Λ-domination is for real, the perturbation might not reenter the Hubble volume.

where the q-exponent has changed because t_q is slightly q-dependent. The details of this q-dependence related to the slow roll parameters ϵ and δ, has to be evaluated for the specific slow roll potential under consideration. Generically however, as we have seen, slow roll inflation leads to a nearly scale invariant power spectrum for the variable $\mathcal{R}$, at least for those modes that leave the Hubble radius during inflation. This concept is explained in Fig. 2.1.

2.3.2. Evolution in the radiation dominated era

We have seen in the previous section how the quantum fluctuations of the inflaton field would give rise to curvature perturbations, encoded in the variable $\mathcal{R}$. But what has this

variable to do with the density fluctuations of matter in our Universe today? To answer this question we first of all have to find out, how this perturbation in $\mathcal{R}$ is transferred to the usual matter. After inflation had ended, the Universe was completely empty as the rapid growth of the scale factor diluted all possibly preexisting fluids. The matter that makes up our Universe was only created in the reheating period after the end of inflation. That the physical processes in this era did not erase all traces of inflation is due to the constancy of $\mathcal{R}$ outside the Hubble radius. This is for example discussed in [53] and later in a paper by Weinberg [54]. In his book[4] this is formulated as a theorem: "Whatever the contents of the Universe, there are two independent isentropic physical scalar solutions of the Newtonian gauge field equations for which the quantity $\mathcal{R}_q$ is time-independent in the limit $q/a \ll H$". The scalar metric components are then

$$\Phi_q(t) = \Psi_q(t) = \mathcal{R}_q \left[-1 + \frac{H(t)}{a(t)} \int_{\mathcal{T}}^{t} a(t') \, \mathrm{d}t' \right] \tag{2.86}$$

and the perturbation of any four scalar $s(x)$ is

$$\delta s_q(t) = -\frac{\mathcal{R}_q \dot{\bar{s}}(t)}{a(t)} \int_{\mathcal{T}}^{t} a(t') \, \mathrm{d}t' \tag{2.87}$$

and the perturbation of the velocity potential is

$$\delta u_q(t) = -\frac{\mathcal{R}_q}{a(t)} \int_{\mathcal{T}}^{t} a(t') \, \mathrm{d}t' \,, \tag{2.88}$$

where $\mathcal{T}$ is an arbitrary initial time.

This theorem transports the curvature perturbations induced by the inflaton to the perturbations in the density of the fields that exist when the respective mode reenters the Hubble radius. Of course, the mere existence of these solutions does not mean that the Universe was in a state described by one of them in its early stage of evolution. However, observations seem to indicate that the perturbations in the early Universe were indeed of isentropic nature. At the moment there is no hint for isocurvature or entropy perturbations. Therefore, these solutions seem to be close to what actually happened.

Fluid equations To describe the early phase of the hot plasma we will examine the fluid equations for a perturbed FRW metric in synchronous gauge as introduced in Sec. 2.2.2. The equations describing this case are Eq. (2.50) for the metric perturbation and the conservation equations (2.51) and (2.52) for the different fluids that are important at

[4] See [45] page 247.

this time, i.e. dark matter, Baryons, photons and neutrinos. Writing down the equations for these fluids and transforming them into Fourier space leads to

$$\frac{d}{dt}\left(a^2\Psi\right) = -4\pi G a^2\left(\delta\varrho_{Dq} + \delta\varrho_{Bq} + 2\delta\varrho_{\gamma q} + 2\delta\varrho_{\nu q}\right) \tag{2.89a}$$

for the evolution of the metric perturbation,

$$\begin{aligned}
\delta\dot{\varrho}_{Dq} + 3H\delta\varrho_{Dq} &= -\bar{\varrho}_D\Psi_q && (2.89b)\\
\delta\dot{\varrho}_{Bq} + 3H\delta\varrho_{Bq} - \left(q^2/a^2\right)\bar{\varrho}_B\delta u_{Bq} &= -\bar{\varrho}_B\Psi_q && (2.89c)\\
\delta\dot{\varrho}_{\gamma q} + 4H\delta\varrho_{\gamma q} - \left(4q^2/3a^2\right)\bar{\varrho}_\gamma\delta u_{\gamma q} &= -\left(4/3\right)\bar{\varrho}_\gamma\Psi_q && (2.89d)\\
\delta\dot{\varrho}_{\nu q} + 4H\delta\varrho_{\nu q} - \left(4q^2/3a^2\right)\bar{\varrho}_\nu\delta u_{\nu q} &= -\left(4/3\right)\bar{\varrho}_\nu\Psi_q && (2.89e)
\end{aligned}$$

for the energy conservation and

$$\begin{aligned}
\frac{1}{3}\delta p_{\gamma q} + \partial_t\left[\left(\frac{4}{3}\bar{\varrho}_\gamma + \bar{\varrho}_B\right)\delta u_{\gamma q}\right] + 3H\left(\frac{4}{3}\bar{\varrho}_\gamma + \bar{\varrho}_B\right)\delta u_{\gamma q} &= 0 && (2.89f)\\
\frac{1}{4}\delta p_{\nu q} + \partial_t\left[\bar{\varrho}_\nu\delta u_{\nu q}\right] + 3H\bar{\varrho}_\nu\delta u_{\nu q} &= 0 && (2.89g)
\end{aligned}$$

for the momentum conservation. Here, the equations of state $w_\gamma = w_\nu = 1/3$ and the plasma condition $\delta u_{\gamma q} = \delta u_{Bq}$ is used. q is again the comoving wavenumber and the q-sub-indices indicate that also the perturbations have been transformed to Fourier space. The equations become simpler when we introduce fractional perturbations, i.e. divided by the the average density and pressure:

$$\delta_{\alpha q} = \frac{\delta\varrho_{\alpha q}}{\bar{\varrho}_\alpha + \bar{p}_\alpha}\,. \tag{2.90}$$

Note that this definition slightly differs by a numerical factor taking into account the equations of state from the usual definition $\delta\varrho_{\alpha q}/\bar{\varrho}_\alpha$. This definition allows to write the equations (2.89a)–(2.89g) above in the compact form

$$\frac{d}{dt}\left(a^2\Psi_q\right) = -4\pi G a^2\left(\bar{\varrho}_D\delta_{Dq} + \bar{\varrho}_B\delta_{Bq} + \frac{8}{3}\bar{\varrho}_\gamma\delta_{\gamma q} + \frac{8}{3}\bar{\varrho}_\nu\delta_{\nu q}\right) \tag{2.91a}$$

for the evolution of the potential and

$$\begin{aligned}
\dot{\delta}_{Dq} &= -\Psi_q && (2.91b)\\
\dot{\delta}_{Bq} - \left(q^2/a^2\right)\delta u_{Bq} &= -\Psi_q && (2.91c)\\
\dot{\delta}_{\gamma q} - \left(q^2/a^2\right)\delta u_{\gamma q} &= -\Psi_q && (2.91d)\\
\dot{\delta}_{\nu q} - \left(q^2/a^2\right)\delta u_{\nu q} &= -\Psi_q && (2.91e)\\
\frac{d}{dt}\left(\frac{(1+R)\,\delta u_{\gamma q}}{a}\right) &= -\frac{1}{3a}\delta_{\gamma q} && (2.91f)\\
\frac{d}{dt}\left(\frac{\delta u_{\nu q}}{a}\right) &= -\frac{1}{3a}\delta_{\nu q} && (2.91g)
\end{aligned}$$

for the fluid perturbations, where the definition $R = 3\bar{\varrho}_B/4\bar{\varrho}_\gamma$ was used. Although they look quite simple individually, the mutual coupling makes it impossible to solve them analytically in the general case. There are, however, several limits in which they may be simplified enough to arrive at an analytic solution that is not too far from the numerically determined one.

Early matching One is the epoch shortly after inflation when all fractional perturbations are assumed to be equal, an assumption made in view of the lack any signature of non-adiabaticity. Setting

$$\delta_{\gamma q} = \delta_{Bq} = \delta_{Dq} = \delta_{\nu q} =: \delta_q \tag{2.92}$$

and using the approximation that this early epoch was radiation dominated, i.e. that

$$\bar{\varrho}_R = \bar{\varrho}_\gamma + \bar{\varrho}_\nu \gg \bar{\varrho}_M = \bar{\varrho}_B + \bar{\varrho}_D \tag{2.93}$$

and for early enough time, such that $q/aH \ll 1$, this leads to an equation for the density contrasts

$$\frac{d}{dt}\left(a^2\dot{\delta}_q\right) = \frac{32}{3}\pi G a^2 \bar{\varrho}_R \delta_q \,. \tag{2.94}$$

The radiation domination implies $a(t) \propto \sqrt{t}$ and with the background Friedman equation $8\pi G/3\bar{\varrho}_R = 1/4t^2$ one has a simple second order differential equation for $\delta_q(t)$. This equation has two solutions, a growing one with $\delta_q(t) \propto t$ and a decaying one $\delta_q(t) \propto 1/t$. For the growing mode the remaining equations give

$$\delta_q(t) = At \;\;;\;\; \Psi_q(t) = -A \;\;;\;\; \delta u_q(t) = -\frac{2t^2}{9}A \,, \tag{2.95}$$

as leading growing contribution and we may now use Eq. (2.58) to relate the constant A to the inflationary epoch. Eq. (2.58) results in

$$A = \frac{1}{2}\frac{q^2}{a^2 H}\mathcal{R}_q \,, \tag{2.96}$$

when neglecting δu_q and so

$$\delta_q = \delta_{\gamma q} = \delta_{Bq} = \delta_{Dq} = \delta_{\nu q} = \frac{1}{4}\frac{q^2}{a^2H^2}\mathcal{R}^o_q \,, \tag{2.97}$$

$$\psi_q = -\frac{1}{2}\frac{q^2}{a^2 H}\mathcal{R}^o_q \,, \tag{2.98}$$

$$\delta u_q = \delta u_{\gamma q} = \delta u_{\nu q} = -\frac{1}{36}\frac{q^2}{a^2H^3}\mathcal{R}^o_q \,, \tag{2.99}$$

which justifies neglecting δu_q in (2.96) and in the derivation of (2.94), because the term with δu_q is one order higher in $q/aH \ll 1$.

These solutions, even though very limited in their range of applicability for q outside the horizon and early times, are still important as they fix the normalization of the future evolution of the modes. By the constant gauge invariant variable $\mathcal{R}_q^o$ they are connected to the inflationary era. This allows us to predict the primordial power spectrum of the matter perturbations from the inflationary form (2.85).

Evolution until decoupling In its evolution from the early state discussed in the previous section up to the time of decoupling, the Universe passes from the radiation dominated era to a matter dominated one. For modes outside the Hubble radius during the whole time, i.e. $q/aH \ll 1$, there is a solution that covers the time evolution of the perturbations in both eras. The difference to the result above is just that now $\bar{\varrho}_M$ is no longer negligible and $a(t)$ passes therefore from $a(t) \propto \sqrt{t}$ to $a(t) \propto t^{2/3}$. So it is convenient to express the result in terms of the scale factor

$$\delta_q = \frac{4q^2\mathcal{R}_q^o}{5H_{EQ}^2 a^2}\left(16 + 8\frac{a}{a_{EQ}} - 2\left(\frac{a}{a_{EQ}}\right)^2 + \left(\frac{a}{a_{EQ}}\right)^3 - 16\sqrt{1+\frac{a}{a_{EQ}}}\right) , \tag{2.100}$$

where the prefactor has been chosen to match the solution (2.97) for $t \to 0$. The solution goes from a $a^2(t) \propto t$ evolution in the radiation dominated era to a $a(t) \propto t^{2/3}$ evolution in the matter dominated era. Therefore the super Hubble scale perturbations in synchronous gauge grow more slowly in the matter era than in the radiation era.

To extend the result to smaller scales, we may consider modes that are still bigger than the Hubble scale at matter radiation equality, but which enter the Hubble radius during the matter dominated era. This translates into $\bar{\varrho}_R \ll \bar{\varrho}_M$ and with the simplifying assumption that $\bar{\varrho}_B \ll \bar{\varrho}_D$, (2.91a) and (2.91b) combine to

$$\ddot{\delta}_{Dq} + 2H\dot{\delta}_{Dq} - 4\pi G\bar{\varrho}_D\delta_{Dq} = 0 . \tag{2.101}$$

This equation (known as the Meszaros equation) will be important in all what follows as it describes the evolution of the matter density perturbations on large scales up to today. As above, there are again two solutions to this equations, a growing and a decaying one. During matter domination, they go with the scale-factor and cosmic time as $\delta_D(t) \propto a(t) \propto t^{2/3}$ and $\delta_D(t) \propto a(t)^{-3/2} \propto t^{-1}$ respectively.

To match (2.100) at scales around the Hubble radius we have to choose the proportionality constant to give

$$\delta_{Dq} = \frac{2}{5}\kappa^2\frac{a}{a_{EQ}}\mathcal{R}_q^o \Rightarrow \Psi_q = -\frac{2}{5}\kappa^2\frac{H_{EQ}}{\sqrt{a/a_{EQ}}}\mathcal{R}_q^o , \tag{2.102}$$

with $\kappa = \sqrt{2}q/(a_{EQ}H_{EQ})$. For the other perturbations things are more complicated, as now, inside the Hubble radius, we cannot neglect $(q^2/a^2)\,\delta u_q$ terms any more. This couples the equations and leads to oscillations in the baryon and photon component.

They are linked before recombination and may, in the approximation of moderately long wavelength, be written as

$$\delta_{\gamma q} = \delta_{Bq} = \frac{3}{5}\mathcal{R}_q^o \left(1 + 3R - \frac{\cos\left(\varphi\left(t\right)\right)}{\left(1+R\right)^{1/4}}\right) \ , \tag{2.103}$$

where $R = 3\bar{\varrho}_B/4\bar{\varrho}_\gamma$ and the phase φ is a function of t. The important lesson from this equation is, that the overall amplitude of the perturbation in the baryons is constant in this era, i.e. up to the time of recombination, because the baryonic plasma sound speed $c_{SB}^2 \neq 0$. In contrast to that, the dark matter perturbations that become smaller than the Hubble radius during this epoch, when matter dominates but before decoupling, continue to grow. This difference is one of the important cosmological arguments for the existence of dark matter. Observations today show larger density fluctuations than there could be in a Universe made of baryonic matter, as δ_{Bq} has less time to grow. Fig. 2.2 illustrates this point.

After the discussion of super horizon modes and those that enter the Hubble radius in the matter dominated era, we finally have to consider the modes that enter already in the radiation dominated era. The equations for these modes are a mess (even though the physics behind is simple) and so we will just discuss the result, being

$$\delta_{Dq} = 9\mathcal{R}_q^o \frac{a}{a_{EQ}}\mathcal{T}_l\left(q\right) + \frac{48\pi G\bar{\varrho}_\gamma}{q^2/a^2}\mathcal{R}_q^o\left(2+R\right)\left(1+R\right)^{3/4} e^{-\int_0^t \Gamma dt}\cos\left(\varphi\left(t\right)\right) \ , \tag{2.104}$$

$$\delta_{Bq} = \delta_{\gamma q} = \frac{a}{a_{EQ}t^2}\frac{\left(1+3R\right)}{q^2/a^2}\mathcal{R}_q^o\mathcal{T}_l\left(q\right) - \frac{3\mathcal{R}_q^o}{\left(1+R\right)^{1/4}} e^{-\int_0^t \Gamma dt}\cos\left(\varphi\left(t\right)\right) \ , \tag{2.105}$$

where $\mathcal{T}_l\left(q\right) = \left(-7/2 + \gamma_E + \ln\left(4\kappa/\sqrt{3}\right)\right)$, $\kappa = \sqrt{2}q/\left(a_{EQ}H_{EQ}\right)$ and Γ is Silk damping. Here again we remark that the baryon perturbations are not growing during matter domination. The dark matter perturbations create wells in the gravitational potential that enhance the baryon density perturbation growth after decoupling (see Fig. 2.2).

The transfer function All the previous results were for specific limits. However, for what follows we will need the spectrum of dark matter perturbations for the whole range of scales, from large to small q. This can only be done numerically, because depending on when the mode entered the Hubble radius the growth will be different. As we have seen, the small scale modes in (2.104), that entered during the radiation dominated era, have a different q dependence than those modes that entered during matter dominance (2.102).

The numerical calculation leads to fitting functions for what is called the *transfer function* that take the different evolution of perturbations on different scales before decoupling into account. After baryon decoupling, the matter component in dark matter and baryons evolves independently from the other components as described by equation (2.102). Until the onset of nonlinear evolution or dark energy domination, the perturbation

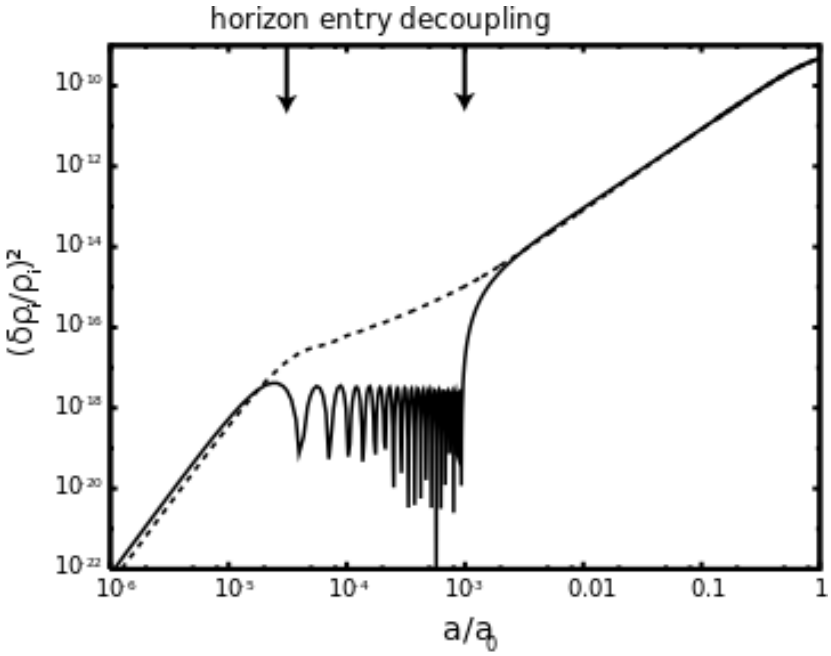

Figure 2.2. Comparison of the evolution of a dark matter perturbative mode with a baryonic mode of the same wavenumber k. The wavelength of the mode corresponds to ≈ 4 Mpc today. When the mode enters the Hubble radius the dark matter perturbation, shown as the dashed line, continues to grow. The baryon perturbation stops to grow and starts to oscillate due to its coupling to the photon bath. After decoupling the baryons fall into the potential wells prepared by the dark matter. Therefore, the perturbation grows rapidly and ends up at the same level as the dark matter perturbation at this time. Picture from Wikipedia.[5]

grows linearly with the scale factor on all scales. Therefore, we may write the evolution in the matter dominated era after baryon decoupling in the form

$$\delta_{Dq} = \frac{2}{5}\kappa^2 \frac{a}{a_{EQ}} \mathcal{R}_q^o \mathcal{T}(q) \ , \tag{2.106}$$

and define the transfer function $\mathcal{T}(q)$ by this equation. We already saw two limits of this transfer function. For small q, i.e. large scales, $\mathcal{T}(q) \to 1$ giving (2.102) and on small scales for $q \gg 1$, it goes to (2.104) $\mathcal{T}(q) \to \frac{45}{2\kappa^2}\left(-7/2 + \gamma_E + \ln\left(4\kappa/\sqrt{3}\right)\right)$. The fitting formula that interpolates between these limits, which we will use in the following

[5]From http : //en.wikipedia.org/wiki/File : Structure_mode_history.svg in the version of 17.07.2012

has been given by Eisenstein and Hu [55] and reads

$$\begin{aligned} \mathcal{T}(q) &= \frac{L_0}{L_0 + C_0 q^2} , \\ L_0(q) &= \ln(2e + 1.8q) , \\ C_0(q) &= 14.2 + \frac{731}{1 + 62.5q} , \end{aligned} \tag{2.107}$$

where their q is defined as

$$q = \frac{k}{h\,\mathrm{Mpc}^{-1}} \Theta_{2.7}^2 / \Gamma , \tag{2.108}$$

with $\Gamma = \Omega_0 h$ and $\Omega_0 = \Omega_C + \Omega_B$. $\Theta_{2.7}$ is the deviation of the CMB temperature from 2.7K. In the case that we do not ignore the effect of baryons on the correlation function, the shape is slightly different. This is encoded in a modification of the shape parameter Γ which becomes

$$\Gamma_{\mathrm{eff}}(k) = \Omega_0 h \left(\alpha_\Gamma + \frac{1 - \alpha_\Gamma}{1 + (0.43ks)^4} \right) , \tag{2.109}$$

where the new parameters are determined by a fit to numerical results of CMBfast to

$$s = \frac{44.5 \ln(9.83/\Omega_0 h^2)}{\sqrt{1 + 10 (\Omega_b h^2)^{3/4}}} \,\mathrm{Mpc} , \tag{2.110}$$

$$\alpha_\Gamma = 1 - 0.328 \ln\left(431 \Omega_0 h^2\right) \frac{\Omega_b}{\Omega_0} + 0.38 \ln\left(22.3 \Omega_0 h^2\right) \left(\frac{\Omega_b}{\Omega_0}\right)^2 . \tag{2.111}$$

This fixes the transfer function over all scales and encodes the difference in the growth of perturbations, that enter the Hubble radius at different times in the evolution.

With these relations we have reached the goal of this section: to follow the initial perturbations created by inflation through the radiation dominated era up to the moment of recombination. This gives the shape of the linear dark matter power spectrum, defined in (2.15) and (2.63) by

$$P(q) = |\delta_{Dq}|^2 = \frac{4}{25} \kappa^4 \left(\frac{a}{a_{EQ}}\right)^2 \left|\mathcal{R}_q^o\right|^2 \mathcal{T}^2(q) = A \left(\frac{a}{a_{EQ}}\right)^2 q^{n_S} \mathcal{T}^2(q) , \tag{2.112}$$

where we used the q-dependence of $\mathcal{R}_q^o$, Eq. (2.84), that is $\mathcal{R}_q^o \propto q^{-3/2-2\epsilon-\delta}$. A is a normalization constant that can be either determined from the CMB as we will discuss in Sec. 2.3.3, or fixed by normalizing the matter fluctuations in a sphere of radius $8h^{-1}$Mpc, i.e. σ_8, to a certain value. We will choose this latter possibility in most cases. n_S is $n_S = 1 - 4\epsilon - 2\delta$. For slow roll inflation there is only a small deviation of n_S from one. This is also seen in the observations and is called scale invariant spectrum in the sense of Eq. (2.26) and Eq. (2.123).

Eq. (2.112) not only gives the initial spectrum at a specific instant in time, but over the whole matter dominated era, because on small scales baryons and photons decouple. Therefore, oscillations in the plasma, that were mediated by the baryons into the dark matter sector, do not longer lead to the second term in (2.104). Consequently, on these scales as on the large scales we have a simple growth of the overall amplitude with a, described by the first term. On large scales (2.102) this is the case anyhow. As the growth of modes outside the horizon (2.100) is the same as for the large scale modes inside the horizon, the modes that enter later have the same amplitude. Therefore, they do not change the shape of the transfer function any more and Eq. (2.112) describes the linear power spectrum throughout the matter dominated era. The only modifications will arise on small scales by nonlinear growth in the late Universe and by the onset of dark energy domination. We will discuss the modifications due to dark energy in Sec. 2.3.4.

2.3.3. Normalization to the CMB

The easiest way to see how the amplitude of the power spectrum of the dark matter distribution imprints itself on the CMB is by focusing on what is called the Sachs Wolfe effect.[6] It encodes the influence of the gravitational potential on the temperature fluctuations in the CMB. This influence is twofold: First of all, the temperature at a given point is redshifted by the local gravitational potential $\phi(\mathbf{x})$ as

$$\frac{\Delta T(\hat{n})}{T_0} = \delta\phi(r_L\hat{n}) \ , \tag{2.113}$$

where $\Delta T(\hat{n}) = T(\hat{n}) - T_0$, $\hat{n}$ is the direction in the sky and r_L is the comoving coordinate distance of the surface of last scattering. The second effect of a local gravitational potential is that it changes the rate of expansion. This modifies the time when the Universe has cooled down to $3000K$, the approximate temperature of decoupling. The time is affected by $\delta\phi(r_L\hat{n}) = \delta t/t$ which is plausible when interpreting the gravitational potential in the post Newtonian way of the Newtonian gauge (2.2.2) (which has a modified time component). The temperature decays as $T(t_0) = T_i/a(t)$, so this gives rise to a density perturbation in the matter dominated era around decoupling of

$$\frac{\Delta T(\hat{n})}{T_0} = -\frac{\delta a}{a} = -\frac{2}{3}\frac{\delta t}{t} = -\frac{2}{3}\delta\phi(r_L\hat{n}) \ . \tag{2.114}$$

The sum of the two contributions is therefore

$$\left(\frac{\Delta T(\hat{n})}{T_0}\right)_{SW} = \frac{1}{3}\delta\phi(r_L\hat{n}) \ . \tag{2.115}$$

[6] There are also intrinsic temperature fluctuations, fluctuations due to the Doppler effect and fluctuations due to the late time integrated Sachs-Wolfe effect. All of those can be shown to be sub-dominant in a certain part of the angular CMB power-spectrum for adiabatic initial perturbations. For a discussion of these terms see e.g. [45].

As this gravitational potential is to be interpreted in the Newtonian gauge we have to relate it to the dark matter perturbations via the analogue of the Poisson equation

$$\nabla^2\delta\phi\left(\mathbf{x},t\right)=-4\pi Ga\left(t\right)^2\delta\varrho_D\left(\mathbf{x},t\right)\Rightarrow\delta\phi\left(\mathbf{q},t\right)=-4\pi G\left(\frac{a\left(t\right)}{q}\right)^2\bar{\varrho}_D\delta_{Dq}\left(t\right)\ . \tag{2.116}$$

Using the perturbation (2.102), the fluctuation of the potential is

$$\delta\phi\left(\mathbf{q}\right)=-\frac{3}{5}\alpha\left(\mathbf{q}\right)\mathcal{R}_q^o\ , \tag{2.117}$$

where $\alpha\left(\mathbf{q}\right)$ is a stochastic phase factor as introduced in Sec. 2.2.3.

From this, one could derive the power spectrum of the temperature fluctuations in Fourier space. However, in the observation of the CMB it is more useful to use a decomposition into spherical harmonics and not plane waves. This means

$$\mathbb{E}\left[\Delta T\left(\hat{n}\right)\Delta T\left(\hat{n}'\right)\right]=\sum_\ell C_\ell\left(\frac{2\ell+1}{4\pi}\right)P_\ell\left(\hat{n}\cdot\hat{n}'\right)\ , \tag{2.118}$$

where P_ℓ are the Legendre polynomials. It is now common to give the coefficients C_ℓ instead of the normal power spectrum. They are determined by

$$C_\ell=\frac{1}{4\pi}\int\mathrm{d}^2\hat{n}\mathrm{d}^2\hat{n}'P_\ell\left(\hat{n}\cdot\hat{n}'\right)\mathbb{E}\left[\Delta T\left(\hat{n}\right)\Delta T\left(\hat{n}'\right)\right]\ . \tag{2.119}$$

With

$$\delta\phi\left(\mathbf{x}\right)=\int\mathrm{d}^3qe^{i\mathbf{q}\cdot\mathbf{x}}\delta\phi_q=\int\mathrm{d}^3q\delta\phi_q\sum_\ell\left(2\ell+1\right)i^\ell P_\ell\left(\hat{q}\cdot\hat{n}\right)j_\ell\left(qr\right)\ , \tag{2.120}$$

this gives for

$$\mathbb{E}\left[\Delta T\left(\hat{n}\right)\Delta T\left(\hat{n}'\right)\right]_{SW}=\frac{4\pi}{9}T_0^2\sum_\ell\left(2\ell+1\right)P_\ell\left(\hat{n}\cdot\hat{n}'\right)\int_0^\infty q^2dq\mathcal{P}_\phi\left(q\right)j_\ell^2\left(qr\right)\ , \tag{2.121}$$

where $\mathcal{P}_\phi\left(q\right)\delta\left(\mathbf{q}-\mathbf{q}'\right)=\mathbb{E}\left[\delta\phi_{\mathbf{q}}\delta\phi_{\mathbf{q}'}\right]$ and so the Sachs Wolfe C_ℓ's are

$$C_{\ell,SW}=\frac{16\pi^2}{9}T_0^2\int_0^\infty q^2dq\mathcal{P}_\phi\left(q\right)j_\ell^2\left(qr\right)\ . \tag{2.122}$$

As the spectrum $\mathcal{P}_\phi\left(q\right)$ by (2.117) is proportional to $\left|\mathcal{R}_q^o\right|^2$, it is a power law $\mathcal{P}_\phi\left(q\right)=N_\phi^2q^{n-4}$ and thus (2.122) may be integrated to

$$C_{\ell,SW}=\frac{16\pi^3 2^{n-4}\Gamma\left(3-n\right)r_L^{1-n}N_\phi^2T_0^2}{9\Gamma^2\left(\frac{4-n}{2}\right)}\frac{\Gamma\left(\ell+\frac{n-1}{2}\right)}{\Gamma\left(\ell+2-\frac{n-1}{2}\right)}\ , \tag{2.123}$$

where r_L is the comoving coordinate distance to the surface of last scattering. For the case that the spectrum goes just like q^{-3}, i.e. for $n = 1$, the C_ℓ's do no longer depend on the absolute scale r_L. This is one reason why this spectrum is called scale invariant. It is also known as Harrison Zel'dovich spectrum. In this $n = 1$ case the C_ℓ's further simplify to

$$C_{\ell,SW} = \frac{8\pi^2 N_\phi^2 T_0^2}{9\ell\,(\ell+1)}\,. \tag{2.124}$$

Therefore, if $\ell\,(\ell+1)\,C_\ell$ is plotted, the spectrum should be approximately constant in the range where the Sachs Wolfe effect is the dominant contribution. This is the case for $10 \lesssim \ell \lesssim 100$. So the magnitude of the C_ℓ's in this range gives a first hint on the absolute value of the density perturbations. By a fit of (2.123) to the Cosmic Background Explorer (COBE) data in the range of $4 \lesssim \ell \lesssim 40$ one obtained the so called COBE normalization of the spectrum which in terms of the N_ϕ used here gives $N_\phi = 8.7 \times 10^{-6}$. Via $N_\phi^2 = \frac{9}{25}\left|\mathcal{R}_q^o\right|^2$ from Eq. (2.117), this connects observations and the theoretical quantities above. More generally if written as

$$\left|\mathcal{R}_q^o\right|^2 = N^2 q^{-3}\left(\frac{q/a_0}{k_\mathcal{R}}\right)^{n_S-1}\,, \tag{2.125}$$

the COBE normalization gives $N^2 = 2.1 \times 10^{-10}$. When compared to the WMAP results given in terms of $\Delta^2_\mathcal{R}(k)$, which is connected to $\left|\mathcal{R}_q^o\right|^2$ by

$$\Delta^2_\mathcal{R}(k) = \frac{k^3}{2\pi^2}\mathcal{P}_\mathcal{R}(k) \quad ; \quad \mathcal{P}_\mathcal{R}(k) = (2\pi)^3\left|\mathcal{R}_q^o\right|^2 \tag{2.126}$$

the measured value of $\Delta^2_\mathcal{R}(k_0) = 2.42 \times 10^{-9}$ gives $N^2 = 1.93 \times 10^{-10}$. This leads in the normalization of (2.112) to

$$A = \frac{4}{25}\kappa^4\left|\mathcal{R}_q^o\right|^2 = \frac{4}{25}\left(\frac{19.3\,(q/a_0)}{\Omega_m h^2}\right)^4 N^2 q^{-3}\left(\frac{q/a_0}{k_\mathcal{R}}\right)^{n_S-1} = 1.4 \times 10^{-2}\,, \tag{2.127}$$

for $a_0 = 1$, $\Omega_m = 0.27$, $h = 0.7$ and $n_S \approx 1$.

2.3.4. The recent evolution

Finally, we want to continue the evolution of the perturbations beyond the matter dominated era. In the recent Universe the takeover of the dark energy component leads to a suppression of the growth in the matter perturbations. By assuming dark energy to be a cosmological constant, the corresponding fluid equation (2.91a) is the same as there are no dark energy perturbations in this case. This means that (2.101) still describes the evolution of the dark matter perturbations in the Λ-dominated phase. The only modification that has to be taken into account is the different evolution of the scale-factor

and the Hubble rate with cosmic time. To this end, it is useful to rewrite the equation (2.101) in terms of the scale factor

$$\dot{a}^2 \left(\frac{d^2}{da^2} \delta_{Dq} \right) + \frac{3}{2} a \left(H^2 + H_0^2 \Omega_\Lambda \right) \left(\frac{d}{da} \delta_{Dq} \right) = \frac{3}{2} H_0^2 \frac{\Omega_m}{a^3} \delta_{Dq} \, . \tag{2.128}$$

The growing solution to this equation is then

$$D\left(a\right) = \frac{a}{a_0} \, {}_2F_1 \left(1, \frac{1}{3}; \frac{11}{6}; -\frac{\Omega_\Lambda}{\Omega_m} \left(\frac{a}{a_0} \right)^3 \right) \, , \tag{2.129}$$

where we decomposed $\delta_{Dq} = A\left(q\right) D\left(a\right)$. The function ${}_2F_1$ is the Gauss hypergeometric function. In the limit of $\Omega_\Lambda \to 0$ it goes to 1. This recovers the correct behavior for matter domination. Its expansion in terms of the scale-factor begins with $D\left(a\right) \to 1 - \frac{2}{11} \left(\frac{a}{a_0} \right)^3$ for $a \ll a_0$, so for early times $D\left(a\right)$ also asymptotically goes like a as expected. Using the same normalization as before, we therefore have for the density perturbations

$$\delta_{Dq} = \frac{2}{5} \kappa^2 \frac{D\left(a\right)}{D\left(a_{EQ}\right)} \mathcal{R}_q^o \mathcal{T}\left(q\right) \, , \tag{2.130}$$

which means that the spectrum scales as $D^2\left(a\right) / D^2\left(a_{EQ}\right)$.

This concludes the journey on which we followed the perturbation from its birth in the quantum fluctuations of the inflating primordial Universe up to the dark energy domination today. Now we have reviewed all the knowledge about the linear perturbation spectrum that will be crucial in the following. To visualize the results we collected, Fig. 2.3 shows the form of the power spectrum (2.112) and the correlation function and matter fluctuations in a sphere. The power spectrum is plotted as a function of $k = 2\pi/r$. It shows the typical form of a CDM spectrum: a scale invariant part on large scales where it grows as k and then a suppression for the modes that entered the horizon already before decoupling. In this regime of large k, i.e. small scales, it decreases like k^{-2}.

The corresponding correlation function falls below one at a few h^{-1}Mpc and then decreases steeply. It falls below zero at a scale slightly above $100h^{-1}$Mpc and then goes to zero as r^{-4}. The same r^{-4} dependence is also the limiting behavior of σ^2 whereas on small scales where we find more structure, it flattens. σ itself goes from its value at $8h^{-1}$Mpc of 0.8 to 10^{-5} on horizon scales.

With the tools described in this and the previous sections, we can finally look at some data.

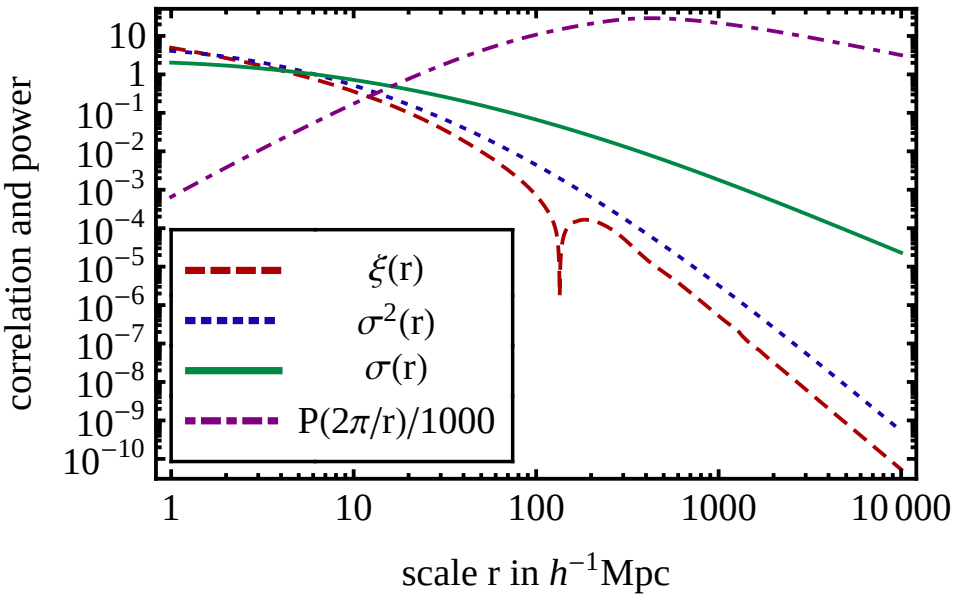

Figure 2.3. Dependence of the ΛCDM correlation function, power spectrum and matter fluctuations on the scale r. The input is the fitting form of the power spectrum of Eq. (2.112). The plot shows it as a function of $k = 2\pi/r$. On small scales it goes like k^{-2}, on large scales as k^1. For σ^2 this means by Eq. (2.23) a decay like r^{-1} in the beginning and r^{-4} on large scales. The correlation function has a similar behavior but experiences a zero crossing at a scale of around $100h^{-1}$Mpc (the sharp dip in this double logarithmic plot).

3. Structure in the observations

3.1. Recent observations

There are plenty of observations that measure aspects of the matter distribution of the Universe directly or indirectly, like radio surveys, weak lensing measurements or cluster searches. However, in this section we will only have a closer look on those observations which are most important for the results of this work and whose techniques are most developed: the measurements of the primordial inhomogeneities imprinted in the CMB, and the large galaxy redshift surveys in the late Universe. Together with the supernova data, those observations gave rise to the popular concordance model and are therefore two pillars of today's cosmology.

3.1.1. Cosmic microwave background inhomogeneities

As recalled in Sec. 1.1.2, the early Universe, after the period of accelerated expansion during inflation, was dominated by radiation. After the Universe had heated up sufficiently, the photons coupled to the charged particles and formed a hot plasma. The acoustic waves that propagated in this plasma, left their imprint in the over and under-density of the plasma. These density fluctuations influenced the photon temperature and led to hotter and cooler regions in the plasma. When the temperature fell below approximately 3000K, the formerly free electrons combined with the protons to form neutral hydrogen. The interaction rate of the photons therefore decreased drastically and enabled them to propagate freely until today. In this way these photons, that redshifted to the microwave region of the electromagnetic spectrum in the following evolution, carry information about the over-density field of the Universe at the time of recombination. They provide information about the initial conditions for cosmic structure formation.

Until the release of newer data from the Planck Satellite, the best measurement of the cosmic microwave background at large scales is still from the Wilkinson Microwave and Anisotropy Probe (WMAP) mission. The angular power spectrum of the temperature field is shown in Fig. 3.1. As we have seen in Sec. 2.3.3, its overall normalization is related to the matter power spectrum that we will be interested in in the following. The data shows the approximate constancy for small ℓ that by Eq. (2.124) was the indication of a scale invariant spectrum. Of course this constancy is not perfect as it is overlayed by other effects that we neglected in the derivation of Eq. (2.124). Taking those into account, however, the fit with the full model spectrum confirms the scale invariance.

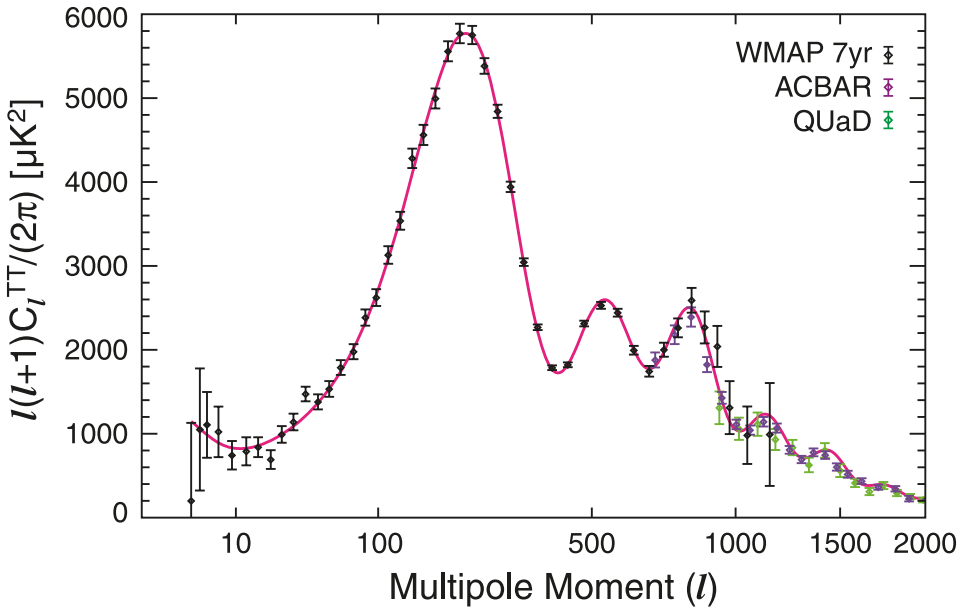

Figure 3.1. Angular power spectrum of the primordial fluctuations of the CMB temperature field. The angular power is given in terms of the magnitude of the coefficients C_ℓ in the expansion of the two-point correlation function into spherical harmonics. The coefficients are multiplied by $\ell\,(\ell+1)\,/2\pi$ to compensate for the overall decrease with this factor of a scale invariant spectrum (see Sec. 2.3.3 for details). The figure was taken from the WMAP7 paper [41]. ACBAR (Arcminute Cosmology Bolometer Array Receiver) and QUaD (QUEST at DASI) are two South Pole based CMB experiments.

The wiggles on top of the spectrum that globally scales as $1/\ell\,(\ell+1)$ are the imprints of the sound waves propagating in the plasma in the early Universe. They contain information about the ratio of baryonic matter to dark matter, and about the angular diameter distance to the surface of last scattering.

The excellent fit of the theoretical curve in Fig. 3.1 to the measured data and the high accuracy of the measurement of the temperature correlations gave rise to what is sometimes called precision cosmology. In combination with other measurements, the precision for many of the basic cosmic parameters is better than 1% and summarized in table 3.1.

3.1.2. Large scale structure surveys

In contrast to the measurement of the initial conditions of structure formation, by looking at the CMB, large scale structure surveys determine the distribution of galaxies in the late Universe. The largest surveys up to today are the 2dF survey [56], the Sloan Digital Sky Survey (SDSS) [57] and the WiggleZ survey [58]. Especially the SDSS is particularly useful, as it covers with an extension of approximately 8200 square degrees about 20% of

Table 3.1. Summary of the currently best values of the cosmological parameters of the ΛCDM model as published in [41].

Class	Parameter	WMAP 7-year Mean	WMAP+BAO+H_0 Mean
Primary	$100\Omega_b h^2$	$2.249^{+0.056}_{-0.057}$	2.255 ± 0.054
	$\Omega_c h^2$	0.1120 ± 0.0056	0.1126 ± 0.0036
	Ω_Λ	$0.727^{+0.030}_{-0.029}$	0.725 ± 0.016
	n_s	0.967 ± 0.014	0.968 ± 0.012
	τ	0.088 ± 0.015	0.088 ± 0.014
	$\Delta^2_{\mathcal{R}}(k_0)$[a]	$(2.43 \pm 0.11) \times 10^{-9}$	$(2.430 \pm 0.091) \times 10^{-9}$
Derived	σ_8	$0.811^{+0.030}_{-0.031}$	0.816 ± 0.024
	H_0	70.4 ± 2.5 km/s/Mpc	70.2 ± 1.4 km/s/Mpc
	Ω_b	0.0455 ± 0.0028	0.0458 ± 0.0016
	Ω_c	0.228 ± 0.027	0.229 ± 0.015
	$\Omega_m h^2$	$0.1345^{+0.0056}_{-0.0055}$	0.1352 ± 0.0036
	z_{reion}[b]	10.6 ± 1.2	10.6 ± 1.2
	t_0[c]	13.77 ± 0.13 Gyr	13.76 ± 0.11 Gyr

[a] $\Delta^2_{\mathcal{R}}(k) = k^3 P_{\mathcal{R}}(k)/(2\pi^2)$ and $k_0 = 0.002$ Mpc^{-1}.

[b] "Redshift of reionization," if the Universe was reionized instantaneously.

[c] The present-day age of the Universe.

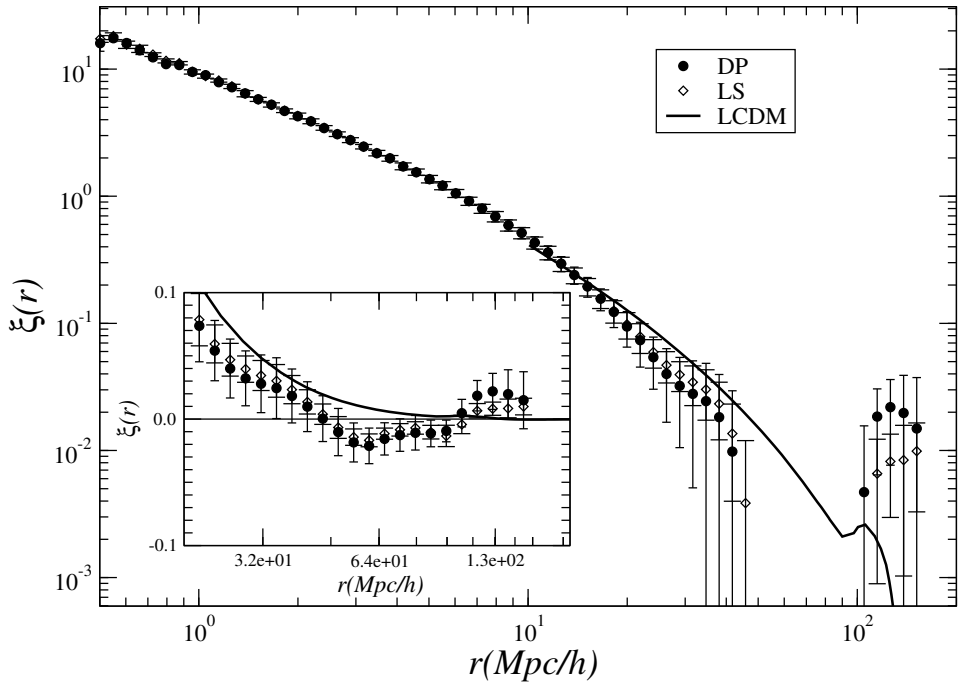

Figure 3.2. Measurement of the correlation function (2.6) in the SDSS DR7 galaxy sample. The analysis was performed by Sylos Labini *et. al* in [60]. They use two different estimators for the correlation function. The Davis Peebles estimator (DP), which we will describe in Eq. (3.11) and the Landy Szalay estimator (LS), Eq. (3.12).

the sky. In addition this area is, apart from 3 separated stripes, connected to one filled region, whereas the 2dF and WiggleZ survey have a more stripe like geometry. This allows to use more robust methods for the characterization of structures using full shell estimators for the correlation function [44, 59] or Minkowski functionals like in [48] and Sec. 3.2.

The result of an estimation of the two-point correlation function from the seventh data release of the SDSS project is shown in Fig. 3.2. It decays like a power law with an index of -1.3 on small scales turning over to -2 on larger scales. The comparison with the ΛCDM model correlation function shows good agreement on small and intermediate scales, but the sample size is not yet sufficient to definitely determine the position of the zero crossing. In the data this seems to occur at smaller redshift than for the model, but this may be related to finite size effects.

Complementary to the estimation of the correlation function, one may also determine the power spectrum of the fluctuations from the data. This has been done in [61] with the result shown in Fig. 3.3.

Also in this case the data agree quite well with the theoretical model power spectrum on the scales where we expect linear theory to hold. For larger k, i.e. smaller scales

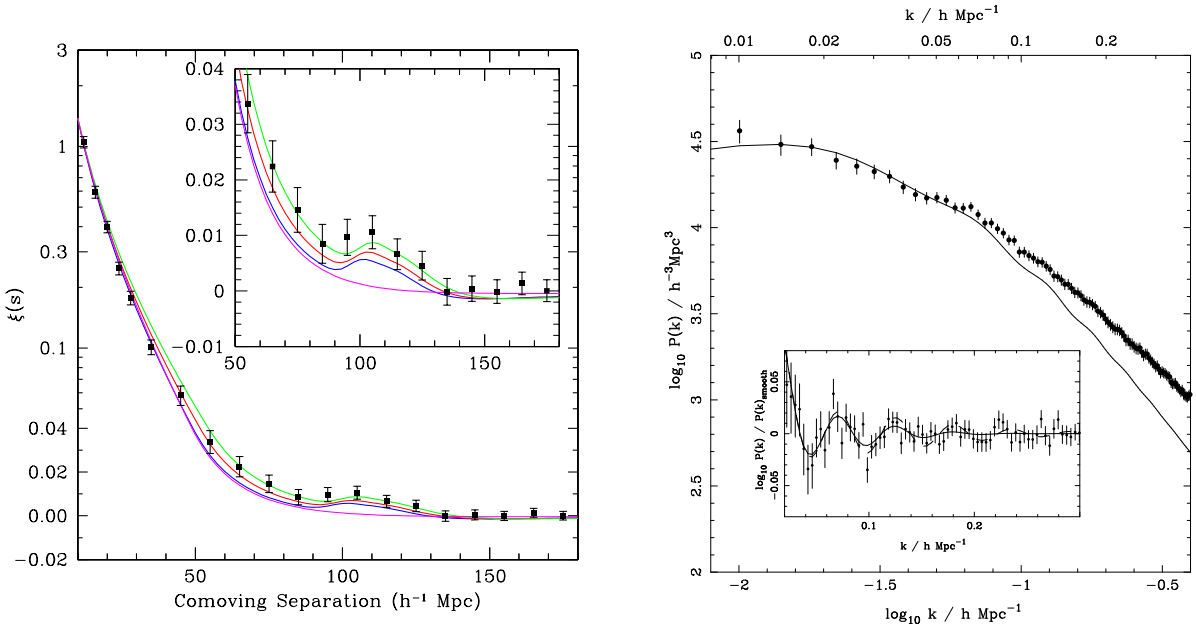

Figure 3.3. First measurements of the BAO in the SDSS DR5 galaxy data. The left plot shows the first detection of the BAO peak in the correlation function in [62]. For the right plot, [61] used the estimation of the power spectrum to isolate the wiggles shown in the inset. In addition, the overall shape nicely fits the theoretical linear power spectrum in the range of scales where it is applicable.

there is a growing deviation from the linear theory power spectrum. This is due to non-linear structure formation and can be modeled by better calculation techniques like renormalized perturbation theory (RPT) [63, 64]. On large scales, i.e. for small k, there is, analogously to the case of the correlation function, not yet enough data to detect the turnover in the power spectrum. This will change with the completion of the third part of the SDSS [36].

Baryon Acoustic Oscillations The inset in Fig. 3.3 shows the baryon acoustic oscillations (BAO) in the data. BAO are the analogue to the wiggles in the CMB power spectrum of Fig. 3.1. They form when the over-density in the baryons, left over from the initial sound waves, are imprinted in the overall matter distribution. To clarify this, Fig. 3.4 shows the evolution of the over-densities in the different energy components of the Universe. For simplicity let us consider a single over-density peak sitting on top of a homogeneous background Universe. This initial configuration is shown in the first graph in Fig. 3.4. The radial dark matter profile is centered around zero, whereas the relativistic components have already moved out due to the higher pressure in the over-density. The plasma of baryons and electrons is coupled to the photons. The plasma over-density continues to expand into the surrounding homogeneous Universe due to its pressure. At

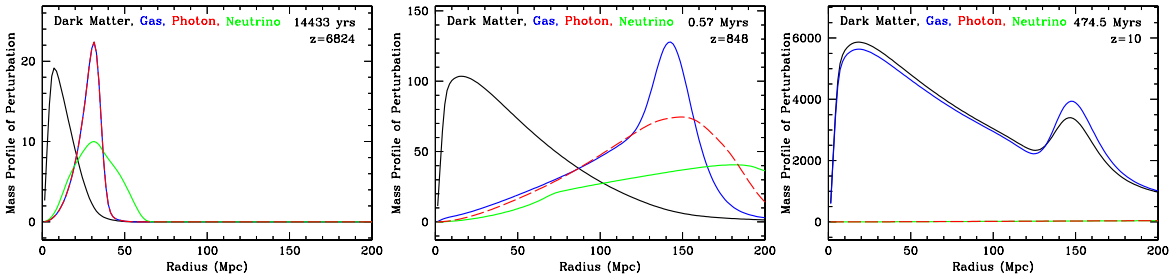

Figure 3.4. Simple model to explain the emergence of the baryon acoustic peak in the correlation function. The sequence follows the evolution of an over-dense peak in an otherwise homogeneous Universe. In the initial stage, the perturbation is the same for all energy density components. In the subsequent evolution the pressure drives out the relativistic components. When baryons and photons decouple, the baryons are left behind and form the characteristic over-density at the distance the sound wave had traveled before decoupling. In the later stages, the infall of matter on the over-density leads to a growth of the overall over-density. During the infall the baryon peak also collects dark matter and gets therefore imprinted in the overall matter density. Pictures from [65].

recombination photons and baryons decouple and only the photon over-density continues to be driven outwards. In the baryon component, the surviving peak of the density wave stays approximately at the scale that it had reached at the time of decoupling. In the following, gravitational instability leads to a spherically symmetric inflow of cold dark matter and baryons from the surrounding homogeneous Universe. This inflow feeds the overall growth of the over-density. As the homogeneous part is supposed to have the average decomposition of 4/5 dark matter and 1/5 baryons, in the end the peak that was mainly baryonic in the beginning has nearly the same ratio of dark to baryonic matter as the average Universe. Therefore the peak should be visible in all observations that probe the matter density profile.

Leaving this idealized situation, one can imagine the inhomogeneous primordial Universe to be made up of many such over-dense peaks. The result should therefore be an enhancement in the correlation function at the scale that corresponds to the radius that the sound wave had traveled outwards until the time of decoupling. This peak in the correlation function is then equivalent to wiggles in the power spectrum, because a localized feature in real space becomes an oscillatory feature in Fourier space. The existence of these BAO has first been detected in real space in [62] and the corresponding data is shown in Fig. 3.3. Besides the presentation in [61] from which Fig. 3.3 is taken, the oscillations in the power spectrum have been analyzed more recently for the entire SDSS sample in [66]. Also in the WiggleZ data, these BAO have been found [67].

The big advantage of these BAO is, that they specify a sharp scale in the otherwise smooth power spectrum/correlation function. As we can determine the primordial sound

speed with the CMB, the scale is known quite precisely. This makes BAO to a standard ruler for the determination of the angular diameter distance. In addition they can be probed in all eras of the Universe by measuring the matter correlation function at the respective time. This allowed [67] to put strong constraints on deviations of the distance redshift relation from the ΛCDM prediction.

We will examine in Sec. 5.4.2 how this determination could potentially be affected by inhomogeneities in the Universe, but find out that, on the scales probed by today's surveys, there seems to be no influence from inhomogeneously varying evolution histories.

3.2. Characterization of the structure in the SDSS

After the description of the methods that are used to characterize structure in the Universe and the short digression in the evolution history of matter perturbations, we will turn in this section to an analysis of the SDSS (luminous red galaxy (LRG)) data on large scale structure. There have been many studies with this data concentrating on the correlation function [62, 68, 60], the power spectrum [61], BAO [62, 69, 66], redshift space distortions [70, 71] and Minkowski functionals [48]. These latter approaches, however, mainly focused on the excursion set method and did not work with the boolean grain model. As this model works directly with the point distribution and does not pre-average the galaxy distribution to give smooth density contours, it is more directly related to the intrinsic properties of the distribution of the individual galaxies. Also the exact theoretical understanding of the behavior of the Minkowski functionals in the boolean grain model, expressed by Eqs. (2.39)–(2.40), demonstrates the usefulness of this model in addition to the previous approaches.

3.2.1. The luminous red galaxy data

The data that is used for the determination of the Minkowski functionals is provided by Kazin[1] [69]. It contains preprocessed SDSS data, selected with the following requirements: the galaxy has a SDSS spectrum, is not in an area around bright stars, has a sector completeness of at least 60%, a redshift in the range $0.16 - 0.47$ and a color- and k-corrected magnitude between -21.2 and -23.1. The details of the selection can be found in [69]. After this pre-selection, the sample contains $105,831$ LRGs. The distribution in the sky is shown in Fig. 3.5. Beside the main region with right ascension (ra) between $120°$ and $260°$ and a declination (dec) between $-5°$ and $70°$, there are three additional stripes in the southern hemisphere (in the opposite direction) and a small displaced patch in the northern sky. As we need a large connected volume for the analysis, we can only use the bulk. In order to have well defined angular boundaries we furthermore cut out a region with ra $\in [132°, 235°]$ and dec $\in [-1°, 60°]$. The resulting patch of the angular window is shown in Fig. 3.5. In addition to these selection processes we have to assure

[1] http://cosmo.nyu.edu/~eak306/SDSS-LRG.html

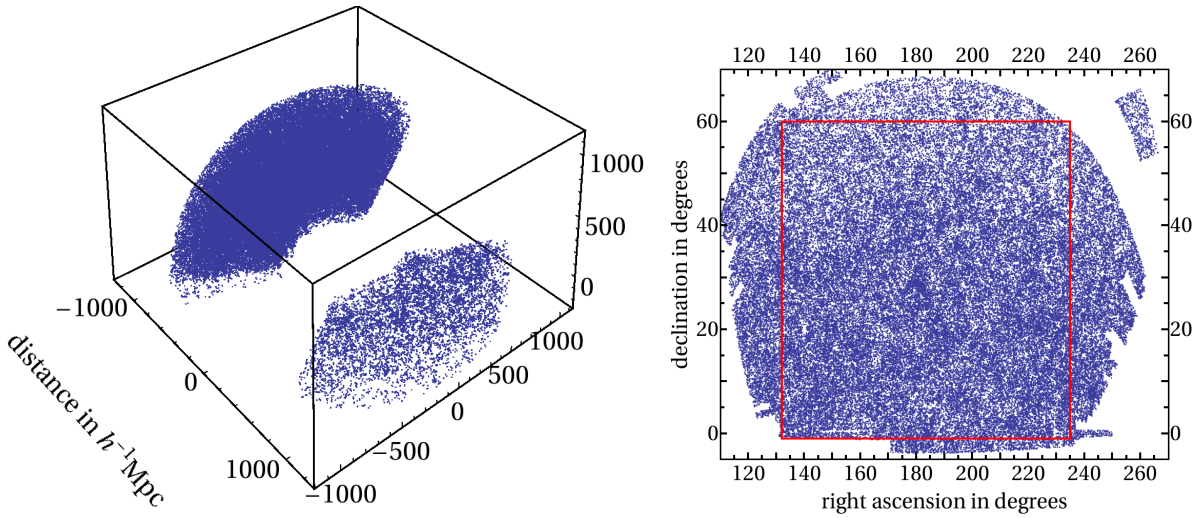

Figure 3.5. SDSS DR7 LRG sample analyzed using the Minkowski functionals. On the left hand side a projection on the full sample. We only use the connected left part. This part is shown on the right hand side. The red square shows the boundaries of the angular cut used.

that the sample is volume limited. As mentioned in [69], this is the case for galaxies that have a redshift below 0.35. The magnitude redshift distribution is shown in Fig. 3.6.

With these selections we arrive at a volume limited sample of 41, 375 LRGs in a redshift range of $z \in [0.16, 0.35]$. Unfortunately, the quality of the sample seems not to be very good as is shown in Fig. 3.6. For an ideal volume limited sample one would expect the average number density of galaxies to be constant with redshift. This is not the case here, where the density fluctuations in different shells vary by nearly 30%. This has already been demonstrated in the original use of this sample for [69]. However, as there is no way of a selection that would lead to a consistent homogeneous sample we will have to use the data as they are.

For comparison to the ΛCDM model the LasDamas project [72, 73] conducted a number of large scale structure N-body simulations[2] trying to model the distribution of the luminous red galaxies. We will use their mock samples in the next section for comparison and the estimation of errors.

To find the Minkowski functionals in position space, we finally convert the redshifts into comoving distances using the distance redshift relation of a ΛCDM model with $\Omega_\Lambda \approx 0.73$. This is done for the SDSS data as well as the mocks in the same way. Of course it would also be possible to consider the redshift space Minkowski functionals.

[2] Available at http://lss.phy.vanderbilt.edu/lasdamas/overview.html

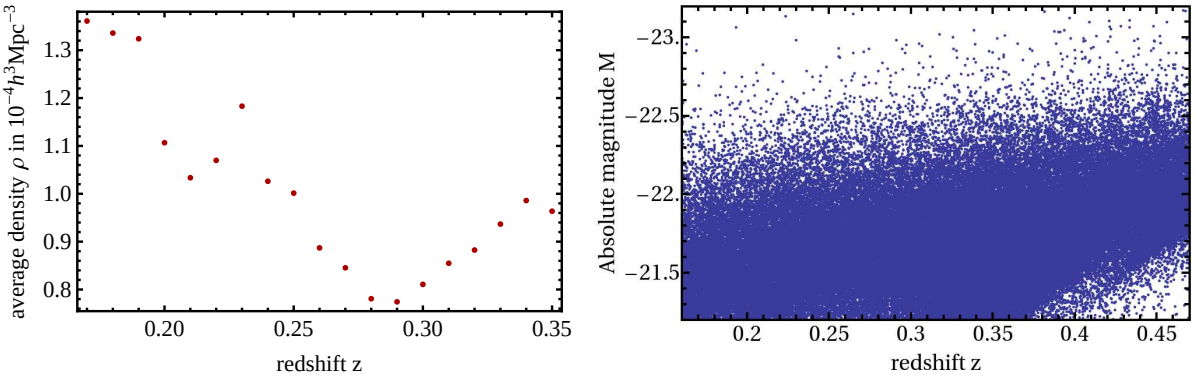

Figure 3.6. Number density in shells of constant thickness centered on the indicated redshifts. This shows, that the number density in the sample is not constant as would be expected from a perfect volume limited sample. Right: Magnitude redshift distribution of the galaxies in the sample. The sample is volume limited up to a redshift of 0.35.

3.2.2. The Minkowski functionals of luminous red galaxies

For the calculation of Minkowski functionals from the sample described in the previous section, we use a code written by Jens Schmalzing and Matthias Ostermann, advertised in [74]. The code was adapted to the problem regarding computational speed and inclusion of the boundaries chosen above. It uses the approximation described in [46] to efficiently calculate the Minkowski functionals of the boolean grain model. We normalize the results such that the maximal value of the theoretical functionals for a Poisson distribution corresponding to the measured sample density, is 1.

The result when applied to the selected 41,375 LRGs is shown in Fig. 3.7. The data points from the SDSS volume are clearly deviating from the Poisson case of a sample without structure. The Minkowski functionals for this case have been calculated using the formulae (2.39)–(2.40) and the sample density of $n = 9.59 \times 10^{-5} h^3 \mathrm{Mpc}^{-3}$. The blue band (consisting of three lines, the average and lines for $\pm$ the error) shows the result for the functionals averaged over 40 mocks. The fact that the band nature is nearly not visible signifies that the fluctuation in the Minkowski functionals of the simulated samples do not vary much. For the volume functionals the results of their determination from the data are marginally consistent with the ΛCDM mocks within the errors. In view of the small error bars, the deviations for the other Minkowski functionals are significant. As the functionals are very robust tracers of the morphology, the observed deviations would imply a very different morphology in the simulations and in the data. If this is due to a slightly different average densities in the mock samples as compared to the data sample, or if the simulations have other, more severe, problems remains to be seen.

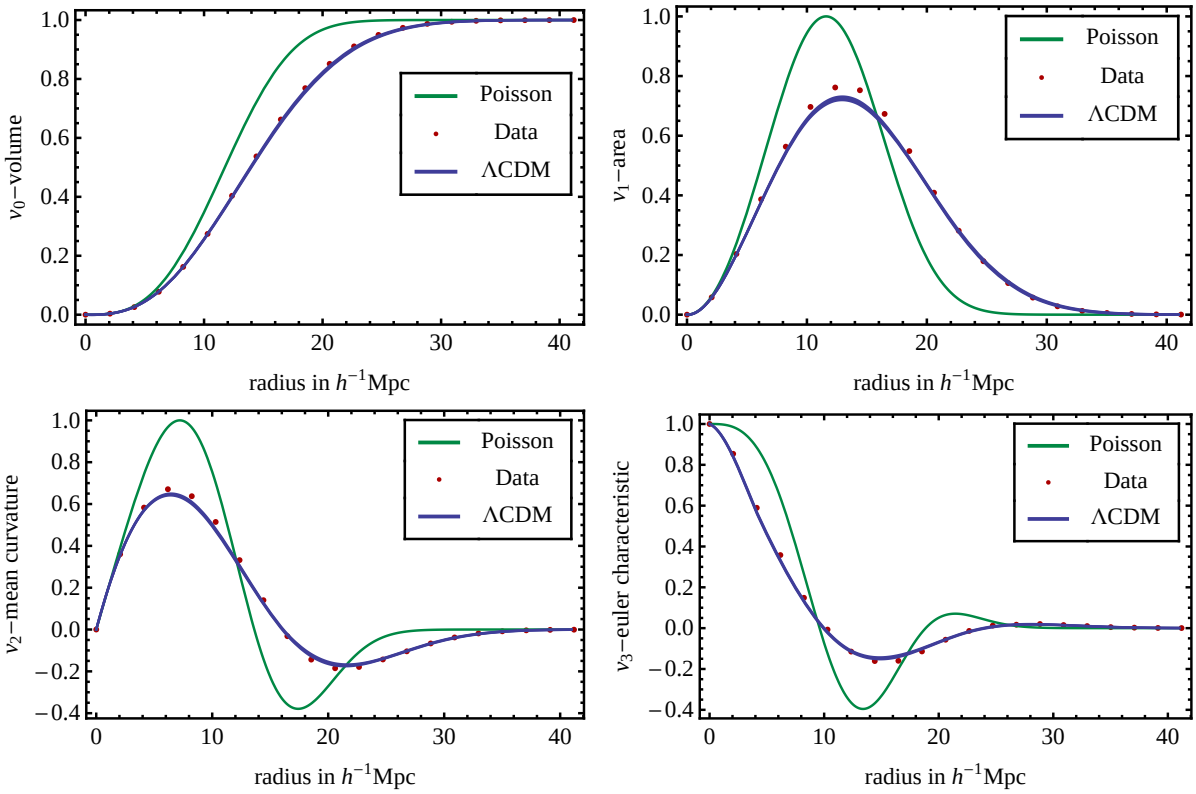

Figure 3.7. Minkowski functionals for the full volume limited region within our angular and redshift cuts. The green solid line gives the values of a pure Poisson point distribution for comparison. The blue solid bands are the Minkowski functionals for the ΛCDM model, as derived from the LasDamas simulation data [72, 73, 75]. The smallness of the band shows that the fluctuations between different realizations are not very large. The red data points derived from the observed sample are at best marginally consistent with the ΛCDM mocks.

Sample homogeneity To check for variations of the Minkowski functionals in different parts of the sample, which occur for example for the estimation of the correlation function [76, 60], we divide the sample into two mainly independent parts and calculate the resulting Minkowski functionals. The two regions are shown in Fig. 3.8. They are the maximal cubes that fit into the sample. The overlap of the two cubes is less than 20%. The choice is a compromise between sample size and independence. The number of points in each cube is approximately $10,000$. The surrounding spherical shells give the boundaries of the volume limited region we selected.

For the comparison of the two cubes, we first calculate the Minkowski functionals in the two cubes. From the result we subtract the average of the functionals determined from the mocks to emphasize deviations from this average, which consequently forms the zero line. The fluctuations of the functionals in the 40 simulated samples is taken to

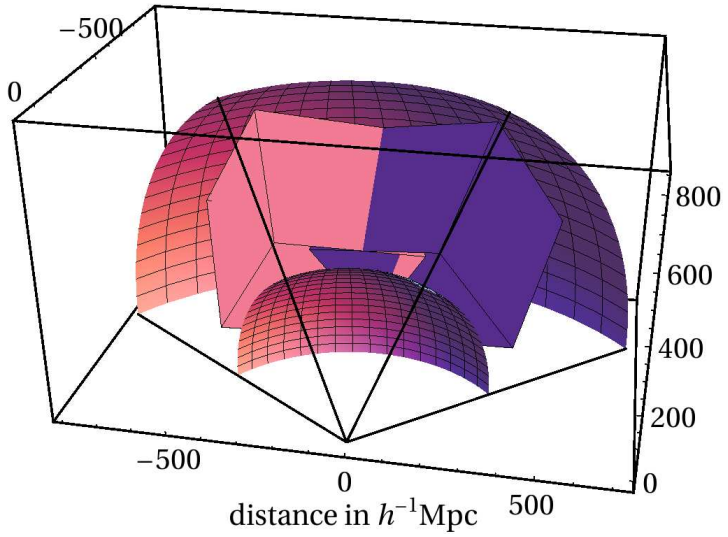

Figure 3.8. Position of the two maximal cubes used to separate the sample into two subsamples with a clear length scale. The "sails" give the $z = 0.16$ and $z = 0.35$ boundaries of our cut sample.

be a measure of the error. Therefore, it is attached to the data points to indicate their possible fluctuation. The result is shown in Fig. 3.9. It indicates that the ΛCDM model, which is the zero line, is consistent with the Minkowski functional data for both boxes. Also, the two boxes are consistent with each other, even if in some cases the other data points lie in the two sigma region of the errors rather than the one sigma region.

To see whether this conclusion holds true also for smaller sample size, we shrink the size of the cubes. For this test it is helpful to compare boxes, as we can attribute a certain scale to the sample size for which we determine the functionals. If we had divided the sample just in two equal wedges this correspondence would not be that clear.

Inspecting the distribution in the left cube, we arrive at the Minkowski functionals shown in Fig. 3.10. Again, the green solid line is the Poisson case. The blue band gives the average mock Minkowski functionals and the variance for 40 mocks. The lines are the connected data points for the cubes of the respective scale. The fact that the band nature of the blue line is clearer here shows, that the error has significantly increased by decreasing the sample size from 40,000 to 10,000 points.

As the density fluctuates more for the smaller sample we tried to account for this by renormalizing the functionals by a shift of scale $R \to R\left(\frac{\varrho_m}{\varrho_i}\right)^{1/3}$. Here ϱ_m is the global mean density and ϱ_i the density of the respective smaller cube. This removes the main effect of a modified density, namely the change in scale of the position at which the deviation from the Poisson case occurs. The problem however is, that it induces a small deviation in the scale of the correlation function that is probed. This may be seen in the

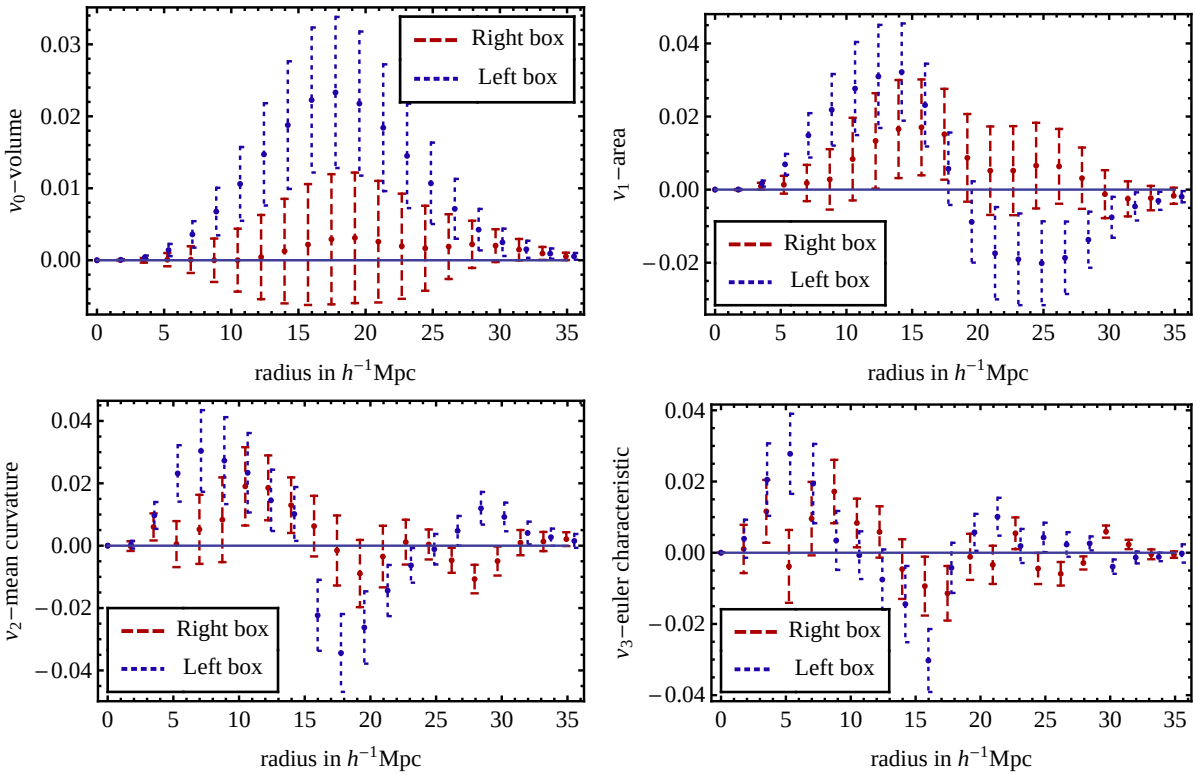

Figure 3.9. Check for consistency of the two cubic subsamples of Fig. 3.8. The data points show the value of the Minkowski functionals of the right and left cube respectively from which we have subtracted the average Minkowski functionals derived from the mock samples for the same cubes. The error bars are determined from the fluctuations between the 40 mock samples. The data of the two cubes are consistent with each other (within the errors) and with the ΛCDM model, represented by the zero line.

theoretical formula (2.40). Evaluating it for the volume Minkowski functional gives

$$\begin{aligned} \varrho_i \overline{V}_0(R) &= \frac{4\pi}{3}\varrho_i R^3 + \sum_{n=1}^{\infty} \frac{(-\varrho_i)^{n+1}}{(n+1)!} \times \\ &\times \int_{\mathcal{D}} \mathrm{d}^3x_1 \ldots \mathrm{d}^3x_n \mathrm{d}^3x \xi_{n+1}(x_1, x_{12}, \ldots)\, \theta(R - |\mathbf{x}|)\, \theta(R - |\mathbf{x} - \mathbf{x}_1|) \ldots . \end{aligned} \tag{3.1}$$

The volume of the intersection of the several balls has been expressed here by an integration over the θ-function $\theta(x)$ which is 0 for $x < 0$ and 1 for $x > 0$. The shift in

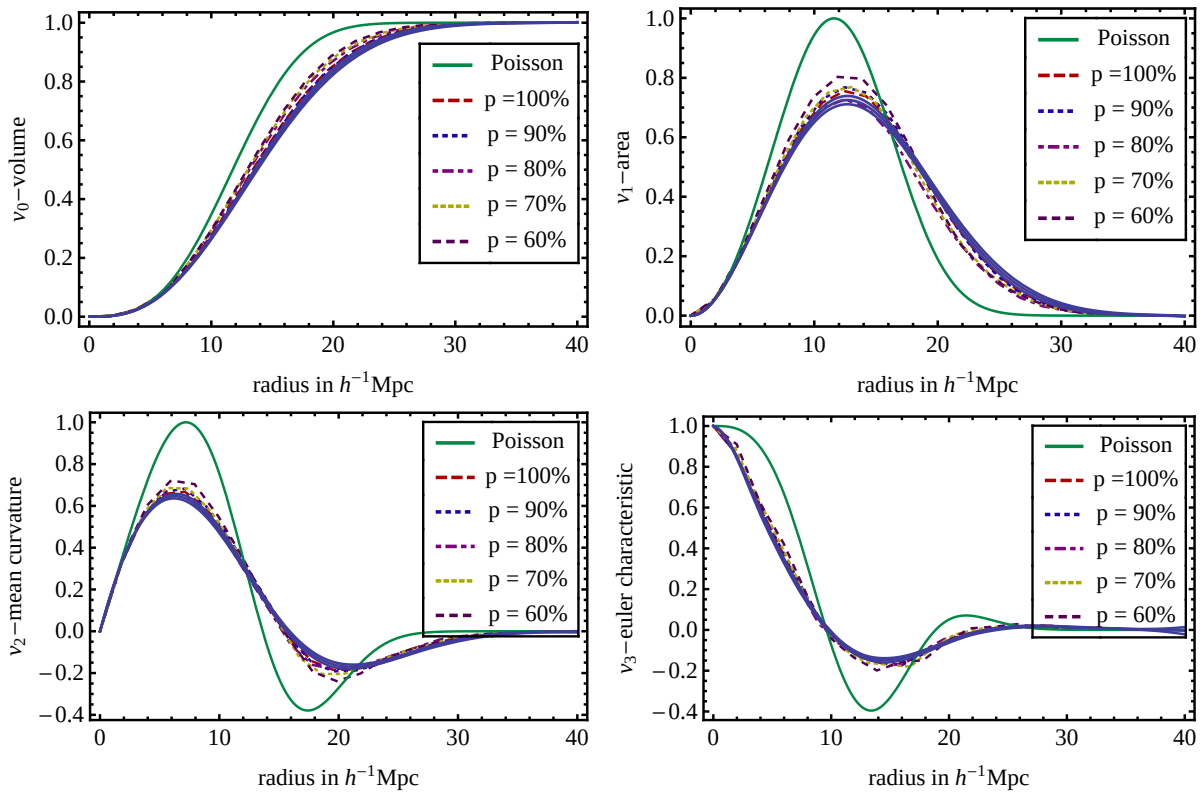

Figure 3.10. Comparison of the Minkowski functionals of the left cube for different scales. The dashed and dotted lines show the functionals for cubes that were obtained by shrinking all sides of the original cube with the factor indicated. In addition the Poisson case is shown in green and the band corresponding to the 100% cube is shown for 40 mocks. The fluctuation occurring for the smallest scales indicate that the precision is no longer very high when shrinking the box that much. However, all the smaller cubes lead to a very similar shape.

scale changes now the ϱ_i, but also induces a stretching in the correlation functions

$$\begin{aligned}\varrho_i \overline{V}_0(R) &= \frac{4\pi}{3}\varrho_m R^3 \\ &\quad + \sum_{n=1}^{\infty} \frac{(-\varrho_m)^{n+1}}{(n+1)!} \int_{\mathcal{D}} \mathrm{d}^3x_1 \ldots \mathrm{d}^3x_n \mathrm{d}^3x \xi_{n+1}\left(\left(\frac{\varrho_m}{\varrho_i}\right)^{\frac{1}{3}} x_1, \left(\frac{\varrho_m}{\varrho_i}\right)^{\frac{1}{3}} x_{12} \ldots\right) \\ &\quad \times\theta\left(\left(\frac{\varrho_m}{\varrho_i}\right)^{\frac{1}{3}} (R - |\mathbf{x}|)\right) \theta\left(\left(\frac{\varrho_m}{\varrho_i}\right)^{\frac{1}{3}} (R - |\mathbf{x} - \mathbf{x}_1|)\right) \ldots . \end{aligned} \tag{3.2}$$

For the distributions we are looking at, the shift induced in the correlation functions has a smaller effect on the value than the shift in scale. Therefore the transformation increases the comparability.

Indeed, if we look at Fig. 3.10, the results of the smaller boxes are quite similar to the global one. As also the error bars for the smaller boxes are larger than for the global box, the result looks quite consistent with the ΛCDM simulation for all the scales considered.

3.2.3. Deviations from Gaussianity

The Minkowski functionals for the boolean grain model may also be used as an indication for the non-Gaussianity of a point distribution. In the Gaussian case the expansion of Eq. (2.40) already ends at $n = 1$, because for a Gaussian distribution, all the cumulants (2.10) for $n > 2$ are zero. The only non-vanishing connected correlation function is therefore the two-point function, which means for the expansion (2.40) that it reduces to

$$\overline{V}_\mu = V_\mu(B) - \frac{\varrho_0}{2}\int_{\mathcal{D}} \mathrm{d}^3x_1 \xi_2(|\mathbf{x}_1|)\, V_\mu(B \cap B_{\mathbf{x}_1}) \ . \tag{3.3}$$

Therefore the Minkowski functionals of a Gaussian distribution are easy to determine when we know the functionals for the intersection of two balls. The intersection being a spherical lens, it is not very hard to find volume and surface. The integral mean curvature is given in [77] and so the corresponding functionals are

$$V_0 = \frac{1}{12}\pi(2R - r)^2(r + 4R) \ , \tag{3.4}$$

$$V_1 = \frac{1}{3}\pi R(2R - r) \ , \tag{3.5}$$

$$V_2 = \frac{1}{6}\sqrt{4R^2 - r^2}\left(\pi - 2\arccos\left(\frac{r}{2R}\right) + 4\sqrt{\frac{2R - r}{2R + r}}\right) \ , \tag{3.6}$$

$$V_3 = 1 \ , \tag{3.7}$$

where R is the radius of the balls and r is the integration variable corresponding to their distance. For $r > 2R$ all four Minkowski functionals are zero, as then the balls do no longer intersect. With this information, the integration (3.3) can be carried out if we know the correlation function of the sample.

It is interesting to note, that for the volume functional the first and only correction to the Poisson term simply consists of the matter fluctuations in a sphere $\sigma(R)$ as defined in (2.16). This can be seen if we express the volume functional of the intersection of spheres in Eq. (3.3) by an integration over two θ-functions like in the previous section. Eq. (3.3) becomes

$$\overline{V}_0 = \frac{4\pi}{3}R^3 - \frac{\varrho_0}{2}\int_{\mathcal{D}} \mathrm{d}^3x_1 \int_{\mathcal{D}} \mathrm{d}^3x \xi_2(|\mathbf{x}_1|)\, \theta(R - |\mathbf{x}|)\, \theta(R - |\mathbf{x} - \mathbf{x}_1|) \ . \tag{3.8}$$

With a change of variables from $\mathbf{x}_1 = \mathbf{x} - \mathbf{x}_2$ and assuming that $\mathcal{D}$ is large enough, this leads to

$$\overline{V}_0 = \frac{4\pi}{3}R^3\left(1 - \frac{\frac{4\pi}{3}R^3\varrho_0}{2}\frac{1}{\left(\frac{4\pi}{3}R^3\right)^2}\int_{\mathcal{D}} \mathrm{d}^3x_2 \int_{\mathcal{D}} \mathrm{d}^3x \xi_2(|\mathbf{x}_2 - \mathbf{x}|)\, W_R(\mathbf{x}_2)\, W_R(\mathbf{x})\right)$$

$$= \frac{4\pi}{3} R^3 \left(1 - \frac{\frac{4\pi}{3} R^3 \varrho_0}{2} \sigma^2 (R) \right) , \tag{3.9}$$

by the definition (2.19). Here, $W_R(\mathbf{x})$ is again the window function for a ball of radius R, i.e. $\theta(R - |\mathbf{x}|)$. This shows how the volume Minkowski functional is directly related to the fluctuations in the density field. For the higher functionals there is no such direct correspondence to other quantities, but they are also quite simple. $\overline{V}_3$ for example is just

$$\overline{V}_3 = 1 - 2\pi\varrho_0 \int_0^{2R} \xi_2(r)\, r^2 \mathrm{d}r \, . \tag{3.10}$$

We want to compare these theoretical functionals to the data for a distribution that is still close to a Gaussian distribution. To this end, we use a slice of the very large simulation (VLS) of the Virgo consortium [78] at a redshift of $z = 5$. This simulation contains 512^3 dark matter points in a cube of side-length $479h^{-1}$Mpc. We randomly select $100,000$ of these points. For these we estimate the correlation function and the density fluctuations in spheres σ.

For the estimation of the correlation function we use two different estimators: The Davis-Peebles (DP) estimator and the Landy-Szalay (LS) estimator as described in [79, 80, 44, 60]. Both estimators are based on counting neighbours at certain distances. Besides the data points D they also need a random sample with the same survey geometry. In this case we just create a cube of Poisson points. The correlation function is estimated by

$$\xi_E^{DP}(r) = \frac{2N_R}{N_D - 1} \frac{DD(r)}{DR(r)} - 1 \tag{3.11}$$

where $DD(r)$ is the number of data-data distances in the interval $[r - \Delta/2, r + \Delta/2]$. $DR(r)$ are the data-random distances in the same interval and N_D and N_R are the total number of data and random points respectively. The more refined LS estimator is based on the same principle of pair counting, and uses the prescription

$$\xi_E^{LS}(r) = \frac{N_R(N_R - 1)}{N_D(N_D - 1)} \frac{DD(r)}{DR(r)} - 2\frac{N_R - 1}{N_D} \frac{DR(r)}{RR(r)} + 1 \tag{3.12}$$

where $RR(r)$ obviously is the number of random-random distances that lie in the $[r - \Delta/2, r + \Delta/2]$ interval. As discussed in [60], the fact that this estimator is the minimal variance estimator for a Poisson distribution (as shown in [80]), does not mean that it is necessarily also more efficient when applied to other distributions (see also [44]). Therefore we will show the results for both estimators.

To find an estimate of σ, we simply apply the defining formula (2.16), i.e. we count for $10,000$ random locations in the sample how many points N lie in a sphere of a certain radius R. Then we calculate the fluctuations in the number of points for each radius by the formula

$$\sigma_{SPP}^2(R) = \frac{\overline{N^2(R)} - \overline{N(R)}^2}{\overline{N(R)}^2} , \tag{3.13}$$

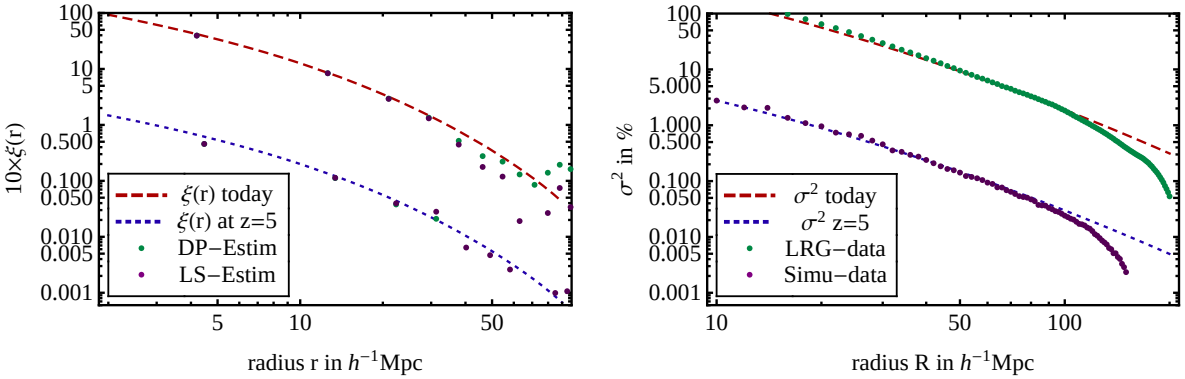

Figure 3.11. Estimation of the correlation function and the matter fluctuations from the analyzed samples. On the left hand side the result of an estimation of the correlation function of the LRG sample and a slice of the VLS at $z = 5$. The estimation is done using the DP and LS estimator that yield consistent results on the relevant scales. On the right hand side an estimation of σ^2 from the same samples. The deviation for large scales is spurious and due to finite size effects. The lines give the best fit two both samples using the shape of the ΛCDM power spectrum as given in Eq. (2.112).

where the ensemble average $\overline{O}$ is over the sample of $10,000$ random locations. As we are in the discrete case of a stochastic point process (SPP), σ^2 has an additional shot noise term. We have to subtract this term before we find the continuous σ^2 we need. The shot noise contribution to σ^2 is just $1/(\varrho V_R)$ where V_R is the volume of the sphere of radius R. More explicitly

$$\sigma^2_{SPP}(R) - \frac{1}{\varrho_0 V_R} = \frac{1}{V_R^2}\int_{\mathcal{D}} \mathrm{d}^3x_1 \int_{\mathcal{D}} \mathrm{d}^3x_2 \xi_2(|\mathbf{x}_1 - \mathbf{x}_2|) W_R(\mathbf{x}_1) W_R(\mathbf{x}_2) = \sigma^2(R) \quad (3.14)$$

as given by Eq. (2.19).

The results for the estimation of both quantities, σ and ξ, for the VLS [78] are shown in Fig. 3.11 as the points around the blue dotted curve. The curve is determined using the ΛCDM power spectrum given in Eq. (2.112). From this spectrum we calculate the correlation function and the density fluctuations and adjust the overall normalization such that it fits the data. For the case of the simulation data, the result for the normalization corresponds to a σ_8 today of $\sigma_8(a = 1) = 0.9$, which is what was plugged into the simulation. As Fig. 3.11 shows, this gives an acceptable fit for both, ξ and σ. Note, that for ξ the two estimators give the same result for nearly all points in the range of interest. For σ we have extended the plot range to larger values of R to demonstrate from which scale on the results become limited by the size of the sample. That this effect occurs is due to the fact that for larger and larger radius there are less and less independent spheres in the sample. At around $100h^{-1}$Mpc, which corresponds roughly to spheres with a diameter of 41% of the sample, the mutual dependence of the points of different

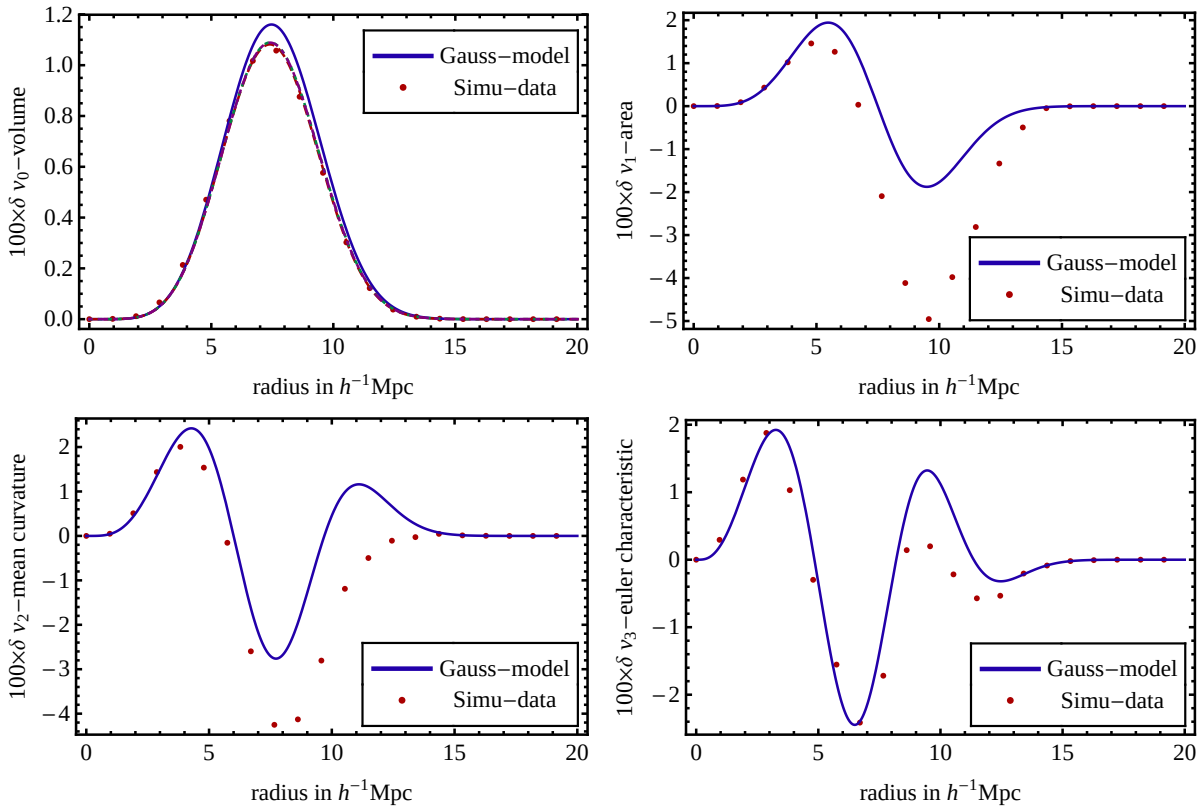

Figure 3.12. Comparison of the Minkowski functionals of the $z = 5$ slice of the VLS with the ones derived from (2.39), (2.40) under the assumption of a Gaussian distribution, i.e. Eq. (3.3). In all cases we subtracted the functionals from the Poisson Minkowski functionals (corresponding to the green solid line in Fig. 3.7), to emphasize the effect. For the volume functional we also added the higher order results for a Log-Normal distribution. The data show already for this small redshift a clear deviation from the Gaussian case. It is most prominent in the higher functionals v_1 and v_2.

spheres tends to equalize their number. Therefore, the fluctuation from sphere to sphere is suppressed with respect to the true value. Supposedly this true value is given by the dotted line determined using the theoretical power spectrum.

With this properly normalized spectrum we calculate the theoretical expectations for the Minkowski functionals in the case of a Gaussian distribution. Fig. 3.12 shows them together with the data determined from the same sample of 100, 000 points for which we estimated ξ and σ above. The plot shows the deviation of the Minkowski functionals from the corresponding case of a Poisson distribution. It is interesting to see, that even at this early stage, the distribution deviates significantly from a Gaussian one. As we have only one sample we cannot estimate the errors like above using mock catalogs. However, the values for the 40, 000 points in the previous section indicate that for the larger sample of

100,000 and for a smaller absolute magnitude of the correlation function, the deviation observed is not due to a statistical fluctuation.

To demonstrate that this is the case and that we can explain the deviation by a theoretical model we calculated the effect of higher orders in the series expansion (2.40). To be able to do this we chose a log-normal distribution as hypothesis, which will be justified in 4.5.2. It resembles the Gaussian distribution described in Sec. 2.1.1, but has as probability distribution in the discrete case (2.28) the form

$$p\left(\left\{\varrho\left(\mathbf{r}_i;\Delta V\right)/\varrho_0\right\}\right) = B\left(\varrho\left(\mathbf{r}_i;\Delta V\right)/\varrho_0\right) e^{-\frac{1}{2}\sum_{i,j}(\log(\varrho(\mathbf{r}_i;\Delta V)/\varrho_0)-\mu_i)A_{ij}(\log(\varrho(\mathbf{r}_j;\Delta V)/\varrho_0)-\mu_j)} . \tag{3.15}$$

For a single cell, without the correlation to other cells encoded in A_{ij}, the distribution is

$$p\left(\varrho/\varrho_0\right) = \frac{1}{\left(\varrho/\varrho_0\right)\sqrt{2\pi\sigma^2}} e^{-\frac{1}{2\sigma^2}\left(\log(\varrho/\varrho_0)-\mu\right)^2} , \tag{3.16}$$

with mean

$$\mathbb{E}\left[\varrho/\varrho_0\right] = e^{\mu+\frac{\sigma^2}{2}} \tag{3.17}$$

and variance

$$\mathbb{E}\left[\left(\varrho/\varrho_0\right)^2\right] - \mathbb{E}\left[\varrho/\varrho_0\right]^2 = \left(e^{\sigma^2}-1\right) e^{2\mu+\sigma^2} . \tag{3.18}$$

As we need the cumulants (2.10) we have to determine the joint expectation values of several variables. This gives

$$\mathbb{E}\left[\prod_{i\in B} X_i\right] = e^{\sum_i \mu_i + \frac{1}{2}\sum_{ij} A^{-1}_{ij}} , \tag{3.19}$$

where the X_i are again the distributions of the i-th cell, $X_i = \hat{\varrho}\left(\mathbf{x}_i\right)/\varrho_0$ and A^{-1}_{ij} are the elements of the inverse matrix to the matrix A. The sums in the exponents run over the indices corresponding to the X_i in the product $\prod_{i\in B} X_i$. For the first two expectation values this means

$$\mathbb{E}\left[X_1\right] = e^{\mu_1+\frac{1}{2}A^{-1}_{11}} , \tag{3.20}$$

$$\mathbb{E}\left[X_1 X_2\right] = e^{\mu_1+\mu_2+\frac{1}{2}A^{-1}_{11}+A^{-1}_{12}+\frac{1}{2}A^{-1}_{22}} . \tag{3.21}$$

With (2.10), this leads to the second cumulant

$$\kappa\left(X_1, X_2\right) = e^{\mu_1+\mu_2+\frac{1}{2}A^{-1}_{11}+\frac{1}{2}A^{-1}_{22}}\left(-1+e^{A^{-1}_{12}}\right) = \tilde{\xi}\left(\mathbf{x}_{12}\right) . \tag{3.22}$$

This means that unlike in the Gaussian case, the relation of the matrix elements A^{-1}_{ij} to the correlation function of the density field is no longer given by (2.29), but rather by

$$A^{-1}_{ij} = \log\left(1+\tilde{\xi}\left(\mathbf{r}_i,\mathbf{r}_j\right)\right) . \tag{3.23}$$

This modified dependence on $\tilde{\xi}$ comes from the fact that the over-density field $X_i = \hat{\varrho}\left(\mathbf{x}_i\right)/\varrho_0$ has as its average the value 1. So $\mathbb{E}\left[X_1\right] = 1$ and (3.20) fix the parameter

μ_i in the distribution (3.15) to be $\mu_i = -\frac{1}{2}A_{ii}^{-1}$. This directly leads to (3.23) for the components of A_{ij}^{-1}.

With these two conditions all parameters of the distribution (3.15) are fixed. Using (3.19) and (2.10) we can now calculate in principle all higher connected correlation functions for a multivariate log normal distribution having a given two-point correlation function. In practice however this quickly leads to long expressions, because of the rapid increase of the combinatorial component, the number of partitions B needed in Eq. (2.10). Therefore we are limited to the connected correlation functions up to ξ_5.

Using the ξ's constructed in this way we can evaluate the series (2.40) up to an index $n = 4$. However, this is not possible for all four Minkowski functionals. For V_1 and V_2 the problem is to determine the values of the intersection of three balls $V_\mu\left(B \cap B_{\mathbf{x}_1} \cap B_{\mathbf{x}_2}\right)$. While this is straightforward for V_0 and V_3 for the other two functionals this would imply the search for suitable parametrizations of the body resulting from the intersection. Especially for V_3 this would be hard in view of the complicated expression (3.6) for V_2 for two balls. This is why we restrict ourselves to the calculation of the higher order terms for V_0.

The result of the inclusion of these higher order terms for the sample drawn from the VLS is shown in the first plot of Fig. 3.12. In addition to the Gaussian component (3.9) the other three lines show the result for v_0 when including terms in the sum (2.40) up to $n = 4$. The first correction to the Gaussian result by $n = 2$ is still quite large, whereas the following corrections are small enough that they do not lead to a visible shift in the curve.

To investigate a case where also the higher corrections make a difference, we apply the whole procedure to another slice of the VLS, one with $z = 2$. The estimation of the correlation function gives a normalization to $\sigma_8\left(a = 1\right) = 0.87$. With this correlation function measured from the particular sample under consideration, we find the curves shown in Fig. 3.13. They show a big first correction to the Gaussian result and smaller corrections for the $n = 3$ and $n = 4$ terms. The correlation function amplitude seems to be small enough to still lead to a rapid convergence.

This is no longer the case for the Universe today. For the SDSS LRG sample one of the necessary conditions for having a Gaussian point process, i.e. $\varrho \int_A d\mathbf{y}\xi_2\left(|\mathbf{y}|\right) \leq 1$, is no longer satisfied (see [81] for a discussion of these conditions). Therefore it is clear that we will need higher order correlation functions. Under the assumption that the distribution is not a Gaussian, but a log normal one, we arrive at the corrections shown in Fig. 3.14. For this plot we use again the SDSS LRG sample and in particular the left one of the boxes of Fig. 3.8. From the $10,000$ galaxies contained in this sample we determine v_0, which was already shown in Fig. 3.10. We subtract the Poisson values and arrive at the points in Fig. 3.14. The determination of the normalization of the correlation function needed for the calculation of the theoretical functionals gives a $\sigma_8\left(a = 1\right) = 1.5$. The result of the fit is shown in Fig. 3.11. Compared with the dark matter particles in the VLS, this means that the luminous red galaxies have a strong bias of $b = 1.7$. Using the fitting formula (2.112) of the power spectrum to derive the connected correlation

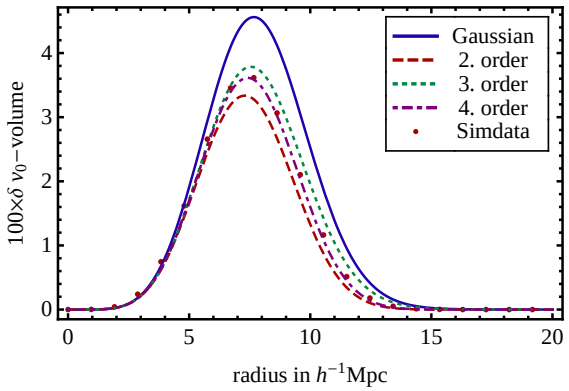

Figure 3.13. Comparison of the volume Minkowski functional of the VLS at $z = 2$ with the ones derived under the assumption of a Log normal distribution. We subtracted the Poisson case to make the deviations more visible. Unlike in Fig. 3.12, the higher order terms now produce sizable corrections.

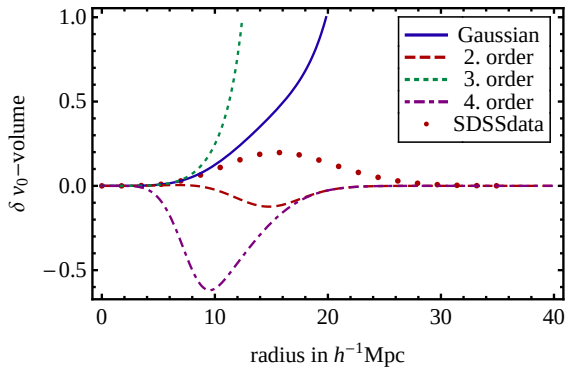

Figure 3.14. Same as Fig. 3.13 but for the SDSS LRG sample, i.e. the actual structure at a redshift of $z = 0$. The corrections stemming from the log normal distribution are now too large to give convergence already for a small number of terms.

functions up to ξ_5 we finally find the curves in Fig. 3.14.

This shows that the distribution of LRGs is not only strongly non-Gaussian, but also that the higher order terms in (2.40) are too large to give the convergence value already by an expansion that uses only the first terms of the series. Like for the series of the exponential function it resembles, one would have to calculate the terms until the factor $(n + 1)!$ is important enough to lead to a converging behavior. Unfortunately this is beyond the computational capacities at hand and therefore we will not know if the late Universe would also have been describable by the assumed log normal distribution.

In any case the examples in this section demonstrate the usefulness of Minkowski functionals for today's Universe as they contain all of the higher order correlation functions.

4. Backreaction of structure on the expansion of the Universe

So far, we discussed the standard picture of structure formation in the Universe. It is based on the assumption that the Einstein equations (1.1) would be valid on average, i.e. if we use them for a homogeneous and isotropic matter source and an "average metric" in form of the FRW metric (1.2). That this is not necessarily true was perhaps most clearly discussed by Ellis in 1983 [7]. There, he investigated the different possibilities for the scales at which the Einstein equations would be valid. He concluded, that the reasonable assumption that they are local equations for the full inhomogeneous metric would lead to the emergence of effective terms. They would arise from the smoothing procedure that allows the description of the larger scales. Since then, and especially after being related to the dark energy problem by [14], there has been a lively debate on whether those corrections would be important or not. The debate has led to a Focus issue of Classical and Quantum Gravity with the interesting contributions [82, 83, 84, 85, 86, 87, 88, 89, 19, 90].

The problem is known under the name of "cosmological backreaction" and has been analyzed mainly within cosmic perturbation theory as introduced in Sec. 2.2. The main result in this perturbative framework was of course that the corrections are perturbatively small and of the order of a 10^{-5} contribution to the cosmic energy budget at the Hubble scale. Some of these perturbative approaches may be found in [11, 14, 15, 16, 17, 12, 13]. However, there have also been doubts concerning the validity of perturbation theory in the late Universe [20]. Once standard perturbation theory breaks down at first order, all other orders become important as well. So there is no indication on the final result from the low order terms. Recently, people have tried to overcome this problem by using a gradient expansion technique that breaks down order by order [91].

All of these perturbative approaches, however, assume that the Universe is describable by the split into a background that is independent of the inhomogeneities and small perturbations to this background. This can only be true on large scales, where, following Ellis, we do not know the precise form of the Einstein equations due to the correction terms arising from the smoothing. This indicates that perturbation theory might not be the best tool for a proof that the corrections when going to the large, homogeneous scales, are negligible. Therefore, there have been attempts to address the problem in non-perturbative frameworks [92, 23, 28, 27, 29, 25, 26]. However, this is in most cases highly speculative, as the complexity of the problem requires simplifying assumptions that may be even less justified than the assumption of the split into background and small perturbation. This means that they can at best be regarded as toy models.

In the present chapter we want to contribute a new analysis to the discussion both in the perturbative and non-perturbative case. The perturbative analysis will have advantages over the standard framework, because for a given perturbative order it may describe systems with a higher degree of nonlinearity. The non-perturbative model will shed some light on one of the toy models discussed previously in the literature. We start by introducing in Sec. 4.1 the specific averaging framework that we will use. Sec. 4.2 discusses the technical realization of the perturbative approximation we employ. Sec. 4.3 gives the results of the calculation of the effects of inhomogeneities in this approximation and Sec. 4.4 presents the quantitative results. Finally Sec. 4.5 discusses connections to other calculations in the literature. Sections 4.2 to 4.4 contain parts that will be published in [40].

4.1. Averaging in an inhomogeneous Universe

As mentioned above, there is at present no consensus on the question whether or not effective terms that arise from a smoothing of small scale inhomogeneities, would be large enough to make a significant contribution to the overall evolution history of the Universe. Analogously, there is also no consensus on what smoothing technique would be the right one to address this question. The complete solution to the problem would involve the construction of a sort of "average tensor" on an average space-time manifold, giving an explicit meaning to the FRW background that is postulated to describe this smoothed out state. The main difficulty in doing this is, that two tensors cannot be compared if they are given at two separate space-time positions. So to average them, they have to be transported to the same location. This is difficult to describe unambiguously.

In this line there have been several attempts to the averaging of tensors on general space-times, e.g. by Zalaletdinov [8, 9] or Carfora [10, 93]. Unfortunately, due to the difficulty of the problem, they all have conceptual problems and often introduce complications that make it hard to derive reliable predictions for the effects under consideration here. Therefore, we will constrain ourselves to the conceptually easiest way of capturing the departure from homogeneity in these emerging correction terms. For the sake of definiteness, we will also neglect a number of influences that contribute to the correction terms, but that are to hard to implement in this context. This means that the idealized situation here may be altered by future more refined treatments, but it will describe effects that are definitely part of the problem. It may therefore be seen as a first step in the resolution of the full problem.

4.1.1. The Buchert Equations

The simplified framework that we are working in is sometimes called the Buchert framework of averaging [94, 95, 32]. It circumvents the problems of the more general tensor averaging frameworks by concentrating on scalar quantities. They have the

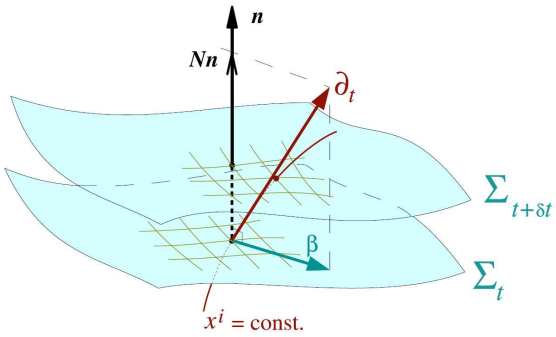

Figure 4.1. Split of the space-time into time orthogonal hypersurfaces Σ. The "distance" between the surfaces can be scaled by the lapse N. The coordinate grid on two different surfaces may be displaced by the shift vector $\vec{\beta}$. For comoving dust one can choose $N = 1$ and $\vec{\beta} = 0$. Picture from [96].

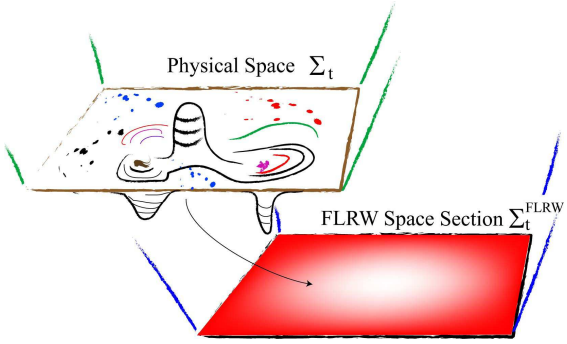

Figure 4.2. Sketch of relativistic structure formation. As the coordinate grid is comoving, there is no motion of particles within the spatial hypersurfaces. Over- and underdensities are therefore only created by curving these hypersurfaces. When passing to the Friedmannian picture, we assume that the internal curvature averages to zero and the external curvature averages to $K = \dot{a}/a$. Picture from [97].

advantage that they can be compared at different positions. Therefore, defining an averaging process for them is straightforward. As they are a special case of the more general tensors, all more refined theories will have to include them in the same way as presented here, at least in the limit of the approximations made. Luckily, it is also the scalar part that is most interesting for cosmology, so we can go quite far despite this restriction.

To define the scalar quantities that we want to average, the Buchert approach uses a specific form of the Arnowitt-Deser-Misner (ADM) formalism to split the four metric into a temporal and a spatial component

$$ {}^4\mathbf{g} = -dt^2 + {}^3\mathbf{g} \;\; ; \;\; {}^3\mathbf{g} = g_{ab}\, dX^a \otimes dX^b \; . \tag{4.1} $$

This split is adapted to the situation in cosmology where we want to describe a "time evolution" from the "beginning" until "today". The time that is used here is the proper time of the observer. To be able to perform this split we have to assume that the cosmic fluid is rotation-less, because any rotation would prevent us from finding an unambiguous foliation of space-time. Of course this is a strong restriction and it is questionable, if the late Universe may still be described by such an approximation. In addition to the restriction to a non-rotating fluid, we will also only consider the effect of the non-relativistic matter component that is pressureless and therefore often called "dust". As dark matter seems to make up a large fraction of the matter in the Universe,

this should capture the main effect.

With these restrictions, (4.1) is a foliation into spatial hypersurfaces of constant cosmic time, where cosmic time is now defined in the restframe of the dust fluid that makes up the Universe. This is sketched in Fig. 4.1. t is a label for a given spatial three hypersurfaces of constant cosmic time. So, the time direction is orthogonal to the hypersurfaces. The coordinate system in the three hypersurfaces is attached to the cosmic fluid and therefore called comoving. In this description galaxies do not have peculiar velocities, because the whole effect of structure formation is described by matter curving the spatial manifold. The two types of curvature that arise during this process are extrinsic curvature K and intrinsic Ricci curvature R. The situation is sketched in Fig. 4.2.

The extrinsic curvature is defined as[1]

$$K_{ij} := -u_{\mu;\nu} h^{\mu}{}_{i} h^{\nu}{}_{j} \ , \tag{4.2}$$

where u_μ is the four velocity of the fluid and $h_{\mu\nu}$ is a projector into the three hypersurface of constant cosmic time. As we are only considering dust and our spatial coordinates are comoving, $n_\mu = u_\mu = (-1, 0, 0, 0)$ where n_μ is the direction perpendicular to the spatial hypersurface. The projectors are $h_{\mu\nu} := g_{\mu\nu} + n_\mu n_\nu$.

Written in these coordinates and for a dust fluid, Einstein's equations (1.1) simplify to a set of evolution equations for the dynamical quantities

$$\dot{\varrho}\,(X,t) = K\varrho\,(X,t) \ , \tag{4.3a}$$
$$\partial_t g_{ij} = -2 g_{ik} K^{k}{}_{j} \ , \tag{4.3b}$$
$$\partial_t K^{i}{}_{j} = K K^{i}{}_{j} + \mathcal{R}^{i}{}_{j} - (4\pi G \varrho\,(X,t) + \Lambda)\,\delta^{i}{}_{j} \ , \tag{4.3c}$$

supplied by a set of constraint equations

$$\frac{1}{2}\left(\mathcal{R} + K^2 - K^{i}{}_{j} K^{j}{}_{i}\right) = 8\pi G \varrho\,(X,t) + \Lambda \ , \tag{4.3d}$$
$$K^{i}{}_{j\|i} - K_{|j} = 0 \ . \tag{4.3e}$$

$\mathcal{R}$ is the Ricci curvature of the spatial hypersurface and $\|i$ and $|j$ denote the covariant and the partial three derivative respectively.

To switch from the geometrical description to a maybe more familiar one in terms of kinematical quantities, one can express the extrinsic curvature tensor in terms of the expansion tensor of the fluid by

$$K_{ij} := -u_{\mu;\nu} h^{\mu}{}_{i} h^{\nu}{}_{j} \quad \rightarrow \quad -K_{ij} = \Theta_{ij} = \sigma_{ij} + \frac{1}{3}\theta g_{ij} \ . \tag{4.4}$$

In this form, the expansion tensor Θ_{ij} only captures the symmetric part of the decomposition of the fluid velocity gradient into its symmetric and antisymmetric component

[1] As usual Latin indices denote coordinates in three space, Greek indices those of the four dimensional space-time. The semicolon ; denotes the covariant four derivative.

$u_{\mu;\nu} = u_{(\mu;\nu)} + u_{[\mu;\nu]}$. However, Θ_{ij} contains the whole evolution of the fluid, because we do not allow for rotations and so $u_{[\mu;\nu]}h^{\mu}{}_{i}h^{\nu}{}_{j} = 0$. In its decomposition (4.4), Θ_{ij} divides into the local expansion rate $\theta = \theta(X,t)$ and the traceless shear σ_{ij} of the fluid. From σ_{ij} one constructs the shear scalar $\sigma^2 = \frac{1}{2}\sigma^{ij}\sigma_{ij}$.

With these replacements, the system of ADM equations in terms of the kinematical quantities reads,

$$\begin{aligned}
\frac{1}{2}\mathcal{R} + \frac{1}{3}\theta^2 - \sigma^2 &= 8\pi G\varrho + \Lambda \,, && (4.5a)\\
\sigma^{i}{}_{j\|i} &= \frac{2}{3}\theta_{|j} \,, && (4.5b)\\
\dot{\varrho} &= -\theta\varrho \,, && (4.5c)\\
\partial_t g_{ij} &= 2g_{ik}\sigma^{k}{}_{j} + \frac{2}{3}\theta g_{ij} \,, && (4.5d)\\
\partial_t \sigma^{i}{}_{j} &= -\theta\sigma^{i}{}_{j} - \mathcal{R}^{i}{}_{j} + \left(4\pi G\varrho - \frac{1}{3}\theta^2 - \frac{1}{3}\dot{\theta} + \Lambda\right)\delta^{i}{}_{j} \,, && (4.5e)
\end{aligned}$$

which still is completely equivalent to the Einstein equations for irrotational dust. It is therefore valid for arbitrary densities ϱ and so still describes the fully inhomogeneous evolution. Therefore, these equations are a good starting point for the derivation of an average cosmology. So the next step will be to define the average we use.

The averaging procedure As mentioned above, the process of averaging is in this restricted case much simpler than in the general tensorial case. For a three scalar $f(t,X)$ we define it as

$$\langle f\rangle_{\mathcal{D}}(t) := \frac{\int_{\mathcal{D}} f(t,X)\,\mathrm{d}\mu_g}{\int_{\mathcal{D}}\mathrm{d}\mu_g} \;;\; \mathrm{d}\mu_g := \sqrt{{}^{(3)}g(t,X)}\mathrm{d}^3X \,, \tag{4.6}$$

where $\mathcal{D}$ is a comoving domain on the spatial hypersurfaces with the volume $V_{\mathcal{D}} = \int_{\mathcal{D}}\mathrm{d}\mu_g$. Unlike in the usual case, where a volume average is defined with respect to a fixed background, the introduction of the Riemannian volume element $\mathrm{d}\mu_g$ implies that in this case, the dynamical background evolution plays a role. A direct consequence is that the volume expansion rate, related to the metric by

$$\theta(t,X) = \sqrt{{}^{(3)}g(t,X)}^{-1}\partial_t\left(\sqrt{{}^{(3)}g(t,X)}\right) \,, \tag{4.7}$$

is also position dependent for a general inhomogeneous metric ${}^{(3)}g(t,X)$. When we take the time derivative of Eq. (4.6)

$$\partial_t\langle f\rangle_{\mathcal{D}} = \langle\partial_t f\rangle_{\mathcal{D}} + \langle f\,\theta\rangle_{\mathcal{D}} - \langle f\rangle_{\mathcal{D}}\langle\theta\rangle_{\mathcal{D}} \,, \tag{4.8}$$

we immediately find that this influences the average. The time evolution of the average is no longer the same as the average of the time evolved quantity f. Or to put it short:

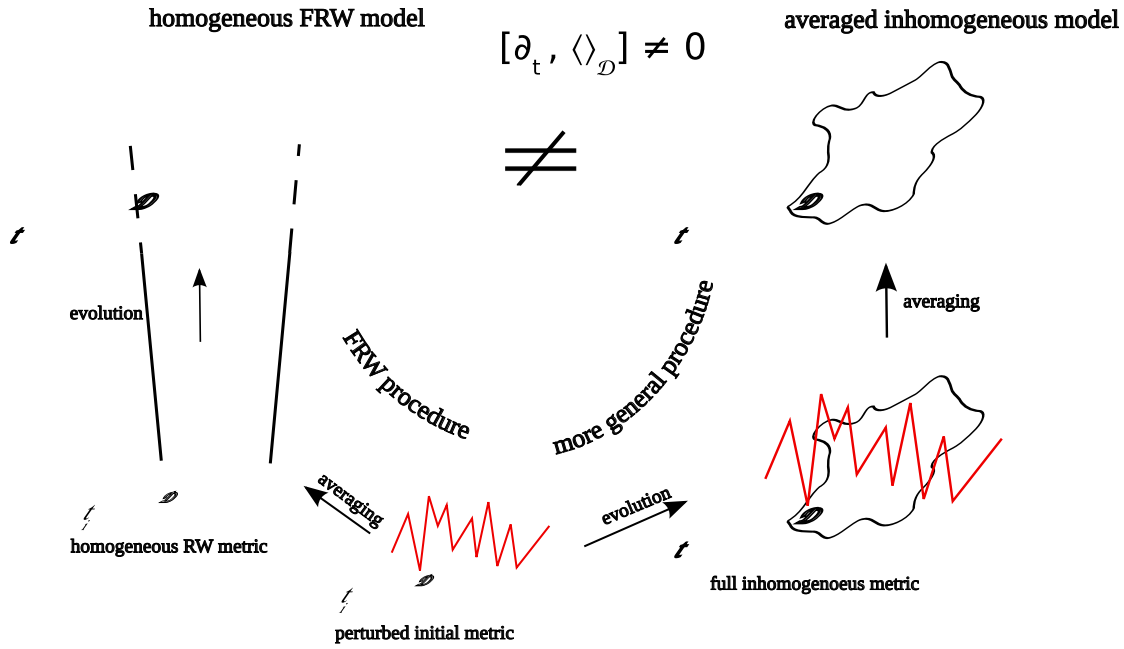

Figure 4.3. Sketch of the difference of the averaging framework to the standard picture. Instead of pre-averaging and then evolving the average patch one should only average after having taken the full inhomogeneous evolution into account. The resulting averages will differ as we see from Eq. (4.8). The question by how much they differ is one aspect of the averaging problem.

Time evolution and averaging do not commute. Note, that for a homogeneous expansion rate this would be the case, as one could simply factor θ out of the spatial average $\langle \ldots \rangle_{\mathcal{D}}$. This non-commutation is one source for the emergence of effective terms in an average description. The difference to the standard case with an assumed average metric is sketched in Fig. 4.3.

One of the most interesting cases where the time evolution of the average of a scalar quantity differs from the full time evolution is the expansion rate itself. Inserting $\theta\,(X,t)$ into Eq. (4.8) gives

$$\partial_t \langle\theta\rangle_{\mathcal{D}} = \langle\partial_t\,\theta\rangle_{\mathcal{D}} + \left\langle\theta^2\right\rangle_{\mathcal{D}} - \langle\theta\rangle^2_{\mathcal{D}}\ . \tag{4.9}$$

This has the unexpected property, that the change in the average expansion rate, that is the acceleration of the average expansion, may be positive even if locally at every point $\partial_t\,\theta < 0$. This can occur, because the variance of expansion rates $\langle\theta^2\rangle_{\mathcal{D}} - \langle\theta\rangle^2_{\mathcal{D}}$ is positive and may, in some cases, outweigh the first term. This means that the average expansion of the domain $\mathcal{D}$ may accelerate even in the case of a dust Universe that we are considering.

This acceleration of the average expansion rate is simply due to the definition of the average. It weights regions according to their volume. Regions that are expanding faster,

however, will also increase their volume faster than regions that are expanding more slowly. If we start from a situation where fast and slowly expanding regions have similar volume, the average expansion rate in the beginning is unaffected by the weighting. In the following however, the faster expanding regions will systematically also gain in the weighting as their faster expansion leads to a bigger volume. If this gain is rapid enough, the average expansion rate of the domain $\mathcal{D}$ may even rise instead of decline. Eventually however, the volume average will be dominated by the fastest expanding region and therefore the amount of time during which average acceleration may occur is limited. This final state with the fastest expanding region dominating the whole Universe is then again a fairly homogeneous situation. In the end, the decrease of the expansion rate of the one homogeneous expanding region will be equal to the decrease of the average.

The question if such a situation can arise, or if Eq. (4.9) is of no practical use for the Universe that we are living in, is one of the currently unsolved puzzles. For a matter dominated Universe, the question may be related to the equations that govern the emergence of different expansion rates in different regions when given the initial density fluctuation in the matter fluid. These are the fluid equations (4.5a)–(4.5e). The equations for the three scalars that we are interested in are the scalar parts of these equations. They read

$$\frac{1}{3}\theta^2 = 8\pi G\varrho - \frac{1}{2}\mathcal{R} + \sigma^2 + \Lambda \,, \tag{4.10a}$$

$$\dot{\theta} + \frac{1}{3}\theta^2 = -4\pi G\varrho - 2\sigma^2 + \Lambda \,, \tag{4.10b}$$

$$0 = \dot{\varrho} + \theta\varrho \,. \tag{4.10c}$$

Not surprisingly this is not a complete set of equations for the time evolution of the four unknown quantities θ, σ^2, $\mathcal{R}$ and ϱ. To close this system of equations one would also have to include the evolution equation for the shear, which is not a scalar equation any more. Therefore we cannot use it in the present context of a scalar averaging scheme. Without using spatial averaging one could attempt to solve the local equations. However, this would be equivalent to solving the full Einstein equations for a generally inhomogeneous dust Universe. This is not possible. Already the specification of realistic initial conditions in the matter density ϱ would be too complicated. We therefore have to live with the restriction that the system of equations no longer closes and we will sketch below possible ways that have been used to circumvent the problem.

4.1.2. Average evolution of inhomogeneous Universes

Averaging Eqs. (4.10a)–(4.10c) finally yields the equations that we will be exploring in the following

$$3H_{\mathcal{D}}^2 = 8\pi G \langle \varrho \rangle_{\mathcal{D}} - \frac{1}{2}\langle \mathcal{R} \rangle_{\mathcal{D}} - \frac{1}{2}\mathcal{Q}_{\mathcal{D}} + \Lambda \,, \tag{4.11a}$$

$$3\frac{\ddot{a}_{\mathcal{D}}}{a_{\mathcal{D}}} = -4\pi G \langle \varrho \rangle_{\mathcal{D}} + \mathcal{Q}_{\mathcal{D}} + \Lambda \,, \tag{4.11b}$$

$$0 = \partial_t \langle \varrho \rangle_{\mathcal{D}} + 3H_{\mathcal{D}} \langle \varrho \rangle_{\mathcal{D}} \,. \tag{4.11c}$$

They are evolution equations for the average scale factor or equivalently the average Hubble rate

$$a_{\mathcal{D}}(t) := \left(\frac{V_{\mathcal{D}}}{V_{\mathcal{D}_\mathrm{i}}}\right)^{\frac{1}{3}} \;;\; H_{\mathcal{D}} := \frac{\dot{a}_{\mathcal{D}}}{a_{\mathcal{D}}} = \frac{1}{3}\langle \theta \rangle_{\mathcal{D}} \,. \tag{4.12}$$

This means that the scale factor is defined via the Riemannian volume of a domain and not directly from a quantity in the inhomogeneous metric. The quantity $\mathcal{Q}_{\mathcal{D}}$ that occurs here is called kinematical backreaction. It is one of several types of backreaction the importance of which is not yet settled. It is defined by

$$\mathcal{Q}_{\mathcal{D}} := \frac{2}{3}\left(\left\langle \theta^2 \right\rangle_{\mathcal{D}} - \langle \theta \rangle_{\mathcal{D}}^2\right) - 2\left\langle \sigma^2 \right\rangle_{\mathcal{D}} = \left\langle K^2 - K_{ij}K^{ij} \right\rangle_{\mathcal{D}} - \frac{2}{3}\langle K \rangle_{\mathcal{D}}^2 \tag{4.13}$$

and therefore encodes the difference of the variance of the expansion rates and the "variance" of the shear. As the two variances themselves are inherently positive, the result may have either sign. This leads to the unexpected effect mentioned above that also in a dust Universe we may have an accelerated expansion, but this time of the kinematically defined average scale-factor $a_{\mathcal{D}}$. The condition reads

$$4\pi G \langle \varrho \rangle_{\mathcal{D}} < \mathcal{Q}_{\mathcal{D}} \,, \tag{4.14}$$

so the fluctuation in the expansion rate within the averaging domain $\mathcal{D}$ has to be large enough to overcome the shear and the average matter density of the Universe.

Another interesting consequence of the set of equations (4.11a)–(4.11c) is, that it leads to a nontrivial curvature evolution. This can be seen by determining the integrability condition connecting (4.11a) and (4.11b). With the help of (4.11c) this yields

$$a_{\mathcal{D}}^{-2}\partial_t\left(a_{\mathcal{D}}^2\langle \mathcal{R} \rangle_{\mathcal{D}}\right) = -a_{\mathcal{D}}^{-6}\partial_t\left(a_{\mathcal{D}}^6\mathcal{Q}_{\mathcal{D}}\right) \,. \tag{4.15}$$

This means that only for $\mathcal{Q}_{\mathcal{D}} = 0$ or $\mathcal{Q}_{\mathcal{D}} \propto a_{\mathcal{D}}^{-6}$ the inhomogeneities and the intrinsic curvature decouple and we recover the standard FRW curvature evolution as $\langle \mathcal{R} \rangle_{\mathcal{D}} \propto a_{\mathcal{D}}^{-2}$ like in Eq. (1.3a). In all other cases the curvature evolution will be modified. We will see this explicitly in the evaluation of the model that we will examine below.

As already mentioned, there is no explicit solution to the above equations as the system does not close. This is the same situation as in the Friedmannian case where one first has

to impose an equation of state for the fluid. In the average case considered here, however, the fluid is an effective one. Therefore, there is no natural choice for an equation of state. The energy density and pressure of the effective fluid may be expressed as

$$\begin{aligned} \varrho_{\mathrm{eff}}^{\mathcal{D}} &= \langle\varrho\rangle_{\mathcal{D}} - \frac{1}{16\pi G}\mathcal{Q}_{\mathcal{D}} - \frac{1}{16\pi G}\langle\mathcal{R}\rangle_{\mathcal{D}} \ ; \\ p_{\mathrm{eff}}^{\mathcal{D}} &= -\frac{1}{16\pi G}\mathcal{Q}_{\mathcal{D}} + \frac{1}{48\pi G}\langle\mathcal{R}\rangle_{\mathcal{D}} \ . \end{aligned} \tag{4.16}$$

Using these definitions in Eqs. (4.11a)–(4.11c), the resulting equations

$$3H_{\mathcal{D}}^2 = 8\pi G\varrho_{\mathrm{eff}}^{\mathcal{D}} - \frac{3k_{\mathcal{D}_{\mathrm{i}}}}{a_{\mathcal{D}}^2} + \Lambda \ ; \tag{4.17a}$$

$$3\frac{\ddot{a}_{\mathcal{D}}}{a_{\mathcal{D}}} = -4\pi G(\varrho_{\mathrm{eff}}^{\mathcal{D}} + 3p_{\mathrm{eff}}^{\mathcal{D}}) + \Lambda \ ; \tag{4.17b}$$

$$0 = \dot{\varrho}_{\mathrm{eff}}^{\mathcal{D}} + 3H_{\mathcal{D}}\left(\varrho_{\mathrm{eff}}^{\mathcal{D}} + p_{\mathrm{eff}}^{\mathcal{D}}\right) \ . \tag{4.17c}$$

underline this formal correspondence to the homogeneous case of Eq. (1.3a).

This correspondence is remarkable by itself. In the whole derivation we did not assume homogeneity and isotropy, but the final result can be written in the same form as the Friedmann equations derived under exactly these assumptions. This means that the Friedmann equations indeed capture the average evolution of the Universe, but the fluids that govern those equations are effective ones. They will not only contain the ordinary fluids with their microscopic equations of state, but an effective fluid with an unknown one $p_{\mathrm{eff}}^{\mathcal{D}} = \beta\left(\varrho_{\mathrm{eff}}^{\mathcal{D}}, a_{\mathcal{D}}\right)$. This cosmic equation of state, that would close the system of average equations, is therefore not easily determined by known microscopic physics [98].

To probe the space of possible solutions to the equations (4.11a)–(4.11c), or equivalently (4.17c), one may use constant equations of state like in the Friedmannian case. By Eq. (4.11c), the matter component already has an equation of state, which is $p_{\mathrm{eff}}^{\mathcal{D}} = 0$. For the effective component of $\mathcal{Q}_{\mathcal{D}}$ and $\langle\mathcal{R}\rangle_{\mathcal{D}}$, which we will call X-matter, a constant equation of state parameter means

$$w_X = \frac{p_{\mathrm{eff}}^{\mathcal{D}}}{\varrho_{\mathrm{eff}}^{\mathcal{D}} - \langle\varrho\rangle_{\mathcal{D}}} \ \Rightarrow \ \mathcal{Q}_{\mathcal{D}} = \langle\mathcal{R}\rangle_{\mathcal{D}}\,\frac{w_X + \frac{1}{3}}{1 - w_X} \ , \tag{4.18}$$

and with the integrability (4.15) this implies

$$\mathcal{Q}_{\mathcal{D}} \propto \langle\mathcal{R}\rangle_{\mathcal{D}} \propto a_{\mathcal{D}}^{-3(1+w_X)} \ , \tag{4.19}$$

or by calling $n = -3\,(1 + w_X)$

$$\mathcal{Q}_{\mathcal{D}} = r^{\mathcal{D}}\langle\mathcal{R}\rangle_{\mathcal{D}} = r^{\mathcal{D}}\mathcal{R}_{\mathcal{D}_i}a_{\mathcal{D}}^n \ , \ \text{with} \ \ r^{\mathcal{D}} = -\frac{n+2}{n+6} \ . \tag{4.20}$$

This means that apart from the case where the two components decouple, i.e. for $Q_{\mathcal{D}} \propto a_{\mathcal{D}}^{-6}$ and $\langle\mathcal{R}\rangle_{\mathcal{D}} \propto a_{\mathcal{D}}^{-2}$, the scaling laws have the same exponent. The space probed

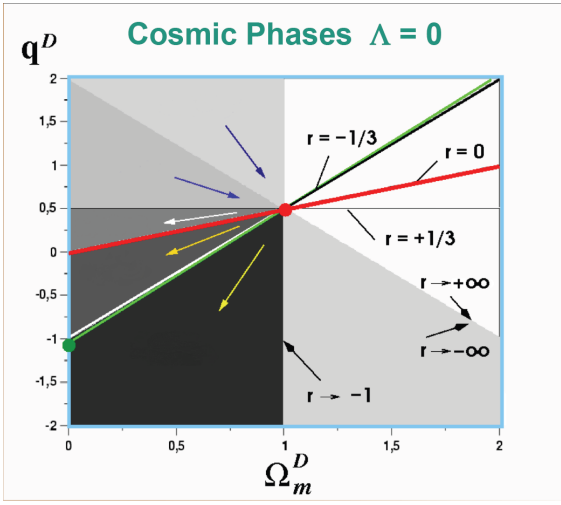

Figure 4.4. "Phase space" for the solutions of the averaged equations. Scaling solutions with $\mathcal{Q}_\mathcal{D} \propto a_\mathcal{D}^n$ with $n = -2\frac{1+3r}{1+r}$ form straight lines. The solutions for different r are shown. The arrows in the different sectors represent the directions of instability. Picture from [23].

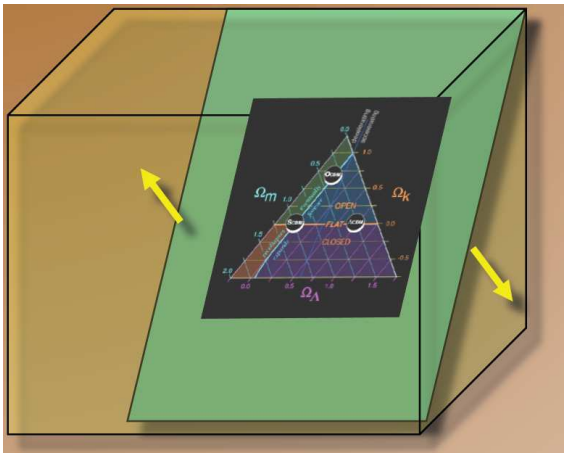

Figure 4.5. Enlargement of the solution space in the case of the average cosmology. The known "cosmic triangle" $\Omega_m = \frac{8\pi G}{3H^2}\varrho$, $\Omega_\Lambda = \frac{\Lambda}{3H^2}$ and $\Omega_k := -\frac{k}{a^2H^2}$ is complemented by the backreaction $\mathcal{Q}_\mathcal{D}$ to form a "cosmic quartet". There is a priori no reason why the solutions in this larger solution space should coincide with the plane of the standard model solutions. (Picture: *Buchert, priv. comm.*)

by these scaling solutions is shown in Fig. 4.4. With the definition of dimensionless cosmic parameters from (4.11a)–(4.11c) of the form

$$\begin{aligned} \Omega_m^\mathcal{D} &:= \frac{8\pi G}{3H_\mathcal{D}^2}\langle\varrho\rangle_\mathcal{D}\,, \quad \Omega_\Lambda^\mathcal{D} := \frac{\Lambda}{3H_\mathcal{D}^2}\,, \\ \Omega_\mathcal{R}^\mathcal{D} &:= -\frac{\langle\mathcal{R}\rangle_\mathcal{D}}{6H_\mathcal{D}^2} \quad, \quad \Omega_\mathcal{Q}^\mathcal{D} := -\frac{\mathcal{Q}_\mathcal{D}}{6H_\mathcal{D}^2}\,, \end{aligned} \tag{4.21}$$

and a deceleration parameter

$$q^\mathcal{D} := -\frac{\ddot{a}_\mathcal{D}}{a_\mathcal{D}}\frac{1}{H_\mathcal{D}^2} = \frac{1}{2}\Omega_m^\mathcal{D} + 2\Omega_\mathcal{Q}^\mathcal{D} - \Omega_\Lambda^\mathcal{D}\,, \tag{4.22}$$

one may show that for $\Lambda = 0$ the scaling solutions are straight lines in the $\left(\Omega_m^\mathcal{D}, q^\mathcal{D}\right)$-plane of Fig. 4.4. As we find from Eqs. (4.11a)–(4.11c), these lines are given by

$$q^\mathcal{D} = \frac{2r^\mathcal{D}}{1+r^\mathcal{D}} + \frac{1}{2}\left(\frac{1-3r^\mathcal{D}}{1+r^\mathcal{D}}\right)\Omega_m^\mathcal{D} - \left(\frac{1+3r^\mathcal{D}}{1+r^\mathcal{D}}\right)\Omega_\Lambda^\mathcal{D}\,. \tag{4.23}$$

They are shown in Fig. 4.4 for $\Omega_\Lambda^{\mathcal{D}} = 0$ and different values of $r^{\mathcal{D}}$. The EdS model with $\Omega_m^{\mathcal{D}} = 1$ and $q^{\mathcal{D}} = 0.5$ sits in the middle of the diagram. The diagram is useful to visualize the results of the dynamical analysis in [23] and the refined one in [99]. They have shown that the standard Friedmann model solutions are unstable. The EdS model is a saddle point and in some cases the Friedmannian solutions are even repellors. This is not surprising, as the activation of the inhomogeneity degree of freedom that led to the fourth cosmic parameter in (4.21), also yields an enlargement of the solution space as sketched in Fig. 4.5. It is at least plausible that the activation of this degree of freedom reduces the stability of the Friedmann background solutions.

The "Morphon" Field To close this introductory section on the Buchert model of averaging, we write the X-matter energy component in form of a scalar field. This is a nice way to make contact to work that has been done in quintessence scenarios for the late time evolution of the Universe. The correspondence is made via the effective energy density (4.16) by defining the scalar field density and pressure as

$$\varrho_{\rm eff}^{\mathcal{D}} =: \langle\varrho\rangle_{\mathcal{D}} + \varrho_\Phi^{\mathcal{D}} \quad ; \quad p_{\rm eff}^{\mathcal{D}} =: p_\Phi^{\mathcal{D}} \, . \tag{4.24}$$

They obey the scalar field equations

$$\varrho_\Phi^{\mathcal{D}} = \epsilon\frac{1}{2}\dot\Phi_{\mathcal{D}}^2 + U_{\mathcal{D}} \quad ; \quad p_\Phi^{\mathcal{D}} = \epsilon\frac{1}{2}\dot\Phi_{\mathcal{D}}^2 - U_{\mathcal{D}} \, , \tag{4.25}$$

where $\epsilon = \pm 1$ is used to switch between a standard and a phantom scalar field. The kinetic and potential energy are then related to backreaction and curvature by

$$U_{\mathcal{D}} = -\frac{\langle\mathcal{R}\rangle_{\mathcal{D}}}{24\pi G} \quad ; \quad -\frac{1}{8\pi G}\mathcal{Q}_{\mathcal{D}} = \epsilon\dot\Phi_{\mathcal{D}}^2 - U_{\mathcal{D}} \, . \tag{4.26}$$

So the curvature plays the role of the potential for the structure of the Universe and a transfer of energy to the kinetic part enlarges the amount of backreaction that might in principle contribute to the effect of dark energy.

It is also interesting to see that the integrability condition (4.15) gives for Φ the equation

$$\ddot\Phi_{\mathcal{D}} + 3H_{\mathcal{D}}\dot\Phi_{\mathcal{D}} + \epsilon\frac{\partial}{\partial\Phi_{\mathcal{D}}}U(\Phi_{\mathcal{D}}, \langle\varrho\rangle_{\mathcal{D}}) \;=\; 0 \, , \tag{4.27}$$

which can be recognized as the classical Klein Gordon equation of a homogeneous scalar field. For the class of scaling solutions introduced above, one may determine the potential needed to arrive at these solutions. It reads

$$U(\Phi_{\mathcal{D}}) = \frac{2}{3}\left((1+r)\frac{\Omega_{\mathcal{R}}^{\mathcal{D}_{\rm i}}}{\Omega_m^{\mathcal{D}_{\rm i}}}\right)^{\frac{3}{n+3}} \langle\varrho\rangle_{\mathcal{D}_{\rm i}} \sinh^{\frac{2n}{n+3}}\left(\frac{(n+3)}{\sqrt{-\epsilon n}}\sqrt{2\pi G}\Phi_{\mathcal{D}}\right) \, , \tag{4.28}$$

and belongs to a class of models in quintessence scenarios that have already been shown to lead to accelerated expansion to the Universe.

4.2. Lagrangian form of the Einstein equations

As mentioned in the introduction to this chapter, we want to set up a perturbative framework that is more adapted to the mildly nonlinear situation than the standard perturbation theory of Sec. 2.2. To achieve this we use a relativistic extension of the famous Zel'dovich approximation (used in the present context in [30]), recently formulated in [31]. The special formulation will allow to have a close correspondence to the Newtonian version of the approximation, which will give some insight into the relevance of genuine relativistic terms. The fundamental building blocks of the approximation are the coframes arising from a decomposition of the metric. Thus, we will first formulate the equations discussed above in terms of these coframes and then show how they are used for the relativistic Zel'dovich approximation (RZA).

4.2.1. Coframe decomposition of Einsteins Equations

Following the derivation in [31], we decompose the three metric of the spatial hypersurfaces of the foliation of Sec. 4.1.1 into coframes

$$ {}^{(3)}\mathbf{g} = \delta_{ab}\boldsymbol{\eta}^a \otimes \boldsymbol{\eta}^b \quad \Longrightarrow \quad g_{ij} = \delta_{ab}\eta^a{}_i\eta^b{}_j \,. \tag{4.29} $$

The non-coordinate indices a, b label the coframes. This choice of the non-coordinate basis, in which the coframes are connected by δ_{ab}, implies, that in general they have a non-trivial initial value $\eta^a{}_i\,(t_0) = \mathring{\eta}^a{}_i$. This initial value contains the initial perturbations to the three metric. We will see below that δ_{ab} is not the only possible choice and decide for another, more convenient possibility.

As we saw in Sec. 4.1.1, for the kind of backreaction that we want to quantify, the Riemannian volume element and therefore the metric determinant $J = \sqrt{g}$ plays an important role. In terms of coframes it reads

$$ J = \frac{1}{6}\epsilon_{abc}\epsilon^{ikl}\eta^a{}_i\eta^b{}_k\eta^c{}_l \,. \tag{4.30} $$

The coframe fields are accompanied by their inverses, the frames $e_a{}^i$ defined by

$$ e_a{}^i\eta^a{}_j = \delta^i{}_j \quad \Longrightarrow \quad e_a{}^i = \frac{1}{2J}\epsilon_{abc}\epsilon^{ikl}\eta^b{}_k\eta^c{}_l \,. \tag{4.31} $$

This allows to express the expansion tensor, defined in (4.4), in terms of the coframes via the relation (4.3b)

$$ \Theta^i{}_j = \dot{\eta}^a{}_j e_a{}^i = \frac{1}{2J}\epsilon_{abc}\epsilon^{ikl}\dot{\eta}^a{}_j\eta^b{}_k\eta^c{}_l \,, \tag{4.32} $$

and of course also the rest of the equations (4.3a)–(4.3e) may be written explicitly in

terms of coframes, giving rise to what [31] call the Lagrange Einstein system:

$$\begin{aligned}
\delta_{ab}\ddot{\eta}^{a}{}_{[i}\eta^{b}{}_{j]} &= 0 && (4.33a)\\
\frac{1}{2}\epsilon_{abc}\epsilon^{ikl}\ddot{\eta}^{a}{}_{i}\eta^{b}{}_{k}\eta^{c}{}_{l} &= \Lambda J - 4\pi G\mathring{J}\mathring{\varrho} && (4.33b)\\
\left(\epsilon_{abc}\epsilon^{ikl}\dot{\eta}^{a}{}_{j}\eta^{b}{}_{k}\eta^{c}{}_{l}\right)_{\|i} &= \left(\epsilon_{abc}\epsilon^{ikl}\dot{\eta}^{a}{}_{i}\eta^{b}{}_{k}\eta^{c}{}_{l}\right)_{\|j} && (4.33c)\\
\epsilon_{abc}\epsilon^{mkl}\dot{\eta}^{a}{}_{m}\dot{\eta}^{b}{}_{k}\eta^{c}{}_{l} &= 16\pi G\mathring{J}\mathring{\varrho} + 2\Lambda J - JR && (4.33d)\\
\frac{1}{2}\Big(\epsilon_{abc}\epsilon^{ikl}\ddot{\eta}^{a}{}_{j}\eta^{b}{}_{k}\eta^{c}{}_{l} &- \frac{1}{3}\epsilon_{abc}\epsilon^{mkl}\ddot{\eta}^{a}{}_{m}\eta^{b}{}_{k}\eta^{c}{}_{l}\delta^{i}{}_{j}\Big) &&\\
+\Big(\epsilon_{abc}\epsilon^{ikl}\dot{\eta}^{a}{}_{j}\dot{\eta}^{b}{}_{k}\eta^{c}{}_{l} &- \frac{1}{3}\epsilon_{abc}\epsilon^{mkl}\dot{\eta}^{a}{}_{m}\dot{\eta}^{b}{}_{k}\eta^{c}{}_{l}\delta^{i}{}_{j}\Big) &&\\
&= -J\tau^{i}{}_{j}\,, && (4.33e)
\end{aligned}$$

where $\mathring{J}$ and $\mathring{\varrho}$ are the initial values of J and ϱ. $\tau^{i}{}_{j}$ is the tracefree part of the Ricci tensor

$$R^{i}{}_{j} = \delta_{ab}\left(\eta^{a}{}_{k}{}^{\|k\|i} - \eta^{a}{}_{k}{}^{\|i\|k}\right)\eta^{b}{}_{j}\,. \tag{4.34}$$

This gives the explicit dependence of the fluid equations (4.3a)–(4.3e) on the coframes which are now the only dynamical variables. For more details see [31].

4.2.2. The relativistic Zel'dovich approximation

The coframe split of the metric is useful, because it allows to generalize the Newtonian Zel'dovich approximation [30] in a straight forward way. This approximation is most easily expressed in a Lagrangian formulation of the fluid equations. The central element is the time dependent mapping $\mathbf{f}(\cdot,t):\mathbf{X}\mapsto\mathbf{x}$ that takes the time independent Lagrangian coordinates $\mathbf{X}$ to the Eulerian fluid coordinates $\mathbf{x}$. For details see [30] and references therein. The Newtonian Zel'dovich approximation then consists in perturbing this mapping by

$$\mathbf{x} = \mathbf{f}^{Z}(\mathbf{X},t) = a(t)\Big(\mathbf{X} + \xi(t)\,\nabla_0\psi(\mathbf{X})\Big)\,, \tag{4.35}$$

where $\nabla_0\psi(\mathbf{X})$ is the gradient of the initial Newtonian potential.

This Newtonian form may be generalized to GR using the coframes. The definition that [31] gives for the relativistic Zel'dovich approximation (RZA) is:

Definition: "Relativistic Zel'dovich Approximation"
We consider the 9 functions in the co-frame coefficients as the only variables in the full set of ADM equations for the matter model "irrotational dust" within a flow-orthogonal foliation of space-time. We then consider the general linearized solution for these coefficients. The approximation "RZA" consists in exactly evaluating any other field as a functional of the linearized solution, without performing further approximations or truncations.

The fact that the linearized solution is used to full extent in the expressions will lead to a better precision of the approximation especially for the kinematical backreaction variable as we will discuss below. The perturbation theory is set up in the same way as in the Newtonian case by splitting the coframes into background and perturbation

$$\boldsymbol{\eta}_H^{\ a} = \eta_{H\,i}^{\ a}\, \boldsymbol{d}X^i := a(t)\boldsymbol{\eta}_H^{\ a}(t_{\mathbf{i}}) \ , \quad \eta_{H\,i}^{\ a} := a(t)\delta_{\ i}^{\ a} \ , \tag{4.36}$$

where $a(t)$ is a background solution of the standard Friedmann equations (1.3a). The RZA is then defined in analogy to (4.35) by

$$\boldsymbol{\eta}^{\ a} = a(t)\left(\boldsymbol{\eta}_H^{\ a}\left(t_{\mathbf{i}}\right) + \mathbf{P}^{\ a}\right) \ , \tag{4.37}$$

so each of the three coframes is perturbed with inhomogeneous deformation one-forms $\mathbf{P}^{\ a}(t, X^k)$. They may be further specified by

$$\mathbf{P}^{\ a} = \xi(t)\dot{P}_{\ i}^{a}\ \boldsymbol{d}X^i \ , \tag{4.38}$$

which means in explicit coordinate form

$${}^{\mathrm{RZA}}\eta_{\ i}^{a}\left(t, X^k\right) := a\left(t\right)\left(N^{a}{}_{i} + \xi(t)\dot{P}_{\ i}^{a}\right) \ , \tag{4.39}$$

where $N^{a}{}_{i} := {}^{\mathrm{RZA}}\eta_{\ i}^{a}\left(t_{\mathbf{i}}, X^k\right)$ and $\dot{P}_{\ i}^{a} = \dot{P}_{\ i}^{a}\left(t_{\mathbf{i}}, X^k\right)$. The time evolution $\xi\left(t\right)$ is given by

$$\xi(t) := (q(t) - q(t_{\mathbf{i}}))/\dot{q}(t_{\mathbf{i}}) \ . \tag{4.40}$$

Plugging this form of the perturbation into the Einstein equations in coframe form (4.33a)–(4.33e) gives an evolution equation for the $q\left(t\right)$ that reads

$$\ddot{q}(t) + 2\frac{\dot{a}(t)}{a(t)}\dot{q}(t) + \left(3\frac{\ddot{a}(t)}{a(t)} - \Lambda\right)q(t) = 0 \ . \tag{4.41}$$

It is interesting to see that we recover here the equation for the time evolution of a dark matter perturbation that we already encountered in standard perturbation theory in Eq. (2.101). This is already indicates that the two approaches are quite comparable. We will elaborate on this correspondence in Sec. 4.5.

There are two solutions of interest to this equation: First, the solution for matter domination that gives $q\left(t\right) \propto a\left(t\right)$ and led to Eq. (2.102). Second, the solution for ΛCDM domination as given in Eq. (2.129).

Before we use this expression to determine the backreaction term, let us elaborate on a subtlety in the choice of initial conditions. The expression of the metric tensor in terms of non-integrable co-frames:

$$g_{ij} := G_{ab}\eta_i^a\eta_j^b \ , \tag{4.42}$$

allows two different treatments of the initial displacements. One can either include them into G_{ab} which means that the non-coordinate basis is orthogonal, but not orthonormal.

Or one can choose G_{ab} to be orthonormal (being the standard assumption), but then one has to deal with the initial values of the co-frames. To have both at a time, i.e. ${N^a}_i = \delta^a_i$ and $G_{ab} = \delta_{ab}$, is not possible as this would mean that the RZA initial metric would be Euclidean. This would disable any time-evolution of this metric as pointed out in [100]. As a nontrivial time-evolution of the metric is what we are interested in, there are only two options:

- $O1$: if ${\tilde{N}^a}_i = \delta^a_i + {P^a}_i$, with ${P^a}_i := P^a_i(t_{\mathbf{i}}, X^k)$ and ${P^a}_i \neq 0$, then $\mathbf{G}$ can be restricted to $\boldsymbol{\delta}$, and the co-frames and the metric read ${}^{\mathrm{RZA}}\tilde{\eta}^a_i\left(t, X^k\right) := a\left(t\right)\left(\delta^a_i + {P^a}_i + \xi(t)\dot{P}^a_i\right)$ $g_{ij} := \delta_{ab}\tilde{\eta}^a_i\tilde{\eta}^b_j$.
- $O2$: by appropriate coordinate transformations, one may set ${N^a}_i$ in Eq. (4.39) to δ^a_i; the transformation then sends $\dot{P}^a_i \to \dot{\mathscr{P}}^a_{\ i} = \delta^a_j\,{}^{\mathrm{RZA}}\tilde{e}^j_{\ b}\left(t_{\mathbf{i}}, X^k\right)\dot{P}^b_{\ i}$, and all informations about the initial geometrical inhomogeneities are contained in $\mathbf{G}$. The co-frames become ${}^{\mathrm{RZA}}\eta^a_{\ i}\left(t, X^k\right) := a\left(t\right)\left(\delta^a_i + \xi(t)\dot{\mathscr{P}}^a_{\ i}\right)$ the metric $g_{ij} := G_{ab}\eta^a_i\eta^b_j$ and $G_{ab} = \delta_{cd}{\tilde{N}^c}_a{\tilde{N}^d}_b$.

The utility of a non-orthonormal basis in some situations has already been pointed out by Chandrasekhar [101]. As we are facing such a situation, we will choose $O2$ in the following. This leads to more concise formulas.

4.3. Backreaction in the RZA

With the technical tools described in the previous section we are now in the position to evaluate the kinematical backreaction (4.13) in this approximation.

4.3.1. Backreaction and curvature in terms of coframes

To arrive at a concise expression we first of all define a new average

$$\langle\mathcal{A}\rangle_{\mathcal{C}_\mathcal{D}} = \frac{1}{V_{\mathcal{D}_\mathbf{i}}}\int_{\mathcal{D}} \mathrm{d}^3X\mathcal{A}\,, \tag{4.43}$$

where $V_{\mathcal{D}_\mathbf{i}} = \int_{\mathcal{D}_\mathbf{i}}\mathrm{d}^3X = \int_{\mathcal{D}_\mathbf{i}} J(X^i, t_i)\mathrm{d}^3X$ is the volume of the initial domain $\mathcal{D}_\mathbf{i}$ for $J(X^i, t_i) = 1$. It is related to the definition (4.6) by

$$\langle\mathcal{A}\rangle_\mathcal{D} = \frac{\langle\mathcal{A}J\rangle_{\mathcal{C}_\mathcal{D}}}{\langle J\rangle_{\mathcal{C}_\mathcal{D}}}\,, \tag{4.44}$$

because J defined in (4.30), is just the metric determinant. It is related to the average scale factor $a_\mathcal{D}$ of equation (4.12) by

$$a^3_\mathcal{D}\left(t\right) = \frac{V_\mathcal{D}\left(t\right)}{V_{\mathcal{D}_\mathbf{i}}} = \langle J\rangle_{\mathcal{C}_\mathcal{D}}\,. \tag{4.45}$$

Using (4.13), $K_{ij} = -\Theta_{ij}$ and (4.32) we may easily express $\mathcal{Q}_{\mathcal{D}}$ in terms of coframes as

$$\mathcal{Q}_{\mathcal{D}} = \frac{1}{\langle J\rangle_{\mathcal{C}_{\mathcal{D}}}}\left\langle \epsilon_{abc}\epsilon^{ikl}\dot{\eta}^{a}{}_{i}\dot{\eta}^{b}{}_{k}\eta^{c}{}_{l}\right\rangle_{\mathcal{C}_{\mathcal{D}}} - \frac{2}{3}\left(\frac{\left\langle \dot{J}\right\rangle_{\mathcal{C}_{\mathcal{D}}}}{\langle J\rangle_{\mathcal{C}_{\mathcal{D}}}}\right)^{2}\,, \tag{4.46}$$

where J is

$$J = \frac{1}{6}\epsilon_{abc}\epsilon^{ikl}\eta^{a}{}_{i}\eta^{b}{}_{k}\eta^{c}{}_{l}\,. \tag{4.47}$$

In our case, the coframes $\eta^{a}{}_{i}$ are restricted to the RZA

$${}^{\mathrm{RZA}}\eta^{a}{}_{i}\left(t, X^{k}\right) := a(t)\left(\delta^{a}{}_{i} + \xi(t)\dot{\mathscr{P}}^{a}{}_{i}\right)\,. \tag{4.48}$$

It is interesting to remark, that the expression (4.46), which in the present form contains the full coframes (4.48), actually only depends on the reduced coframes ${}^{\mathrm{RZA}}\tilde{\eta}^{a}{}_{i}\left(t, X^{k}\right) = {}^{\mathrm{RZA}}\eta^{a}{}_{i}\left(t, X^{k}\right)/a\left(t\right)$. The reason for this simplification is that the backreaction term does not depend on the full expansion tensor $\Theta^{i}{}_{j}$, but only on the peculiar expansion tensor $\theta^{i}{}_{j} := \Theta^{i}{}_{j} - H(t)\delta^{i}{}_{j}$. To see this, we write (4.13) in terms of the invariants of the expansion tensor $K_{ij} = -\Theta_{ij}$ as

$$\mathcal{Q}_{\mathcal{D}} = 2\left\langle \mathbf{II}(\Theta^{i}{}_{j})\right\rangle_{\mathcal{D}} - \frac{2}{3}\left\langle \mathbf{I}(\Theta^{i}{}_{j})\right\rangle^{2}_{\mathcal{D}}\,. \tag{4.49}$$

Using the separation into Hubble flow and peculiar expansion $\theta^{i}{}_{j} := \Theta^{i}{}_{j} - H(t)\delta^{i}{}_{j}$ the invariants become

$$\begin{aligned}
\mathbf{I}(\Theta^{i}{}_{j}) &= 3H + \mathbf{I}(\theta^{i}{}_{j})\,,\\
\mathbf{II}(\Theta^{i}{}_{j}) &= 3H^{2} + 2H\,\mathbf{I}(\theta^{i}{}_{j}) + \mathbf{II}(\theta^{i}{}_{j})\,,\\
\mathbf{III}(\Theta^{i}{}_{j}) &= H^{3} + H^{2}\mathbf{I}(\theta^{i}{}_{j}) + H\mathbf{II}(\theta^{i}{}_{j}) + \mathbf{III}(\theta^{i}{}_{j})\,.
\end{aligned} \tag{4.50}$$

Inserting Eqs. (4.50) into Eq. (4.49), we find that backreaction only depends on the invariants of the peculiar-expansion tensor:

$$\mathcal{Q}_{\mathcal{D}} = 2\left\langle \mathbf{II}\left(\theta^{i}{}_{j}\right)\right\rangle_{\mathcal{D}} - \frac{2}{3}\left\langle \mathbf{I}\left(\theta^{i}{}_{j}\right)\right\rangle^{2}_{\mathcal{D}}\,. \tag{4.51}$$

This non-trivial result demonstrates that the backreaction effects do not depend on the Hubble flow: backreaction is only due to peculiar-expansion.

For the evaluation of (4.46) we use (4.48) in (4.47) to find for J

$${}^{\mathrm{RZA}}\mathrm{J} = a^{3}(t)\mathfrak{J}\,, \tag{4.52}$$

Beside the background scaling a^{3} there is the *peculiar-volume deformation*

$$\mathfrak{J}(t, X^{k}) := 1 + \xi(t)\mathrm{I}_{\mathbf{i}} + \xi^{2}(t)\mathrm{II}_{\mathbf{i}} + \xi^{3}(t)\mathrm{III}_{\mathbf{i}}\,, \tag{4.53}$$

that contains the principal scalar invariants of the perturbation coframe

$$\mathrm{I}_{\mathbf{i}} := \mathrm{I}\left(\dot{\mathscr{P}}^a{}_i\right);\ \mathrm{II}_{\mathbf{i}} := \mathrm{II}\left(\dot{\mathscr{P}}^a{}_i\right);\ \mathrm{III}_{\mathbf{i}} := \mathrm{III}\left(\dot{\mathscr{P}}^a{}_i\right)\ . \tag{4.54}$$

These invariants of the matrix $\dot{\mathscr{P}}^a{}_i$ are given by

$$\begin{aligned}
\mathrm{I}\left(\dot{\mathscr{P}}^a{}_i\right) &:= \frac{1}{2}\epsilon_{abc}\epsilon^{ijk}\dot{\mathscr{P}}^a{}_i\delta^b{}_j\delta^c{}_k\ , \\
\mathrm{II}\left(\dot{\mathscr{P}}^a{}_i\right) &:= \frac{1}{2}\epsilon_{abc}\epsilon^{ijk}\dot{\mathscr{P}}^a{}_i\dot{\mathscr{P}}^b{}_j\delta^c{}_k\ , \\
\mathrm{III}\left(\dot{\mathscr{P}}^a{}_i\right) &:= \frac{1}{6}\epsilon_{abc}\epsilon^{ijk}\dot{\mathscr{P}}^a{}_i\dot{\mathscr{P}}^b{}_j\dot{\mathscr{P}}^c{}_k\ .
\end{aligned} \tag{4.55}$$

The first term of (4.46) is also easily evaluated for the coframes (4.48), and so

$${}^{\mathrm{RZA}}\mathcal{Q}_{\mathcal{D}} = \frac{\dot{\xi}^2\left(\gamma_1 + \xi\gamma_2 + \xi^2\gamma_3\right)}{\left(1 + \xi\left\langle \mathrm{I}_{\mathbf{i}}\right\rangle_{\mathcal{C}_{\mathcal{D}}} + \xi^2\left\langle \mathrm{II}_{\mathbf{i}}\right\rangle_{\mathcal{C}_{\mathcal{D}}} + \xi^3\left\langle \mathrm{III}_{\mathbf{i}}\right\rangle_{\mathcal{C}_{\mathcal{D}}}\right)^2}\ , \tag{4.56}$$

with

$$\begin{cases}
\gamma_1 := 2\left\langle \mathrm{II}_{\mathbf{i}}\right\rangle_{\mathcal{C}_{\mathcal{D}}} - \frac{2}{3}\left\langle \mathrm{I}_{\mathbf{i}}\right\rangle^2_{\mathcal{C}_{\mathcal{D}}}\ , \\
\gamma_2 := 6\left\langle \mathrm{III}_{\mathbf{i}}\right\rangle_{\mathcal{C}_{\mathcal{D}}} - \frac{2}{3}\left\langle \mathrm{II}_{\mathbf{i}}\right\rangle_{\mathcal{C}_{\mathcal{D}}}\left\langle \mathrm{I}_{\mathbf{i}}\right\rangle_{\mathcal{C}_{\mathcal{D}}}\ , \\
\gamma_3 := 2\left\langle \mathrm{I}_{\mathbf{i}}\right\rangle_{\mathcal{C}_{\mathcal{D}}}\left\langle \mathrm{III}_{\mathbf{i}}\right\rangle_{\mathcal{C}_{\mathcal{D}}} - \frac{2}{3}\left\langle \mathrm{II}_{\mathbf{i}}\right\rangle^2_{\mathcal{C}_{\mathcal{D}}}\ .
\end{cases} \tag{4.57}$$

The need for all these definitions shows that the result is quite ugly for a simple first order treatment. This complication occurs, because we do not truncate the final expression consistently at first order. We will examine the shortcomings of this approach in section 4.3.2.

If we did a consistent truncation to first order in (4.56), we would find zero, because the leading order term γ_1 is already of second order. This agrees with the result in [15, 16, 17]. There, they also find that first-order perturbations give already the correct second-order term for backreaction. The reason for this is that, by (4.51), $\mathcal{Q}_{\mathcal{D}}$ only depends on the peculiar expansion field θ^i_j. This latter does not have a zeroth order term, so the second order of θ^2 consists of the squared first order terms only and has no genuine second-order contribution. This means that (4.56) contains the correct second-order result as we will show explicitly in Sec. 4.5.1. This leading order contribution decays in an EdS Universe with the background scale-factor as $1/a$, because $\dot{\xi}^2 = \dot{a}^2 \propto 1/a$.

Curvature To calculate the curvature in the RZA we have to express it as a functional of the perturbed coframes. To this end we combine (4.10a) and (4.10b) to eliminate the density and use the definition of the expansion rate (4.4) to find

$${}^3\mathcal{R} = 6\mathrm{II}(\Theta^i{}_j) - 4\mathrm{I}^2(\Theta^i{}_j) - 4\dot{\mathrm{I}}(\Theta^i{}_j) + 6\Lambda\ , \tag{4.58}$$

where the invariants are defined in (4.55). Averaging this we arrive at

$$ {}^{\mathrm{RZA}}\langle\mathcal{R}\rangle_{\mathcal{D}} = -\left\{\frac{\left\langle\ddot{\mathfrak{J}}\right\rangle_{\mathcal{C}_{\mathcal{D}}}}{\langle\mathfrak{J}\rangle_{\mathcal{C}_{\mathcal{D}}}} + 3\left(\frac{\ddot{\xi}}{\dot{\xi}} + 4\frac{\dot{a}}{a}\right)\frac{\left\langle\dot{\mathfrak{J}}\right\rangle_{\mathcal{C}_{\mathcal{D}}}}{\langle\mathfrak{J}\rangle_{\mathcal{C}_{\mathcal{D}}}}\right\} + 6\frac{k}{a^2}\,, \tag{4.59} $$

which is now written in terms of the Jacobian $\mathfrak{J}$ (4.52). For the EdS background that we are looking at, this means

$$ \begin{aligned} {}^{\mathrm{RZA}}\langle\mathcal{R}\rangle_{\mathcal{D}} \;=\; & \frac{-10H_{\mathrm{i}}\dot{\xi}^2}{a}\frac{\langle\mathbf{I_i}\rangle_{\mathcal{C}_{\mathcal{D}}} + 2\langle\mathbf{II_i}\rangle_{\mathcal{C}_{\mathcal{D}}}\xi + 3\langle\mathbf{III_i}\rangle_{\mathcal{C}_{\mathcal{D}}}\xi^2}{1+\xi\langle\mathbf{I_i}\rangle_{\mathcal{C}_{\mathcal{D}}} + \xi^2\langle\mathbf{II_i}\rangle_{\mathcal{C}_{\mathcal{D}}} + \xi^3\langle\mathbf{III_i}\rangle_{\mathcal{C}_{\mathcal{D}}}} \\ & +\dot{\xi}^2\frac{2\langle\mathbf{II_i}\rangle_{\mathcal{C}_{\mathcal{D}}} + 6\langle\mathbf{III_i}\rangle_{\mathcal{C}_{\mathcal{D}}}\xi}{1+\xi\langle\mathbf{I_i}\rangle_{\mathcal{C}_{\mathcal{D}}} + \xi^2\langle\mathbf{II_i}\rangle_{\mathcal{C}_{\mathcal{D}}} + \xi^3\langle\mathbf{III_i}\rangle_{\mathcal{C}_{\mathcal{D}}}} \end{aligned} \tag{4.60} $$

in terms of the invariants (4.54). We see that the curvature term has a first-order contribution, whereas the leading order of the backreaction term (4.56) was a second-order contribution. In addition, for the EdS background the time evolution of the leading contribution is $\propto a^{-2}$ because $\dot{\xi}^2 \propto a^{-1}$. With the correspondence procedure that we will describe in more detail in Sec. 4.5.1, we recover the same term as Li and Schwarz [15, 16, 17].

4.3.2. Newtonian limit and self consistency

The final expression of the backreaction term in the RZA, Eq. (4.56), has an interesting counterpart in the Newtonian framework. In [30] it was shown that in the Newtonian setting the backreaction can be expressed by

$$ {}^{\mathrm{NZA}}\mathcal{Q}_{\mathcal{D}} = \frac{\dot{\xi}^2\;(\Upsilon_1 + \xi\Upsilon_2 + \xi^2\Upsilon_3)}{\left(1+\xi\langle\mathbf{I_i}\rangle_{\mathcal{D}_{\mathrm{i}}} + \xi^2\langle\mathbf{II_i}\rangle_{\mathcal{D}_{\mathrm{i}}} + \xi^3\langle\mathbf{III_i}\rangle_{\mathcal{D}_{\mathrm{i}}}\right)^2}\,, \tag{4.61} $$

with

$$ \Upsilon_1 \;:=\; 2\langle\mathbf{II_i}\rangle_{\mathcal{D}_{\mathrm{i}}} - \frac{2}{3}\langle\mathbf{I_i}\rangle^2_{\mathcal{D}_{\mathrm{i}}}\quad, \tag{4.62} $$

$$ \Upsilon_2 \;:=\; 6\langle\mathbf{III_i}\rangle_{\mathcal{D}_{\mathrm{i}}} - \frac{2}{3}\langle\mathbf{I_i}\rangle_{\mathcal{D}_{\mathrm{i}}}\langle\mathbf{II_i}\rangle_{\mathcal{D}_{\mathrm{i}}}\quad, \tag{4.63} $$

$$ \Upsilon_3 \;:=\; 2\langle\mathbf{I_i}\rangle_{\mathcal{D}_{\mathrm{i}}}\langle\mathbf{III_i}\rangle_{\mathcal{D}_{\mathrm{i}}} - \frac{2}{3}\langle\mathbf{II_i}\rangle^2_{\mathcal{D}_{\mathrm{i}}}\quad. \tag{4.64} $$

Here, the invariants are related to the gradient of the Newtonian potential ψ that figures in definition (4.35)

$$ \mathbf{I_i} := \mathbf{I}\left(\psi^{|i}_{\;|j}\right)\quad,\quad \mathbf{II_i} = \mathbf{II}\left(\psi^{|i}_{\;|j}\right)\quad,\quad \mathbf{III_i} := \mathbf{III}\left(\psi^{|i}_{\;|j}\right)\,. \tag{4.65} $$

The definition of the invariants is given in (4.55). In addition to the different meaning of the invariants there is only one other modification with respect to the RZA result: The average over the initial domain $\mathcal{D}_{\mathbf{i}}$ is now in flat Newtonian space.

The correspondence to the Newtonian result is of course not surprising as the construction used was chosen analogously to the Newtonian case. It was shown in [31] that in the limit where we send the non-integrable coframes $\eta^a_{\ i}$ to integrable ones via

$$\eta^a_{\ i} \to {}^N\eta^a_{\ i} = f^a_{\ |i} \ , \tag{4.66}$$

the resulting equations reduce to the Newtonian fluid equations in their Lagrangian form. f is the Lagrangian mapping of (4.35) and so the Newtonian perturbation one-forms correspond then directly the gradients of the Newtonian potential

$${}^N\dot{P}^a_{\ i} = \psi^{|a}_{\ \ |i} \ . \tag{4.67}$$

This explains the close correspondence of the results.

Consistency checks To test to which extent the expressions derived above are self consistent, we can plug the results for the backreaction term (4.56) and the curvature (4.60) into the integrability condition (4.15). The result in the case of the EdS model is

$$-\frac{6H_0\Omega_m}{a^2\left(t\right)\left\langle\mathfrak{J}\right\rangle_{\mathcal{C}_\mathcal{D}}}\dot{\xi}\frac{\mathrm{d}^2}{\mathrm{d}\xi^2}\left\langle\mathfrak{J}\right\rangle_{\mathcal{C}_\mathcal{D}} = 0 \ . \tag{4.68}$$

So the integrability condition is satisfied if $\frac{\mathrm{d}^2}{\mathrm{d}\xi^2}\left\langle\mathfrak{J}\right\rangle_{\mathcal{C}_\mathcal{D}} = 0$, because all other terms are intrinsically non-zero. This means however that $2\left\langle\mathrm{II}_{\mathbf{i}}\right\rangle_{\mathcal{C}_\mathcal{D}} + 3\xi\left\langle\mathrm{III}_{\mathbf{i}}\right\rangle_{\mathcal{C}_\mathcal{D}} = 0$ and so the expressions for the curvature and the backreaction term are strictly speaking only consistent if

$$\begin{cases} a^3_\mathcal{D} = 1 + \xi(t)\left\langle\mathrm{I}_{\mathbf{i}}\right\rangle_{\mathcal{C}_\mathcal{D}} \ , \\ \left\langle\mathrm{II}_{\mathbf{i}}\right\rangle_{\mathcal{C}_\mathcal{D}} = 0 = \left\langle\mathrm{III}_{\mathbf{i}}\right\rangle_{\mathcal{C}_\mathcal{D}} \ . \end{cases} \tag{4.69}$$

This encodes the fact that the RZA is only a first-order scheme. As we will see below in Sec. 4.5.1, the backreaction expression is correct to second order, so it is $\mathcal{Q}_\mathcal{D}$ that is "more correct". We will use this in 4.4 and derive the curvature directly from the backreaction term by integrating (4.15) and not from its expression (4.60).

The same problem arises when we compare the expression from (4.56) with an alternative expression of $\mathcal{Q}_\mathcal{D}$ in terms of the average scale factor. For the EdS background that we use here, Eq. (4.11b)

$$\mathcal{Q}_\mathcal{D} = 3\frac{\ddot{a}_\mathcal{D}}{a_\mathcal{D}} + 4\pi G\left\langle\varrho\right\rangle_\mathcal{D} \tag{4.70}$$

is a direct expression of $\mathcal{Q}_\mathcal{D}$ in terms of $a_\mathcal{D}$ and $\left\langle\varrho\right\rangle_{\mathcal{D}_{\mathbf{i}}}$. This allows us to use (4.45) and (4.52) to determine $\mathcal{Q}_\mathcal{D}$. The result is that the two expressions for $\mathcal{Q}_\mathcal{D}$ disagree. They

again differ by a genuine second-order term proportional to $\langle \mathbf{II_i} \rangle_{\mathcal{C}_\mathcal{D}}$. We circumvent this problem by integrating (4.70) to obtain $a_\mathcal{D}$ from $\mathcal{Q}_\mathcal{D}$ directly.

Both problems do not arise if we use a consistent second-order treatment. So far, however, this is only possible in the Newtonian limit described above as we have the full form of the perturbations to the coframes (or the displacements in that case) only for the Newtonian Lagrangian perturbation theory. The generalization to a relativistic perturbation theory is work in progress [102].

4.4. The average evolution

After deriving the general expression for the backreaction term in the previous section, we will now proceed with the evaluation of the results. It has been shown in [30] that the Newtonian Zel'dovich approximation (NZA) of [30] gives the same result as the exact calculation in the case of a plane symmetric collapse as well as in the case of a spherical collapse. This surprising result for two kinematically orthogonal exact solutions has been used by [30] to stress the power of the NZA. If the approximation is correct in those limits it might also do well for the intermediate regime of a mixture of the two forms of collapse. As the NZA and the RZA are closely related by (4.66), we will check in the following section if these results remain valid in the RZA.

4.4.1. RZA results in highly symmetric Universes

The exact solutions of the equations of general relativity that correspond to the limiting cases discussed in the NZA [30], are the anisotropic plane collapse model and the spherically symmetric Lemaître-Tolman-Bondi model.

Plane collapse The metric ansatz we use for the study of the plane-symmetric case reads

$$ds^2 = -dt^2 + a\left(t\right)^2 \left(dx^2 + dy^2 + \left(1 + P\left(z,t\right)\right)^2 dz^2\right) \ , \tag{4.71}$$

In the case of the NZA, plane symmetry is imposed by using initial conditions with $\mathbf{II}\left(\theta_{ij}\right) = 0 = \mathbf{III}\left(\theta_{ij}\right)$. It is therefore important that for this metric ansatz we also find vanishing higher invariants of the peculiar expansion tensor: $\mathbf{II}\left(\theta_{ij}\right) = 0 = \mathbf{III}\left(\theta_{ij}\right)$. The first invariant is non-trivial and reads

$$\mathbf{I}\left(\theta^i{}_j\right) = \frac{\dot{P}\left(z,t\right)}{1 + P\left(z,t\right)} \ . \tag{4.72}$$

The equation determining the time-evolution of $P\left(z,t\right)$ was in the Newtonian case simply

$$\dot{\Theta} + \Theta^k_l \Theta^l_k = -4\pi G \varrho + \Lambda \ , \tag{4.73}$$

which gave

$$\ddot{P}\left(z,t\right)+2\frac{\dot{a}}{a}\dot{P}\left(z,t\right)=4\pi G\varrho_{H}P\left(z,t\right)\ . \tag{4.74}$$

Hence, the Newtonian plane collapse had two solutions,

$$P\left(z,t\right)=aC_{1}\left(z\right)+\frac{C_{2}\left(z\right)}{a^{3/2}}\ , \tag{4.75}$$

a growing and a decaying one. In the relativistic case, however, there are more constraints. In the Lagrange-Einstein-System (4.33a)–(4.33e), also a link to the scalar curvature comes in:

$$\dot{\Theta}^{i}_{j}+\Theta\Theta^{i}_{j} = \left(4\pi G\varrho+\Lambda\right)\delta^{i}_{j}-\mathcal{R}^{i}_{j}\ ; \tag{4.76}$$

$$\Theta^{2}-\Theta^{k}_{l}\Theta^{l}_{k} = 16\pi G\varrho+2\Lambda-\mathcal{R}\ . \tag{4.77}$$

These two equations combined also give Eq. (4.73) for the relativistic case. Additionally, however, they have to be satisfied individually. As the plane-symmetric metric ansatz Eq. (4.71) implies that $\mathcal{R}^{i}{}_{j}=0$, the relativistic solution space is not the same as the Newtonian one. For the Hamilton constraint Eq. (4.77) we find

$$\frac{\dot{a}}{a}\dot{P}\left(z,t\right)=-4\pi G\varrho_{H}P\left(z,t\right)\ , \tag{4.78}$$

which is now, for $\mathcal{R}=0$, only a differential equation of first order with the solution

$$P\left(z,t\right)=\frac{C\left(z\right)}{a^{3/2}}\ . \tag{4.79}$$

This $P\left(z,t\right)$ also satisfies Eq. (4.76), but one of the solutions of the Newtonian case has disappeared.

Taking $P\left(z,t\right)=:\xi\left(t\right)\dot{\mathscr{P}}^{a}{}_{i}\left(z,t_{i}\right)$, with $\xi\left(t\right)=\left(q\left(t\right)-q\left(0\right)\right)/\dot{q}\left(0\right)$ and using the expression of Eq. (4.51), we find for the backreaction term

$$\mathcal{Q}_{\mathcal{D}}^{\text{plane}}=-\frac{2}{3}\left\langle\mathbf{I}\left(\theta^{i}{}_{j}\right)\right\rangle_{\mathcal{D}}^{2}=-\frac{2}{3}\left(\frac{\dot{\xi}\left\langle\mathbf{I_{i}}\right\rangle_{\mathcal{C}_{\mathcal{D}}}}{1+\xi\left\langle\mathbf{I_{i}}\right\rangle_{\mathcal{C}_{\mathcal{D}}}}\right)^{2}\ , \tag{4.80}$$

where $\mathbf{I_{i}}=\mathbf{I}\left(\theta^{i}{}_{j}\right)\Big|_{t_{i}}=\mathbf{I}\left(\dot{\mathscr{P}}^{a}{}_{i}\left(z,t_{i}\right)\right)$. This shows that the plane-symmetric metric is, as in the Newtonian case, a particular exact solution that is contained in the solutions of the RZA. Note again, however, that this solution in the RZA as well as for the plane-symmetric metric does not have the growing mode that was present in the Newtonian solution. This is due to the vanishing scalar curvature for cylindrical symmetry and the relation to the Hamilton constraint that did not exist in the Newtonian case. (Note that the integrability condition (4.15) is satisfied by this solution.) This is another interesting

example of a case in which a class of Newtonian solutions may not automatically provide a solution of general relativity.

For negative $\langle \mathbf{I_i} \rangle_{\mathcal{D}_i}$, corresponding to over-dense regions, $\mathcal{Q}_{\mathcal{D}}^{\text{plane}}$ is diverging at some time when $1 + \xi(t) \langle \mathbf{I_i} \rangle_{\mathcal{D}_i}$ approaches zero, even though the solution is decaying. Our special initial conditions imply a one-dimensional symmetry of inhomogeneities on a three-dimensional background (cylindrical symmetry), and the diverging $\mathcal{Q}_{\mathcal{D}}^{\text{plane}}$ is supposed to mimic the highly anisotropic pancake collapse in the three-dimensional situation.

Spherical collapse The metric ansatz that describes the spherical collapse in the relativistic setting is of course the Lemaître-Tolman-Bondi (LTB) model. The ansatz for the line element is

$$ds^2 = -dt^2 + \frac{R'^2(t,r)}{1+2E(r)}dr^2 + R^2(t,r)d\Omega^2 \ , \tag{4.81}$$

where E is a free function of r satisfying $E(r) > -1/2$; the prime denotes partial differentiation with respect to r.
In this metric, the scalar parts of Einstein's field equations read:

$$4\pi\varrho(t,r) = \frac{M'(r)}{R'(t,r)R^2(t,r)} \ , \tag{4.82}$$

and

$$\frac{1}{2}\dot{R}^2(t,r) - \frac{GM(r)}{R(t,r)} = E(r) \ , \tag{4.83}$$

with M being another free function of r; the dot denotes partial time-derivative. Using the relation between the expansion tensor and the metric tensor,

$$\Theta^i{}_j := \frac{1}{2}g^{ik}\dot{g}_{kj} \ , \tag{4.84}$$

the averaged scalar invariants of the expansion tensor can be calculated:

$$\left\langle \mathbf{I}(\Theta^i{}_j) \right\rangle_{LTB} = \frac{4\pi}{V_{LTB}} \int_0^{r_{\mathcal{D}}} \frac{\partial_r \left(\dot{R}R^2\right)}{\sqrt{1+2E}} dr \ ; \tag{4.85}$$

$$\left\langle \mathbf{II}(\Theta^i{}_j) \right\rangle_{LTB} = \frac{4\pi}{V_{LTB}} \int_0^{r_{\mathcal{D}}} \frac{\partial_r \left(\dot{R}^2R\right)}{\sqrt{1+2E}} dr \ ;$$

$$\left\langle \mathbf{III}(\Theta^i{}_j) \right\rangle_{LTB} = \frac{4\pi}{3V_{LTB}} \int_0^{r_{\mathcal{D}}} \frac{\partial_r \left(\dot{R}^3\right)}{\sqrt{1+2E}} dr \ , \tag{4.86}$$

where the Riemannian volume of an LTB-domain is given by

$$V_{LTB} = \frac{4\pi}{3} \int_0^{r_{\mathcal{D}}} \frac{\partial_r \left(R^3\right)}{\sqrt{1+2E}} dr \ . \tag{4.87}$$

The average curvature on the LTB domain is

$$\langle \mathcal{R} \rangle_{LTB} = -\frac{16\pi}{V_{LTB}} \int_0^{r_\mathcal{D}} \frac{\partial_r (ER)}{\sqrt{1+2E}} dr \ . \tag{4.88}$$

As was shown already in [103], there are two cases for which we find relations between the invariants without having to solve the system (4.82) and (4.83) explicitly: the first one is a separable solution $R(t,r)$ of the form

$$R(t,r) = f(t) \cdot g(r) \ . \tag{4.89}$$

The second case is an LTB domain with $E(r) = E$. The restriction $E = cst.$ corresponds to self-similar LTB solutions if we require at the same time that the function $M(r) \propto r$ [104].

In both cases, one can show for $R(t,0) = 0$:

$$\begin{aligned} \left\langle \mathbf{II}(\Theta^i{}_j) \right\rangle_{LTB} &= \frac{1}{3} \left\langle \mathbf{I}(\Theta^i{}_j) \right\rangle^2_{LTB} \ , \\ \left\langle \mathbf{III}(\Theta^i{}_j) \right\rangle_{LTB} &= \frac{1}{27} \left\langle \mathbf{I}(\Theta^i{}_j) \right\rangle^3_{LTB} \ . \end{aligned} \tag{4.90}$$

Combining these terms in the backreaction $\mathcal{Q}_{LTB}$ given by Eq. (4.49), we get for a spherically symmetric $E = cst.$–domain or a separable $R(t,r)$:

$$\mathcal{Q}_{LTB} = 0 \ . \tag{4.91}$$

In the case $E = cst.$, Eq. (4.88) gives

$$\langle \mathcal{R} \rangle_{LTB} = -\frac{12E}{R^2(r_\mathcal{D})} \ . \tag{4.92}$$

This implies that $\langle \mathcal{R} \rangle_{LTB}$ decreases when we increase the size of the averaging domain, because R is a growing function of $r_\mathcal{D}$.

These results show, that also for the spherical symmetric configuration the GR version of the Zel'dovich approximation is less accurate than the Newtonian one. In the Newtonian case the approximation was still reproducing the exact result for all possible spherical distributions of matter. In the GR case this is no longer the case. Only in two very special cases the correspondence still holds. This shows again that the curvature that comes in in the GR case and the additional constraint equations lead to a bigger variety of solutions. These are no longer summarized by the simple approximation.

4.4.2. Amount of backreaction on different scales

After the comparison to exact GR results in the previous section, we now turn to the evaluation of the magnitude of $\mathcal{Q}_\mathcal{D}$ in the cosmological context. The result (4.56)

describing the backreaction term in the RZA implies that at leading order it decays with the scale-factor like $1/a$. However, to quantify its importance it is not the absolute, but the relative magnitude compared to other cosmic parameters that counts. The dominant contribution in the late Universe, the matter density, goes like $1/a^3$. Therefore, the influence of the backreaction contribution grows like a^2. We evaluate the importance of this growth in the standard cosmological picture, starting with a nearly homogeneous and isotropic initial state. To this end we only need to determine the magnitude of the three invariants of the perturbation one-forms $\dot{\mathscr{P}}^a_{\ i}$ and use them in (4.56). The context of the standard scenario implies that the calculation of the initial values is performed in a Universe model that is close to spatially flat. If we additionally neglect tensor modes, we are in the limit described in Sec. 4.3.2. We therefore assume that our initial conditions for the invariants of $\dot{\mathscr{P}}^a_{\ i}$ are given by the values of $\langle \mathbf{I_i} \rangle_{\mathcal{D}_i}$, $\langle \mathbf{II_i} \rangle_{\mathcal{D}_i}$ and $\langle \mathbf{III_i} \rangle_{\mathcal{D}_i}$ from [30]. By the formal analogy of Eq. (4.56) to the one of [30], this means that most of the results of [30] are still valid in the RZA context. There are however also some new phenomena that emerge due to the fact that, unlike in the NZA of [30], the RZA develops non-vanishing scalar curvature. In this section, we will therefore comment on which results of [30] remain valid and discuss where the GR description brings in new phenomena.

Determination of initial conditions In [30] it was shown, that the averaged initial invariants that we will use also here, have vanishing ensemble expectation values

$$\mathbb{E}\left[\langle \mathbf{I_i} \rangle_{\mathcal{D}_i}\right] = \mathbb{E}\left[\langle \mathbf{II_i} \rangle_{\mathcal{D}_i}\right] = \mathbb{E}\left[\langle \mathbf{III_i} \rangle_{\mathcal{D}_i}\right] = 0 \,. \tag{4.93}$$

However, for a specific domain, any of the volume-averaged invariants may be positive or negative. These invariants fluctuate with a certain variance variance, e.g., $\sigma^2_{\mathbf{I}}(R) = \mathbb{E}\left[\langle \mathbf{I_i} \rangle^2_{\mathcal{B}_R}\right]$. In our calculation of the time-evolution of $a_{\mathcal{D}}(t)$, we consider one-σ fluctuations of the averaged invariants for spherical domains of radius R, e.g. $\langle \mathbf{I_i} \rangle_{\mathcal{B}_R} = \pm\sigma_{\mathbf{I}}(R)$. [30] showed how these fluctuations are linked to the matter power spectrum. As indicated, $\sigma_{\mathbf{I}}(R)$ will explicitly depend on the radius of the initial domain, but implicitly also on the shape of the power spectrum. [30] used a standard CDM power spectrum normalized to $\sigma_8 = 1$ and $h = 0.5$. In addition to the EdS model considered there, we also present some values for a standard ΛCDM background with $\Omega_\Lambda \approx 0.73$, $h = 0.7$ and $\sigma_8 = 0.8$.

It is important to stress that we choose to use one-σ fluctuations in the invariants. This means that, when we use them to construct other parameters the values obtained will not correspond to one-σ fluctuations of this parameter. For the initial value of $\mathcal{Q}_{\mathcal{D}}$ for example a one-σ fluctuation of the invariants is related to a one-σ fluctuation of $\mathcal{Q}_{\mathcal{D}}$ by

$$\sigma^2\left[{}^{\mathrm{RZA}}\mathcal{Q}_{\mathcal{D}_i}\right] \;=\; 4\sigma^2_{\mathbf{II}}(R) - \frac{8}{3}Cov\left(\langle \mathbf{I_i} \rangle^2_{\mathcal{D}_i}, \langle \mathbf{II_i} \rangle_{\mathcal{D}_i}\right) + \frac{8}{9}\sigma^4_{\mathbf{I}}(R) \,. \tag{4.94}$$

where the the covariance of $\langle \mathbf{I_i} \rangle^2_{\mathcal{D}_i}$ and $\langle \mathbf{II_i} \rangle_{\mathcal{D}_i}$ is non-zero (in contrast to the covariance of $\langle \mathbf{I_i} \rangle_{\mathcal{D}_i}$ and $\langle \mathbf{II_i} \rangle_{\mathcal{D}_i}$ for example). On the other hand, calculating ${}^{\mathrm{RZA}}\mathcal{Q}_{\mathcal{D}_i}$ with one-σ

fluctuations for the invariants yields

$$^{\mathrm{RZA}}\mathcal{Q}_{\mathcal{D}_\mathrm{i}} = 2\sigma_{\mathbf{II}}\left(R\right) - \frac{2}{3}\sigma^2_{\mathbf{I}}\left(R\right) \ . \tag{4.95}$$

In an abuse of language we will nevertheless speak of one-σ fluctuations in the following, but one should keep in mind that we mean those of the initial invariants (except for Fig. 4.6). In the case of $^{\mathrm{RZA}}\mathcal{Q}_{\mathcal{D}_\mathrm{i}}$, for large values of R, the two prescriptions coincide as $\sigma^2_{\mathbf{I}}\left(R\right)$ drops off faster than $\sigma_{\mathbf{II}}\left(R\right)$.

Scale-dependence of initial conditions From the very definition of the averaged parameters it seems natural that all averaged quantities would be scale-dependent and drop off with growing domain $\mathcal{D}$. That this is not necessarily the case shows the example of the initial expansion- and shear-fluctuations. In the RZA they are given by

$$\begin{aligned}\left\langle\theta^2\right\rangle_{\mathcal{D}} - \left\langle\theta\right\rangle^2_{\mathcal{D}} &= \left\langle\mathbf{I}\left(\dot{\mathscr{P}}^a_{\ i}\right)^2\right\rangle_{\mathcal{D}} - \left\langle\mathbf{I}\left(\dot{\mathscr{P}}^a_{\ i}\right)\right\rangle^2_{\mathcal{D}} \ , \\ \left\langle\sigma^2\right\rangle_{\mathcal{D}} &= \frac{1}{3}\left\langle\mathbf{I}\left(\dot{\mathscr{P}}^a_{\ i}\right)^2\right\rangle_{\mathcal{D}} - \left\langle\mathbf{II}\left(\dot{\mathscr{P}}^a_{\ i}\right)\right\rangle_{\mathcal{D}} \ .\end{aligned} \tag{4.96}$$

Using the acceleration equation in terms of co-frames (4.33b), one can show that for the RZA $\mathbf{I}\left(\dot{\mathscr{P}}^a_{\ i}\right) = -\delta$, where δ is the local density contrast. This means that also in the RZA, as already in the Newtonian case, the expectation values of expansion- and shear-fluctuations are no longer scale-dependent. They are rather given by

$$\begin{aligned}\mathbb{E}\left[\left\langle\theta^2\right\rangle_{\mathcal{D}} - \left\langle\theta\right\rangle^2_{\mathcal{D}}\right] &= H^2_{\mathbf{i}}\left(\int_{\mathbb{R}^3}\mathrm{d}^3k P_{\mathbf{i}}\left(k\right) - \sigma^2_{\mathbf{I}}\left(R\right)\right) \ , \\ \mathbb{E}\left[\left\langle\sigma^2\right\rangle_{\mathcal{D}}\right] &= \frac{1}{3}H^2_{\mathbf{i}}\int_{\mathbb{R}^3}\mathrm{d}^3k P_{\mathbf{i}}\left(k\right) \ ,\end{aligned} \tag{4.97}$$

where we again made use of the assumed approximate flatness of the initial Universe model, necessary to use the Fourier transformation. Interestingly, only part of the expected expansion fluctuations still contains information about the domain $\mathcal{D}$. The other part and the shear is domain-independent. Calculating the value of this integral may be used to estimate the importance of backreaction, if the shear fluctuations were negligible. To this end we calculate

$$\mathbb{E}\left[^{\mathrm{RZA}}\Omega^{\mathcal{D}_0}_{\mathcal{Q},trunc}\right] = -\frac{1}{9H^2_{\mathcal{D}_0}}\mathbb{E}\left[\left\langle\theta^2\right\rangle_{\mathcal{D}_0} - \left\langle\theta\right\rangle^2_{\mathcal{D}_0}\right] \ , \tag{4.98}$$

where 0 stands for today and we did the time-evolution from the initial time up to today with the leading a^{-1} mode of Eq. (4.56) only. A quantitative estimate with an exponential IR cut-off at the Hubble scale and UV cut-off at 1 kpc then yields $\mathbb{E}\left[^{\mathrm{RZA}}\Omega^{\mathcal{D}_0}_{\mathcal{Q},trunc}\right] \approx 0.73$. This illustrates the well-known fact that the expansion- and

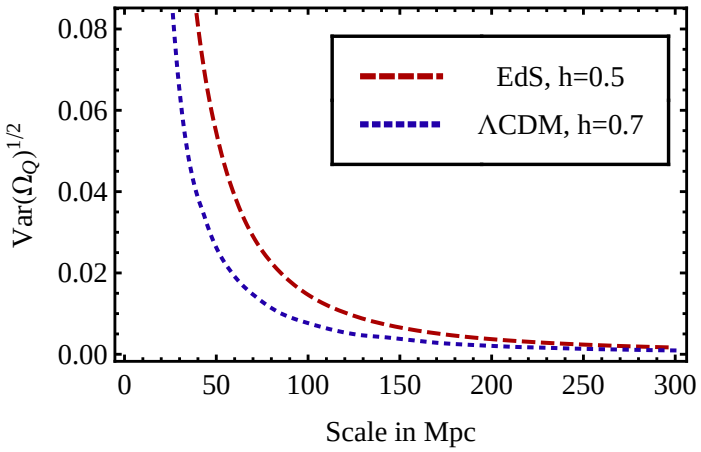

Figure 4.6. One-σ fluctuations of $\Omega_{\mathcal{Q}}^{\mathcal{D}_0}$ as a function of scale for (i) an EdS model ($h = 0.5$, $\sigma_8 = 1$) and (ii) a ΛCDM model ($\Omega_\Lambda \approx 0.73$, $h = 0.7$, $\sigma_8 = 0.8$).

shear-fluctuations by themselves are important even in a perturbative framework. In the backreaction term, however, they combine in a way that leaves only the domain-dependent contribution in the second term of the expansion fluctuations. In the Newtonian framework this is expected by the fact that $\mathcal{Q}_\mathcal{D}$ can be written as a surface term. In GR it is not a necessity, but in the linear RZA the cancellation is still effective. For higher orders, however, this is no longer true and [18] reported the survival of a domain-independent contribution to $\mathcal{Q}_\mathcal{D}$ at second order.

To close this section we calculate, as an illustration of the scale-dependence of the parameters, the backreaction term $\mathcal{Q}_\mathcal{D}$. It will imprint its scale-dependence on the other parameters and is therefore particularly interesting. To get a feeling for the magnitude of the values, we evolve it again with the a^{-1} mode until today and normalize it with $H^2_{\mathcal{D}_0}$ to get $\Omega_{\mathcal{Q}}^{\mathcal{D}_0}$. The result is shown in Fig. 4.6. We plot the one-σ fluctuation of $\Omega_{\mathcal{Q}}^{\mathcal{D}_0}$ with the correct sigma interpretation of Eq. (4.94). The result shows that only below the assumed homogeneity scale of about 150 Mpc the backreaction term is at least a per-cent contribution. For larger scales it becomes negligible. This explains that in the following all parameters converge to their background values for large $\mathcal{D}$.

Evolution of the scale factor $a_\mathcal{D}$ Having specified our initial conditions we can now calculate the average scale factor ${}^{\mathrm{RZA}}a_\mathcal{D}$ directly by integrating Eq. (4.11b). The input is the average density

$$\langle \varrho \rangle_\mathcal{D} = \frac{a^3}{a^3_\mathcal{D}} \varrho_H \left(1 + \langle \delta\,(t_\mathbf{i}) \rangle_{\mathcal{D}_\mathbf{i}}\right) = \frac{a^3}{a^3_\mathcal{D}} \varrho_H \left(1 - \langle \mathbf{I_i} \rangle_{\mathcal{D}_\mathbf{i}}\right), \tag{4.99}$$

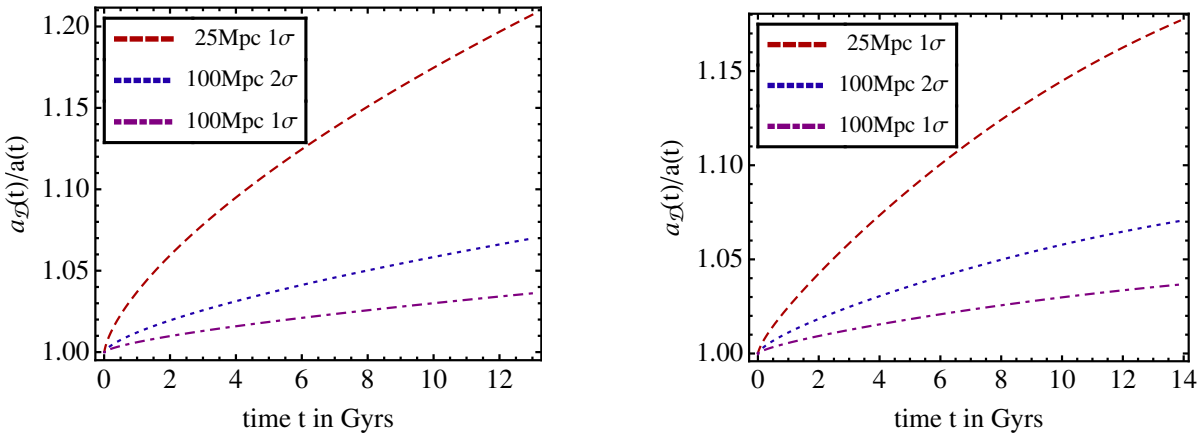

Figure 4.7. Evolution of the volume scale factor, normalized by the background scale factor, on typical under-dense domains of 25 and 100 Mpc, and on a domain that is a 2−sigma under-density fluctuation in the initial conditions on 100 Mpc. On the left the evolution for an EdS background with $\Omega_m = 1$ ($h = 0.5$, $\sigma_8 = 1$) and on the right for a ΛCDM background with $\Omega_m = 0.27$ ($h = 0.7$, $\sigma_8 = 0.8$).

and the RZA of the backreaction term Eq. (4.56). The initial conditions for ${}^{\mathrm{RZA}}a_{\mathcal{D}}$ are $a_{\mathcal{D}_\mathrm{i}} = 1$ and

$$\dot{a}_{\mathcal{D}}\left(t_\mathrm{i}\right) = \dot{a}\left(t_\mathrm{i}\right)\left(1 + \frac{1}{3}\left\langle \mathbf{I}_\mathrm{i}\right\rangle_{\mathcal{D}_\mathrm{i}}\right) \ . \tag{4.100}$$

As mentioned, the evolution of the dynamical quantities $a_{\mathcal{D}}$, $H_{\mathcal{D}} = \dot{a}_{\mathcal{D}}/a_{\mathcal{D}}$ and $q_{\mathcal{D}} = -(\ddot{a}_{\mathcal{D}}/a_{\mathcal{D}})/H_{\mathcal{D}}^2$ turns out to coincide with those of [30] for our choice of initial conditions. This means that the large deviations from the background values for some of these quantities, that have been found in [30], also occur in the RZA. In the case of the volume deceleration parameter $q_{\mathcal{D}}$ for one-σ fluctuations this leads to deviations of 30% on a scale of 100 Mpc.

The effects on $a_{\mathcal{D}}$ and $H_{\mathcal{D}}$ are smaller, but may also become important for special regions, more than one σ away from the background. In the relativistic framework the deviations of the volume scale factor $a_{\mathcal{D}}$ from the background scale factor $a(t)$ can also be interpreted as giving the strength of perturbations to the metric, since the calculation of the volume just involves the metric determinant, and not higher derivatives of the metric. Taking the cube of this deviation gives us a typical strength for the volume fluctuation, e.g. for one-sigma fluctuations on the scale of 100 Mpc we find a 12 percent effect, see Figure 4.7 for the evolution of the scale factors.

Evolution of the density parameters With the results obtained for the scale-factor we may now also inspect the time evolution of the cosmic parameters (4.21). We show them for scales of 25, 50 and 100 Mpc. From (4.100) we see, that a negative sign of

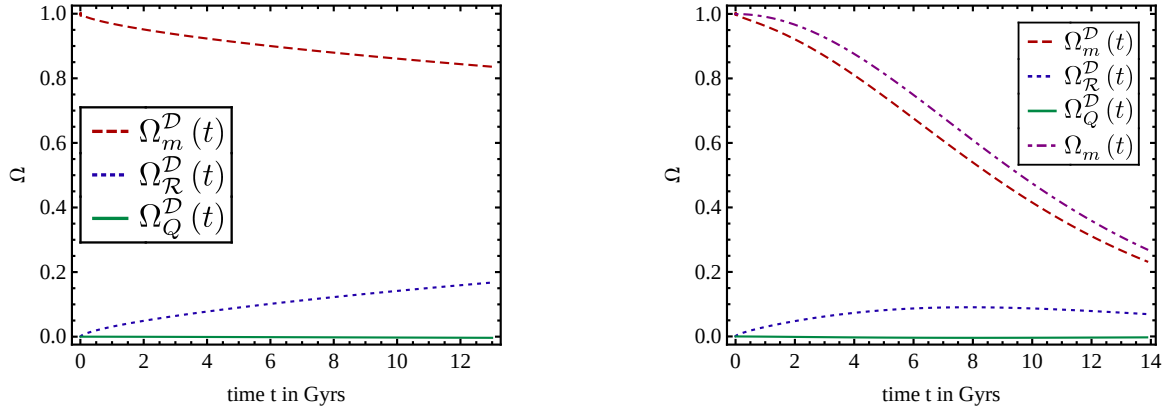

Figure 4.8. Evolution of the domain-dependent cosmological parameters of Eq. (4.21) with cosmic time. One background is the EdS model with $\Omega_m = 1$ ($h = 0.5$, $\sigma_8 = 1$) (left), the other one the ΛCDM model with $\Omega_m = 0.27$ ($h = 0.7$, $\sigma_8 = 0.8$) (right; the background density parameter is plotted here as the upper curve). The figure shows values for an expanding domain of 100 Mpc radius with one-σ fluctuations of the initial invariants of the perturbation one-form.

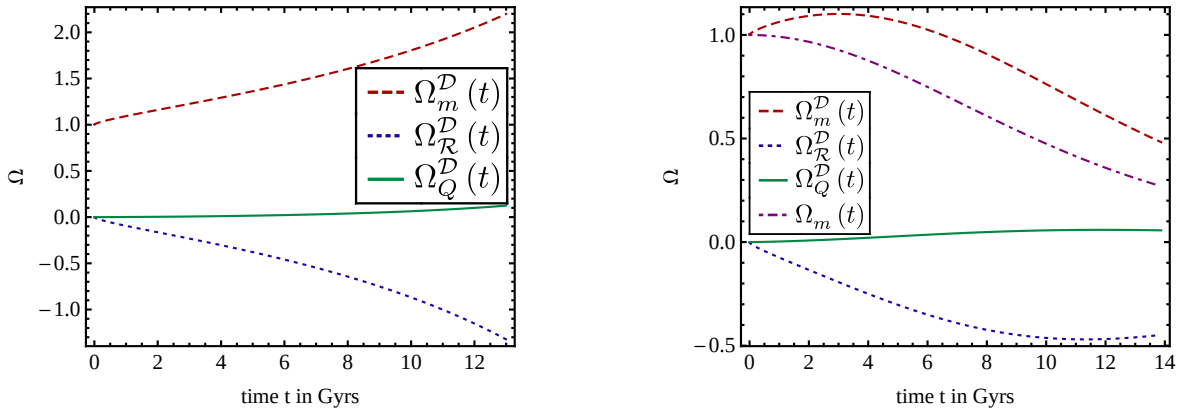

Figure 4.9. Evolution of the domain-dependent cosmological parameters of Eq. (4.21) with cosmic time. On the left the background is an EdS model with $\Omega_m = 1$ ($h = 0.5$, $\sigma_8 = 1$), on the right a ΛCDM model with $\Omega_m = 0.27$ ($h = 0.7$, $\sigma_8 = 0.8$). The figure shows values for a collapsing domain of 50 Mpc radius with one-σ fluctuations of the initial invariants of the perturbation one-form.

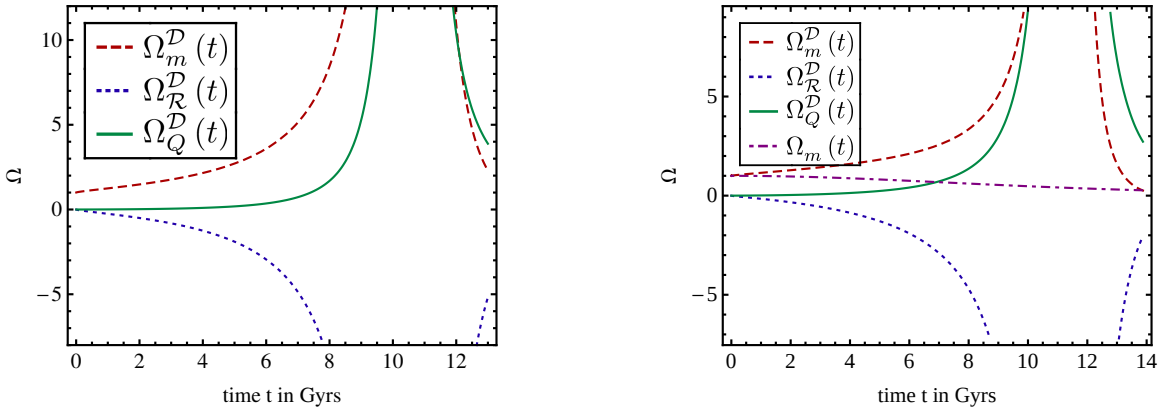

Figure 4.10. This figure corresponds to Fig. 4.9, but shows the corresponding values for a collapsing domain of one-σ fluctuations on the scale of 25 Mpc. On this scale we appreciate a singular pancake collapse; it illustrates that the backreaction term now becomes not only qualitatively but also quantitatively significant. To demonstrate that this is due to an increasing $\Omega_{\mathcal{Q}}^{\mathcal{D}}$, we additionally plot the ratios $\Omega_{\mathcal{Q}}^{\mathcal{D}}/\Omega_m^{\mathcal{D}}$ and $\Omega_{\mathcal{R}}^{\mathcal{D}}/\Omega_m^{\mathcal{D}}$ in Fig. 4.11.

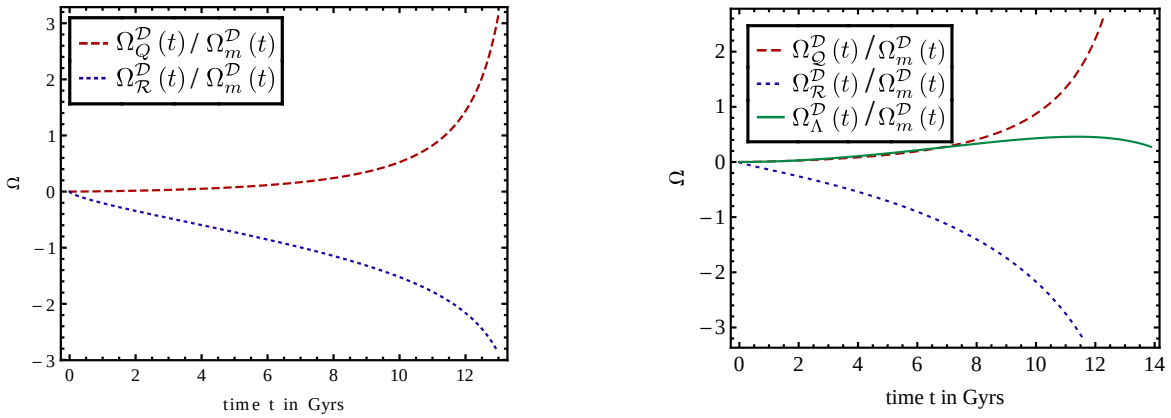

Figure 4.11. Ratios of $\Omega_{\mathcal{Q}}^{\mathcal{D}}/\Omega_m^{\mathcal{D}}$, $\Omega_{\mathcal{R}}^{\mathcal{D}}/\Omega_m^{\mathcal{D}}$ and $\Omega_\Lambda^{\mathcal{D}}/\Omega_m^{\mathcal{D}}$ for the EdS model (left) and the ΛCDM model (right) for a scale of 25 Mpc. Around the time when the collapse begins (from Fig. 4.10 this is around 11 Gyrs), i.e. where $H_{\mathcal{D}}$ goes to zero and changes sign, backreaction and curvature become the dominant contributions.

$\langle \mathbf{I_i} \rangle_{\mathcal{D}_i}$ leads to a collapsing domain, a positive sign to an expanding domain. This is the result of the relation of the first invariant to the density contrast which is $\mathbf{I}\left(\dot{\mathscr{P}}^a_{\ i}\right) = -\delta$ and was shown below (4.96). So a negative $\langle \mathbf{I_i} \rangle_{\mathcal{D}_i}$ leads to a positive over-density and collapses and inversely.

The results for an over-density of a radius of 50 and an under-density of a radius of 100 Mpc respectively, are shown in Fig. 4.9 and Fig. 4.8. It is interesting to see that even on scales of 100 Mpc, where the modification to the scale-factor is only $\approx 4\%$, the deviation of the cosmic parameters from their background values $\Omega_k = 0$ and $\Omega_m = 1$ may be as big as $\approx 20\%$. Locally, on domains of a radius of 50 Mpc, the deviations are even bigger than 100%. We will investigate in Sec. 5.4 how these strong fluctuations fundamentally limit our ability to measure important cosmic parameters.

For the ΛCDM background the matter density parameter is also reduced with respect to the background value and again we have curvature emerging from a flat background. Today, however, it is not as big as in the EdS case, since the cosmological constant dominates.

The figures also show, that even for a small value of $\Omega^{\mathcal{D}}_{\mathcal{Q}}$, the fluctuations in the curvature are sizable. This contributes to the cosmic energy budget locally. Observations that derive the existence of a low matter content $\Omega^{\mathcal{D}}_m < 1$ from local observations, have to take into account that on these scales the value of $\Omega^{\mathcal{D}}_m$ is not necessarily representative for the background Universe. Cosmic curvature and backreaction may reduce or enhance the value of $\Omega^{\mathcal{D}}_m$ according to the existence of a local under- or over-density.

For the smallest scales shown in Fig. 4.10, we encounter the collapse of the domain. During the collapse, backreaction is not only qualitatively a new contribution, but also quantitatively important as can be seen from Fig. 4.11. This might modify the dynamics of the collapse with respect to the standard description.

4.5. Comparison to other quantitative estimations

We have investigated in the last sections how the amount of backreaction may be determined in the perturbative RZA. This naturally leads to two questions: a) How do the results obtained in the RZA compare to other results from cosmic perturbation theory, and b) do these results remain valid when we try to go to nonlinear models. Regarding a), there are quite a lot of papers that do this calculation in different flavors of cosmological perturbation theory. The Newtonian gauge results of [11, 12, 13] and the synchronous gauge results of [14, 15, 16, 17] are hereby relatively consistent. We will choose in Sec. 4.5.1 the work of Li and Schwarz [15, 16, 17] for comparison. This is because it is closest to the RZA in that it uses synchronous comoving gauge and treats all interesting quantities systematically.

For the task b) the situation is not as comfortable. There are some papers that try to build toy models to extend the validity of the estimations to the non-linear regime. But either they are ad hoc, by postulating an equation of state [23, 25, 26], or they are very

idealized [27]. We will choose the second possibility and discuss the model of Räsänen [27]. In Sec. 4.5.2 we will determine the amount of kinematical backreaction it delivers and see how this compares to the RZA results.

4.5.1. Perturbative models

Comparison to the results of Li and Schwarz The limit of Sec. 4.3.2, in which we reduce the non-integrable coframes to integrable ones, is also the one in which we may compare our results to those obtained by Li and Schwarz [15, 16, 17] in the standard perturbation theory framework. They decompose the line element as

$$\mathrm{d}s^2 = a^2(\eta)\left\{-\mathrm{d}\eta^2 + \left[\left(1-2\psi^{(1)}\right)\delta_{ij} + D_{ij}\chi^{(1)}\right]\mathrm{d}x^i\mathrm{d}x^j\right\}, \tag{4.101}$$

with $D_{ij} = \partial_i\partial_j - \frac{1}{3}\Delta\delta_{ij}$, and solve the perturbation equations to find for the first order scalar metric perturbations

$$\psi^{(1)} = \frac{\eta^2}{18}\Delta\varphi(\mathbf{x}) + \frac{5}{3}\varphi(\mathbf{x}) , \tag{4.102}$$

$$\chi^{(1)} = -\frac{\eta^2}{3}\varphi(\mathbf{x}) , \tag{4.103}$$

where the peculiar gravitational potential $\varphi(\mathbf{x})$ is given by the cosmological Poisson equation

$$\Delta\varphi(\mathbf{x}) = 4\pi G\varrho_H a^2\delta(\mathbf{x},t) \ . \tag{4.104}$$

The equation relates the potential to the density perturbation $\varrho(\mathbf{x},t) = \varrho_H(t)(1+\delta(\mathbf{x},t))$.

With the results (4.102) and (4.103) their line element is given by

$$\mathrm{d}s^2 = -\mathrm{d}t^2 + a^2(t)\left[\left(1-\frac{10}{3}\varphi(\mathbf{x})\right)\delta_{ij} - 3t_i^2\frac{a}{a_i}\partial_i\partial_j\varphi(\mathbf{x})\right]\mathrm{d}x^i\mathrm{d}x^j \ . \tag{4.105}$$

This form emerges by fixing an ambiguity in the definition of $\psi^{(1)}$ and $\chi^{(1)}$ such that $\chi^{(1)}$ has no constant part independent of a. With any other choice there would be additional constant terms proportional to $\partial_i\partial_j\varphi(\mathbf{x})$ in the metric. We will see that our choice in the RZA case was a different one.

To come to a direct comparison, we first rewrite the Eqs. (4.33b) and (4.33d) for the first-order ansatz (4.37) in the form

$$\eta^a_{\ i} = a(t)\left[\delta^a_{\ i} + P^a_{\ i}(X,t)\right] \ . \tag{4.106}$$

Eq. (4.33b) is to first order

$$\ddot{P}(X,t) + 2H\dot{P}(X,t) = -4\pi G\varrho_H\left(\mathring{P} - P + \delta_{\mathbf{i}}\right) \ , \tag{4.107}$$

where $P = P^i{}_i(X,t)$, $\mathring{P} = P^i{}_i(X,t_0)$ and $\delta_{\mathbf{i}}$ is defined as

$$\varrho = \mathring{\varrho}\frac{\mathring{J}}{J} = \left(\frac{a_i}{a}\right)^3 (\mathring{\varrho}_0 + \mathring{\varrho}_1)\frac{1+\mathring{P}}{1+P} = \left(\frac{a_i}{a}\right)^3 \mathring{\varrho}_0\left(1+\delta_{\mathbf{i}} - P + \mathring{P}\right) . \tag{4.108}$$

Eq. (4.33d) becomes

$$H\dot{P}(X,t) = 4\pi G\varrho_H(t)\left(-P+\mathring{P}+\delta_{\mathbf{i}}\right) - \frac{1}{4}{}^{(1)}R , \tag{4.109}$$

where the first order Ricci curvature is given by

$${}^{(1)}R = -\frac{4}{a^2}\mathring{P}^k{}_{[k}{}^{|l}{}_{|l]} . \tag{4.110}$$

We may solve these equations for the coframe perturbations in the limit discussed in Sec. 4.3.2. Sending them to integrable ones

$$P^i{}_j(X,t) = \Psi(X)\,\delta^i{}_j + \xi(t)\,\psi^{|i}{}_{|j}(X) \tag{4.111}$$

and using the EdS model to be specific, we find from (4.107) that

$$\Rightarrow \delta_{\mathbf{i}} = -\psi^{|i}{}_{|i}(X) , \tag{4.112}$$

which is the analogue of Eq. (4.104). From (4.109) Ψ is determined to be $\frac{5}{2}\psi = \Psi$. As we work with the same coordinate system in both cases, we may compare the normalization of the potentials by equating the initial density contrasts in the two Poisson equations (4.104) and (4.112). This reveals

$$\varphi = -\frac{2}{3}\frac{1}{t_i^2}\psi , \tag{4.113}$$

where t_i is the initial cosmic time. Combining the above expressions shows, that the metric ${}^{\mathrm{RZA}}g_{ij}(t,X^k) = \delta_{ab}\eta^a{}_i\eta^b{}_j$ is

$${}^{\mathrm{RZA}}g_{ij}(t,X^k) = a^2(t)\left(\delta_{ij}+P_{ij}(X,t)\right) = a^2(t)\left(\delta_{ij} - \frac{10}{3}\varphi\delta_{ij} - 3t_i^2\xi(t)\partial_i\partial_j\varphi\right) . \tag{4.114}$$

For the EdS model used by Li and Schwarz in the derivation of (4.105), the RZA variable $\xi(t)$ is $\xi(t) = a(t) - 1$. This completes the analogy of the first order RZA metric (4.114) with the standard perturbation theory metric (4.105).

Backreaction The RZA as defined in Sec. 4.2.2, however, is not merely a first order scheme. It comes with the prescription not to do a consistent truncation to a given order, but to evaluate the kinematical quantities in their exact form in terms of coframes, using

the first-order perturbed coframes. This approximation has proven to be useful in the Newtonian case and this is also the case in the determination of the backreaction term.

In the strict interpretation of a first order scheme and with a consistent truncation, backreaction would be zero. From Eq. (4.56) we immediately see that the leading order term is of second order. This second order contribution is

$$ {}^{(2)}\mathcal{Q}_{\mathcal{D}} = \dot{\xi}^2 \left(2 \left\langle \mathrm{II} \left(\dot{\mathscr{P}}^a_{\ i} \right) \right\rangle_{\mathcal{C}_{\mathcal{D}}} - \frac{2}{3} \left\langle \mathrm{I} \left(\dot{\mathscr{P}}^a_{\ i} \right) \right\rangle^2_{\mathcal{C}_{\mathcal{D}}} \right) . \tag{4.115} $$

In the limit discussed in Sec. 4.3.2, in which we can make the comparison to the Li Schwarz results [15, 16, 17], it becomes

$$ {}^{(2)}\mathcal{Q}_{\mathcal{D}} = \dot{\xi}^2 \left(2 \left\langle \mathbf{II} \left(\psi^{|i}_{\ |j} \right) \right\rangle_{\mathcal{D}_\mathrm{i}} - \frac{2}{3} \left\langle \mathbf{I} \left(\psi^{|i}_{\ |j} \right) \right\rangle^2_{\mathcal{D}_\mathrm{i}} \right) . \tag{4.116} $$

This is the same as in the standard perturbation theory results of Li and Schwarz [15, 16, 17], which reads

$$ \mathcal{Q}_{\mathcal{D}} = \frac{t_i^2}{a} \left(\langle (\Delta\varphi)^2 \rangle - \langle \partial^i \partial_j \varphi \partial^j \partial_i \varphi \rangle - \frac{2}{3} \langle \Delta\varphi \rangle^2 \right) = \frac{t_i^2}{a} \left(2 \left\langle \mathbf{II} \left(\varphi^{|i}_{\ |j} \right) \right\rangle_{\mathcal{D}_\mathrm{i}} - \frac{2}{3} \left\langle \mathbf{I} \left(\varphi^{|i}_{\ |j} \right) \right\rangle^2_{\mathcal{D}_\mathrm{i}} \right) . \tag{4.117} $$

As discussed below Eq. (4.41), in the EdS case $\xi = a - 1$ and therefore $\dot{\xi}^2 = \dot{a}^2 = \frac{4}{9} a^{-1} t_i^{-2}$. By taking into account Eq. (4.113) one may figure out that the prefactor is also the same.

The fact that the first-order perturbative expansion is sufficient for the backreaction term comes from Eq. (4.51). There, we have shown that the backreaction term does not depend on the complete expansion tensor, but merely on the peculiar one $\theta^i_{\ j} := \Theta^i_{\ j} - H(t)\delta^i_{\ j}$. This subtracts the zeroth order term, so the second order backreaction stems from the square of the first order. The intrinsic second-order term is relevant at third order only. This is different for the curvature term, which explains why we did not find consistent results to second order in Sec. 4.3.2.

Finally, we want to go one order higher in the comparison. This is of course no longer possible with the approximation discussed above, which is only a first order scheme. This is not a problem, as the comparison is anyway possible in the limit of integrable coframes only. In this limit however, as we saw in Sec. 4.3.2, we are back to the Newtonian perturbation theory. So we may use the Newtownian results of Lagrangian perturbation theory. A summary of the third order results is given in [105]. From there, we take the displacement (4.35) to be

$$ \begin{aligned} \vec{f} \;=\; & a\,\vec{X} \;+\; q_z(a)\,\nabla_0 \mathcal{S}^{(1)}(\vec{X}) \;+\; q_{zz}(a)\,\nabla_0 \mathcal{S}^{(2)}(\vec{X}) \\ & + q^a_{zzz}(a)\,\nabla_0 \mathcal{S}^{(3a)}(\vec{X}) \;+\; q^b_{zzz}(a)\,\nabla_0 \mathcal{S}^{(3b)}(\vec{X}) \;-\; q^c_{zzz}(a)\,\nabla_0 \times \vec{\mathcal{S}}^{(3c)}(\vec{X}) \,, \end{aligned} \tag{4.118} $$

where the time dependence of the different orders is given by

$$q_z = \left(\frac{3}{2}\right)\left(a^2 - a\right) , \tag{4.119a}$$

$$q_{zz} = \left(\frac{3}{2}\right)^2\left(-\frac{3}{14}a^3 + \frac{3}{5}a^2 - \frac{1}{2}a + \frac{4}{35}a^{-\frac{1}{2}}\right) , \tag{4.119b}$$

$$q^a_{zzz} = \left(\frac{3}{2}\right)^3\left(-\frac{1}{9}a^4 + \frac{3}{7}a^3 - \frac{3}{5}a^2 + \frac{1}{3}a - \frac{16}{315}a^{-\frac{1}{2}}\right) , \tag{4.119c}$$

$$q^b_{zzz} = \left(\frac{3}{2}\right)^3\left(\frac{5}{42}a^4 - \frac{33}{70}a^3 + \frac{7}{10}a^2 - \frac{1}{2}a + \frac{4}{35}a^{\frac{1}{2}} + \frac{4}{105}a^{-\frac{1}{2}}\right) , \tag{4.119d}$$

$$q^c_{zzz} = \left(\frac{3}{2}\right)^3\left(\frac{1}{14}a^4 - \frac{3}{14}a^3 + \frac{1}{10}a^2 + \frac{1}{2}a - \frac{4}{7}a^{\frac{1}{2}} + \frac{4}{35}a^{-\frac{1}{2}}\right) , \tag{4.119e}$$

and the different orders of $\mathcal{S}$ may be determined from the equations

$$\Delta_0\mathcal{S}^{(1)} = \mathbf{I}\left(\mathcal{S}_{,i,k}\right)\, t_0 , \tag{4.120a}$$

$$\Delta_0\mathcal{S}^{(2)} = 2\mathbf{II}\left(\mathcal{S}^{(1)}_{,i,k}\right) , \tag{4.120b}$$

$$\Delta_0\mathcal{S}^{(3a)} = 3\mathbf{III}\left(\mathcal{S}^{(1)}_{,i,k}\right) , \tag{4.120c}$$

$$\Delta_0\mathcal{S}^{(3b)} = \sum_{a,b,c}\epsilon_{abc}\,\frac{\partial\left(\mathcal{S}^{(2)}_{,a},\mathcal{S}^{(1)}_{,b},X_c\right)}{\partial\left(X_1,X_2,X_3\right)} , \tag{4.120d}$$

$$\left(\Delta_0\vec{\mathcal{S}}^{(3c)}\right)_k = \epsilon_{pq[j}\frac{\partial\left(\mathcal{S}^{(2)}_{,i]},\mathcal{S}^{(1)}_{,p},X_q\right)}{\partial\left(X_1,X_2,X_3\right)} . \tag{4.120e}$$

Using the prescription (4.66), we may evaluate (4.47) for the volume deformation. With (4.45) this gives the average scale factor

$$\begin{aligned} a_{\mathcal{D}}\left(t\right) = a\left(t\right)\Bigg(1 + \frac{q_z}{a}\left\langle\mathbf{I_i}\right\rangle_{\mathcal{D}_\mathbf{i}} + \left(2\frac{q_{zz}}{a} + \left(\frac{q_z}{a}\right)^2\right)\left\langle\mathbf{II_i}\right\rangle_{\mathcal{D}_\mathbf{i}} + \\ + \left(\left(\frac{q_z}{a}\right)^3 + 3\frac{q^a_{zzz}}{a}\right)\left\langle\mathbf{III_i}\right\rangle_{\mathcal{D}_\mathbf{i}} + 2\left(\frac{q_z}{a}\frac{q_{zz}}{a} + \frac{q^b_{zzz}}{a}\right)\left\langle\mathbf{II}^{(1,2)}_\mathbf{i}\right\rangle_{\mathcal{D}_\mathbf{i}}\Bigg)^{1/3} . \end{aligned} \tag{4.121}$$

Here we use the Newtownian potential of the correspondence as well as the Newtonian average $\langle O\rangle_{\mathcal{D}_\mathbf{i}}$. This means that these invariants are the invariants (4.65) of the gradients of the potential $\psi = \frac{3}{2t_i^2}\mathcal{S}$

$$\mathbf{I_i} := \mathbf{I}\left(\psi^{|i}_{\ |j}\right) \quad , \quad \mathbf{II_i} = \mathbf{II}\left(\psi^{|i}_{\ |j}\right) \quad , \quad \mathbf{III_i} := \mathbf{III}\left(\psi^{|i}_{\ |j}\right) , \tag{4.122}$$

defined analogously to (4.55). The new invariant $\mathbf{II}^{(1,2)}_\mathbf{i}$ is related to $\psi^{(2)} = \left(\frac{3}{2}\right)^2\mathcal{S}^{(2)}$ by

$$\mathbf{II}^{(1,2)}_\mathbf{i} = \frac{1}{2}\left(\psi^{|j}_{\ |j}\psi^{|k(2)}_{\ \ |k} - \psi^{|k}_{\ |j}\psi^{|j(2)}_{\ \ |k}\right) . \tag{4.123}$$

With this volume scale factor we can determine the third order backreaction term from (4.11b) which is

$$\mathcal{Q}_{\mathcal{D}} = 3\frac{\ddot{a}_{\mathcal{D}}}{a_{\mathcal{D}}} + 4\pi G\frac{a^3}{a_{\mathcal{D}}^3}\varrho_H\left(1 - \langle \mathbf{I_i}\rangle_{\mathcal{D}_\mathbf{i}}\right) \ , \tag{4.124}$$

where $\varrho_H(t)$ is the background density and we have seen in (4.112) that the density perturbation $\delta_\mathbf{i}$ is related to the first invariant of the potential by $\delta_\mathbf{i} = -\mathbf{I_i}$. In the scheme used in the derivation of (4.118), the choice was made to put all matter perturbations into the first-order density perturbation, so $\varrho = \frac{a^3}{a_{\mathcal{D}}^3}\varrho_H\left(1 - \langle \mathbf{I_i}\rangle_{\mathcal{D}_\mathbf{i}}\right)$ is the complete inhomogeneous density to all orders.

With these definitions and equations we can finally derive the third-order contribution to the backreaction term. It has several components, two of them decaying and one of them constant in time. This constant part reads

$${}^{(3)}\mathcal{Q}_{\mathcal{D}} = \frac{4}{3}\langle \mathbf{I_i}\rangle^3_{\mathcal{D}_\mathbf{i}} - \frac{74}{21}\langle \mathbf{I}\rangle_{\mathcal{D}_\mathbf{i}}\langle \mathbf{II_i}\rangle_{\mathcal{D}_\mathbf{i}} - \frac{12}{7}\left\langle \mathbf{II}_\mathbf{i}^{(1,2)}\right\rangle_{\mathcal{D}_\mathbf{i}} + 6\langle \mathbf{III_i}\rangle_{\mathcal{D}_\mathbf{i}} \ . \tag{4.125}$$

This can be compared to the result obtained by Li and Schwarz [17] which reads[2]

$$\begin{aligned}\mathcal{Q}_0 \ = \ & \frac{t_i^4}{2}\langle\Delta\varphi\rangle\left(\langle(\Delta\varphi)^2\rangle - \langle\partial^i\partial_j\varphi\partial^j\partial_i\varphi\rangle - \frac{2}{3}\langle\Delta\varphi\rangle^2\right) \\ & + t_i^4\Bigg[-3\langle\partial^i\partial_j\varphi\partial^j\partial_k\varphi\partial^k\partial_i\varphi\rangle + \frac{45}{14}\langle\partial^i\partial_j\varphi\partial^j\partial_i\varphi\Delta\varphi\rangle - \frac{3}{14}\langle(\Delta\varphi)^3\rangle \\ & \quad + \frac{18}{7}\langle\partial^i\partial_j\varphi\partial^j\partial_i\psi_0\rangle - \frac{15}{7}\langle\partial^i\partial_j\varphi\partial^j\partial_i\varphi\rangle\langle\Delta\varphi\rangle \\ & \quad + \frac{15}{7}\langle\Delta\varphi\rangle\langle(\Delta\varphi)^2\rangle - \frac{5}{3}\langle\Delta\varphi\rangle^3\Bigg] \ .\end{aligned} \tag{4.126}$$

Of course this has first to be written in the same form to be comparable. Converting the potentials with the correspondence (4.113), being $\varphi = -\frac{2}{3}\frac{1}{t_i^2}\psi$, and using the definitions (4.122) and (4.123), we arrive at exactly the same expression as the one in the Newtonian limit, i.e. (4.125). This is also the case for the next order. This allows us to give the expression for the fourth order backreaction term in appendix B.

One could object that this result was obvious as we are solving the equations for the same dust fluid. However, it is not a priori clear that the Newtonian fluid equations should give the same result as standard cosmological perturbation theory in the GR case. The result implies that the contributions calculated by Li and Schwarz [15, 16, 17], that were calculated by keeping only the fastest growing terms, are the Newtonian ones. For those there is the theorem that they are boundary terms decaying with a spherical enlargement of the averaging domain. So the fastest growing contributions

[2]Note that we have reestablished the version of $\mathcal{Q}_0$ in terms of the background scale factor a. The conversion from the $a_{\mathcal{D}}$ to a dependence leads to the inclusion of the first line.

to the perturbative expression of the backreaction term are all boundary terms (in the sense that they decay when we increase the domain of averaging and in contrast to the constant domain independent 10^{-5} terms derived e.g. in [18]). This has already been mentioned by Räsänen [20] and is important when considering the large scale effects of cosmological backreaction. The question whether the inhomogeneities would renormalize the background with an effective cosmological constant will therefore not be decided by the terms presented here, but rather the sub-leading contributions (see [20] for a discussion). For the small scale results that we discuss in Sec. 4.4.2, however, these are the most important contributions.

4.5.2. Non-perturbative models

The results obtained in the RZA are not only consistent with other perturbative treatments as discussed in the previous section. They also provide a nice description of the properties of a model that was constructed to describe non-perturbative features. This model was introduced by Räsänen in [27]. There, he investigated the average evolution of an ensemble of regions that are over- or under-dense respectively. For the distribution of peaks and under-densities he used the statistics for a Gaussian random field given by the BBKS paper [106]. The evolution of the individual regions was described by the spherical collapse model that treats the peaks as "small Universes" with positive or negative curvature. In this model he evaluated the expansion rate and the acceleration parameter.

In a similar way as Räsänen we want to ask the question what the backreaction and structure evolution in such a model looks like. Unlike him, however, we do not only want to treat the extreme peaks and troughs, but describe the complete Universe systematically also for not very over- or under-dense regions in the spirit of [26]. As we have seen in Sec. 2.1.1, the density field smoothed over regions of a certain size by the prescription (2.27) is, for a Gaussian random field, approximately given by a Gaussian distribution. The variance of this Gaussian distribution is related to the correlation function of the underlying Gaussian field by Eq. (2.29). This enables us to create our test Universes in a simple way: We calculate from the ΛCDM power spectrum (2.112) the density fluctuations σ by (2.23) in boxes that correspond to the density smoothing (2.27). We will refer to this model as MultiDomain model. For each of the boxes we determine an initial over-density $1+\delta_{\mathcal{D}_j}$ by generating Gaussian random numbers with mean 1 and variance σ. Then we let each individual region j evolve like a FRW Universe with curvature by the equation

$$\left(\frac{\dot{a}_j}{a_j}\right)^2 = H_{\mathbf{i}}^2\left(\Omega_{m,\mathbf{i}}\left(1+\delta_{\mathcal{D}_j}\right)\left(\frac{a_{\mathbf{i}}}{a_j}\right)^3 + \left(1-\Omega_{m,\mathbf{i}}\left(1+\delta_{\mathcal{D}_j}\right)-\Omega_{\Lambda,i}\right)\left(\frac{a_{\mathbf{i}}}{a_j}\right)^2 + \Omega_{\Lambda,i}\right), \tag{4.127}$$

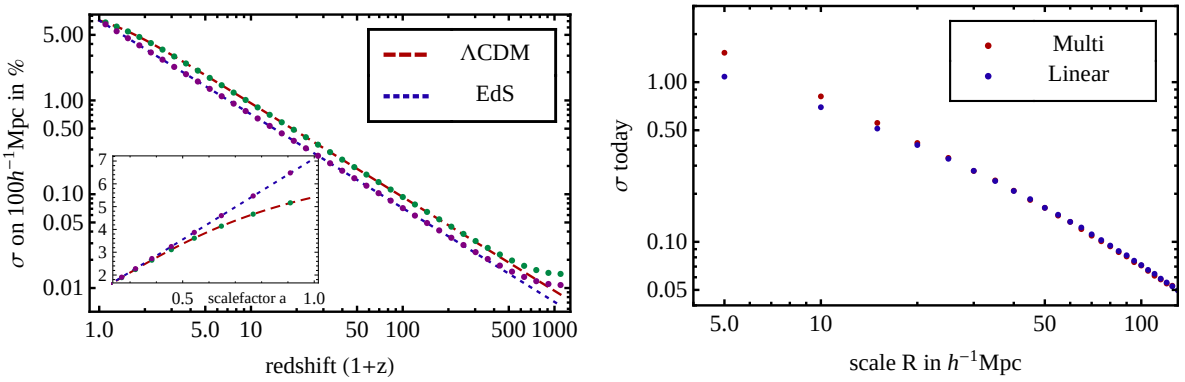

Figure 4.12. The growth of the matter fluctuations in a sphere of radius $100h^{-1}$Mpc. The dashed lines represent the linear growth function $D(a)$ which is equal to a in the EdS case. The dots are the result of the MultiDomain model. The inset zooms into the evolution today, i.e. around a scale-factor of $a_0 = 1$. For better distinction the curves are normalized such that they are the same today.

where an $\mathbf{i}$ denotes the initial value of the respective quantity and j indexes the domain (we choose the same initial value for the scale-factors of all domains so $a_{j,\mathbf{i}} =: a_\mathbf{i}$). To determine the initial values $H_\mathbf{i}$, $\Omega_{\Lambda,\mathbf{i}}$ and $\Omega_{m,\mathbf{i}}$ we use the values that we find from a ΛCDM ($H_0 = 70\frac{km}{sMpc}$, $\Omega_{m,0} = 0.27$) or an EdS ($H_0 = 50\frac{km}{sMpc}$, $\Omega_{m,0} = 1$) model with $\delta_{\mathcal{D}_j} = 0$. This means $\Omega_{\Lambda,\mathbf{i}} = 1 - \Omega_{m,\mathbf{i}}$ and so

$$\left(\frac{\dot{a}_j}{a_j}\right)^2 = H_\mathbf{i}^2 \left(\Omega_{m,\mathbf{i}} \left(1 + \delta_{\mathcal{D}_j}\right) \left(\frac{a_\mathbf{i}}{a_j}\right)^3 - \Omega_{m,\mathbf{i}} \delta_{\mathcal{D}_j} \left(\frac{a_\mathbf{i}}{a_j}\right)^2 + (1 - \Omega_{m,\mathbf{i}})\right) . \tag{4.128}$$

With the evolution of the individual scale factors, we may then calculate the over-density of the regions at later times, because we assume that they are independent. So the matter content is conserved and the over-density evolution for a given domain is

$$\delta_{\mathcal{D}_j}(t) = \left(\frac{a}{a_j}\right)^3 \left(1 + \delta_{\mathcal{D}_j}(t_\mathbf{i})\right) - 1 . \tag{4.129}$$

We calculate this evolution for 10,000 domains starting with our Gaussian initial conditions and the ΛCDM power spectrum (2.112) at a redshift of $z = 1100$. At several intermediate time (= redshift) steps we calculate the variance of the emerging over-density distribution. We consider the increased volume of the under-dense domains, by calculating an effective number of domains of the given scale. So a domain that ends up with a volume two times larger than the average counts twice. The results are shown in Fig. 4.12. At early times the points do not quite agree with the linear growth function that describes the growth of the clustering strength related to an increasing σ. However,

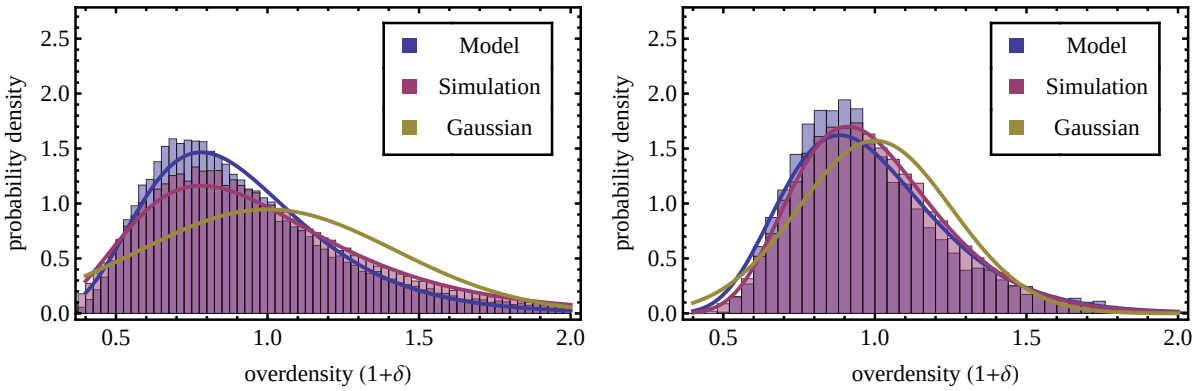

Figure 4.13. Density distribution for boxes of $7.5h^{-1}$Mpc and $15h^{-1}$Mpc side-length at a redshift of $z = 3$. The blue histogram contains the results of the evolution of the sub-volumes in the MultiDomain model. The red histogram is the result of an analysis of the VLS data [78]. The curves are the best fit log-normal distributions.

this is only due to the choice of a common expansion rate $H_{\mathbf{i}}$ for all domains. This choice hinders the initial growth and leads to lower values of σ. For simplicity we corrected for this by dividing the points by a factor of 0.6 to have the late normalization correct. We will also do this for all plots that follow. Of course, one could also use more refined initial conditions that also provide a correct value for the perturbed expansion rate. By choosing not to do this we demonstrate nicely how the growth of σ comes about by the different Hubble expansion on different domains, which emerges due to the perturbation in the density after the necessary relaxation time.

The interesting consequence of Fig. 4.12 now is, that once the initial phase is over, the growth in σ follows exactly the result from linear theory. Also the scale dependence follows the linear result for scales where linear theory is supposed to be applicable. For a more detailed picture, the full distribution of over-densities in the different regions at a redshift of $z = 3$ is shown in Fig. 4.13. It has already evolved away from a Gaussian distribution and is now approximately described by a Log-Normal distribution. For comparison to possible effects of nonlinear structure, we determined the over-density distribution for boxes of the same size from of the Very Large Simulation project data (VLS) [78]. We see, that the shape of the distribution is also in the simulation of Log-Normal type. In addition the shapes of distributions for the model and the simulation are quite close, even if for small scales they begin to deviate. This may be due to the unclear treatment of regions that have collapsed to zero volume at the time of evaluation. This happens earlier on small scales, so the deviation occurs there first.

Finally, we want to compare the result of the growth of the average scale factor to the predictions from the calculation above. The average scale factor for the overall domain is

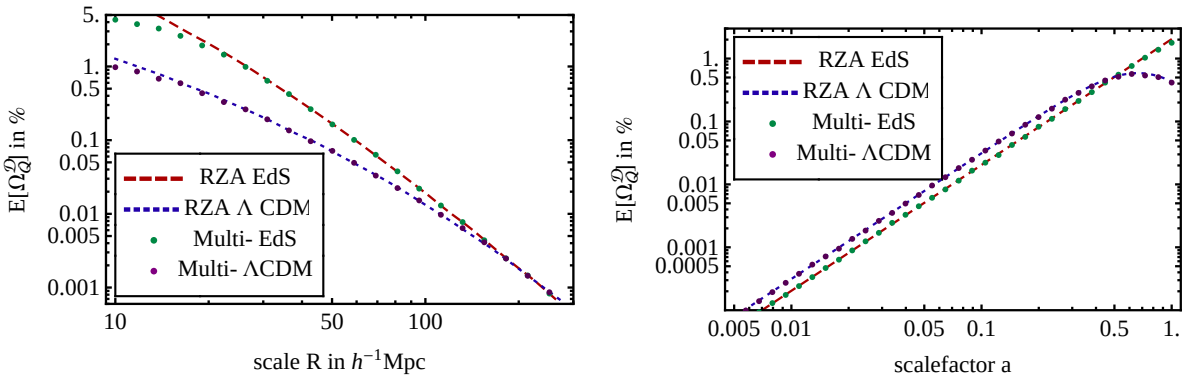

Figure 4.14. Values of Omega-backreaction as determined from the MultiDomain model for ΛCDM and EdS (dots). The lines represent the ensemble expectation value of $\Omega_{\mathcal{Q}}^{\mathcal{D}}$ as determined from perturbation theory. Left: Scale dependence today. Right: Time evolution on a scale of $20h^{-1}$Mpc.

given by

$$a_{\mathcal{D}} = \left(\frac{1}{N} \sum_{j=1}^{N} \left(\frac{a_j}{a_{\mathbf{i}}} \right)^3 \right)^{1/3} . \tag{4.130}$$

This allows us again to calculate $\Omega_{\mathcal{Q}}^{\mathcal{D}}$ from (4.11b) by

$$\mathcal{Q}_{\mathcal{D}} = 3\frac{\ddot{a}_{\mathcal{D}}}{a_{\mathcal{D}}} + 4\pi G \frac{a^3}{a_{\mathcal{D}}^3} \varrho_H \left(1 + \delta_{\mathbf{i}}\right) , \tag{4.131}$$

which is in the MultiDomain model and for today

$$\Omega_{\mathcal{Q}}^{\mathcal{D}_0} = -\frac{1}{2}\frac{1}{H_{\mathcal{D}_0}^2} \left(\frac{\ddot{a}_{\mathcal{D}_0}}{a_{\mathcal{D}_0}} + \frac{1}{2a_{\mathcal{D}_0}^3} H_{\mathbf{i}}^2 \Omega_{m,\mathbf{i}} \frac{1}{N} \sum_{j=1}^{N} \left(1 + \delta_{j,\mathbf{i}}\right) - H_{\mathbf{i}}^2 \Omega_{\Lambda,\mathbf{i}} \right) . \tag{4.132}$$

To compare this to the perturbative result, we use equation (4.116). So the ensemble expectation value for the backreaction on the domain, that is formed by the union of the different sub-domains j, becomes in the EdS case

$$\mathbb{E}\left[\mathcal{Q}_{\mathcal{D}}\right] = -\frac{2}{3}\dot{a}^2 \mathbb{E}\left[\langle \mathbf{I}_{\mathbf{i}} \rangle_{\mathcal{D}_{\mathbf{i}}}^2\right] , \tag{4.133}$$

and in the ΛCDM case

$$\mathbb{E}\left[\mathcal{Q}_{\mathcal{D}}\right] = -\frac{2}{3}\dot{D}\left(a\right)^2 \mathbb{E}\left[\langle \mathbf{I}_{\mathbf{i}} \rangle_{\mathcal{D}_{\mathbf{i}}}^2\right] , \tag{4.134}$$

where the function $D\left(a\right)$ is given by (2.129). In Fig. 4.14 we compare these theoretical predictions to the outcome (4.132) of our calculation for the Gaussian distributed domains.We find that the scale dependence as well as the time evolution of the expectation

value of the kinematical backreaction term is well described by our theoretical model. Of course, this was anticipated from the result of Fig. 4.12, namely that the matter fluctuations grow as in linear theory. But it is not completely evident that the more complicated expression (4.132) gives the linear theory result. In addition, it is interesting to see what order of magnitude the effect has. The fact that it is only a few per-cent effect on small scales and rapidly decreases on large scales shows, that it is unlikely to have a big effect within the standard cosmological framework. If there is not something drastically happening in the interaction of the different regions, kinematical backreaction remains at the 10^{-5} level on the Hubble scale.

5. The influence of structure on observations

In the previous chapter we saw, that even the inhomogeneous Universe may on average be described by equations that look like the standard Friedmann equations, derived under the assumption of homogeneity and isotropy. These average equations however contain effective terms that will modify the dynamics of the expansion of the Universe. The evaluation of these terms in the framework of Lagrangian perturbation theory in the previous section showed that there are no global effects to be expected if the standard perturbative result is correct. However, Fig. 4.6 made clear that local fluctuations are there and may be important even in a perturbative treatment and even in Newtonian theory. Of course, the fluctuations are not limited to the backreaction parameter, but also occur in the other cosmic parameters. There, as we have seen in Sec. 4.4.2, the curvature is systematically more important than the backreaction component. In addition, as we will see, its fluctuations stay important up to much larger scales than the fluctuations in the backreaction term. In this chapter we will, therefore, investigate the question, how big these fluctuations actually are and to what extent they influence the measurement of important cosmological observables that are determined in the local Universe. Why these local observables are important is discussed in Sec. 5.1. After this short motivation we will complete the picture begun in Sec. 4.4.2 to study in more detail the actual scale dependence of the fluctuations in the cosmic parameters rather than their time dependence. This will lead to concise formulae for the perturbations in Sec. 5.2. Their evaluation for realistic surveys makes use of suitable window functions corresponding to real observations. Their implementation is discussed in Sec. 5.3. Sec. 5.4 then presents the variations that occur in observables of the local cosmic structure. We will see that they present fundamental limitations to the accuracy of a measurement of especially the Hubble flow. From Sec. 5.2 on, the text is basically the one that we published in [39].

5.1. Cosmic variance

The theoretical limitation of the precision with which we are in principle able to infer global cosmic parameters from observations is often called cosmic variance. Especially for the CMB this limitation is well studied. It is most important for the measurement of the C_ℓ's on large scales, but has also to be taken into account in the determination of the errors on higher order multipoles if the instrumental uncertainties are small enough.

For the Planck mission this means for example that cosmic variance is the dominant error up to multipoles of $\ell \approx 2500$. This fundamental limitation comes from the fact that with the CMB we observe only one realization of the stochastic process that led to these temperature fluctuations. So the number of independent realizations is limited especially for large scales, because we only have one Universe in which we can observe the CMB.

In the case of the late time structure inhomogeneities, the situation is a bit better because we have three dimensional information on the matter distribution. Ultimately however, the situation is similar, as we can only observe one representation of the Universe when we go to large scales, i.e. the one centered on the position of our Milky Way. The situation is even worse if we are interested in the properties of the Universe at a given cosmic time. As all of the cosmologically interesting measurements are based on radiation that travels with the speed of light, we can only observe our past light cone. So when we look at larger and larger scales, we also look further back in time. Therefore, the information that we have about today's Universe is strictly speaking limited to a small volume around us. We will see in the following section that measurements which are local in this sense, play an important role for our current understanding of our Universe. The way this understanding is approached by a theorist and an observer is shown in Fig. 5.1.

5.1.1. The importance of local measurements

The only global measurement that we have is the CMB. All other measurements are more or less local. Current galaxy surveys convincingly probe the Universe up to a redshift of 0.2 (with more sparse recent data up to 0.4-0.5). The supernova measurements reach out to larger redshifts, but they have to be normalized with the measured value of the Hubble expansion today. This quantity is by definition constrained to be measured in our cosmic neighborhood and therefore subject to the biggest uncertainty. This dependence of our conclusions on the correct result of local measurements is nicely visualized by the plot of the WMAP results in Fig. 5.2. It shows the allowed region of parameter space for the curvature and dark energy parameter. The figure nicely illustrates the well known degeneracy in these two parameters, if only data from the WMAP mission is used. The degeneracy emerges, because the oscillatory features in the CMB only fix the distance to the surface of last scattering. This distance, however, may be generated by late time cosmic curvature on the one hand, or a cosmological constant on the other hand. It is only by adding local information that we exclude the large portion of the parameter space that corresponds to a vanishing or small cosmological constant but nonzero curvature. As discussed, this local information partly depends on H_0. Fig. 5.2 demonstrates that its value depends on data that is collected within the nearest 200 Mpc, corresponding to a redshift smaller than 0.1. This is not likely to be a region representable for the whole present day Universe, so we will calculate the fluctuations that we expect between different regions of this size.

A still more radical idea in this line that explores the consequences of our local

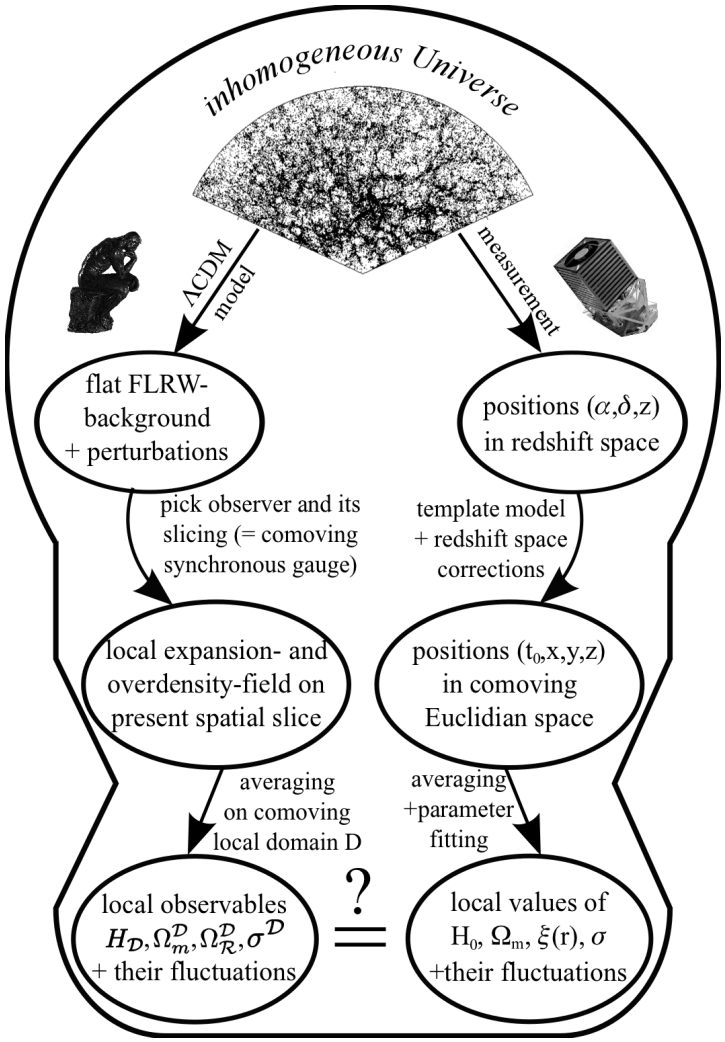

Figure 5.1. Comparison of the theorist's and observer's view on the Universe. Our calculation in comoving synchronous gauge facilitates the description of the boundaries of the experimentally investigated regions in our Universe. Note, that recently there have been attempts by [107] to directly relate the two upper circles. This was done by calculating the predictions for the quantities in redshift space explicitly from the perturbed ΛCDM model.

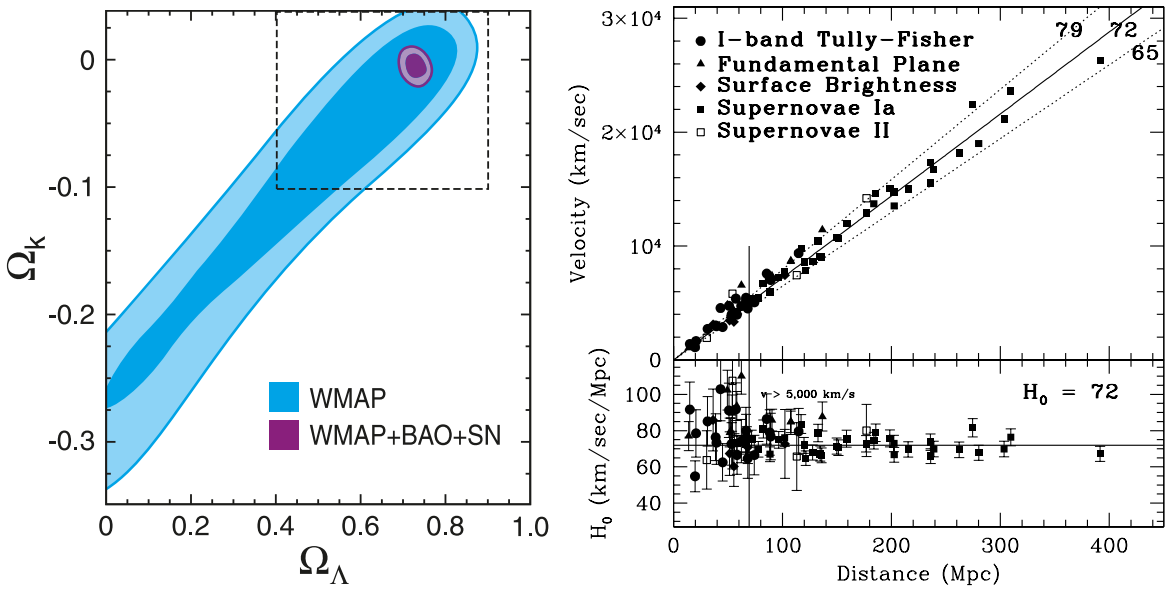

Figure 5.2. Left: Illustration of the importance of local information for the determination of cosmic curvature. As the WMAP results only fix the distance to the surface of last scattering, there is an ambiguity concerning the reason for this distance. It could either be due to curvature or due to Λ. The local structure information then fixes it to be Λ. Graph from [109]. Right: Measurement of the Hubble constant H_0 by different methods. Most of them, except for certain supernovae, are within a region of 200 Mpc around us. Graph from [110].

environment not being a typical region of the Universe, is the idea that we live close to the center of a giant under-density. If this under-density has the right properties it might be able to explain the observations without having to introduce a cosmological constant. However, the isotropy of the CMB places severe constraints on our allowed displacement from the center of the under-density, rendering these models highly non-Copernican (see e.g. [108] for a test of the void model with observations).

5.1.2. Ensemble variance of averaged observables

As already mentioned above, we will be interested in the following to what extent cosmic parameters (4.21) for a given domain-size $\mathcal{D}$ may change from position to position in the Universe solely by the influence of the observed cosmic inhomogeneities. To this end, we formally would have to calculate the variance for the parameters evaluated on domains equivalent to $\mathcal{D}$, but placed at different locations in our spatial slice. For an ergodic process, however, this is the same as the variance of an ensemble average over

many realizations of the Universe keeping the domain $\mathcal{D}$ fixed, but changing the initial conditions of the matter distribution. This is the quantity that we calculate in theory and therefore we have to rely on the assumption of ergodicity when comparing our results with the observation. In our case this ensemble average is taken over quantities that are volume averages. This means that for any observable O there are two different averages involved. The domain averaging, $\langle O\rangle_{\mathcal{D}}$, and the ensemble average, $\overline{O}$. We assume that both averaging procedures commute.

The fluctuations are then characterized by the variance with respect to the ensemble averaging process,

$$\sigma\left(\langle O\rangle_{\mathcal{D}}\right) := \left(\overline{\langle O\rangle_{\mathcal{D}}^2} - \overline{\langle O\rangle_{\mathcal{D}}}^2\right)^{\frac{1}{2}} \quad . \tag{5.1}$$

An example for a common observable calculated in this manner would be σ_8 as the ensemble r.m.s. fluctuation of the matter density field. Other observables that we will concentrate on are the matter parameter $\Omega_m^{\mathcal{D}}$ and the curvature parameter $\Omega_{\mathcal{R}}^{\mathcal{D}}$ as well as the Hubble rate $H_{\mathcal{D}}$. To evaluate their fluctuations we use the results of Li and Schwarz [15, 16, 17] who determined the inhomogeneous corrections to the average background value in standard cosmic perturbation theory. Even though they determine the correction up to second order, we will only need the linear result. This is because the fluctuations (5.1) in an observable that has a first order perturbation are of first order, but the second term in the expansion of the fluctuations is already of third order. Formally this has been shown in [17] by decomposing O into successive orders $O = O^{(0)} + O^{(1)} + O^{(2)} + \cdots$. For a Gaussian distribution we may then express (5.1) as

$$\sigma\left(O\right) = \sqrt{\overline{\left(O^{(1)}\right)^2}}\left(1 + \frac{\overline{\left(O^{(2)}\right)^2} - \left(\overline{O^{(2)}}\right)^2 + 2\overline{O^{(1)}O^{(3)}}}{2\overline{\left(O^{(1)}\right)^2}}\right) \quad , \tag{5.2}$$

This shows, that the second order term vanishes. This is of course not the case for observables as $\Omega_{\mathcal{Q}}^{\mathcal{D}}$, that do not have a first order contribution as we have seen in Sec. 4.3.1. Their lowest order contribution to $\sigma\left(O\right)$ is then of second order. We have seen in Fig. 4.6 that the fluctuations rapidly decay and are already at 100 Mpc of the order of a per-cent only. As the galaxy surveys that we will calculate our results for, already probe volumes that are much larger than that, we will not be interested in the variance for $\Omega_{\mathcal{Q}}^{\mathcal{D}}$ in this chapter.

5.2. Fluctuations in the cosmic parameters

We now turn to the calculation of the fluctuations in the cosmic parameters. We use results from standard perturbation theory in synchronous comoving gauge, as obtained by [15, 16, 17]. We will connect these results to the matter density fluctuations σ as the fundamental quantity. This will allow an easy evaluation of the importance of the fluctuations in the next section.

5.2.1. Inhomogeneous cosmic parameters

Using the notation of [15, 16, 17], the perturbed line element

$$\mathrm{d}s^2 = a^2(\eta)\left\{-\mathrm{d}\eta^2 + \left[\left(1-2\psi^{(1)}\right)\delta_{ij} + D_{ij}\chi^{(1)}\right]\mathrm{d}x^i\mathrm{d}x^j\right\} \tag{5.3}$$

defines the metric potentials $\psi^{(1)}(\eta,\mathbf{x})$ and $\chi^{(1)}(\eta,\mathbf{x})$, where η denotes conformal time and $D_{ij} = \partial_i\partial_j - \frac{1}{3}\delta_{ij}\Delta$. By writing the perturbed metric in this form, we constrain ourselves to a flat background. In contrast to chapter 4, we will use here $a_0 = 1$ for today's scale factor. The quantities that we are mainly interested in are the expansion rate and the spatial curvature. The former follows from the expansion tensor and reads

$$\theta = \frac{3}{a}\left(\frac{a'}{a} - \psi^{(1)\prime}\right) , \tag{5.4}$$

where $()'$ stands for the derivative with respect to conformal time. Calculating the spatial Ricci curvature from the above metric yields

$$\mathcal{R} = \frac{12}{a^2}\left(2\frac{a'}{a}\psi^{(1)\prime} + \psi^{(1)\prime\prime}\right) . \tag{5.5}$$

By the covariant conservation of the energy momentum tensor, $\psi^{(1)}$ is related to the matter density contrast $\delta(\eta,\mathbf{x})$ by

$$\psi^{(1)} = \frac{1}{3}\delta - \bar{\zeta}(\mathbf{x}) \quad \delta(\eta,\mathbf{x}) := \frac{\varrho^{(1)}}{\varrho^{(0)}} . \tag{5.6}$$

$\bar{\zeta}(\mathbf{x})$ is a constant of integration that plays no role in the following, because θ and $\mathcal{R}$ involve only time derivatives of $\psi^{(1)}$.

As we are using conformal time, the evolution equation of the density perturbations (2.101) is of the slightly modified form

$$\delta'' + \frac{a'}{a}\delta' = \frac{4\pi G\varrho_0^{(0)}}{a}\delta , \tag{5.7}$$

but the solution in terms of a for a ΛCDM Universe is of course still the same as in (2.129) namely

$$\delta(a,\mathbf{x}) = \frac{D(a)}{D(1)}\delta_0(\mathbf{x}), \text{ with } D(a) = a\,{}_2F_1\left(1,\frac{1}{3};\frac{11}{6};-ca^3\right), \quad \text{and } c \equiv \frac{\Omega_\Lambda}{\Omega_m} . \tag{5.8}$$

Here, $\delta_0(\mathbf{x})$ is the density perturbation today, $D(a)$ is the growth factor and ${}_2F_1$ is a hypergeometric function. In the following we denote today's value of the growth factor by $D_0 \equiv D(1)$.

Plugging this solution into (5.4) and using (5.6), we find the local expansion rate

$$\frac{1}{3}\theta(a,\mathbf{x}) = H_0\sqrt{\frac{\Omega_m}{a^3}}\sqrt{1+ca^3}\left(1-\frac{1}{3}f\left(a\right)\delta\left(a,\mathbf{x}\right)\right)\ , \tag{5.9}$$

expressed in terms of the growth rate

$$f\left(a\right) := \frac{\mathrm{d}\ln D\left(a\right)}{\mathrm{d}\ln a} = \frac{5\frac{a}{D(a)}-3}{2\left(1+ca^3\right)}\ . \tag{5.10}$$

From (5.5) we find the local spatial curvature

$$\mathcal{R}(a,\mathbf{x}) = 10\frac{1}{a^2}H_0^2\Omega_m\frac{\delta_0(\mathbf{x})}{D_0}\ . \tag{5.11}$$

From these quantities we can define local Ω functions,

$$\Omega_m\left(a,\mathbf{x}\right) = \frac{1}{1+ca^3}\left[1+\left(1+\frac{2}{3}f\left(a\right)\right)\delta\left(a,\mathbf{x}\right)\right]\ , \tag{5.12a}$$

$$\Omega_{\mathcal{R}}\left(a,\mathbf{x}\right) = -\left[\frac{1}{1+ca^3}+\frac{2}{3}f\left(a\right)\right]\delta\left(a,\mathbf{x}\right)\ , \tag{5.12b}$$

$$\Omega_\Lambda\left(a,\mathbf{x}\right) = \frac{ca^3}{\left(1+ca^3\right)}\left[1+\frac{2}{3}f\left(a\right)\delta\left(a,\mathbf{x}\right)\right]\ , \tag{5.12c}$$

$$\Omega_{\mathcal{Q}}\left(a,\mathbf{x}\right) = 0\ , \tag{5.12d}$$

demonstrating that the importance of curvature effects grows proportional to the formation of structures. A remarkable property is that $\sum\Omega_i(a,\mathbf{x})=1$ holds not only for the FLRW background, but also at the level of perturbations. For linear perturbations the kinematic backreaction term does not play any role, but becomes important as soon as quadratic terms are considered.

Let us now compare these local quantities with the domain-averaged expansion rate and the spatial curvature [16]. From the definition of the average $\langle\rangle_{\mathcal{D}}$ in (4.6) we find that, in principle, fluctuations in the volume element $d\mu_g$ have to be taken into account. Writing $\mathrm{d}\mu_g = J\mathrm{d}^3x$ with the functional determinant $J = a^3\left(1-3\psi^{(1)}\right)$, the average over the perturbed hypersurface agrees with an average over an unperturbed Euclidean domain

$$\left\langle O^{(1)}\right\rangle_{\mathcal{D}} = \frac{\int_{\mathcal{D}}O^{(1)}J\mathrm{d}\mathbf{x}}{\int_{\mathcal{D}}J\mathrm{d}\mathbf{x}} \simeq \frac{\int_{\mathcal{D}}O^{(1)}\mathrm{d}\mathbf{x}}{\int_{\mathcal{D}}\mathrm{d}\mathbf{x}} =: \left\langle O^{(1)}\right\rangle\ , \tag{5.13}$$

if we restrict our attention to linear perturbations.

We express domain-averaged quantities in terms of the volume scale factor $a_{\mathcal{D}}$, because we assume that the measured redshift in an inhomogeneous Universe is related to the average scale factor. This has been advocated by [21], where the relation

$$(1+z)\approx a_{\mathcal{D}}^{-1} \tag{5.14}$$

has been established. Note that in principle one would have to introduce averaging on some larger scale than $\mathcal{D}$ to connect this background average on some domain $\mathcal{B}$ to the redshift. For the sake of simplicity, and because we content ourselves with small redshifts, we use the same domain $\mathcal{D}$. This limits the validity of the result to small redshifts.

In order to relate a and $a_{\mathcal{D}}$, we start from

$$H_{\mathcal{D}} = \frac{1}{3}\langle\theta\rangle_{\mathcal{D}} = \frac{\dot{a}_{\mathcal{D}}}{a_{\mathcal{D}}} = \frac{1}{a}\frac{a'_{\mathcal{D}}}{a_{\mathcal{D}}} = \frac{1}{a}\left(\frac{a'}{a} - \left\langle\psi^{(1)\prime}\right\rangle\right). \tag{5.15}$$

To first order this relation gives

$$a_{\mathcal{D}} = a\left(1 - \frac{1}{3}\left(\langle\delta\left(a\right)\rangle_{\mathcal{D}} - \langle\delta\left(1\right)\rangle_{\mathcal{D}}\right)\right) . \tag{5.16}$$

We finally obtain the averaged Hubble rate

$$H_{\mathcal{D}} = H_0\sqrt{\frac{\Omega_m}{a_{\mathcal{D}}^3}}\sqrt{1+ca_{\mathcal{D}}^3}\left[1 - \frac{5\frac{a_{\mathcal{D}}}{D(a_{\mathcal{D}})} - 3\frac{D_0}{D(a_{\mathcal{D}})}}{6(1+ca_{\mathcal{D}}^3)}\frac{D(a_{\mathcal{D}})}{D_0}\langle\delta_0\rangle_{\mathcal{D}}\right] \tag{5.17}$$

and the averaged spatial curvature

$$\langle\mathcal{R}\rangle_{\mathcal{D}} = 10\,\Omega_m\frac{H_0^2}{a_{\mathcal{D}}^2}\frac{\langle\delta_0\rangle_{\mathcal{D}}}{D_0}. \tag{5.18}$$

For later convenience we also define the function

$$f_{\mathcal{D}}\left(a_{\mathcal{D}}\right) := \frac{5\frac{a_{\mathcal{D}}}{D_0} - 3}{2(1+ca_{\mathcal{D}}^3)}, \tag{5.19}$$

which is our modified version of the growth rate of Eq. (5.10), multiplied by $D\left(a\right)/D_0$. It basically encodes the deviation of the time evolution of the Hubble perturbation from the time evolution of the ensemble averaged Hubble rate

$$\overline{H_{\mathcal{D}}}\left(a_{\mathcal{D}}\right) = H_0\sqrt{\frac{\Omega_m}{a_{\mathcal{D}}^3}}\sqrt{1+ca_{\mathcal{D}}^3}\,, \tag{5.20}$$

as may be seen from the resulting expression

$$H_{\mathcal{D}} = \overline{H_{\mathcal{D}}}\left(a_{\mathcal{D}}\right)\left(1 - \frac{1}{3}f_{\mathcal{D}}\left(a_{\mathcal{D}}\right)\langle\delta_0\rangle_{\mathcal{D}}\right) . \tag{5.21}$$

In the Einstein-de Sitter limit ($c \to 0$ and $\Omega_m \to 1$) we arrive at

$$\begin{aligned} H_{\mathcal{D}} &= \frac{H_0}{a_{\mathcal{D}}^{3/2}}\left(1 - \frac{1}{3}a_{\mathcal{D}}\langle\delta_0\rangle_{\mathcal{D}}\right) , \\ \langle\mathcal{R}\rangle_{\mathcal{D}} &= 10\frac{H_0^2}{a_{\mathcal{D}}^2}\langle\delta_0\rangle_{\mathcal{D}} . \end{aligned}$$

In order to compare this with the results of [15, 16], we define the peculiar gravitational potential $\varphi(\mathbf{x})$ via

$$\Delta\varphi(\mathbf{x}) \equiv 4\pi G\varrho^{(1)}a^2 = \frac{3}{2}H_0^2\frac{\delta}{a} = \frac{2}{3}\frac{1}{t_0^2}\frac{\delta}{a} \tag{5.22}$$

and obtain

$$\begin{aligned} H_{\mathcal{D}} &= \frac{2}{3t_0}a_{\mathcal{D}}^{-3/2}\left[1-\frac{1}{2}a_{\mathcal{D}}t_0^2\left\langle\Delta\varphi\right\rangle\right], \\ \left\langle\mathcal{R}\right\rangle_{\mathcal{D}} &= \frac{20}{3}a_{\mathcal{D}}^{-2}\left\langle\Delta\varphi\right\rangle. \end{aligned} \tag{5.23}$$

While our results agree for the spatial curvature, $H_{\mathcal{D}}$ is different from the result in [16], because there the assumption $a \ll 1$ was made when applying (5.16).

Let us now turn to the dimensionless $\Omega^{\mathcal{D}}$-parameters. To first order, they may be expressed as

$$\Omega_m^{\mathcal{D}}(a_{\mathcal{D}}) = \frac{1}{1+c\,a_{\mathcal{D}}^3}\left[1+\left(1+\frac{2}{3}f_{\mathcal{D}}(a_{\mathcal{D}})\right)\left\langle\delta_0\right\rangle_{\mathcal{D}}\right], \tag{5.24a}$$

$$\Omega_{\mathcal{R}}^{\mathcal{D}}(a_{\mathcal{D}}) = -\left[\frac{1}{1+c\,a_{\mathcal{D}}^3}+\frac{2}{3}f_{\mathcal{D}}(a_{\mathcal{D}})\right]\left\langle\delta_0\right\rangle_{\mathcal{D}}, \tag{5.24b}$$

$$\Omega_{\Lambda}^{\mathcal{D}}(a_{\mathcal{D}}) = \frac{c\,a_{\mathcal{D}}^3}{1+ca_{\mathcal{D}}^3}\left[1+\frac{2}{3}f_{\mathcal{D}}(a_{\mathcal{D}})\left\langle\delta_0\right\rangle_{\mathcal{D}}\right], \tag{5.24c}$$

$$\Omega_{\mathcal{Q}}^{\mathcal{D}}(a_{\mathcal{D}}) = 0. \tag{5.24d}$$

When taking the limit $\mathcal{D}\to 0$ in Eqs. (5.24a) – (5.24d), we recover the point-wise defined Ω-parameters of Eqs. (5.12a) – (5.12d). This provides a self-consistency check of the averaging framework.

From the expressions for the $\Omega^{\mathcal{D}}$-parameters one can easily calculate the ensemble averages and the ensemble variance. $\overline{\left\langle\delta_0\right\rangle_{\mathcal{D}}} = 0$, since the domain-averaged over-density of $\mathcal{D}$, in general non-zero, averages out when we consider a large number of domains of given size and local density fluctuations drawn from the same (Gaussian) distribution.

Here we adopt the common view that linear theory is a good description of the present Universe at the largest observable scales (which has been questioned recently in [20]). We then find the ensemble average of the curvature parameter $\overline{\Omega_{\mathcal{R}}^{\mathcal{D}}}$ to vanish. For the matter density parameter Eq. (5.24a) yields

$$\overline{\Omega_m^{\mathcal{D}}}(a_{\mathcal{D}}) = \left(1+c\,a_{\mathcal{D}}^3\right)^{-1}. \tag{5.25}$$

This may be used to verify that the relation $\overline{\Omega_m^{\mathcal{D}}}+\overline{\Omega_{\Lambda}^{\mathcal{D}}} = 1$ holds. In addition, this relation implies that $\overline{\Omega_m^{\mathcal{D}}}(a_{\mathcal{D}_0})$ corresponds to today's background matter density parameter:

$$\overline{\Omega_m^{\mathcal{D}}}(a_{\mathcal{D}_0}) = \Omega_m + \mathcal{O}\left(\overline{\left\langle\delta_0^2\right\rangle_{\mathcal{D}}}\right). \tag{5.26}$$

However, this is true at first order in the density contrast only, because in this case ensemble averages agree with background quantities. At higher orders, the ensemble averages differ from the background quantities.

5.2.2. Relating cosmic parameter- and matter-fluctuations

After having convinced ourself that the expectations of the averaged $\Omega^{\mathcal{D}}$-parameters are identical to their ΛCDM background values up to second-order corrections, we now turn to the study of their ensemble variances.

All variances of domain averaged cosmological parameters can be related to the variance of the over-density of the matter distribution, $\sigma\left(\langle\delta_0\rangle_{\mathcal{D}}\right)$.

In order to specify $\langle\delta_0\rangle_{\mathcal{D}}$, we introduce the normalized window function $W_{\mathcal{D}}(X)$ and write

$$\begin{aligned}\langle\delta_0\rangle_{\mathcal{D}} &= \int_{\mathbb{R}^3}\delta_0(\mathbf{x})\,W_{\mathcal{D}}(\mathbf{x})\,\mathrm{d}^3x \\ &= \int_{\mathbb{R}^3}\widetilde{\delta}_0(\mathbf{k})\,\widetilde{W}_{\mathcal{D}}(\mathbf{k})\,\mathrm{d}^3k,\end{aligned} \tag{5.27}$$

A tilde denotes a Fourier-transformed quantity. With the definition of the matter power spectrum

$$\overline{\widetilde{\delta}_0(\mathbf{k})\,\widetilde{\delta}_0(\mathbf{k}')} = \delta^{\mathrm{Dirac}}(\mathbf{k}+\mathbf{k}')\;P_0(k)\,, \tag{5.28}$$

where δ^{Dirac} denotes Dirac's delta function, the ensemble variance of the matter over-density becomes

$$\left(\sigma_{\mathcal{D}_0}\right)^2 := \sigma^2\left(\langle\delta_0\rangle_{\mathcal{D}}\right) = \int_{\mathbb{R}^3}P_0(k)\,\widetilde{W}_{\mathcal{D}}(\mathbf{k})\,\widetilde{W}_{\mathcal{D}}(-\mathbf{k})\,\mathrm{d}^3k. \tag{5.29}$$

For a spherical top hat window function, this expression is the well-known matter variation in a sphere Eq. (2.16), often used to normalize the matter power spectrum by fixing its value for a sphere with a radius of $8h^{-1}$Mpc (σ_8). To calculate this variance, we use the standard ΛCDM power spectrum (2.112). Knowing $\sigma_{\mathcal{D}}$ at a particular epoch of interest, we can calculate all the fluctuations in the cosmic parameters. They read:

$$\delta H_{\mathcal{D}} = \frac{1}{3}\overline{H_{\mathcal{D}}}\left(a_{\mathcal{D}}\right)f_{\mathcal{D}}\left(a_{\mathcal{D}}\right)\sigma_{\mathcal{D}_0}\,, \tag{5.30a}$$

$$\delta\Omega_m^{\mathcal{D}} = \overline{\Omega_m^{\mathcal{D}}}\left(a_{\mathcal{D}}\right)\left(1+\frac{2}{3}f_{\mathcal{D}}\left(a_{\mathcal{D}}\right)\right)\sigma_{\mathcal{D}_0}\,, \tag{5.30b}$$

$$\delta\Omega_{\mathcal{R}}^{\mathcal{D}} = \overline{\Omega_m^{\mathcal{D}}}\left(a_{\mathcal{D}}\right)\left(1+\frac{2}{3}\frac{f_{\mathcal{D}}\left(a_{\mathcal{D}}\right)}{\overline{\Omega_m^{\mathcal{D}}}\left(a_{\mathcal{D}}\right)}\right)\sigma_{\mathcal{D}_0}\,, \tag{5.30c}$$

$$\delta\Omega_\Lambda^{\mathcal{D}} = \overline{\Omega_\Lambda^{\mathcal{D}}}\left(a_{\mathcal{D}}\right)\frac{2}{3}f_{\mathcal{D}}\left(a_{\mathcal{D}}\right)\sigma_{\mathcal{D}_0}\,, \tag{5.30d}$$

$$\delta\Omega_{\mathcal{Q}}^{\mathcal{D}} = \mathcal{O}\left(\left(\sigma_{\mathcal{D}_0}\right)^2\right)\,, \tag{5.30e}$$

where e.g. $\delta\Omega_\Lambda^{\mathcal{D}}$ denotes the square root of the variance, $\delta\Omega_\Lambda^{\mathcal{D}} := \sigma\left(\Omega_\Lambda^{\mathcal{D}}\right)$. $\overline{\Omega_m^{\mathcal{D}}}$, $\overline{H_{\mathcal{D}}}$ and $f_{\mathcal{D}}\left(a_{\mathcal{D}}\right)$ were defined in Eq. (5.25), (5.20) and (5.19) and $\overline{\Omega_\Lambda^{\mathcal{D}}} = 1 - \overline{\Omega_m^{\mathcal{D}}}$.

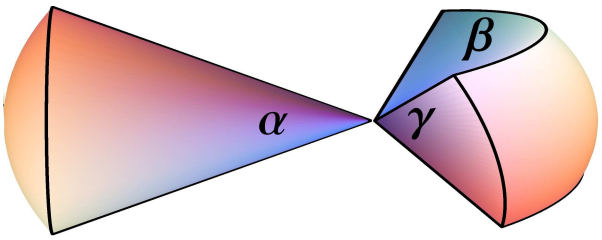

Figure 5.3. The two survey geometries considered (separately). A simple cone with one single opening angle α and a slice given by two angles β and γ.

These variances are the minimum ones that one can hope to obtain by measurements of regions of the Universe of size $\mathcal{D}$. They do not include any observational uncertainties, nor biasing or sampling issues. They are intrinsic to the inhomogeneous dark matter distribution that governs the evolution of the Universe.

Equations (5.30a) to (5.30e) are interesting in two respects: Firstly, our expression for $\delta H_{\mathcal{D}}$ is simpler than the one in [111], nevertheless, both results agree. Secondly, Eqs. (5.30a) to (5.30e) quantify the connection between fluctuations in cosmological parameters and inhomogeneities in the distribution of matter. If we choose "today" as our reference value, Eqs. (5.30a) to (5.30d) allow us to predict the domain averaged cosmological parameters:

$$\begin{array}{rcccl} H_{\mathcal{D}} & = & H_0 & \pm & \frac{1}{3} H_0 \, f_{\mathcal{D}_0} \quad \sigma_{\mathcal{D}_0} \\ \Omega_m^{\mathcal{D}} & = & \Omega_m & \pm & \Omega_m \left(1 + \frac{2}{3} f_{\mathcal{D}_0}\right) \quad \sigma_{\mathcal{D}_0} \\ \Omega_{\mathcal{R}}^{\mathcal{D}} & = & 0 & \pm & \left(\Omega_m + \frac{2}{3} f_{\mathcal{D}_0}\right) \quad \sigma_{\mathcal{D}_0} \\ \Omega_{\Lambda}^{\mathcal{D}} & = & \Omega_\Lambda & \pm & \frac{2}{3} \Omega_\Lambda \, f_{\mathcal{D}_0} \quad \sigma_{\mathcal{D}_0} \end{array} \tag{5.31}$$

with

$$f_{\mathcal{D}_0} \equiv f_{\mathcal{D}}\left(a_{\mathcal{D}_0}\right) = \frac{\Omega_m}{2}\left(5 D_0^{-1} - 3\right) \approx \left\{ \begin{array}{ll} 0.5 & \Lambda\text{CDM} \\ 1.0 & \text{EdS} \end{array} \right. , \tag{5.32}$$

where we assumed $\Omega_m = 0.3$ for ΛCDM. More generally, for $\Omega_m > 0.1$, $f_{\mathcal{D}_0}$ may be approximated by [112, 55]

$$f_{\mathcal{D}_0} \approx \frac{1}{140}\left(2 + 140\,\Omega_m^{4/7} - \Omega_m - \Omega_m^2\right). \tag{5.33}$$

From the knowledge of $\sigma_{\mathcal{D}_0}$ we may therefore easily derive the variation of cosmological parameters. To relate our calculations to real surveys, we elaborate in the next section on how to calculate $\sigma_{\mathcal{D}_0}$ for several survey geometries.

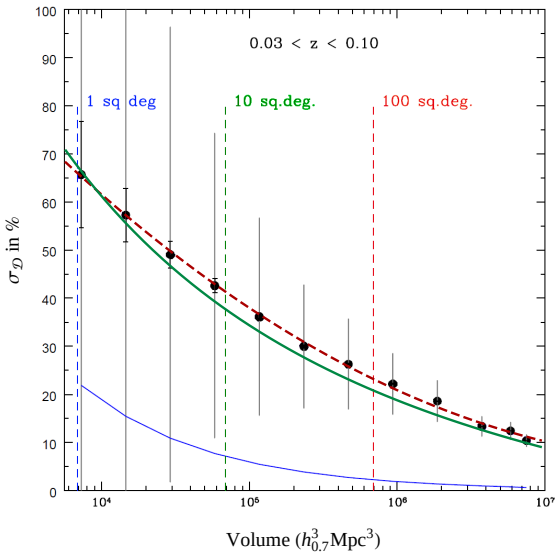

Figure 5.4. Variance of the matter density, $\sigma_{\mathcal{D}}$, as a function of the observed domain volume. Data were derived from the SDSS main sample by [113]. The dashed (red) line shows the fit of [113] to the data, the solid (green) line is our result including the sample variance [solid (blue) line at the bottom].

5.3. Matter and curvature fluctuations

5.3.1. Influence of the survey geometry

Observations of the Universe are rarely full-sky measurements and typically sample domains much smaller than the Hubble volume. We therefore must address the problem of the survey geometry. Effects from a limited survey size are in particular important for deep fields, as studied for example in [114]. While in their case, for small angles and deep surveys, approximating the observed volume by a rectangular geometry is appropriate, it probably is not appropriate for the bigger survey volumes that we have in mind.

We therefore chose two different geometries that resemble observationally relevant ones. Firstly, we used a simple cone with a single opening angle α. The second geometry is a slice described by two angles β and γ for the size in right ascension and declination respectively. In the radial direction we assumed a top hat window, whose cut-off value corresponds to the depth of the survey. Both shapes are shown in Fig. 5.3.

To calculate $\sigma_{\mathcal{D}_0}$ for both geometries, we used a decomposition into spherical harmonics. This allowed us to derive an expression for the expansion coefficients in terms of a series in $\cos(2n\alpha)$ for the cone and a similar one for the slice, depending on trigonometric functions of β and γ. The radial coefficients were calculated numerically from the ΛCDM power spectrum (2.112). It includes the effect of baryons on the overall shape and

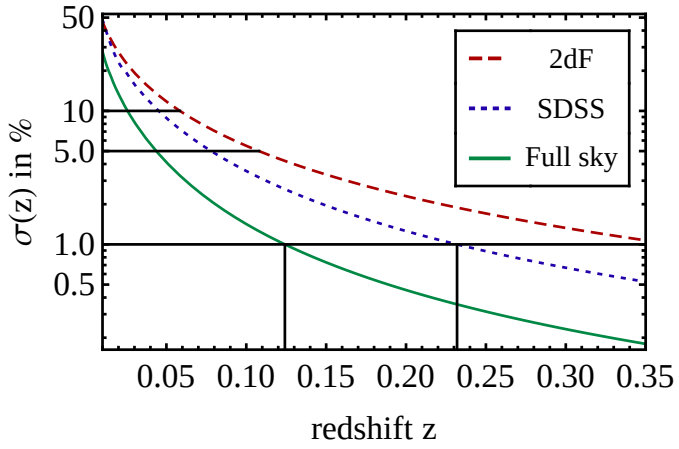

Figure 5.5. Variance of the matter density, $\sigma_{\mathcal{D}}$, for survey geometries resembling the 2dFGRS, the SDSS and a hypothetical full sky survey as a function of maximum redshift considered. We find that the determination of the local $\sigma_{\mathcal{D}}$ below redshifts of 0.1 (corresponding to ~ 400 Mpc) is fundamentally limited by cosmic variance to the 1% level.

amplitude of the matter power spectrum, but does not model baryon acoustic oscillations. The calculation of the coefficients is explained in appendix A.

All plots use best-fit ΛCDM values from WMAP 7yr as summarized in table 3.1; $\Omega_b = 0.0456$, $\Omega_{cdm} = 0.227$ and $n_s = 0.963$. The power spectrum is normalized to $\sigma_8 = 0.809$.

To ensure that the result of our calculation for the slice-like geometry and a standard ΛCDM power spectrum is reasonable, we compared it with an analysis of SDSS data by [113]. In Fig. 5.4 we show this comparison of their r.m.s. matter over-density $\sigma_{\mathcal{D}}$ obtained from the SDSS main galaxy sample, in terms of its angular extension (and hence the volume). The dashed line going through the points shows their empirical fit to the data. The solid green line shows our result for the cosmic variance of a slice with respective angular extension (for $\beta = \gamma$), plus their sample variance. Note that our result is not a fit to SDSS data, but is a prediction based on the WMAP 7yr data analysis. Additionally, the real SDSS window function is slightly more complicated than our simplistic window, thus perfect agreement is not to be expected.

For the full SDSS volume, $\sigma_{\mathcal{D}_0}$ is shown in Fig. 5.5. For comparison we also added the smaller, southern hemisphere 2dF survey and a hypothetical full sky survey. For the two surveys, we assumed an approximate angular extension of 120°×60° for SDSS and for the two fields of the 2dF survey 80°×15° and 75°×10°. The ongoing BOSS survey corresponds to the plot for the SDSS geometry, because it will basically have the same angular extension. Because it will target higher redshifts, it is not in the range of our calculation, however. As a rough statement (the precise value depends on the redshift),

one may say that the 2dF survey is a factor of 5 and the SDSS survey a factor of 2.5 above the variance of a full sky survey. This is interesting because the SDSS survey covers approximately only 1/6 of the full sky and the 2dF survey only 1/20. This is due to the angular dependence of $\sigma_{\mathcal{D}}$. We find that fluctuations drop quickly as we increase small angles and flattens at large angles.

From Fig. (5.5) we see that the cosmic variance of the matter density for the SDSS geometry is 5% at a depth of $z \approx 0.08$ and still 1% out to $z \approx 0.23$. Note, however, that the extension of the domain of (spatial) averaging to a redshift of 0.35 is clearly not very realistic because lightcone effects will become relevant with increasing extension of the domain. The assumption that this domain would be representative for a part of the hypersurface of constant cosmic time becomes questionable. We expect, however, that in this range evolution effects will only be a minor correction to the result presented here because of the following estimation:

The main effect we miss by approximating the lightcone by a fixed spatial hypersurface is evolution in the matter density distribution. To specify what "region that is not too extended spatially" means, one should therefore estimate the maximum evolution in a given sample. This can be done by determining the growth of the density contrast in the outermost (and therefore oldest) regions of the sample. In the linear regime considered here, the evolution of the density contrast is given by $\delta(z) = \delta_0 D(0)/D(z)$. Therefore, lightcone corrections should be smaller than $\epsilon_l = 1 - D(z)/D(0)$ which is $\epsilon_l \approx 5\%$ for $z = 0.1$ and $\epsilon_l \approx 14\%$ for $z = 0.3$. Therefore, the order of magnitude of our results should be correct on a wider range of scales, but on scales above $z = 0.3$ the corrections to our calculation are expected to pass beyond 15%.

These effects can be taken into account with the new method of light cone averaging developed by [115].

Finally, it should be noted that for large volumes the actual shape of the survey geometry is not very important. As long as all dimensions are bigger than the scale of the turnover of the power spectrum, the deviation of the cosmic variance for our shapes, compared to those of a box of equal volume, is at the percent level. To reach this result, we compared $\sigma_{\mathcal{D}_0}$ for the slice-like geometry to its value for a rectangular box of the same volume. We used a slice for which $\beta = \gamma$. The box was constructed to have a quadratic basis and the same depth as the slice in radial direction. Therefore the base square of the box is smaller than the square given by the two angles of the slice. The result of this comparison is that the deviation of $\sigma^{rect}_{\mathcal{D}_0}$ from the value for the slice is at most 6% for angles above $\beta \approx 10°$. For smaller angles the deviation becomes bigger and redshift-dependent. This is caused by the changing shape of the power spectrum at small scales. The large angle behavior confirms an observation of [113]. They found that the cosmic variance in the SDSS dataset was the same for both of the two geometries they considered.

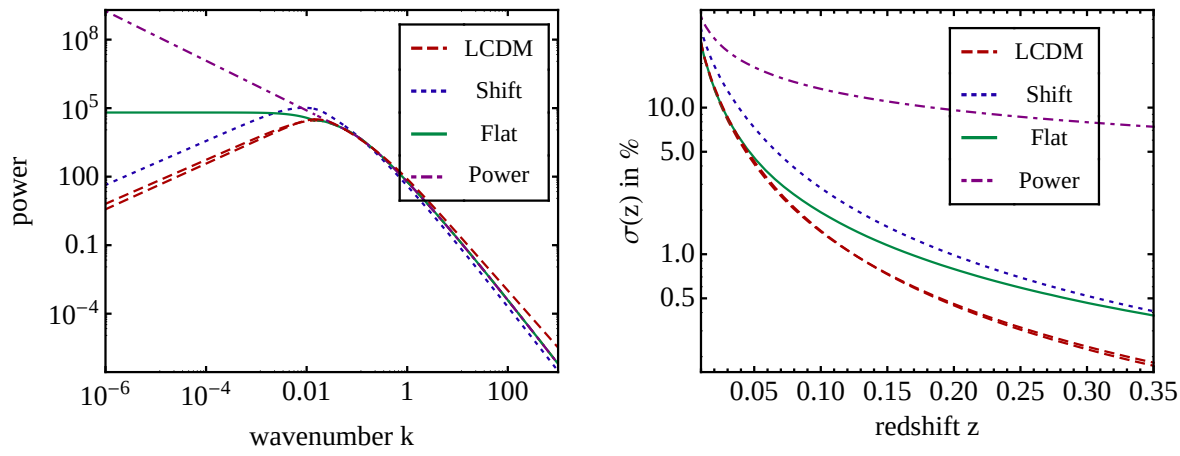

Figure 5.6. Modified power spectra (left panel) and their corresponding matter fluctuations σ (right panel). The red dashed line is the standard ΛCDM spectrum. The blue dotted line corresponds to a spectrum where the turnover in the spectrum has just been shifted to larger scales. The green solid line is a spectrum with a flat large scale behavior and the purple dashed dotted line is a spectrum with a modified power law. In the two latter cases there is no zero crossing of the correlation function at all. The right hand side clearly shows that if the zero crossing is not there or at larger scales, our results would be underestimating the large scale fluctuations.

Non-standard Power spectra All of the results above assume the standard shape of the power spectrum (2.112). However, there has been some discussion on whether the ΛCDM correlation function really fits the data on large scales. In [60] the authors claim that the transition of the correlation function to negative values seems to be at larger values than expected. In order to explore what order of magnitude the corrections would be if the correlation function was different, we show in Fig. 5.6 the values of σ for different possibilities: A simple shift of the zero crossing to larger scales, but with the same form, a flat spectrum on large scales and a modified power law. All three possibilities would lead to an enhancement of the fluctuations due to cosmic structure. In the case of the modified power law even by a factor of 20. If this confusion remains will become clear with the availability of the BOSS galaxy data, as they allow to probe the scales of the zero crossing of the correlation function more reliably.

5.3.2. Importance of curvature fluctuations

After the general study of the effect of the shape of the observational domain $\mathcal{D}$ on $\sigma_{\mathcal{D}_0}$, one may ask for which parameter the fluctuations are most important.

The three lowest lines in the plot of Fig. 5.7 show that this is the case for the curvature fluctuations. The two lowest lines, showing the fluctuations $\delta\Omega_m$ and $\delta H_{\mathcal{D}_0}/H_{\mathcal{D}_0}$ for

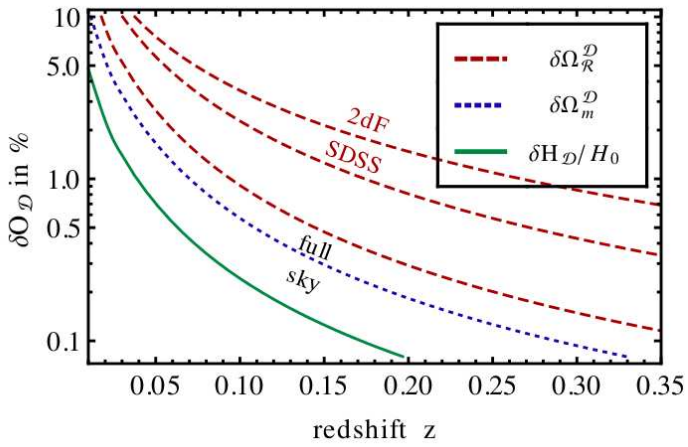

Figure 5.7. Top three lines: the expected r.m.s. fluctuation of the curvature parameter, $\delta\Omega_{\mathcal{R}}^{\mathcal{D}}$, for geometries resembling the 2dFGRS, the SDSS, and a full sky. The two lowest lines are the expected r.m.s. fluctuations of the parameters $\Omega_m^{\mathcal{D}_0}$ and $H_{\mathcal{D}_0}$ for a full-sky survey extending to the respective redshift. The curvature fluctuations turn out to be higher than all other fluctuations.

the full sphere, lie a factor of 1.6 and 3.8, respectively, below the respective curvature fluctuations $\delta\Omega_{\mathcal{R}}^{\mathcal{D}}$. Therefore the fluctuations of Ω_m play a smaller role for all Universes with $\Omega_m < 1$. The uncertainty in $H_{\mathcal{D}_0}$, which has been in the focus of the investigations so far [116, 16, 111], contributes even less to the distortion of the geometry, as we shall discuss in Section 5.4.2.

What this means for real surveys, such as the 2dF or the SDSS survey, is shown by the three upper lines in Fig. 5.7. They compare $\delta\Omega_{\mathcal{R}}^{\mathcal{D}}$ for the slices observed by these surveys to that of a full sky measurement. $\delta\Omega_{\mathcal{R}}^{\mathcal{D}}$ is bigger than one percent up to a redshift of 0.18 for the SDSS and 0.28 for the 2dF survey and it does not drop below 0.001 for values of z as high as 0.5. This may seem very low, but it has been shown that getting the curvature of the Universe wrong by 1‰ already affects our ability to measure the dark energy equation of state $w(z)$ [117]. Of course one has to keep in mind that for high redshifts one has to be careful with the values presented here because they are based on the assumption that the observed region lies on one single spatial hypersurface. Because this approximation worsens beyond a redshift of 0.1, there may be additional corrections to the size of the fluctuations stemming from lightcone effects.

To investigate the curvature fluctuations for more general geometries, we show in Fig. 5.8 the angular and radial dependence of the curvature fluctuation $\delta\Omega_{\mathcal{R}}^{\mathcal{D}}(\alpha)$ for the cone-like window of Fig. 5.3.

On the l.h.s. of Fig. 5.8 we evaluate the angular dependence. For a survey that only reaches a redshift of 0.1, the fluctuations are still higher than 0.01 for a half-sky survey. It is interesting to note that for a deeper survey, $\delta\Omega_{\mathcal{R}}^{\mathcal{D}}(\alpha)$ grows much faster when α is

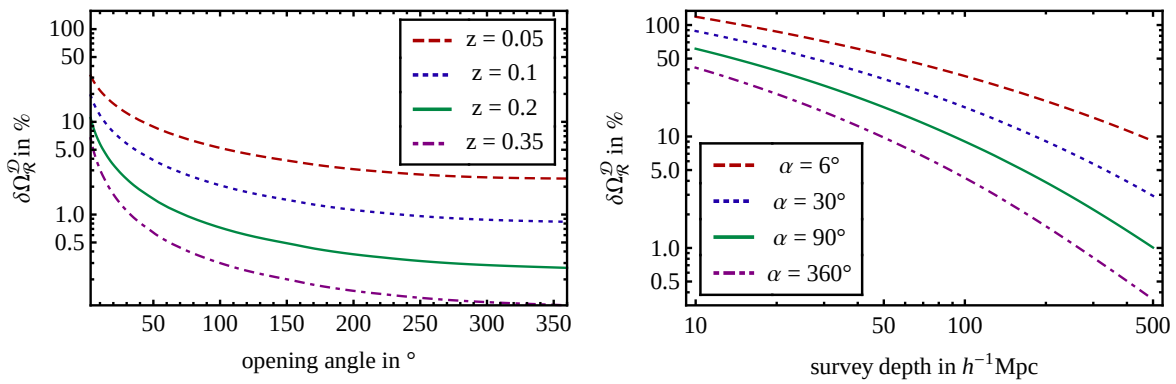

Figure 5.8. Cosmic variance of the curvature parameter. *Left panel:* Dependence of $\delta\Omega_{\mathcal{R}}^{\mathcal{D}}$ on the opening angle of the cone-like survey geometry of Fig. 5.3 for different top hat depths of the survey. *Right panel:* Dependence of $\delta\Omega_{\mathcal{R}}^{\mathcal{D}}$ on the depth of the survey. For a small cone of 6° opening angle we expect curvature fluctuations of 10% up to $450h^{-1}$Mpc.

reduced than for a shallow survey. This is because $\sigma_{\mathcal{D}_0}(R)$ changes from a relatively weak R^{-1} decay to a R^{-2} decay on larger scales. For $z = 0.35$, this behavior dominates and a decrease in α increases $\sigma_{\mathcal{D}_0}(R, \alpha)$ stronger than in the R^{-1} regime.

On the r.h.s. of Fig. 5.8 we show the dependence of $\delta\Omega_{\mathcal{R}}^{\mathcal{D}}$ on the survey depth for some opening angles of the cone-like window. For narrow windows the fluctuation in $\Omega_{\mathcal{R}}^{\mathcal{D}}$ stays high, even beyond the expected homogeneity scale of $100h^{-1}$Mpc. For $R = 200h^{-1}$Mpc and a 6° window, for example, it is still at $\delta\Omega_{\mathcal{R}}^{\mathcal{D}} \approx 0.2$. For smaller beams these fluctuations persist even out to much longer distances. Therefore they play an important role for deep field galaxy surveys, as shown in [114, 113] for the matter density fluctuations. But even for wider angles, fluctuations in curvature persist on sizable domains. If one recalls that the distance given for the full sphere of 360° is its radius, this means that regions in the Universe as big as $540h^{-1}$Mpc have typical curvature fluctuations on the order of 1%. This is not that small because the last scattering surface at $z \approx 1100$ is only $9600h^{-1}$Mpc away. One of these regions therefore fills more than 5% of the way to that surface.

To put these values into perspective, we compare the WMAP 5yr confidence contours [109] on the curvature parameter with those that may in principle be derived from the 2dF or the SDSS survey in Fig. 5.9. Because they only sample a finite size of the Universe, one cannot be sure that this value is indeed the background value and not only a local fluctuation. The cosmic variance induced by this finite size effect is, for the 2dF survey volume up to $z \approx 0.2$, shown by the two second-largest (red) ellipses. The two innermost (blue) ones depict the minimum possible error using the SDSS survey volume up to $z \approx 0.3$. Clearly, the determination of $\Omega_{\mathcal{R}}^{\mathcal{D}}$ may perhaps be improved by a factor of two if one were to eliminate all other sources of uncertainty. This may be less if lightcone

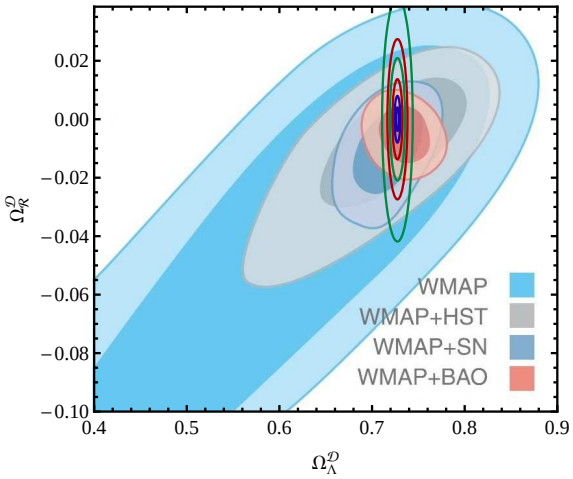

Figure 5.9. Minimum confidence contours in $\Omega_{\Lambda}^{\mathcal{D}}$ and $\Omega_{\mathcal{R}}^{\mathcal{D}}$ achievable in different volumes through fluctuations of matter. The green (outermost) ellipses are the 95% and 68% contours for the volume from which the HST data are drawn. The next inner (red) ones are for a survey of the size of the 2dF survey up to $z = 0.2$. In the middle there is a small double ellipse in blue, showing the values for the SDSS volume up to $z = 0.3$. The background image depicts the results from WMAP 5 [109]. They give the experimental values and uncertainties on these parameters for a combination of various experimental probes.

effects play a non-negligible role already for $z \approx 0.3$.

Fig. 5.10 shows the dependence of the curvature fluctuation on the considered cosmology. For this study we fixed the spectral index and the normalization of the spectrum to $n_s = 0.963$ and $\sigma_8 = 0.809$, respectively. We varied each of the other parameters one after another, while keeping the remaining ones fixed to the concordance values. We used the SDSS geometry out to a redshift of $z = 0.09$ as a reference value at which we conducted this investigation, because the concordance values lead to a $\delta\Omega_{\mathcal{R}}^{\mathcal{D}}$ of 0.01 for this configuration. Interestingly enough, the dependence on the Ω_m parameter is very weak. This means that the value does not differ much for the flat ΛCDM model and the EdS model. This is surprising, because the prefactor of $\sigma_{\mathcal{D}_0}$ in (5.30c) changes by a factor of 3 from about 5/11 for ΛCDM to 5/3 for EdS. This rise, however, is compensated for by a drop of the value of $\sigma_{\mathcal{D}_0}$. The reason for this drop is that a higher Ω_m leads to more power on small scales. Because we kept the integrated normalization fixed at a given value of σ_8, this means less power on large scales, i.e. at $z = 0.09$. Moreover, a variation of the Hubble constant h and the baryon fraction f_b has only a small effect around the concordance value. $\delta\Omega_{\mathcal{R}}^{\mathcal{D}}$ changes significantly only for more extreme values of f_b and h.

5.4. Hubble and geometry fluctuations

5.4.1. Inhomogeneity uncertainties in the Hubble scale

Local fluctuations of the Hubble expansion rate have already been considered in the literature [118, 119, 116, 111]. Here we wish to add two new aspects.

The first one is on the measurement of $H(z)$ itself. Experiments that try to measure H as a function of z, like the WiggleZ survey [120], do this by measuring a "local" average $H(z_m)$ in a region around the redshift z_m. These regions should not be too small to keep the effects of local fluctuations small. On the other hand they cannot be enlarged in an arbitrary way because then the redshift z_m becomes less and less characteristic for the averaging domain. In other words, for an increasingly thicker shell Δz, the evolution of $H(z)$ begins to play a role. Therefore, one may find the optimal thickness of the averaging shells over which the variation in the expansion rate

$$\mathrm{Var}\left[H(z)\right] = \frac{1}{V_{\mathcal{D}}}\int H[z(r)]^2 W_{\mathcal{D}}\left(r\right)\mathrm{d}^3 r - \left(\frac{1}{V_{\mathcal{D}}}\int H[(z(r)]W_{\mathcal{D}}\left(r\right)\mathrm{d}^3 r\right)^2 \quad (5.34)$$

equals the variance imposed by the inhomogeneous matter distribution. The corresponding shells are shown in Fig. 5.11. It should be noted that the error for the first bin is certainly underestimated in our treatment, which rests on linear perturbation theory. Taking into account higher orders, which become dominant at small scales, will certainly increase it. Of course, in these measurements the survey geometries will not necessarily be close to the SDSS or the 2dF geometry, but they are shown to illustrate survey geometries that do not cover the full sky.

Secondly, we wish to note that the relation between fluctuations in the Hubble expansion rate and fluctuations in the matter density offers the interesting possibility to determine the evolution of the growth function for matter perturbations from the variances of the Hubble rate measured at different redshifts. A direct measurement of the growth function by a determination of σ_8 at different epochs is difficult, because one never examines the underlying dark matter distribution. Therefore one has to assume that the observed objects represent the same clustering pattern as the underlying dark matter (this is the problem of bias). It is well known that there is bias and its modeling typically has to rely on assumptions.

An interesting bypass is to look at the variation of local expansion rates at different redshifts. The assumption that the luminous objects follow the local flow is more likely and the assumption that this local flow is generated by the inhomogeneities of the underlying dark matter distribution is also reasonable. A similar idea leads to the attempt to use redshift-space distortions to do so [66]. The fact that one considers fluctuations means that we would not have to know the actual value of $H\left(z\right)$, but only the local variation at different redshifts.

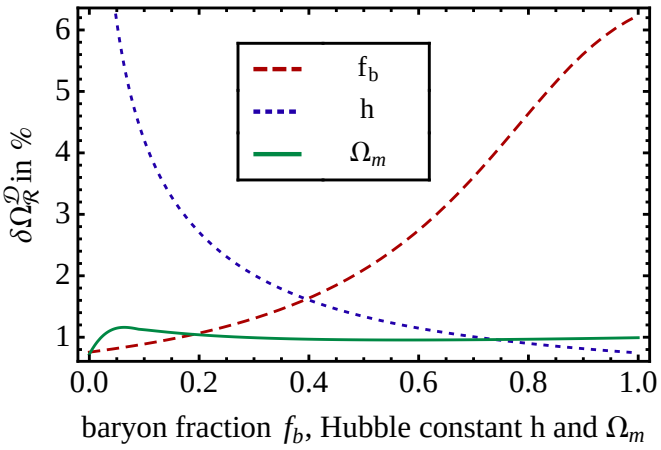

Figure 5.10. Dependence of $\delta\Omega^{\mathcal{D}}_{\mathcal{R}}$ on some cosmological parameters for a spherical domain extending to $z = 0.09$. The basis is the ΛCDM model with $\Omega_b = 0.0456$, $\Omega_{cdm} = 0.227$, $h = 0.7$, $n_s = 0.963$ and $\sigma_8 = 0.809$. For this model and for the chosen redshift, $\delta\Omega^{\mathcal{D}}_{\mathcal{R}} \approx 0.01$. We then varied $\Omega_m = \Omega_b + \Omega_{cdm}$, $f_b = \Omega_b/\Omega_m$ and h between 0 and 1, holding the other parameters fixed at their aforementioned values. Because σ_8 is fixed, the fluctuation in $\Omega^{\mathcal{D}}_{\mathcal{R}}$ is nearly independent on Ω_m.

This variation, defined as

$$\delta_H = \frac{H_{\mathcal{D}} - \overline{H}_{\mathcal{D}}(a_{\mathcal{D}})}{\overline{H}_{\mathcal{D}}(a_{\mathcal{D}})} \,, \tag{5.35}$$

has the fluctuations of Eq. (5.30a)

$$\sigma\left(\delta_H\right) = \frac{1}{3}\overline{H_{\mathcal{D}}}\left(a_{\mathcal{D}}\right) f_{\mathcal{D}}\left(a_{\mathcal{D}}\right) \sigma_{\mathcal{D}_0} \,. \tag{5.36}$$

If we were to measure this quantity at different redshifts, we could, without knowledge of the absolute normalization of $H_{\mathcal{D}}(z)$, determine $f_{\mathcal{D}}(a_{\mathcal{D}})$ only from the variance and therefore the constant $c = \Omega_\Lambda/\Omega_m$.

Note that in the standard case, where the background redshift is identified with the observed one, $f_{\mathcal{D}}(a_{\mathcal{D}})$ is simply replaced by the growth rate $f(a) = \frac{\mathrm{d}\ln D(a)}{\mathrm{d}\ln a}$, and measuring the Hubble fluctuations would yield a direct measurement of f. In the real world, where the redshift captures the structure on the way from the source to us, it is not directly the background redshift. One would rather measure the modified "growth rate" $f_{\mathcal{D}}(a_{\mathcal{D}})$. The difference between these two quantities is small in our range of validity for $f_{\mathcal{D}}(a_{\mathcal{D}})$, however (corrections of linear order in the perturbations).

5.4.2. Fluctuations of the acoustic scale

Let us now turn to the effect of fluctuations caused by inhomogeneities on the local distance estimates. An important distance measure, recently used in BAO experiments, is D_V. It was introduced in [62] and mixes the angular diameter distance and the comoving coordinate distance to the BAO ring. It is measured through the BAO radius perpendicular to the line of sight $r_\perp$ and the comoving radius parallel to the line of sight $r_\parallel$.

$$r_{bao} := \left(r_\parallel r_\perp^2\right)^{\frac{1}{3}} = D_V\left(z\right)\Delta\theta^2\frac{\Delta z}{z} \tag{5.37}$$

One can, therefore, determine the distance D_V to the corresponding redshift, if the comoving radius of the baryon ring r_{bao} is known. This may be achieved by a measurement of the angle of the BAO ring on the sky $\Delta\theta$ and its longitudinal extension $\Delta z/z$. The precise definition of D_V is derived from the expressions of the comoving distances $r_\parallel$ and $r_\perp$:

$$r_\parallel = \int_z^{z+\Delta z}\frac{c}{H(z')}\mathrm{d}z' \approx \frac{c\Delta z}{H(z)} = \frac{cz}{H(z)}\frac{\Delta z}{z}, \tag{5.38}$$

$$r_\perp = (1+z)\,D_A(z)\Delta\theta, \tag{5.39}$$

from which we find

$$D_V(z) = \left(\frac{cz}{H(z)}D_M^2(z)\right)^{\frac{1}{3}}, \tag{5.40}$$

where D_M is the comoving angular distance

$$D_M(z) = c\left(\sqrt{\Omega_k}H_0\right)^{-1}\sinh\left(\sqrt{\Omega_k}I\left(z\right)\right), \tag{5.41}$$

with

$$I(z) = \int_0^z\frac{H_0}{H(z')}\mathrm{d}z'. \tag{5.42}$$

As already mentioned above, the term $\Omega_\mathcal{Q}^\mathcal{D}$ vanishes in our first-order treatment and the curvature contribution scales as $a_\mathcal{D}^{-2}$. Therefore we may express the Hubble rate as

$$\frac{H_\mathcal{D}(z)}{H_{\mathcal{D}_0}} = \left[(1+z)^3\Omega_m^{\mathcal{D}_0} + (1+z)^2\Omega_\mathcal{R}^{\mathcal{D}_0} + (1-\Omega_m^{\mathcal{D}_0} - \Omega_\mathcal{R}^{\mathcal{D}_0})\right]^{\frac{1}{2}}, \tag{5.43}$$

where we assumed the relation between redshift and average scale factor of Eq. (5.14).

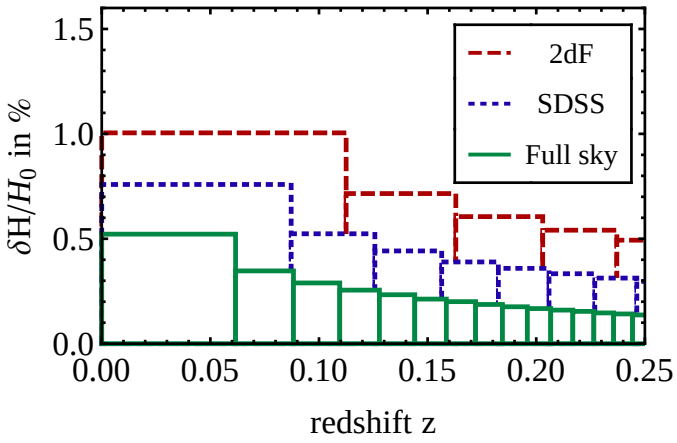

Figure 5.11. Optimal thickness of shells to minimize the variance of $H(z)$ (see text for the two competing effects). The respective error corresponds to the height of the bars, the shells necessary for this purpose to their width.

We may now calculate the fluctuation of D_V,

$$\frac{\delta r_\parallel}{r_\parallel} = \frac{\delta H_{\mathcal{D}_0}}{H_{\mathcal{D}_0}} + \left|\frac{1-(1+z)^2}{2}\frac{H_{\mathcal{D}_0}^2}{H_{\mathcal{D}}(z)^2}\right| \delta\Omega_{\mathcal{R}}^{\mathcal{D}_0} + \left|\frac{1-(1+z)^3}{2}\frac{H_{\mathcal{D}_0}^2}{H_{\mathcal{D}}(z)^2}\right| \delta\Omega_m^{\mathcal{D}_0} \,, \quad (5.44)$$

$$\frac{\delta r_\perp}{r_\perp} = \frac{\delta D_M}{D_{M_0}} = \frac{\delta H_{\mathcal{D}_0}}{H_{\mathcal{D}_0}} + \left|\frac{I(z)^2}{6} + \frac{I'(z)}{I(z)}\right| \delta\Omega_{\mathcal{R}}^{\mathcal{D}_0} + \left|\frac{I'(z)}{I(z)}\right| \delta\Omega_m^{\mathcal{D}_0} \,, \quad (5.45)$$

$$\frac{\delta D_V}{D_V} = \frac{1}{3}\frac{\delta r_\parallel}{r_\parallel} + \frac{2}{3}\frac{\delta r_\perp}{r_\perp} \,, \quad (5.46)$$

where $I'(z)$ denotes a partial derivation with respect to the respective parameter, i.e. $\Omega_{\mathcal{R}}^{\mathcal{D}_0}$ or $\Omega_m^{\mathcal{D}_0}$. Note that $I'(z)$ and $I(z)$ are evaluated on the background ($\Omega_{\mathcal{R}}^{\mathcal{D}_0} = 0$ and $\Omega_m^{\mathcal{D}_0} = \Omega_m$).

We evaluated the magnitude of the fluctuations in D_V, based on the cosmological parameters of the concordance model, as presented in Fig. 5.12. Fluctuations as low as one per cent are reached for much smaller domains than for the cosmic variance of the Ω-parameters. Thus, at first sight it might seem that the BAO measurement of D_V could essentially overcome the cosmic variance limit. Closer inspection of this result reveals that this is not the case. Indeed, the much smaller variation of the distance D_V means that a precise knowledge of the distance measure D_V does not lead to an equivalently good estimate of the cosmic parameters.

Clearly, the systematic uncertainty that we calculated is only a minor effect compared with the errors intrinsic to the actual measurement of the acoustic scale, as a comparison of the three solid (green) lines in Fig. 5.12 shows. The lowest one is the fluctuation of the scale D_V for full spheres of the corresponding size at different places in the Universe. It

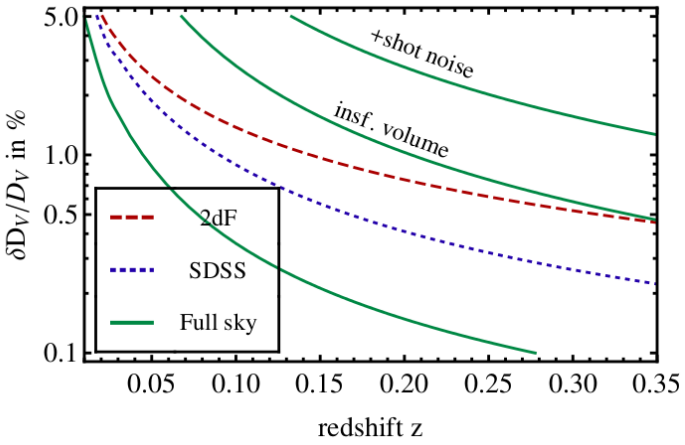

Figure 5.12. Errors on the distance D_V for various survey geometries as a function of maximum redshift. For comparison the error induced by the finite number of BAO modes in the corresponding full sphere volume, calculated with the fitting formula of [121], is shown (insufficient volume). This error is about a factor of 10 bigger than the error from the local volume distortion caused by inhomogeneities that we calculated. Adding a shot noise term, corresponding to a galaxy density of $n = 3 \times 10^{-4} h^3 \mathrm{Mpc}^{-3}$ typical for SDSS and BOSS, we find that the cosmic variance of D_V is a sub-dominant contribution to the error budget.

is therefore the possible local deformation caused by statistical over- or under-densities. The possible precision of a measurement of D_V by BAOs, however, also depends on the number of observable modes. This induces an error if the volume is too small, and in particular when it is smaller than the BAO scale a reasonable measurement is no longer possible. Accordingly, even for a perfect sampling of the observed volume, the error will not be smaller than the solid (green) lines in the middle. If one adds shot noise caused by imperfect sampling by a galaxy density of $n = 3 \times 10^{-4} h^3 \mathrm{Mpc}^{-3}$, typical for SDSS and BOSS, the error increases even more. This means that for the realistic situation where we do not have a sufficiently small perfect ruler to allow for large statistics already for the small volumes considered here, the deformation uncertainty that we calculated remains completely sub-dominant.

6. Conclusion and Outlook

To conclude, let us review what we learned about the influence of structure.

Our analysis of the SDSS LRG data in chapter 3 showed, that Minkowski functionals are a useful tool to characterize cosmic structure. Especially to describe the deviations of the galaxy distributions from a Gaussian distribution, the boolean grain model for Minkowski functionals was found to be helpful. This is, because for the Gaussian case, the exact shape of the Minkowski functional density is known analytically and so every deviation from this shape is a clear indication for non-Gaussianity. This could be demonstrated by a comparison of the functionals of a ΛCDM dark matter simulation [78] at redshift of $z = 5$ and the LRGs today. The simulated $z = 5$ data was still close to the Gaussian form of its initial conditions, but showed already clear deviations. For the late time LRGs, the Gaussian model was way off the actual shape of the functionals, indicating the strong non-Gaussianity of their distribution.

Comparing the Minkowski functionals of the LRGs to those from the mock simulations performed by [73, 75] in the context of the ΛCDM model, that are constructed to reproduce the LRGs with the correct window function of the observed region, we found significant deviations. If this is due to problems of the simulations, or if the effect really points to a discrepancy of the morphology between the LRGs and the underlying ΛCDM dark matter distribution is still under investigation.

After the test of the real cosmic structure in observational galaxy data, we investigate to what extent inhomogeneities of this magnitude influence the average evolution of the Universe on different scales. To this end we use a new form of a relativistic Lagrangian perturbation theory [31], that has the advantage of being conceptually close to the Newtonian theory. Therefore, it is expected that the general solution scheme for higher-order perturbations in Newtonian theory [122] may be generalized to the GR case. We perform a first test and find that the correspondence at lowest order is even a one to one correspondence. Furthermore, we show the equivalence of the first-order solution of the scheme to results of standard perturbation theory from [15, 16, 17]. This shows that the growing mode of their second-order result occurs in the same form in the Newtonian theory. Therefore this contributes only to the surface terms as already remarked by Li in [17].

The close correspondence of the GR result is probably due to the fact that the electric part of the Weyl tensor and the Newtonian tidal tensor are formally closely related [31]. By showing the equivalence of the Newtonian and GR perturbative solution we give an explicit example that this correspondence actually holds.

By a comparison of the Relativistic Zel'dovich approximation (RZA) to exact GR

results we find, that the solutions are more restricted than in the Newtonian case. This demonstrates that there is more to the full general relativistic solutions than what comes directly from the correspondence. So at some point the magnetic part of the Weyl tensor will also play a role in the GR case. From which order on this is the case is also work in progress [102].

Finally, the perturbative scheme allows us to determine quantitatively the influence of the backreaction term and we find it to be scale-dependent and of the order of 1% at 100Mpc. However, the curvature contribution may be as big as 20% on these scales giving rise to a 12% change in the comoving volume of a 100 Mpc sphere. For the ensemble averages, the results are less impressive. However, we could show that the RZA gives the same result as a partitioning model where each of the components evolves individually as an over- or under-dense Friedmann model.

The fact that the fluctuations especially in the curvature are still that large at scales of 100 Mpc motivated the exploration of the backreaction effects for even bigger domains. In the era of precision cosmology, it is crucial to know at which scale the effects are important and when they drop below the measurement precision. We evaluated this question taking into account the real size of the galaxy surveys, i.e. the fact that they are never full sky surveys. We derived useful formulae (5.30a)–(5.30e) that relate the fluctuation in the matter density to the fluctuations in the cosmic parameters.

Especially cosmic curvature was found to fluctuate at the percent level on scales as large as $540h^{-1}$Mpc in diameter. Only a volume-limited sample up to a redshift of 0.5 would be able to constrain the local curvature to 0.1 per cent. This is interesting in view of the BOSS [36] data to appear soon, that should provide such a sample.

For the determination of cosmic distances we found that fluctuations in the local geometry due to inhomogeneities do not limit the precision with which the BAO distance scale can be measured. This is good news for surveys like WiggleZ [58] or BOSS [36] that will constrain the ΛCDM model with the help of BAO measurements, or have already done so [67].

Finally we derived limits on how precisely we will ever know the Hubble rate today. Especially for this quantity local fluctuations are crucial: by looking at larger distances we look in the past and so the volume for the determination of H_0 is limited to a small area around us by definition. We find that this radius is $z \approx 0.06$ and that the uncertainty in H_0 will therefore be bigger than 0.5%.

Outlook There are many interesting lines of research that are opened up by these results. To adapt the determination of the cosmic variance due to local fluctuations to the new galaxy data, one could use the results on light cone averaging as derived by [115]. In this way the evolution effects of the galaxy distribution could be taken into account, which is not done here. One could also extend the analysis to other interesting quantities like the luminosity distance as done by [107]. With new supernova data the fluctuations in the Hubble rate could also be compared to the fluctuations calculated

here, as begun by [123].

In the case of the Lagrangian theory results, the generalization of the perturbative scheme to higher order will allow a new approach to the question up to which point in the evolution the perturbative results are still trustworthy. This is complementary to the gradient expansion approach advocated in [91]. It will be interesting to see up to which order the Newtonian correspondence will hold or at which point GR corrections occur. That this correspondence can never hold for all observables, however, but only for some of them, has recently been shown in [124].

Finally for the deviations of the LRG Minkowski functionals from the ΛCDM simulation data could point to an insufficient understanding of the LRGs as tracers of cosmic structures. It will turn out what kind of new insights we will gain from there.

Bibliography

[1] A. Einstein. *Kosmologische Betrachtungen zur allgemeinen Relativitätstheorie. Sitzungsberichte der Königlich Preußischen Akademie der Wissenschaften (Berlin), Seite 142-152.* 142–152 (1917).

[2] D. N. Spergel, L. Verde, H. V. Peiris, E. Komatsu, M. R. Nolta, et al. *First-Year Wilkinson Microwave Anisotropy Probe (WMAP) Observations: Determination of Cosmological Parameters. ApJS* **148**, 175–194 (2003). arXiv:astro-ph/0302209.

[3] A. G. Riess, A. V. Filippenko, P. Challis, A. Clocchiatti, A. Diercks, et al. *Observational Evidence from Supernovae for an Accelerating Universe and a Cosmological Constant. AJ* **116**, 1009–1038 (1998). arXiv:astro-ph/9805201.

[4] S. Perlmutter, G. Aldering, G. Goldhaber, R. A. Knop, P. Nugent, et al. *Measurements of Omega and Lambda from 42 High-Redshift Supernovae. ApJ* **517**, 565–586 (1999). arXiv:astro-ph/9812133.

[5] M. Scrimgeour, T. Davis, C. Blake, J. B. James, G. Poole, et al. *The WiggleZ Dark Energy Survey: the transition to large-scale cosmic homogeneity. ArXiv e-prints* (2012). arXiv:1205.6812.

[6] C. J. Copi, D. Huterer, D. J. Schwarz, and G. D. Starkman. *Large-Angle Anomalies in the CMB. Advances in Astronomy* **2010** (2010). arXiv:1004.5602.

[7] G. F. R. Ellis. *Relativistic cosmology - Its nature, aims and problems.* In B. Bertotti, F. de Felice, & A. Pascolini (ed.) *General Relativity and Gravitation Conference*, 215–288 (1984).

[8] R. M. Zalaletdinov. *Averaging out the Einstein equations. General Relativity and Gravitation* **24**, 1015–1031 (1992).

[9] R. M. Zalaletdinov. *Towards a theory of macroscopic gravity. General Relativity and Gravitation* **25**, 673–695 (1993).

[10] T. Buchert and M. Carfora. *Regional averaging and scaling in relativistic cosmology. Classical and Quantum Gravity* **19**, 6109–6145 (2002). arXiv:gr-qc/0210037.

[11] S. Räsänen. *Dark energy from back-reaction. J. Cosmology Astropart. Phys.* **2**, 3–+ (2004). arXiv:astro-ph/0311257.

[12] I. A. Brown, G. Robbers, and J. Behrend. *Averaging Robertson-Walker cosmologies. J. Cosmology Astropart. Phys.* **4**, 16–+ (2009). arXiv:0811.4495.

[13] I. A. Brown, J. Behrend, and K. A. Malik. *Gauges and cosmological backreaction. J. Cosmology Astropart. Phys.* **11**, 27–+ (2009). arXiv:0903.3264.

[14] E. W. Kolb, S. Matarrese, and A. Riotto. *On cosmic acceleration without dark energy. New Journal of Physics* **8**, 322–+ (2006). arXiv:astro-ph/0506534.

[15] N. Li and D. J. Schwarz. *Onset of cosmological backreaction. Phys. Rev. D* **76**, 083011–+ (2007). arXiv:gr-qc/0702043.

[16] N. Li and D. J. Schwarz. *Scale dependence of cosmological backreaction. Phys. Rev. D* **78**, 083531–+ (2008). arXiv:0710.5073.

[17] N. Li. *Cosmological backreaction : from the local Hubble expansion rate to dark energy.* Dissertation, Universität Bielefeld (2008). http://bieson.ub.uni-bielefeld.de/volltexte/2008/1372/.

[18] C. Clarkson, K. Ananda, and J. Larena. *Influence of structure formation on the cosmic expansion. Phys. Rev. D* **80**, 083525–+ (2009). arXiv:0907.3377.

[19] C. Clarkson and O. Umeh. *Is backreaction really small within concordance cosmology? Classical and Quantum Gravity* **28**, 164010 (2011). arXiv:1105.1886.

[20] S. Räsänen. *Applicability of the linearly perturbed FRW metric and Newtonian cosmology. Phys. Rev. D* **81**, 103512–+ (2010). arXiv:1002.4779.

[21] S. Räsänen. *Light propagation in statistically homogeneous and isotropic dust universes. J. Cosmology Astropart. Phys.* **2**, 11–+ (2009). arXiv:0812.2872.

[22] S. Räsänen. *Light propagation in statistically homogeneous and isotropic universes with general matter content. J. Cosmology Astropart. Phys.* **3**, 18 (2010). arXiv:0912.3370.

[23] T. Buchert, J. Larena, and J.-M. Alimi. *Correspondence between kinematical backreaction and scalar field cosmologies – the 'morphon field'. Classical and Quantum Gravity* **23**, 6379–6408 (2006). arXiv:gr-qc/0606020.

[24] J. Larena, J.-M. Alimi, T. Buchert, M. Kunz, and P.-S. Corasaniti. *Testing backreaction effects with observations. Phys. Rev. D* **79**, 083011 (2009). arXiv:0808.1161.

[25] X. Roy and T. Buchert. *Chaplygin gas and effective description of inhomogeneous universe models in general relativity. Classical and Quantum Gravity* **27**, 175013–+ (2010). arXiv:0909.4155.

[26] A. Wiegand and T. Buchert. *Multiscale cosmology and structure-emerging dark energy: A plausibility analysis. Phys. Rev. D* **82**, 023523–+ (2010). arXiv:1002.3912.

[27] S. Räsänen. *Evaluating backreaction with the peak model of structure formation. J. Cosmology Astropart. Phys.* **4**, 26–+ (2008). arXiv:0801.2692.

[28] D. L. Wiltshire. *Exact Solution to the Averaging Problem in Cosmology. Physical Review Letters* **99**, 251101 (2007). arXiv:0709.0732.

[29] D. L. Wiltshire. *Average observational quantities in the timescape cosmology. Phys. Rev. D* **80**, 123512 (2009). arXiv:0909.0749.

[30] T. Buchert, M. Kerscher, and C. Sicka. *Back reaction of inhomogeneities on the expansion: The evolution of cosmological parameters. Phys. Rev. D* **62**, 043525–+ (2000). arXiv:astro-ph/9912347.

[31] T. Buchert and M. Ostermann. *Lagrangian theory of structure formation in relativistic cosmology I: Lagrangian framework and definition of a non-perturbative approximation. ArXiv e-prints* (2012). arXiv:1203.6263.

[32] T. Buchert. *Dark Energy from structure: a status report. General Relativity and Gravitation* **40**, 467–527 (2008). arXiv:0707.2153.

[33] M. Giavalisco, H. C. Ferguson, A. M. Koekemoer, M. Dickinson, D. M. Alexander, et al. *The Great Observatories Origins Deep Survey: Initial Results from Optical and Near-Infrared Imaging. ApJ* **600**, L93–L98 (2004). arXiv:astro-ph/0309105.

[34] H.-W. Rix, M. Barden, S. V. W. Beckwith, E. F. Bell, A. Borch, et al. *GEMS: Galaxy Evolution from Morphologies and SEDs. ApJS* **152**, 163–173 (2004). arXiv:astro-ph/0401427.

[35] N. Scoville, R. G. Abraham, H. Aussel, J. E. Barnes, A. Benson, et al. *COSMOS: Hubble Space Telescope Observations. ApJS* **172**, 38–45 (2007). arXiv:astro-ph/0612306.

[36] D. J. Eisenstein, D. H. Weinberg, E. Agol, H. Aihara, C. Allende Prieto, et al. *SDSS-III: Massive Spectroscopic Surveys of the Distant Universe, the Milky Way, and Extra-Solar Planetary Systems. AJ* **142**, 72–+ (2011). arXiv:1101.1529.

[37] D. Schlegel, F. Abdalla, T. Abraham, C. Ahn, C. Allende Prieto, et al. *The BigBOSS Experiment. ArXiv e-prints* (2011). arXiv:1106.1706.

[38] L. Amendola, S. Appleby, D. Bacon, T. Baker, M. Baldi, et al. *Cosmology and fundamental physics with the Euclid satellite. ArXiv e-prints* (2012). arXiv:1206.1225.

[39] A. Wiegand and D. J. Schwarz. *Inhomogeneity-induced variance of cosmological parameters*. *A&A* **538**, A147 (2012). arXiv:1109.4142.

[40] T. Buchert, C. Nayet, and A. Wiegand. *Lagrangian theory of structure formation in relativistic cosmology II: average properties of a generic evolution model. To be published* (2012).

[41] E. Komatsu, K. M. Smith, J. Dunkley, C. L. Bennett, B. Gold, et al. *Seven-year Wilkinson Microwave Anisotropy Probe (WMAP) Observations: Cosmological Interpretation*. *ApJS* **192**, 18–+ (2011). arXiv:1001.4538.

[42] D. Boyanovsky, H. J. de Vega, and D. J. Schwarz. *Phase Transitions in the Early and Present Universe*. *Annual Review of Nuclear and Particle Science* **56**, 441–500 (2006). arXiv:hep-ph/0602002.

[43] C. H. Lineweaver and C. A. Egan. *The Cosmic Coincidence as a Temporal Selection Effect Produced by the Age Distribution of Terrestrial Planets in the Universe*. *ApJ* **671**, 853–860 (2007). arXiv:astro-ph/0703429.

[44] A. Gabrielli, F. Sylos Labini, M. Joyce, and L. Pietronero. *Statistical physics for cosmic structures*. Lecture notes in physics ; 629 (Springer, 2005).

[45] S. Weinberg. *Cosmology* (Oxford University Press, 2008).

[46] K. R. Mecke, T. Buchert, and H. Wagner. *Robust morphological measures for large-scale structure in the Universe*. *A&A* **288**, 697–704 (1994). arXiv:astro-ph/9312028.

[47] H. Hadwiger. *Vorlesungen über Inhalt, Oberfläche und Isoperimetrie*. Die Grundlehren der mathematischen Wissenschaften in Einzeldarstellungen mit besonderer Berücksichtigung der Anwendungsgebiete ; 93 (Springer, 1957).

[48] C. Hikage, J. Schmalzing, T. Buchert, Y. Suto, I. Kayo, et al. *Minkowski Functionals of SDSS Galaxies I : Analysis of Excursion Sets*. *PASJ* **55**, 911–931 (2003). arXiv:astro-ph/0304455.

[49] M. Kerscher, J. Schmalzing, T. Buchert, and H. Wagner. *Fluctuations in the IRAS 1.2 Jy catalogue*. *A&A* **333**, 1–12 (1998). arXiv:astro-ph/9704028.

[50] M. Kerscher, K. Mecke, J. Schmalzing, C. Beisbart, T. Buchert, et al. *Morphological fluctuations of large-scale structure: The PSCz survey*. *A&A* **373**, 1–11 (2001). arXiv:astro-ph/0101238.

[51] J. Schmalzing. *On statistics and dynamics of cosmic structure*. Ph.D. thesis, Ludwig Maximilians Universität München (1999). http://edoc.ub.uni-muenchen.de/449/.

[52] J. M. Bardeen. *Gauge-invariant cosmological perturbations. Phys. Rev. D* **22**, 1882–1905 (1980).

[53] J. Martin and D. J. Schwarz. *Influence of cosmological transitions on the evolution of density perturbations. Phys. Rev. D* **57**, 3302–3316 (1998). arXiv:gr-qc/9704049.

[54] S. Weinberg. *Adiabatic modes in cosmology. Phys. Rev. D* **67**, 123504 (2003). arXiv:astro-ph/0302326.

[55] D. J. Eisenstein and W. Hu. *Baryonic Features in the Matter Transfer Function. ApJ* **496**, 605–+ (1998). arXiv:astro-ph/9709112.

[56] M. Colless, G. Dalton, S. Maddox, W. Sutherland, P. Norberg, et al. *The 2dF Galaxy Redshift Survey: spectra and redshifts. MNRAS* **328**, 1039–1063 (2001). arXiv:astro-ph/0106498.

[57] K. N. Abazajian, J. K. Adelman-McCarthy, M. A. Agüeros, S. S. Allam, C. Allende Prieto, et al. *The Seventh Data Release of the Sloan Digital Sky Survey. ApJS* **182**, 543–558 (2009). arXiv:0812.0649.

[58] M. J. Drinkwater, R. J. Jurek, C. Blake, D. Woods, K. A. Pimbblet, et al. *The WiggleZ Dark Energy Survey: survey design and first data release. MNRAS* **401**, 1429–1452 (2010). arXiv:0911.4246.

[59] F. Sylos Labini and N. L. Vasilyev. *Extension and estimation of correlations in cold dark matter models. A&A* **477**, 381–395 (2008). arXiv:0710.0224.

[60] F. Sylos Labini, N. L. Vasilyev, Y. V. Baryshev, and M. López-Corredoira. *Absence of anti-correlations and of baryon acoustic oscillations in the galaxy correlation function from the Sloan Digital Sky Survey data release 7. A&A* **505**, 981–990 (2009). arXiv:0903.0950.

[61] W. J. Percival, R. C. Nichol, D. J. Eisenstein, J. A. Frieman, M. Fukugita, et al. *The Shape of the Sloan Digital Sky Survey Data Release 5 Galaxy Power Spectrum. ApJ* **657**, 645–663 (2007). arXiv:astro-ph/0608636.

[62] D. J. Eisenstein, I. Zehavi, D. W. Hogg, R. Scoccimarro, M. R. Blanton, et al. *Detection of the Baryon Acoustic Peak in the Large-Scale Correlation Function of SDSS Luminous Red Galaxies. ApJ* **633**, 560–574 (2005). arXiv:astro-ph/0501171.

[63] M. Crocce and R. Scoccimarro. *Renormalized cosmological perturbation theory. Phys. Rev. D* **73**, 063519 (2006). arXiv:astro-ph/0509418.

[64] M. Crocce and R. Scoccimarro. *Memory of initial conditions in gravitational clustering. Phys. Rev. D* **73**, 063520 (2006). arXiv:astro-ph/0509419.

[65] D. J. Eisenstein, H.-J. Seo, and M. White. *On the Robustness of the Acoustic Scale in the Low-Redshift Clustering of Matter*. *ApJ* **664**, 660–674 (2007). arXiv:astro-ph/0604361.

[66] W. J. Percival, B. A. Reid, D. J. Eisenstein, N. A. Bahcall, T. Budavari, et al. *Baryon acoustic oscillations in the Sloan Digital Sky Survey Data Release 7 galaxy sample*. *MNRAS* **401**, 2148–2168 (2010). arXiv:0907.1660.

[67] C. Blake, E. A. Kazin, F. Beutler, T. M. Davis, D. Parkinson, et al. *The WiggleZ Dark Energy Survey: mapping the distance-redshift relation with baryon acoustic oscillations*. *MNRAS* **418**, 1707–1724 (2011). arXiv:1108.2635.

[68] T. Okumura, T. Matsubara, D. J. Eisenstein, I. Kayo, C. Hikage, et al. *Large-Scale Anisotropic Correlation Function of SDSS Luminous Red Galaxies*. *ApJ* **676**, 889–898 (2008). arXiv:0711.3640.

[69] E. A. Kazin, M. R. Blanton, R. Scoccimarro, C. K. McBride, A. A. Berlind, et al. *The Baryonic Acoustic Feature and Large-Scale Clustering in the Sloan Digital Sky Survey Luminous Red Galaxy Sample*. *ApJ* **710**, 1444–1461 (2010). arXiv:0908.2598.

[70] W. J. Percival and M. White. *Testing cosmological structure formation using redshift-space distortions*. *MNRAS* **393**, 297–308 (2009). arXiv:0808.0003.

[71] A. Cabré and E. Gaztañaga. *Clustering of luminous red galaxies - I. Large-scale redshift-space distortions*. *MNRAS* **393**, 1183–1208 (2009). arXiv:0807.2460.

[72] C. McBride, A. Berlind, R. Scoccimarro, R. Wechsler, M. Busha, et al. *LasDamas Mock Galaxy Catalogs for SDSS*. In *American Astronomical Society Meeting Abstracts #213*, vol. 41 of *Bulletin of the American Astronomical Society*, 425.06 (2009).

[73] C. McBride et al. *in prep. tba* (2012).

[74] J. Schmalzing, M. Kerscher, and T. Buchert. *Minkowski Functionals in Cosmology*. In S. Bonometto, J. R. Primack, and A. Provenzale (eds.) *Dark Matter in the Universe*, 281 (1996). arXiv:astro-ph/9508154.

[75] *The simulations used for the Minkowski functional analysis were carried out by the Large Suite of Dark Matter Simulations (LasDamas) project. The data are publicly available at.* http://lss.phy.vanderbilt.edu/lasdamas/.

[76] F. Sylos Labini, N. L. Vasilyev, and Y. V. Baryshev. *Breaking the self-averaging properties of spatial galaxy fluctuations in the Sloan Digital Sky Survey - Data release six*. *A&A* **508**, 17–43 (2009). arXiv:0909.0132.

[77] K. Mecke. *Integralgeometrie in der Statistischen Physik*. Reihe Physik ; 25 (Deutsch, 1994).

[78] *The Very Large Simulation (VLS) used in this paper were carried out by the Virgo Supercomputing Consortium using computers based at Computing Centre of the Max-Planck Society in Garching and at the Edinburgh Parallel Computing Centre. The data are publicly available at.* www.mpa-garching.mpg.de/galform/virgo/vls.

[79] M. Davis and P. J. E. Peebles. *A survey of galaxy redshifts. V - The two-point position and velocity correlations*. *ApJ* **267**, 465–482 (1983).

[80] S. D. Landy and A. S. Szalay. *Bias and variance of angular correlation functions*. *ApJ* **412**, 64–71 (1993).

[81] M. Kerscher. *Constructing, characterizing, and simulating Gaussian and higher-order point distributions*. *Phys. Rev. E* **64**, 056109 (2001). arXiv:astro-ph/0102153.

[82] G. F. R. Ellis. *Inhomogeneity effects in cosmology*. *Classical and Quantum Gravity* **28**, 164001 (2011). arXiv:1103.2335.

[83] K. Bolejko, M.-N. Célérier, and A. Krasiński. *Inhomogeneous cosmological models: exact solutions and their applications*. *Classical and Quantum Gravity* **28**, 164002 (2011). arXiv:1102.1449.

[84] F. Sylos Labini. *Inhomogeneities in the universe*. *Classical and Quantum Gravity* **28**, 164003 (2011). arXiv:1103.5974.

[85] V. Marra and A. Notari. *Observational constraints on inhomogeneous cosmological models without dark energy*. *Classical and Quantum Gravity* **28**, 164004 (2011). arXiv:1102.1015.

[86] D. L. Wiltshire. *What is dust?–Physical foundations of the averaging problem in cosmology*. *Classical and Quantum Gravity* **28**, 164006 (2011). arXiv:1106.1693.

[87] T. Buchert. *Toward physical cosmology: focus on inhomogeneous geometry and its non-perturbative effects*. *Classical and Quantum Gravity* **28**, 164007 (2011). arXiv:1103.2016.

[88] S. Räsänen. *Backreaction: directions of progress*. *Classical and Quantum Gravity* **28**, 164008 (2011). arXiv:1102.0408.

[89] E. W. Kolb. *Backreaction of inhomogeneities can mimic dark energy*. *Classical and Quantum Gravity* **28**, 164009 (2011).

[90] T. Clifton. *Cosmology without averaging. Classical and Quantum Gravity* **28**, 164011 (2011). arXiv:1005.0788.

[91] K. Enqvist, S. Hotchkiss, and G. Rigopoulos. *A gradient expansion for cosmological backreaction. J. Cosmology Astropart. Phys.* **3**, 26 (2012). arXiv:1112.2995.

[92] T. Buchert. *On globally static and stationary cosmologies with or without a cosmological constant and the dark energy problem. Classical and Quantum Gravity* **23**, 817–844 (2006). arXiv:gr-qc/0509124.

[93] M. Carfora. *Renormalization Group and the Ricci flow. ArXiv e-prints* (2010). arXiv:1001.3595.

[94] T. Buchert. *On Average Properties of Inhomogeneous Fluids in General Relativity: Dust Cosmologies. General Relativity and Gravitation* **32**, 105–126 (2000). arXiv:gr-qc/9906015.

[95] T. Buchert. *On Average Properties of Inhomogeneous Fluids in General Relativity: Perfect Fluid Cosmologies. General Relativity and Gravitation* **33**, 1381–1405 (2001). arXiv:gr-qc/0102049.

[96] E. Gourgoulhon. *3+1 Formalism and Bases of Numerical Relativity. ArXiv General Relativity and Quantum Cosmology e-prints* (2007). arXiv:gr-qc/0703035.

[97] T. Buchert and M. Carfora. *On the curvature of the present-day universe. Classical and Quantum Gravity* **25**, 195001–+ (2008). arXiv:0803.1401.

[98] T. Buchert. *LETTER TO THE EDITOR: A cosmic equation of state for the inhomogeneous universe: can a global far-from-equilibrium state explain dark energy? Classical and Quantum Gravity* **22**, L113–L119 (2005). arXiv:gr-qc/0507028.

[99] X. Roy, T. Buchert, S. Carloni, and N. Obadia. *Global gravitational instability of FLRW backgrounds – interpreting the dark sectors. Classical and Quantum Gravity* **28**, 165004 (2011). arXiv:1103.1146.

[100] S. Matarrese and D. Terranova. *Post-Newtonian cosmological dynamics in Lagrangian coordinates. MNRAS* **283**, 400–418 (1996). arXiv:astro-ph/9511093.

[101] S. Chandrasekhar. *The mathematical theory of black holes* (1992).

[102] A. Alles, A. Wiegand, and A. Buchert. *in prep. tba* (2013).

[103] C. Sicka. *Effektive Dynamik inhomogener Kosmologien.* Ph.D. thesis, Ludwig Maximilians Universität München (2003). http://edoc.ub.uni-muenchen.de/1208/.

[104] R. A. Sussman. *Radial asymptotics of Lemaître-Tolman-Bondi dust models. General Relativity and Gravitation* **42**, 2813–2864 (2010). arXiv:1002.0173.

[105] T. Buchert. *Lagrangian Theory of Gravitational Instability of Friedman-Lemaitre Cosmologies - a Generic Third-Order Model for Nonlinear Clustering. MNRAS* **267**, 811 (1994). arXiv:astro-ph/9309055.

[106] J. M. Bardeen, J. R. Bond, N. Kaiser, and A. S. Szalay. *The statistics of peaks of Gaussian random fields. ApJ* **304**, 15–61 (1986).

[107] C. Bonvin and R. Durrer. *What galaxy surveys really measure. Phys. Rev. D* **84**, 063505–+ (2011). arXiv:1105.5280.

[108] T. Biswas, A. Notari, and W. Valkenburg. *Testing the void against cosmological data: fitting CMB, BAO, SN and H_0. J. Cosmology Astropart. Phys.* **11**, 30 (2010). arXiv:1007.3065.

[109] E. Komatsu, J. Dunkley, M. R. Nolta, C. L. Bennett, B. Gold, et al. *Five-Year Wilkinson Microwave Anisotropy Probe Observations: Cosmological Interpretation. ApJS* **180**, 330–376 (2009). arXiv:0803.0547.

[110] W. L. Freedman, B. F. Madore, B. K. Gibson, L. Ferrarese, D. D. Kelson, et al. *Final Results from the Hubble Space Telescope Key Project to Measure the Hubble Constant. ApJ* **553**, 47–72 (2001). arXiv:astro-ph/0012376.

[111] O. Umeh, J. Larena, and C. Clarkson. *The Hubble rate in averaged cosmology. J. Cosmology Astropart. Phys.* **3**, 29 (2011). arXiv:1011.3959.

[112] O. Lahav, P. B. Lilje, J. R. Primack, and M. J. Rees. *Dynamical effects of the cosmological constant. MNRAS* **251**, 128–136 (1991).

[113] S. P. Driver and A. S. G. Robotham. *Quantifying cosmic variance. MNRAS* **407**, 2131–2140 (2010). arXiv:1005.2538.

[114] B. P. Moster, R. S. Somerville, J. A. Newman, and H.-W. Rix. *A Cosmic Variance Cookbook. ApJ* **731**, 113 (2011). arXiv:1001.1737.

[115] M. Gasperini, G. Marozzi, F. Nugier, and G. Veneziano. *Light-cone averaging in cosmology: formalism and applications. J. Cosmology Astropart. Phys.* **7**, 8–+ (2011). arXiv:1104.1167.

[116] X. Shi and M. S. Turner. *Expectations for the Difference between Local and Global Measurements of the Hubble Constant. ApJ* **493**, 519 (1998). arXiv:astro-ph/9707101.

[117] C. Clarkson, M. Cortês, and B. Bassett. *Dynamical dark energy or simply cosmic curvature?* *J. Cosmology Astropart. Phys.* **8**, 11–+ (2007). arXiv:astro-ph/0702670.

[118] E. L. Turner, R. Cen, and J. P. Ostriker. *The relation of local measures of Hubble's constant to its global value.* *AJ* **103**, 1427–1437 (1992).

[119] Y. Wang, D. N. Spergel, and E. L. Turner. *Implications of Cosmic Microwave Background Anisotropies for Large-Scale Variations in Hubble's Constant.* *ApJ* **498**, 1–+ (1998). arXiv:astro-ph/9708014.

[120] C. Blake, K. Glazebrook, T. M. Davis, S. Brough, M. Colless, et al. *The WiggleZ Dark Energy Survey: measuring the cosmic expansion history using the Alcock-Paczynski test and distant supernovae.* *MNRAS* **418**, 1725–1735 (2011). arXiv:1108.2637.

[121] H.-J. Seo and D. J. Eisenstein. *Improved Forecasts for the Baryon Acoustic Oscillations and Cosmological Distance Scale.* *ApJ* **665**, 14–24 (2007). arXiv:astro-ph/0701079.

[122] J. Ehlers and T. Buchert. *Newtonian Cosmology in Lagrangian Formulation: Foundations and Perturbation Theory.* *General Relativity and Gravitation* **29**, 733–764 (1997). arXiv:astro-ph/9609036.

[123] M. Seikel and D. J. Schwarz. *Probing Backreaction Effects with Supernova Data.* In *Cosmic Structure and Evolution* (2009). arXiv:0912.2308.

[124] S. F. Flender and D. J. Schwarz. *Newtonian versus relativistic cosmology.* *ArXiv e-prints* (2012). arXiv:1207.2035.

[125] S. Matarrese, S. Mollerach, and M. Bruni. *Relativistic second-order perturbations of the Einstein-de Sitter universe.* *Phys. Rev. D* **58**, 043504 (1998). arXiv:astro-ph/9707278.

[126] C. Rampf and T. Buchert. *Lagrangian perturbations and the matter bispectrum I: fourth-order model for non-linear clustering.* *J. Cosmology Astropart. Phys.* **6**, 21 (2012). arXiv:1203.4260.

[127] K. Peeters. *Cadabra: a field-theory motivated symbolic computer algebra system.* *Computer Physics Communications* **176**, 550–558 (2007). arXiv:cs/0608005.

[128] K. Peeters. *Introducing Cadabra: a symbolic computer algebra system for field theory problems.* *ArXiv High Energy Physics - Theory e-prints* (2007). arXiv:hep-th/0701238.

A. Window function calculation

In this appendix we write out the window functions explicitly, which were used to find the results in Sec. 5.3 and 5.4. The principal quantity we need is the matter variance today as defined in Eq. (5.29) being

$$(\sigma_{\mathcal{D}_0})^2 := \sigma^2\left(\langle\delta_0\rangle_{\mathcal{D}}\right) = \int_{\mathbb{R}^3} P_0\left(k\right)\widetilde{W}_{\mathcal{D}}\left(\mathbf{k}\right)\widetilde{W}_{\mathcal{D}}\left(-\mathbf{k}\right)\mathrm{d}^3k\ . \tag{A.1}$$

For a ball, the Fourier transformed window function is still simple and was already given in Sec. 2.1.1. The real space window Eq. (2.20)

$$W_{\mathcal{B}(R)}\left(\mathbf{r}\right) = \begin{cases} 1 & R-|\mathbf{r}|>0 \\ 0 & \text{else}\ , \end{cases} \tag{A.2}$$

is transformed to give Eq. (2.21)

$$\widetilde{W}_{\mathcal{B}(R)}\left(\mathbf{k}\right) = \frac{1}{\frac{4\pi}{3}R^3}\int d^3r W_{\mathcal{B}(R)}\left(\mathbf{r}\right)e^{-i\mathbf{k}\cdot\mathbf{r}} = \frac{3\left(\sin kR - kR\cos kR\right)}{\left(kR\right)^3}\ . \tag{A.3}$$

If the integral is not over the full sphere the expressions are unfortunately more complicated. For a general window function given in terms of spherical coordinates we have

$$\widetilde{W}_{\mathcal{D}}\left(\mathbf{k}\right) = \frac{1}{V_{\mathcal{D}}}\int d^3r W_{\mathcal{D}}\left(r,\theta,\varphi\right)e^{-i\mathbf{k}\cdot\mathbf{r}}\ . \tag{A.4}$$

We will be interested in top hat windows, so radial and angular part may be separated as

$$W_{\mathcal{D}}\left(r,\theta,\varphi\right) = W_{\mathcal{D}}\left(r\right)f_{\mathcal{D}}\left(\theta,\varphi\right) \tag{A.5}$$

and $f_{\mathcal{D}}\left(\theta,\varphi\right)$ can in general be decomposed as

$$f_{\mathcal{D}}\left(\theta,\varphi\right) = \sum_{\ell=0}^{\infty}\sum_{m=-\ell}^{\ell}\int c_{\ell m}Y_{\ell m}\left(\theta,\varphi\right)\ , \tag{A.6}$$

with coefficients given by

$$c^{\mathcal{D}}_{\ell m} = \int f_{\mathcal{D}}\left(\theta,\varphi\right)\left[Y^m_\ell\left(\theta,\varphi\right)\right]^\star d\Omega\ . \tag{A.7}$$

This means for $\widetilde{W}_{\mathcal{D}}(\mathbf{k})$ in terms of spherical harmonics

$$\widetilde{W}_{\mathcal{D}}(\mathbf{k}) = \frac{1}{V_{\mathcal{D}}} \sum_{\ell=0}^{\infty} \sum_{m=-\ell}^{\ell} \int W_{\mathcal{D}}(r)\, c_{\ell m}^{\mathcal{D}} Y_{\ell m}(\theta,\varphi)\, e^{-i\mathbf{k}\cdot\mathbf{r}} d^3r \,. \tag{A.8}$$

Using the identity

$$e^{i\vec{k}\vec{r}} = 4\pi \sum_{l=0}^{\infty} \sum_{m=-l}^{l} i^l j_l(kr) \left[Y_l^m(\theta_k,\varphi_k)\right]^{\star} \cdot Y_l^m(\theta_r,\varphi_r) \;, \tag{A.9}$$

we find after some simplification

$$(\sigma_{\mathcal{D}_0})^2 = \int_{\mathbb{R}^3} P_0(k)\, \widetilde{W}_{\mathcal{D}}(\mathbf{k})\, \widetilde{W}_{\mathcal{D}}(-\mathbf{k})\, \mathrm{d}^3k = 4\pi V_{\mathcal{D}}^{-2} \sum_{\ell=0}^{\infty} (2\ell+1)\, R_\ell(r)\, A_\ell(\alpha,\beta) \;, \tag{A.10}$$

where the radial coefficients are

$$\begin{aligned} R_\ell(r) &= V_{\mathcal{D}}^2 \int\int\int P(k)\, k^2 W_{\mathcal{D}}(r_1)\, W_{\mathcal{D}}(r_2)\, r_1^2 j_\ell(kr_1)\, r_2^2 j_\ell(kr_2)\; dk\, dr_1\, dr_2 \\ &= \int_0^{\infty} k^2 P(k) \left(S_\ell(k,R)\right)^2 \; dk \,. \end{aligned} \tag{A.11}$$

For a sharp window in real space $W_{\mathcal{D}}(r) = \Theta(R-r)/V_{\mathcal{D}}$ the coefficients S_ℓ are given by

$$\begin{aligned} S_\ell(R) &= \int \Theta(R-r)\, j_\ell(kr)\, r^2 dr \\ &= \sqrt{\pi} 2^{-\ell-2} R^3 \Gamma\left(\frac{\ell+3}{2}\right) (kR)^\ell \; {}_1\tilde{F}_2\left(\frac{\ell+3}{2}; \ell+\frac{3}{2}, \frac{\ell+5}{2}; -\frac{1}{4}k^2R^2\right) \end{aligned} \tag{A.12}$$

where ${}_1\tilde{F}_2$ is a regularized hypergeometric function. Only the first two coefficients can be expressed by trigonometric functions

$$S_0(R) = -\frac{kR\cos(kR) - \sin(kR)}{k^3} \,, \tag{A.13}$$

$$S_1(R) = -\frac{kR\sin(kR) + 2\cos(kR) - 2}{k^3} \,. \tag{A.14}$$

Comparing S_0 with (A.3) we find that the monopole (the full sphere) comes out correctly.

The angular coefficients in (A.10) read

$$\begin{aligned} A_\ell(\alpha,\beta) &= \int\int P_\ell\left(\cos(\theta_{r_1})\cos(\theta_{r_2}) + \cos(\varphi_{r_1}-\varphi_{r_2})\sin(\theta_{r_1})\sin(\theta_{r_2})\right) \\ &\quad \times f_{\mathcal{D}}(\theta_{r_1},\varphi_{r_1})\, f_{\mathcal{D}}(\theta_{r_2},\varphi_{r_2})\, d\Omega_{r_1} d\Omega_{r_2} \;, \end{aligned} \tag{A.15}$$

where $d\Omega_{r_1} = \sin(\theta_{r_1})\, d\theta_{r_1} d\varphi_{r_1}$. We calculate these integrals for the two angular windows of Fig. 5.3. The slice like geometry has $\varphi \in [0, \alpha]$ and $\theta \in \left[\frac{\pi}{2} - \beta, \frac{\pi}{2} + \beta\right]$ so the windows

$$\begin{aligned} A_\ell(\alpha, \beta) &= \int_0^\alpha \int_0^\alpha \int_{\frac{\pi}{2}-\beta}^{\frac{\pi}{2}+\beta} \int_{\frac{\pi}{2}-\beta}^{\frac{\pi}{2}+\beta} P_\ell\left(\cos(\theta_{r_1})\cos(\theta_{r_2}) + \cos(\varphi_{r_1} - \varphi_{r_2})\sin(\theta_{r_1})\sin(\theta_{r_2})\right) \\ &\quad \times \sin(\theta_{r_1})\sin(\theta_{r_2})\, d\varphi_{r_1} d\varphi_{r_2} d\theta_{r_1} d\theta_{r_2} \end{aligned} \tag{A.16}$$

may be written as

$$\begin{aligned} A_\ell(\alpha, \beta) = \sum_{k=0}^{\lfloor \frac{\ell}{2} \rfloor} \sum_{i=0}^{\ell-2k} & \frac{(-1)^{i+k+\ell} \left(\frac{1}{2}\right)^{3\ell-4k+i} (2\ell - 2k)! \left(\sum_{k=0}^{i} \binom{i}{k} \frac{\sin^2\left(\alpha\left(\frac{i}{2}-k\right)\right)}{\left(\frac{i}{2}-k\right)^2}\right)}{i!k!(\ell-k)!(-i-2k+\ell)!} \\ \times \left(\sum_{m=0}^{i+1} \sum_{j=0}^{-i-2k+\ell} (-1)^j \binom{i+1}{m} \binom{\ell-i-2k}{j} \right. & \left. \frac{\sin(\beta(2j+2k+2m-\ell-1))}{2j+2k+2m-\ell-1} \right)^2 \end{aligned} \tag{A.17}$$

This looks quite ugly, but for our purpose of not too small angular scales this is sufficient. The first few coefficients read

$$A_0(\alpha, \beta) = 4\alpha^2 \sin^2(\beta)\,, \tag{A.18}$$

$$A_1(\alpha, \beta) = \sin^2\left(\frac{\alpha}{2}\right)(2\beta + \sin(2\beta))^2\,, \tag{A.19}$$

$$A_2(\alpha, \beta) = \frac{2}{3}\alpha^2\left(\sin^6(\beta) - 3\sin^2(\beta)\right) + \frac{1}{48}\left(\alpha^2 + \sin^2(\alpha)\right)(9\sin(\beta) + \sin(3\beta))^2 \tag{A.20}$$

Finally when we take the volume into account we find

$$\sigma^2(R, \alpha, \beta) = \left(\frac{2}{3}R^3\alpha\sin\left(\frac{\beta}{2}\right)\right)^{-2} \left(4\pi \sum_{\ell=0}^{\infty} (2\ell+1)\, R_\ell(R)\, A_\ell(\alpha, \beta)\right)\,. \tag{A.21}$$

The geometry of the cone is defined by the angular window function $\varphi \in [0, 2\pi]$ and $\theta \in [0, \beta]$. Note the different meaning of β in this case. The coefficients read

$$\begin{aligned} A_\ell(\beta) = \sum_{k=0}^{\lfloor \frac{\ell}{2} \rfloor} \sum_{i=0}^{\lfloor \frac{1}{2}(\ell-2k) \rfloor} & \frac{\pi^2(-1)^k 2^{-2i-\ell}(2\ell-2k)!}{k!(\ell-k)!(-2i-2k+\ell)!} \\ \times \left(\frac{\Gamma\left(\frac{1}{2}(-2i-2k+\ell+1)\right)}{\Gamma\left(\frac{1}{2}(-2k+\ell+3)\right)} \right. & \left. - \cos^{-2i-2k+\ell+1}(\beta) \sum_{j=0}^{i} \frac{(-1)^j \cos^{2j}(\beta)}{j!(i-j)!\left(\frac{1}{2}(-2i-2k+\ell+1)+j\right)} \right)^2 . \end{aligned} \tag{A.22}$$

Now that there is only one angle involved, they are simpler

$$A_0(\beta) = 4\pi^2(\cos(\beta) - 1)^2\,, \tag{A.23}$$

$$A_1(\beta) = \pi^2 \sin^4(\beta)\,, \tag{A.24}$$

$$A_2(\beta) = \pi^2 \sin^4(\beta)\cos^2(\beta)\,, \tag{A.25}$$

$$A_3(\beta) = \frac{1}{64}\pi^2 \sin^4(\beta)(5\cos(2\beta) + 3)^2\,, \tag{A.26}$$

which also indicates that Eq. (A.22) is not yet the most compact form. But it is good enough for our purpose. The matter fluctuations for the cone are therefore

$$\sigma^2\left(R,\beta\right) = \left(\frac{2}{3}R^3\left(\cos(\beta)-1\right)\right)^{-2}\left(4\pi\sum_{\ell=0}^{\infty}\left(2\ell+1\right)R_\ell\left(R\right)A_\ell\left(\beta\right)\right) . \tag{A.27}$$

For more general geometries the formulae will become even more involved than Eq. (A.17), but there is no conceptual problem to calculate them.

B. Fourth order backreaction

The correspondence discussed in section 4.5.1 allows us to derive the form of the leading order backreaction mode at fourth order. To this end we use the metric

$$\mathrm{d}s^2 = a^2(\eta)\left[-\mathrm{d}\eta^2 + \left(\delta_{ij} + \gamma_{ij}^{(1)} + \gamma_{ij}^{(2)} + \gamma_{ij}^{(3)}\right)\mathrm{d}x^i\mathrm{d}x^j\right] \,, \tag{B.1}$$

where η is the conformal time. The decomposition chosen in [125] is

$$\gamma_{ij}^{(1)} = -2\psi^{(1)}\delta_{ij} + \chi_{ij}^{(1)} \,, \tag{B.2}$$

$$\gamma_{ij}^{(2)} = -\psi^{(2)}\delta_{ij} + \frac{1}{2}\chi_{ij}^{(2)} \,, \tag{B.3}$$

$$\gamma_{ij}^{(3)} = -\frac{1}{3}\psi^{(3)}\delta_{ij} + \frac{1}{6}\chi_{ij}^{(3)} \,. \tag{B.4}$$

The solution to second order is also given in [125] and was used in [17] for the third order expression of the backreaction term. The fastest growing terms are at first order

$$\psi^{(1)} = \frac{\eta^2}{18}\Delta\varphi(\mathbf{x}) \,, \tag{B.5}$$

$$\chi_{ij}^{(1)} = \frac{\eta^2}{9}\Delta\varphi(\mathbf{x})\delta_{ij} - \frac{\eta^2}{3}\partial_i\partial_j\varphi(\mathbf{x}) \tag{B.6}$$

and at second order

$$\psi^{(2)} = \frac{\eta^4}{252}\left[(\Delta\varphi)^2 - \frac{10}{3}\partial^i\partial_j\varphi\partial^j\partial_i\varphi\right] \,, \tag{B.7}$$

$$\chi_{ij}^{(2)} = \frac{\eta^4}{126}\left[\left((\Delta\varphi)^2 - \frac{10}{3}\partial^k\partial_m\varphi\partial^m\partial_k\varphi\right)\delta_{ij} + 7\partial_i\partial_k\varphi\partial^k\partial_j\varphi + 6\partial_i\partial_j\psi_0\right] \,. \tag{B.8}$$

Solving the Einstein equations (1.1) at third order with the metric ansatz (B.1), we now find that

$$\psi^{(3)} = \frac{\eta^6}{162}\left[\partial^{ab}\psi_0\partial_{ab}\varphi + \frac{2}{21}\partial_a^a\varphi\partial_b^b\varphi\partial_c^c\varphi + \frac{1}{14}\partial_a^a\varphi\partial^{bc}\varphi\partial_{bc}\varphi - \frac{1}{6}\partial^{ab}\varphi\partial_a^c\varphi\partial_{bc}\varphi\right] \,, \tag{B.9}$$

$$\begin{aligned}\chi_{ij}^{(3)} = \frac{\eta^6}{9}\Bigg[&\frac{1}{9}\delta_{ij}\left(\partial^{ab}\psi_0\partial_{ab}\varphi + \frac{2}{21}\partial_a^a\varphi\partial_b^b\varphi\partial_c^c\varphi + \frac{1}{14}\partial_a^a\varphi\partial^{bc}\varphi\partial_{bc}\varphi - \frac{1}{6}\partial^{ab}\varphi\partial_a^c\varphi\partial_{bc}\varphi\right) \\ &- \frac{3}{14}\,\partial_{(i}{}^a\psi_0\,\partial_{j)a}\varphi + \frac{1}{6}\,\partial_{ij}\Psi^{(3a)} - \frac{5}{7}\,\partial_{ij}\Psi^{(3b)} + \frac{1}{14}\,\partial_{(i}{}^a\epsilon_{j)ak}T^{(3c)k}\Bigg] \,,\end{aligned} \tag{B.10}$$

where ∂_a^b is a short form for $\partial_a \partial^b$. This again is only the fastest growing term of the third order solution to the Einstein equations. The new potentials used here are the solutions to the defining equations

$$\Delta\psi_0 := -\frac{1}{2}\left[(\Delta\varphi)^2 - \partial^i\partial_j\varphi\partial^j\partial_i\varphi\right] \tag{B.11}$$

$$\Delta\Psi^{(3a)} := \frac{1}{6}\epsilon_{abc}\epsilon^{mnk}\partial_m{}^a\varphi\,\partial_n{}^b\varphi\,\partial_k{}^c\varphi \tag{B.12}$$

$$\Delta\Psi^{(3b)} := -\frac{1}{2}\left[\Delta\varphi\Delta\psi_0 - \partial^i\partial_j\varphi\partial^j\partial_i\psi_0\right] \tag{B.13}$$

$$\Delta T^{(3c)k} := \epsilon^{ijk}\epsilon_{abc}\epsilon^{pnl}\delta_{pi}\partial_j{}^a\psi_0\,\partial_n{}^b\varphi\,\delta_l{}^c\,. \tag{B.14}$$

The complete metric to third order containing the fastest growing terms is then

$$\begin{aligned} g_{ij} &= a^2(\eta)\left[\delta_{ij} - \frac{1}{3}\partial_i\partial_j\varphi\,\eta^2 + \frac{1}{36}\left(\frac{6}{7}\,\partial_i\partial_j\psi_0 + \partial_i{}^b\varphi\,\partial_{jb}\varphi\right)\eta^4\right. \\ &\quad \left. -\frac{1}{216}\left(\frac{6}{7}\,\partial_{(i}{}^b\psi_0\,\partial_{j)b}\varphi - \frac{2}{3}\,\partial_i\partial_j\Psi^{(3a)} + \frac{20}{21}\,\partial_i\partial_j\Psi^{(3b)} - \frac{2}{7}\,\epsilon_{ak(i}\partial^a_{j)}T^{(3c)k}\right)\eta^6\right]\,. \end{aligned} \tag{B.15}$$

Using the correspondence (4.66) we find that in the Newtonian case the metric is given by

$$g_{ij} = \delta_{ab} f^{|a}_{|i} f^{|b}_{|j}\,, \tag{B.16}$$

where the third order solutions of the Lagrangian mapping f have been given in equation (4.118). The potentials $S^{(2)}$, $S^{(3a)}$, $S^{(3b)}$ and $S^{(3c)}$ defined in Eqs. (4.120a)–(4.120e) are up to a factor the same as the ψ_0, $\Psi^{(3a)}$, $\Psi^{(3b)}$ and $T^{(3c)}$ used here. If we plug (4.118) into (B.16), we find also in the Newtonian case (B.15), as expected.

With the metric (B.15), we can then calculate the corresponding expansion tensor

$$\begin{aligned} \Theta^j_i &= \frac{a'}{a}\delta^j_i - \frac{1}{3}\eta\partial^j_i\varphi + \frac{1}{18}\left(\frac{6}{7}\partial^j_i\Psi^{(2)} - \partial^{ja}\varphi\partial_{ia}\varphi\right)\eta^3 + \frac{1}{504}\left[5\partial^a_i\Psi^{(2)}\partial^j_a\varphi + \partial^{ja}\Psi^{(2)}\partial_{ia}\varphi\right. \\ &\quad \left. -\frac{14}{3}\partial_{ab}\varphi\partial^{ja}\varphi\partial^b_i\varphi + \frac{14}{3}\partial^j_i\Psi^{(3a)} - \frac{20}{3}\partial^j_i S^{(3b)} - \partial^{ja}T^{(3c)}_b\epsilon^b_{ai}\eta^5 - \partial^a_i T^{(3c)}_b\epsilon^{jb}_a\right]\eta^5\,. \end{aligned} \tag{B.17}$$

With this expression we are finally able to give the fourth order backreaction term. $\mathcal{Q}_\mathcal{D}$ in terms of the extrinsic curvature is given in Eq. (4.13) by

$$\mathcal{Q}_\mathcal{D} = \left\langle K^2 - K_{ij}K^{ij}\right\rangle_\mathcal{D} - \frac{2}{3}\langle K\rangle^2_\mathcal{D} \tag{B.18}$$

and with the relation between extrinsic curvature and expansion rate $-K_{ij} = \Theta_{ij}$ we find

$$\begin{aligned} {}^{(4)}\mathcal{Q}_\mathcal{D} \propto a\left(\frac{72}{49}\left\langle \mathbf{II}^{(2,2)}_\mathbf{i}\right\rangle_{\mathcal{D}_\mathbf{i}} - 4\left\langle \mathbf{II}^{(1,3a)}_\mathbf{i}\right\rangle_{\mathcal{D}_\mathbf{i}} + \frac{40}{7}\left\langle \mathbf{II}^{(1,3b)}_\mathbf{i}\right\rangle_{\mathcal{D}_\mathbf{i}} + \frac{6}{7}\left\langle \mathbf{II}^{(1,3c)}_\mathbf{i}\right\rangle_{\mathcal{D}_\mathbf{i}} - \frac{90}{7}\left\langle \mathbf{III}^{(1,1,2)}_\mathbf{i}\right\rangle_{\mathcal{D}_\mathbf{i}}\right. \\ \left. \frac{104}{21}\left\langle \mathbf{II}^{(1,2)}_\mathbf{i}\right\rangle_{\mathcal{D}_\mathbf{i}}\langle\mathbf{I_i}\rangle_{\mathcal{D}_\mathbf{i}} - \frac{26}{3}\langle\mathbf{III_i}\rangle_{\mathcal{D}_\mathbf{i}}\langle\mathbf{I_i}\rangle_{\mathcal{D}_\mathbf{i}} - \frac{296}{147}\langle\mathbf{II_i}\rangle^2_{\mathcal{D}_\mathbf{i}} + \frac{122}{21}\langle\mathbf{II_i}\rangle_{\mathcal{D}_\mathbf{i}}\langle\mathbf{I_i}\rangle^2_{\mathcal{D}_\mathbf{i}} - 2\langle\mathbf{I_i}\rangle^4_{\mathcal{D}_\mathbf{i}}\right)\,. \end{aligned} \tag{B.19}$$

Here we again converted the potentials $\varphi \to \psi$ via $\varphi = -\frac{2}{3}\frac{1}{t_i^2}\psi$ and we write the combinations of these ψ potentials in terms of its invariants as

$$\mathbf{I_i} := \frac{1}{2}\epsilon_{abc}\epsilon^{ijk}\psi_{|i}^{|a}\delta^b{}_j\delta^c{}_k \,, \tag{B.20}$$

$$\mathbf{II_i} := \frac{1}{2}\epsilon_{abc}\epsilon^{ijk}\psi_{|i}^{|a}\psi_{|j}^{|b}\delta^c{}_k \,, \tag{B.21}$$

$$\mathbf{III_i} := \frac{1}{6}\epsilon_{abc}\epsilon^{ijk}\psi_{|i}^{|a}\psi_{|j}^{|b}\psi_{|k}^{|c} \,, \tag{B.22}$$

$$\mathbf{II}_\mathbf{i}^{(x,y)} := \frac{1}{2}\epsilon_{abc}\epsilon^{ijk}\Psi_{|i}^{x|a}\Psi_{|j}^{y|b}\delta^c{}_k \,, \tag{B.23}$$

$$\mathbf{III}_\mathbf{i}^{(1,1,2)} := \frac{1}{6}\epsilon_{abc}\epsilon^{ijk}\psi_{|i}^{|a}\psi_{|j}^{|b}\psi_{0|k}^{|c} \,, \tag{B.24}$$

$$\mathbf{II}_\mathbf{i}^{(1,3c)} := \epsilon^{abc}\partial_a^d T_b^{(3c)}\partial_{cd}\varphi \,. \tag{B.25}$$

Here, $O_{|a}$ denotes the partial derivative $\partial_a O$ and Ψ^x may be ψ_0, $\Psi^{(3a)}$ or $\Psi^{(3b)}$. The same expression emerges in the Newtownian case. To show this, we use the fourth order solution of [126] and the same procedure as described in section 4.5.1. We start by writing down the volume scale factor at fourth order

$$a_\mathcal{D}^3 = a^3\left[1 + \langle\mathbf{I_i}\rangle_{\mathcal{D}_\mathbf{i}}\, a + \frac{4}{7}\langle\mathbf{II_i}\rangle_{\mathcal{D}_\mathbf{i}}\, a^2 + \left(\frac{2}{3}\langle\mathbf{III_i}\rangle_{\mathcal{D}_\mathbf{i}} - \frac{8}{21}\left\langle\mathbf{II}_\mathbf{i}^{(1,2)}\right\rangle_{\mathcal{D}_\mathbf{i}}\right)a^3 + \right. \tag{B.26}$$

$$\left.\left(\frac{48}{539}\left\langle\mathbf{II}_\mathbf{i}^{(2,2)}\right\rangle_{\mathcal{D}_\mathbf{i}} - \frac{8}{33}\left\langle\mathbf{II}_\mathbf{i}^{(1,3a)}\right\rangle_{\mathcal{D}_\mathbf{i}} + \frac{80}{231}\left\langle\mathbf{II}_\mathbf{i}^{(1,3b)}\right\rangle_{\mathcal{D}_\mathbf{i}} + \frac{4}{77}\left\langle\mathbf{II}_\mathbf{i}^{(1,3c)}\right\rangle_{\mathcal{D}_\mathbf{i}} - \frac{60}{77}\left\langle\mathbf{III}_\mathbf{i}^{(1,1,2)}\right\rangle_{\mathcal{D}_\mathbf{i}}\right)a^4\right]$$

and use Eq. (4.124) to derive the expression of the corresponding backreaction term. The result is again (B.19). This confirms that the fastest growing GR mode corresponds to the Newtonian mode.

C. List of abbreviations

Abbreviation	Use	Meaning
2dFGRS	3.1.2	Two degree field giant redshift survey: [56]
ADM	4.1.1	Arnowitt-Deser-Misner
BAO	3.1.2	baryon acoustic oscillations
BigBoss	1	Extension of BOSS [37]
BOSS	1	Baryonic Oscillation Spectroscopic Survey
CDM	1	cold dark matter
CMB	3.1.1	cosmic microwave background
COBE	2.3.3	Cosmic Background Explorer
DP	3.2.3	Davis Peebles correlation function estimator [79]
EdS	4.3.1	Einstein-de Sitter
Euclid	1	A European galaxy survey satellite mission [38]
FRW	1	Friedmann-Robertson-Walker
GR	1	general relativity
ISW	1	Integrated Sachs Wolfe Effect
ΛCDM	1	Λ cold dark matter
LTB	4.4.1	Lemaître-Tolman-Bondi
LRG	3.2	luminous red galaxy
LS	3.2.3	Landy Szalay correlation function estimator [80]
NZA	4.3.2	Newtonian Zel'dovich Approximation[30]
RW	1.1.1	Robertson Walker
RZA	4.2	Relativistic Zel'dovich Approximation [31]
SDSS	3.1.2	Sloan Digital Sky Survey
SDSS DR7	3.1.2	Seventh data release Sloan Digital Sky Survey [57]
SDSS-III	3.1.2	Third phase of the Sloan Digital Sky Survey [36]
SPP	2.1	stochastic point process
SSP	2.1	stationary stochastic process
VLS	3.2.3	very large simulation [78]
WiggleZ	3.1.2	An Australian Galaxy survey [58]
WMAP	3.1.1	Wilkinson Microwave Anisotropy Probe [2]
WMAP5	5.3.2	WMAP 5-year data release [109]
WMAP7	3.1.1	WMAP 7-year data release [41]

D. List of symbols and list of figures

Symbol	Definition	Use	Meaning
a		Eq. (1.3a)	scale factor
$a_{\mathcal{D}}$	$= \left(\frac{V_{\mathcal{D}}}{V_{\mathcal{D}_\mathrm{i}}}\right)^{\frac{1}{3}}$	Eq. (4.12)	volume scale factor
$\langle\mathcal{A}\rangle_{\mathcal{C}_{\mathcal{D}}}$	$= \frac{1}{V_{\mathcal{D}_\mathrm{i}}}\int_{\mathcal{D}} \mathrm{d}^3X\mathcal{A}$	Eq. (4.43)	chart average
C_ℓ	$= \frac{\int \mathrm{d}^2\hat{n}\mathrm{d}^2\hat{n}' P_\ell\left(\hat{n}\cdot\hat{n}'\right)\overline{\Delta T(\hat{n})\Delta T(\hat{n}')}}{4\pi}$	Eq. (2.119)	CMB angular power
$\mathcal{D}$		Eq. (4.6)	domain of averaging
$D\left(a\right)$	$= \frac{a}{a_0}\,{}_2F_1\left(1, \frac{1}{3}; \frac{11}{6}; -\frac{\Omega_\Lambda}{\Omega_m}\left(\frac{a}{a_0}\right)^3\right)$	Eq. (2.129)	ΛCDM growth function
D_{ij}	$= \partial_i\partial_j - \frac{1}{3}\Delta\delta_{ij}$	Eq. (4.101)	traceless derivative
$\mathbb{E}\left[O\right]$	$= \overline{O}$	Sec. 2.1	ensemble average
$\langle f\rangle_{\mathcal{D}}\left(t\right)$	$= \frac{\int_{\mathcal{D}} f(t,X)\mathrm{d}\mu_g}{\int_{\mathcal{D}}\mathrm{d}\mu_g}$	Eq. (4.6)	scalar average
$\mathbf{f}^Z\left(\mathbf{X},t\right)$	$= a(t)\Big(\mathbf{X} + \xi\left(t\right)\nabla_0\psi\left(\mathbf{X}\right)\Big)$	Eq. (4.35)	Lagrangian mapping
$f\left(a\right)$	$= \frac{\mathrm{d}\ln D(a)}{\mathrm{d}\ln a}$	Eq. (5.10)	growth rate
$f_{\mathcal{D}}\left(a_{\mathcal{D}}\right)$	$= \frac{5\frac{a_{\mathcal{D}}}{D_0}-3}{2(1+ca_{\mathcal{D}}^3)}$	Eq. (5.19)	average growth rate
G		Eq. (1.3a)	Newton's gravitational constant
$g_{\mu\nu}$	$g_{\mu\nu} = \bar{g}_{\mu\nu} + h_{\mu\nu}$	Eq. (2.41)	metric of space-time
g_{ij}		Eq. (2.41)	3-dimensional spatial metric
$g\left(t_1, t_2, \ldots, t_n\right)$	$= \log\left(\mathbb{E}\left[\exp\left(\sum_{j=1}^n t_j X_j\right)\right]\right)$	Eq. (2.8)	cumulant generating function
h	$= H/\left(100\frac{\mathrm{km}}{\mathrm{sMpc}}\right)$	Sec. 2.3.2	dimensionless Hubble parameter
H	$H = \frac{\dot{a}}{a}$	Eq. (1.3a)	Hubble expansion rate
$H_{\mathcal{D}}$	$= \frac{\dot{a}_{\mathcal{D}}}{a_{\mathcal{D}}} = \frac{1}{3}\langle\theta\rangle_{\mathcal{D}}$	Eq. (4.12)	average Hubble expansion rate
$h_{\mu\nu}$		Eq. (4.2)	projection operator
$h_{\mu\nu}$	$g_{\mu\nu} = \bar{g}_{\mu\nu} + h_{\mu\nu}$	Eq. (2.41)	metric perturbation
$\mathrm{I}\left(\dot{\mathscr{P}}^a{}_i\right)$	$= \frac{1}{2}\epsilon_{abc}\epsilon^{ijk}\dot{\mathscr{P}}^a{}_i\delta^b{}_j\delta^c{}_k$	Eq. (4.55)	1. invariant of a matrix
$\mathrm{II}\left(\dot{\mathscr{P}}^a{}_i\right)$	$= \frac{1}{2}\epsilon_{abc}\epsilon^{ijk}\dot{\mathscr{P}}^a{}_i\dot{\mathscr{P}}^b{}_j\delta^c{}_k$	Eq. (4.55)	2. invariant of a matrix
$\mathrm{III}\left(\dot{\mathscr{P}}^a{}_i\right)$	$= \frac{1}{6}\epsilon_{abc}\epsilon^{ijk}\dot{\mathscr{P}}^a{}_i\dot{\mathscr{P}}^b{}_j\dot{\mathscr{P}}^c{}_k$	Eq. (4.55)	3. invariant of a matrix
$\mathbf{I_i}$	$= \mathbf{I}\left(\psi^{|i}_{\ |j}\right)$	Eq. (4.122)	initial 1. invariant: trace
$\mathbf{II_i}$	$= \mathbf{II}\left(\psi^{|i}_{\ |j}\right)$	Eq. (4.122)	initial 2. invariant
$\mathbf{III_i}$	$= \mathbf{III}\left(\psi^{|i}_{\ |j}\right)$	Eq. (4.122)	initial 3. invariant: determinant
J	$= \frac{1}{6}\epsilon_{abc}\epsilon^{ikl}\eta^a{}_i\eta^b{}_k\eta^c{}_l$	Eq. (4.30)	measure of integral
k		Sec. 2.2.3	physical wave number
K_{ij}	$= -u_{\mu;\nu}h^\mu{}_i h^\nu{}_j$	Eq. (4.2)	extrinsic curvature
n_s		Eq. (2.112)	index of the power spectrum

Symbol	Definition	Use	Meaning
p		Eq. (2.45)	pressure
p_{eff}	$p_{\text{eff}}^{\mathcal{D}} = -\frac{1}{16\pi G}\mathcal{Q}_{\mathcal{D}} + \frac{1}{48\pi G}\langle\mathcal{R}\rangle_{\mathcal{D}}$	Eq. (4.16)	pressure of the effective fluid
$\mathbf{P}^{a}(t, X^{k})$		Eq. (4.37)	coframe perturbation
$\mathcal{P}(q)$	$= \lvert\delta_{Dq}\rvert^2 = Aq^{n_S}\mathcal{T}^2(q)\left(\frac{a}{a_{EQ}}\right)^2$	Eq. (2.112)	ΛCDM power spectrum
$P(\mathbf{k})$	$= \int d^3r\tilde{\xi}(\mathbf{r})\, e^{-i\mathbf{k}\cdot\mathbf{r}}$	Eq. (2.13)	general power spectrum
q	$q = ak$	Sec. 2.2.3	comoving wave number
$q(t)$		Eq. (4.41)	time evolution of perturbation
$q^{\mathcal{D}}$	$= -\frac{\ddot{a}_{\mathcal{D}}}{a_{\mathcal{D}}}\frac{1}{H_{\mathcal{D}}^2}$	Eq. (4.22)	average deceleration factor
$\mathcal{Q}_{\mathcal{D}}$	$= \frac{2}{3}\left(\langle\theta^2\rangle_{\mathcal{D}} - \langle\theta\rangle_{\mathcal{D}}^2\right) - 2\langle\sigma^2\rangle_{\mathcal{D}}$	Eq. (4.13)	kinematical backreaction term
R		Eq. (1.1)	Ricci scalar
R		Eq. (2.16)	scale of observations
$\mathcal{R}$		Eq. (4.3c)	3-dimensional spatial Ricci scalar
$\mathcal{R}_q$	$= -\frac{a^2H}{q^2}\Psi_q + \frac{4\pi Ga^2}{q^2}\delta\varrho_q + H\delta u_q$	Eq. (2.58)	curvature perturbation ...
$\mathcal{R}_q^o$		Eq. (2.84)	... outside the Hubble radius
$R_H(t)$	$= \int \frac{dt}{a(t)}$	Eq. (2.24)	particle horizon
$R_{\mu\nu}$		Eq. (1.1)	Ricci tensor
$\mathcal{R}_{ij}$		Eq. (4.3c)	3-dimensional spatial Ricci tensor
t		Sec. 4.1.1	cosmic time
$T_{\mu\nu}$	$= \bar{p}\bar{g}_{\mu\nu} + (\bar{\varrho} + \bar{p})\,\bar{u}_\mu\bar{u}_\nu$	Eq. (2.45)	energy-momentum tensor
u_μ		Eq. (4.2)	4-velocity
$V_{\mathcal{D}}$	$= \int_{\mathcal{D}} \mathrm{d}\mu_g$	Eq. (4.6)	volume of the domain $\mathcal{D}$
$V_\mu(B)$		Eq. (2.37)	Minkowski functionals of a ball
$\overline{V}_\mu$		Eq. (2.40)	Minkowski functionals with structure
w	$= p/\varrho$	Eq. (1.3a)	equation of state
w_X	$= \frac{p_{\text{eff}}^{\mathcal{D}}}{\varrho_{\text{eff}}^{\mathcal{D}} - \langle\varrho\rangle_{\mathcal{D}}}$	Eq. (4.18)	effective equation of state
$W_{\mathcal{B}(R)}(\mathbf{r})$	$= \begin{cases} \left(\frac{4\pi}{3}R^3\right)^{-1} & R - \lvert\mathbf{r}\rvert > 0 \\ 0 & \text{else} \end{cases}$	Eq. (2.20)	top-hat window function
$\widetilde{W}_{\mathcal{B}(R)}(\mathbf{k})$	$= 3(kR)^{-3}(\sin kR - kR\cos kR)$	Eq. (2.21)	Fourier transformed window
z		Sec. 3.2.1	redshift

Symbol	Definition	Use	Meaning
Δ		Eq. (4.104)	Laplace operator
δ_H	$= \frac{H_{\mathcal{D}} - \overline{H}_{\mathcal{D}}(a_{\mathcal{D}})}{\overline{H}_{\mathcal{D}}(a_{\mathcal{D}})}$	Eq. (5.35)	fluctuation of the Hubble rate
$\delta_{\alpha q}$	$= \frac{\delta \varrho_{\alpha q}}{\bar{\varrho}_\alpha + \bar{p}_\alpha}$	Eq. (2.90)	over-density
δ_{Dq}	$= \frac{2}{5}\kappa^2 \frac{D(a)}{D(a_{EQ})} \mathcal{R}_q^o \mathcal{T}(q)$	Eq. (2.130)	dark matter over-density
η		Eq. (4.101)	conformal time
$\eta^a{}_i$		Eq. (4.29)	metric coframe
θ	$= \Theta^i_i$	Eq. (4.4)	volume expansion rate
Θ_{ij}	$= -K_{ij} = \sigma_{ij} + \frac{1}{3}\theta g_{ij}$	Eq. (4.4)	spatial expansion tensor
Λ		Eq. (1.1)	cosmological constant
$\mathrm{d}\mu_g$	$= \sqrt{{}^{(3)}g(t,X)}\mathrm{d}^3X$	Eq. (4.6)	Riemannian volume element
κ_n	$= \partial_{t_1} \dots \partial_{t_n} g(t_1, t_2, \dots, t_n)\vert_{\mathbf{t}=0}$	Eq. (2.9)	joint cumulants
ν_i		Eq. (2.39)	Minkowski functional densities
ϱ		Sec. 2.1	energy density
$\varrho_{\mathrm{eff}}^{\mathcal{D}}$	$= \langle\varrho\rangle_{\mathcal{D}} - \frac{1}{16\pi G}\mathcal{Q}_{\mathcal{D}} - \frac{1}{16\pi G}\langle\mathcal{R}\rangle_{\mathcal{D}}$	Eq. (4.16)	effective energy density
$\sigma(\langle O\rangle_{\mathcal{D}})$	$= \left(\overline{\langle O\rangle_{\mathcal{D}}^2} - \overline{\langle O\rangle_{\mathcal{D}}}^2\right)^{\frac{1}{2}}$	Eq. (5.1)	ensemble variance
$\sigma^2(R)$	$= \frac{\mathbb{E}\left[M(R)^2\right] - \mathbb{E}[M(R)]^2}{\mathbb{E}[M(R)]^2}$	Eq. (2.16)	matter fluctuations
σ^2	$= \frac{1}{2}\sigma^{ij}\sigma_{ij}$	Eq. (4.4)	shear scalar
$\sigma^2_{\mathcal{D}_0}$	$= \sigma^2(\langle\delta_0\rangle_{\mathcal{D}})$	Eq. (5.29)	matter fluctuations today
σ_{ij}	$\Theta_{ij} = -K_{ij} = \sigma_{ij} + \frac{1}{3}\theta g_{ij}$	Eq. (4.4)	shear tensor
φ	$\Delta\varphi(\mathbf{x}) = 4\pi G \varrho_H a^2 \delta(\mathbf{x}, t)$	Eq. (4.104)	peculiar gravitational potential
$\chi^{(1)}$		Eq. (4.101)	first order scalar perturbation
$\chi(A)$	$= \begin{cases} 1 & A \text{ convex } A \neq \emptyset \\ 0 & A = \emptyset \end{cases}$	Eq. (2.35)	Euler characteristic
$\psi^{(1)}$		Eq. (4.101)	first order scalar perturbation
ψ	$\delta_{\mathbf{i}} = -\psi^{\vert i}{}_{\vert i}(X)$	Eq. (4.112)	NZA potential
Ψ	$= \frac{\partial}{\partial t}\left(\frac{h_{ii}}{2a^2}\right)$	Eq. (2.49)	synchronous metric perturbation
Ω		Eq. (1.4)	energy density parameter for:
Ω_k	$= -\frac{k}{a^2H^2}$	Eq. (1.4)	curvature
Ω_{m}	$= \frac{8\pi G}{3H^2}\varrho$	Eq. (1.4)	matter
Ω_{r}	$= \frac{8\pi G}{3H^2}\varrho_r$	Eq. (1.4)	radiation
Ω_λ	$= \frac{\Lambda}{3H^2}$	Eq. (1.4)	cosmological constant
$\Omega_m^{\mathcal{D}}$	$= \frac{8\pi G}{3H_{\mathcal{D}}^2}\langle\varrho\rangle_{\mathcal{D}}$	Eq. (4.21)	average matter parameter
$\Omega_\Lambda^{\mathcal{D}}$	$= \frac{\Lambda}{3H_{\mathcal{D}}^2}$	Eq. (4.21)	average cosm. const. parameter
$\Omega_{\mathcal{R}}^{\mathcal{D}}$	$= -\frac{\langle\mathcal{R}\rangle_{\mathcal{D}}}{6H_{\mathcal{D}}^2}$	Eq. (4.21)	average curv. parameter
$\Omega_Q^{\mathcal{D}}$	$= -\frac{Q_{\mathcal{D}}}{6H_{\mathcal{D}}^2}$	Eq. (4.21)	backreaction parameter
$\xi_E^{DP}(r)$	$= \frac{2N_R}{N_D - 1}\frac{DD(r)}{DR(r)} - 1$	Eq. (3.11)	Davis Peebles estimator
$\xi_E^{LS}(r)$	$= \frac{N_R(N_R-1)}{N_D(N_D-1)}\frac{DD(r)}{DR(r)} - 2\frac{N_R-1}{N_D}\frac{DR(r)}{RR(r)} + 1$	Eq. (3.12)	Landy Szalay estimator
$\xi(t)$	$= (q(t) - q(t_{\mathbf{i}}))/\dot{q}(t_{\mathbf{i}})$	Eq. (4.40)	RZA evolution function
$\tilde{\xi}(\mathbf{x}_{12})$	$= \overline{\hat{\delta}(\mathbf{x}_1)\hat{\delta}(\mathbf{x}_2)}$	Eq. (2.6)	2 pt. correlation function
$\tilde{\zeta}$	$= \overline{\hat{\delta}(\mathbf{x}_1)\hat{\delta}(\mathbf{x}_2)\hat{\delta}(\mathbf{x}_3)}$,	Eq. (2.7)	3 pt. correlation function

List of Figures

Danksagung

Zu allervörderst möchte ich meinen Eltern für die jahrelange konstante Unterstützung danken, ohne die diese Doktorarbeit nicht entstanden wäre. Wie mir jüngst versichert wurde seid ihr mindestens eine 3 Sigma Fluktuation nach oben weswegen ich mich glücklich schätze. Danke auch meinen Brüdern die zum Durchhalten beigetragen haben.

An dieser Stelle sei auch Rüdiger Örtel und Leonhard Hohe gedankt ohne die ich nicht Physik studiert hätte, und natürlich dem großen Norbert Poncin, dem ich die Begeisterung für die Eleganz der theoretischen Physik verdanke.

Of course I also want to thank my supervisor Dominik Schwarz, for the possibility to learn a lot about cosmology and to always have a critical view on the claims that people make when trying to confirm their favorite model. I am grateful to my collaborator Thomas Buchert for always being available in case of problems.

This work benefited from many discussions with people all over the world. I enjoyed my discussions with Juliane Behrend, Iain Brown, Chris Byrnes, Chris Clarkson, Ruth Durrer, Anastasia Fialkov, Martin Kunz, Valerio Marra, Sabino Matarrese, Giovanni Marozzi, Nathaniel Obadia, Will Percival, Syksy Räsänen, Xavier Roy, Marina Seikel and David Wiltshire.

I thank Francesco Sylos Labini for a great trip to Roma and for help with the LRG galaxy samples, including useful codes for generating point distributions. I thank Lars Andersson for an invitation to the AEI and for interesting discussions and ideas on the MultiDomain model.

I thank Christoph Wiegand for discussions on more and less fundamental problems of physics and for helpful support in fighting the “hidden magic” of Mathematica. I thank Martin Kerscher, Nathaniel Obadia and Thomas Buchert for useful remarks on the final manuscript. I acknowledge financial support by Deutsche Forschungsgemeinschaft (DFG) under grant IRTG 881. Thank goes also to Cornelius Rampf for convincing me to go to the famous 2010 ICTP summer school.

Finalement je suis heureux de pouvoir remercier ma copine JCMDK pour le support moral qui m’a aidé à remonter le moral après des journées frustrantes qui arrivent des fois en recherche. Merci en plus pour me faire découvrir le nouveau monde avec toutes ses bizarrités et sa vue particulière sur la physique et pour zr genafsbezre qr dhnfvzbqb ra dhnfvzrag ornh.

Eigenständigkeitserklärung

Hiermit erkläre ich, dass ich die vorliegende Arbeit mit dem Titel The inhomogeneous Universe: Its average expansion and cosmic variance selbstständig und ohne unerlaubte fremde Hilfe angefertigt habe. Es wurden ausschließlich die angegebenen Quellen und Hilfen benutzt.

Bielefeld, den 08.08.2012

Alexander Wiegand